# Direct electrochemistry
# of redox proteins

**Dirk Heering**

H.A. Heering

# Direct electrochemistry
# of redox proteins

Stellingen

Behorende bij het proefschrift

**Direct electrochemistry of redox proteins**


1    De standaarddeviatie die volgt uit de middeling van midpointpotentialen, gemeten met
     cyclische voltammetry, is verwaarloosbaar ten opzichte van de onzekerheid in de
     waarden indien sprake is van asymmetrische verbreding.
     [dit proefschrift]


2    HiPIPs zijn LowPIPs.
     [Hoofdstuk 6 en 7 van dit proefschrift]


3    In tegenstelling tot de theoretisch met dithioniet haalbare potentiaal, zelfs als de
     onzuiverheid wordt meegenomen in de berekening, is titaan(III)citraat in de praktijk
     een betere reductor.
     [G. Mayhew (1978) *Eur. J. Biochem 85*, 535; A.J.B. Zehnder (1976) *Ph.D. Thesis*,
     Federal Institute of Technology (ETH), Zürich, Zwitserland; Hoofdstuk 3 en 7 van dit
     proefschrift]


4    De aanwezigheid van 15 low-spin lage-potentiaal heemgroepen in hoog-
     molecuulgewicht cytochroom *c* naast één high-spin hoge-potentiaal heemgroep
     suggereert overeenkomsten met het fotosynthese centrum in de chloroplast: de lage
     potentiaal heemgroepen zijn het electrochemische equivalent van een antennesysteem.
     [M.F.J.M. Verhagen *et al.* (1994) *Eur. J. Biochem. 225*, 311.]


5    Pitten is een passief proces.


6    Als zomerdijk de winterdijk vertrouwt, kan Nederland rustig gaan slapen.


7    Door het privatiseren van overheidsinstellingen verliest de staat een belangrijke bron
     van inkomsten, die niet op het innen van belastingen is gebaseerd.


8    De invoering van de angelsaksische onderwijsstructuur zonder ook de intensieve
     begeleiding door tutors over te nemen, komt de kwaliteit van het academisch
     onderwijs niet ten goede.

9    Opportunisme is verre te verkiezen boven dogmatische politiek, maar het aangrijpen van goede kansen moet niet worden verward met het nemen van *ad hoc* besluiten bij gebrek aan visie op de toekomst.

10   Volgens C. Stoll [Het Koekoeksei] is een goed programma, dat passwords versleutelt, vergelijkbaar met een worstmachine waar geen varkens uitkomen als je de slinger terugdraait. Deze metafoor is echter alleen geldig als elk varken een ander kleur gehakt oplevert.

11   Het internet is in sommige opzichten te beschouwen als digitale kaasfondue.
     [vgl. W.M. Pruimboom (1995) proefschrift, Erasmus Universiteit Rotterdam,
     stelling 11]


                         Dirk Heering, Wageningen, 23 oktober 1995.

*What has it got in its pocketsess?*
*Tell us that. It must tell first!*

*Answers were to be guessed, not given!*

[J.R.R. Tolkien, The Hobbit]

# Woord vooraf

De omslag van dit boekje suggereert dat de inhoud het werk is van één persoon, maar dit is, zonder valse bescheidenheid, natuurlijk niet het geval. Velen hebben direct en indirect belangrijke bijdragen geleverd aan de inhoud van mijn proefschrift en aan de werksfeer. Deze opening is dan wel cliché (en er is een risico dat het zelfs regelrechte plagiaat is), maar daarmee niet minder oprecht.

Allereerst wil ik natuurlijk mijn directe werkomgeving, lab 1/2, bedanken: Beste Fred, de jaren in "jouw" lab hebben mij een degelijke wetenschappelijke opvoeding gegeven. Jouw vakkennis, ondersteuning en geduld om voor mij als klankbord op te treden zijn zeer belangrijk geweest. Ik heb er grote waardering voor dat je constant bereid en (soms tot mijn verrassing) in staat was om mij practisch en theoretisch bij te staan.

Ronnie (of moet ik tegenwoordig "mijnheer Ron Wolbert" zeggen?), jij bent zo'n sleutelpersoon waar het lot door wordt gestuurd. Eerst heb je me "geronseld" voor een afstudeervak in de groep van Riet Hilhorst, waar jij toen zat (ik weet het nog goed, het was op de borrel van Veegers college "Regulering"). En later, jij zat toen inmiddels bij Fred, heb je me erop attent gemaakt dat er een interessante OIO-baan beschikbaar was. Het lot kan soms rare sprongen maken want het bleek dat de groep van Fred toen net was verhuisd naar lab 1/2, waar Riet eerst zat. En mijn territorium werd precies dezelfde plek als tijdens mijn afstudeervak. En dat terwijl ik me nog zo voorgenomen had om een AIO-baan buiten Wageningen te zoeken. Natuurlijk bedank ik je ook voor de practische ondersteuning.

Antonio Pierik, jouw enthousiaste hulp heeft mij snel de nukken van ons "huisbeestje" *Desulfovibrio vulgaris* geleerd. Sander Arendsen en Marc Verhagen, bedankt voor jullie hulp en de zeer succesvolle "evaluaties". Yvonne Bulsink, jouw inzet bij het werk aan de HiPIPs was onmisbaar.

Niet alleen "mijn eigen" student Leon Coolen maar ook de vele andere studenten die op lab 1/2 hebben gewerkt verdienen, misschien onverwacht, ook een bedankje. Jullie hebben allemaal een niet te onderschatten invloed op het eindresultaat gehad. Hetzij direct door jullie wetenschappelijke werk of door een aangename toevoeging te leveren aan de algemene sfeer op het lab en de vele discussies over biochemische en andere zaken. Ook al was ik (te) vaak "die AIO die achter zijn computer zit". Ik heb gemerkt dat het geven van onderwijs en uitleg net zo nuttig is voor de student als voor de "leraar".

Mijn promotor, professor Cees Veeger, dank U voor de belangstelling voor mijn werk en de opbouwende kritiek (altijd ingeleid met verontschuldiging "advocaat van de duivel" te spelen). Elles Steensma, het was een gezellige en nuttige samenwerking. Het "itereren" van het manuscript via E-mail ging verrassend goed. Carlo van Mierlo, bedankt voor je steun aan dit project, ondanks je zorgen dat het NMR-werk van Elles erdoor zou worden vertraagd. Zoals ik je beloofd had, het artikeltje is er gekomen. Overige vakgroepsgenoten, de lijst

*Dirk*

# Contents

Chapter 7: Reversible super-reduction of the cubane $[4Fe\text{-}4S]^{(3+;2+;1+)}$ in High Potential Iron-Sulfur protein under non-denaturing conditions: EPR spectroscopic and electrochemical studies.

# Symbols and abbreviations

| | |
|---|---|
| $A$ | surface area |
| $A^{FMN}$ | electrode surface area covered by adsorbed FMN |
| ASR | assimilatory sulfite reductase |
| BisTris | bis[2-hydroxyethyl]iminotris[hydroxymethyl]methane |
| BisTrisPropane | 1,3-bis[tris(hydroxymethyl)methylamino]propane |
| $c$ | concentration |
| $c*$ | bulk-concentration |
| C | dimensionless (normalized) concentration |
| Caps | 3-[cyclohexylamino]-1-propanesulfonate |
| CD | circular dichroism |
| CGRA | *Chromatium gracile* HIPIP |
| Ches | 2-[N-cyclohexylamino]ethanesulfonate |
| CVIN | *Chromatium vinosum* HiPIP |
| $D$ | diffusion coefficient |
| DMSO | dimethylsulfoxide |
| DPV | differential pulse voltammetry |
| $E$ | potential |
| $E_1$ | semiquinone/hydroquinone redox potential |
| $E_2$ | quinone/semiquinone redox potential |
| $E_{high}$ | upper limit of potential scan |
| $E_{low}$ | lower limit of potential scan |
| $E_m$ | midpoint potential |
| $E_{SCE}$ | potential of SCE electrode with respect to NHE |
| $E^o$ | standard redox potential |
| EH1 | *Ectothiorhodospira halophila* iso-1 HIPIP |
| EH2 | *Ectothiorhodospira halophila* iso-2 HIPIP |
| Epps | N-[2-hydroxyethyl]piperazine-N'-[3-propanesulfonate] |
| EPR | electron paramagnetic resonance spectroscopy |
| EV1 | *Ectothiorhodospira vacuolata* iso-1 HIPIP |
| EV2 | *Ectothiorhodospira vacuolata* iso-2 HIPIP |
| $F$ | Faraday constant (96484.6 C/mol) |
| FAD | flavin adenine dinucleotide |
| Fld | flavodoxin |
| FMN | riboflavin-5'-phosphate (flavin mononucleotide) |
| $g$ | concentration gradient or $g$-factor in EPR |
| G | dimensionless concentration gradient |
| GOD | glucose oxidase |

| | |
|---|---|
| Hepes | N-[2-hydroxyethyl]piperazine-N'-[2-ethanesulfonate] |
| HiPIP | high potential iron-sulfur protein |
| $i$ | current |
| $i_{pa}$ | anodic peak current |
| $i_{pc}$ | cathodic peak current |
| $I$ | ionic strength |
| $(p)K_i$ | (-log) protonation constant of species i |
| $k^+$ | comproportionation rate |
| $k^-$ | disproportionation rate |
| $K_1$ | dimensionless comproportionation rate |
| $K_2$ | dimensionless disproportionation rate |
| $k_b$ | heterogeneous rate constant for oxidation |
| $K_b$ | dimensionless heterogeneous rate constant for oxidation |
| $K_{com}$ | comproportionation constant |
| $k_f$ | heterogeneous rate constant for reduction |
| $K_f$ | dimensionless heterogeneous rate constant for reduction |
| $k^\circ, k_s$ | standard heterogeneous rate constant |
| KPi | potassium phosphate buffer |
| LOPTLC | long optical path length thin layer cell |
| Mes | 2-[N-morpholino]ethanesulfonate |
| Mops | 3-[N-morpholino]propanesulfonate |
| morpholin | 1-oxa-4-azacyclohexane |
| $n$ | number of electrons |
| $n_\alpha$ | number of electrons involved in the rate-determining step |
| NHE | normal hydrogen electrode |
| NMR | nuclear magnetic resonance |
| Ox, ox, O, o | oxidized species |
| p$I$ | iso-electric point |
| PS | *Paracoccus* species HIPIP |
| $r$ | distance |
| $R$ | molar gas constant (8.31441 J/mol·K) |
| $r^2$ | correlation coefficient (linear regression) |
| Red, red, R, r | reduced species |
| RGEL | *Rhodocyclus gelatinosus* HiPIP |
| RGLO | *Rhodopila globiformis* HIPIP |
| RSAL | *Rhodospirillum salinarum* iso-2 HIPIP |
| RTEN | *Rhodocyclus tenuis* HiPIP |
| SCE | saturated calomel electrode |
| SCV | staircase cyclic voltammetry |
| Sq, sq, S, s | semiquinone species |

| | |
|---|---|
| $t$ | time or temperature (°C) |
| $T$ | absolute temperature |
| **T** | dimensionless time |
| **Taps** | N-tris[hydroxymethyl]methyl-3-aminopropanesulfonate |
| **TLC** | thin layer cell |
| $t_N$ | normalized time |
| **TPFE** | *Thiocapsa pfennigii* HiPIP |
| **Tricine** | N-tris[hydroxymethyl]methylglycine |
| **TROS** | *Thiocapsa roseopersicina* HiPIP |
| **UV** | ultra violet light |
| $v$ | potential scan rate |
| **VIS** | visible light |
| $x$ | distance (from electrode surface) |
| **X** | dimensionless distance (from the electrode) |
| $x_N$ | normalized distance (from the electrode) |
| $y_i$ | activity coefficient |
| $z$ | number of charge unities |
| $\alpha$ | cathodic transfer coefficient or sampling parameter in SCV |
| $\delta$ | diffusion layer |
| $\Delta E$ | potential step |
| $\Delta E_p$ | peak-to-peak separation |
| $\Delta G^\circ$ | standard Gibbs free energy change |
| $\Delta H^\circ$ | standard enthalpy change |
| $\Delta S^\circ$ | standard entropy change |
| $\Delta S^\circ_{rc}$ | standard entropy change of the reaction center |
| $\varepsilon$ | dielectric constant or molar extinction coefficient |
| $\Theta^{ox}$, $\Theta^{red}$ | relative fraction of oxidized/reduced species |
| $\lambda$ | wavelength or dimensionless diffusion parameter |
| $\lambda_{max}$ | position of absorption maximum |
| $\phi$ | relative coverage of the surface (by adsorbed FMN) |
| $\chi^2$ | sum of squared differences |
| $\sqrt{\pi}\,\chi$ | current function |

# Chapter 1

## General Introduction.

### 1.1    Redox proteins

An important part of the metabolism consists of reduction/oxidation reactions. The proteins involved in these electron transfer reactions are known as redox proteins. These proteins all contain one or more redox active groups. The diversity of these groups is very large, ranging from single transition metal ions coordinated by amino acid side chains, or organic molecules such as flavins, to complexes such as heme, multi-nuclear metal centers and clusters of iron, sulfur and sometimes other metal ions (see *e.g.* [Fraústo da Silva & Williams, 1993]). This offers a large versatility in the binding of substrate and a wide range of available redox potentials. Moreover, the redox potential is modulated by the environment of the cofactor (*i.e.* the peptide). The heterogeneous group of redox proteins includes both the redox enzymes and the proteins that only shuttle electrons between different parts of the metabolism. The enzymes are often large and complex, containing multiple redox centers, while the electron transfer proteins are usually small and have much simpler structures. However, the redox centers present in these electron transferring proteins are also found in enzymes. This makes them ideally suited as model systems for the enzymes, especially to study the influence of the peptide on the redox potential of the cofactor and to study the electron transfer between different proteins and between proteins and electrodes or small reductants/oxidants.

In the context of this thesis the flavins and the iron-sulfur clusters are most important. Flavins are found as cofactor in the electron transferring flavodoxins in the form of riboflavin-5'-phosphate ("flavin mononucleotide", FMN), in enzymes such as glucose oxidase and xanthine oxidase in the form of flavin adenine dinucleotide (FAD), or as covalently bound FAD in *e.g.* succinate dehydrogenase. FMN and FAD consist of a 7,8-dimethylisoalloxazine ringsystem ("flavin"), substituted at N(10) with either a ribityl phosphate or a ribityl adenine diphosphate side chain (Figure 1.1). The isoalloxazine ringsystem exists in three redox states: the fully oxidized quinone state, the one-electron reduced semiquinone state, and the two-electron reduced hydroquinone state. In each of the redox states the ring system can be anionic, neutral or cationic, depending on the pH (Figure 1.2). For free flavin (not bound to protein) and also in a number of flavin-enzymes (especially the hydroxylases) the redox potential of the first reduction step (called $E_2$ according to the convention of Clark [1960]) is higher (less negative) than that of the second step ($E_1$). This results in a net uptake of two electrons and a redox potential equal to the average of $E_1$ and $E_2$. The maximum relative
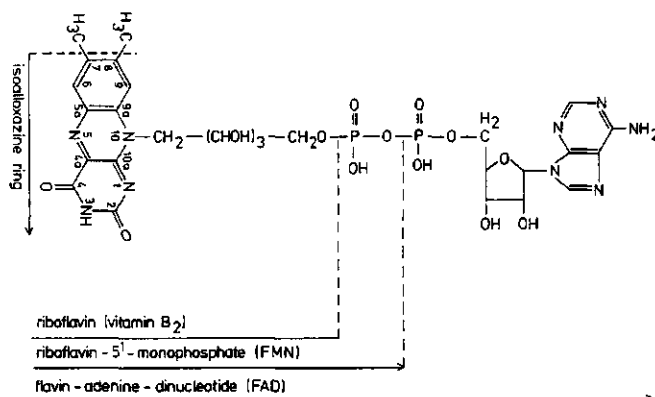
**Figure 1.1.** Structures of flavin cofactors (modified from [Müller, 1981]).
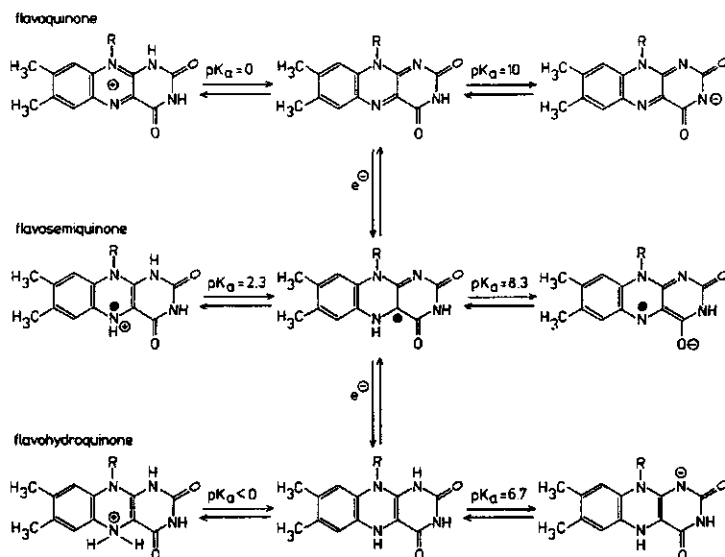


**Figure 1.2.** The structures of the flavin in its three oxidation states (modified from [Müller, 1987]).

amount of flavosemiquinone is determined by the potential difference. However, in flavodoxins and in some flavin-enzymes (dehydrogenases) the semiquinone species is stabilized. This results in a higher quinone/semiquinone potential and a lowering of the semiquinone/hydroquinone potential, and allows for the consecutive transfer of two single electrons [Müller, 1987].

Iron-sulfur proteins contain clusters of iron and acid-labile sulfide ions. The clusters

- 2 -

|     |          |          |          |
|:---:|:--------:|:--------:|:--------:|
| [1Fe] | [2Fe-2S] | [3Fe-4S] | [4Fe-4S] |
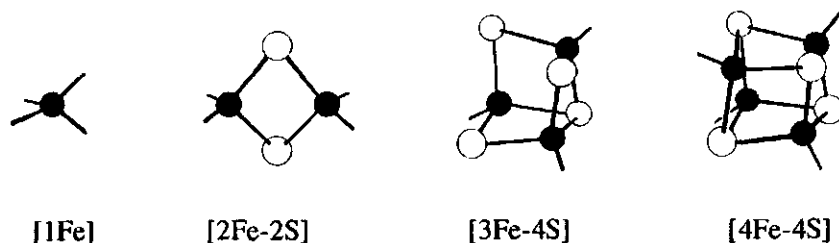
**Figure 1.3.** Examples of iron (sulfur) centers found in redox proteins [Armstrong, 1990].

**Table 1.1.** The different redox states of the [4Fe-4S] cluster.

| Redox state | Formal Fe charges: | | | | EPR-spectrum |
|-------------|------|------|------|------|--------------|
| $[4Fe-4S]^0$   | 2+ | 2+ | 2+ | 2+ | no  |
| $[4Fe-4S]^{1+}$ | 2+ | 2+ | 2+ | 3+ | yes |
| $[4Fe-4S]^{2+}$ | 2+ | 2+ | 3+ | 3+ | no  |
| $[4Fe-4S]^{3+}$ | 2+ | 3+ | 3+ | 3+ | yes |
| $[4Fe-4S]^{4+}$ | 3+ | 3+ | 3+ | 3+ | no  |

are often bound to the protein by cysteine residues coordinating to the iron ions (although not exclusively, *e.g.* the Rieske-type [2Fe-2S] cluster is coordinated by 2 cysteines and 2 histidines [Link *et al.*, 1992 and references cited therein]). Some examples are given in Figure 1.3. The most ubiquitous iron-sulfur cluster in biology is the [4Fe-4S] cluster, a distorted cube with alternating iron and sulfur ions at the corners. The cluster is usually bound to the protein by 4 cysteinyl residues, coordinated to the iron-ions [Cammack, 1992; Lippard & Berg, 1994]. The formal charge of the iron ions can be 2+ or 3+, yielding the theoretical possibility of 5 redox states (see Table 1.1). However, the potential differences between the potentials of the consecutive reduction steps are in the order of 1 Volt, making this cluster in practice a one-electron transferring center. In biology, either the 1+/2+ transition (*e.g.* in ferredoxins) or the 3+/2+ (in high potential iron-sulfur proteins, HiPIPs) is utilized [Carter *et al.*, 1972].

## 1.2   Reduction potentials

As stipulated above, one of the important properties of redox-centers is their reduction potential. For the reversible reduction of species Ox by $n$ electrons

$$Ox + ne^- \rightleftharpoons Red \qquad (1.1)$$

the relation between the concentrations Ox and Red and the potential of the solution $E$ is given by the Nernst-equation

$$E = E^\circ + \frac{RT}{nF}\ln\left(\frac{[Ox]}{[Red]}\right) \qquad (1.2)$$

or

$$\frac{[Ox]}{[Ox] + [Red]} = \frac{1}{1 + \exp\left[-\dfrac{nF}{RT}(E - E^\circ)\right]} \qquad (1.3)$$

where the Faraday constant $F$ is the charge per mol electrons, $R$ is the gas constant and $T$ the absolute temperature. The potential $E^\circ$ at which [Red]=[Ox], usually referred to as the half-wave potential, the (standard) reduction potentials or redox potential is a direct measure of the Gibbs free energy for the reduction reaction:

$$\Delta G^\circ = -nFE^\circ \qquad (1.4)$$

This means that the reduction of a substance by another substance is favoured by a low (more negative) reduction potential and high concentration of the reduced form of the electron-donor (reductor). The enthalpy and entropy of the reduction reaction can be determined by measuring the temperature dependence of the reduction potential.

Because of this direct relation between the potential and the energy difference between the oxidized and the reduced state, the presence of charges around the redox center, hydrogen bonding and polarity of the surrounding peptide/water medium can have a large influence on the redox potential. In water at pH 7 the range of applicable redox potentials under equilibrium conditions is limited by the potential of the $H_2O/O_2$ redox couple of +0.83 V and by that of the $H_2/H^+$ couple of –0.42 V. However, redox potentials that are well outside this range at pH 7 are also encountered in proteins. These potentials can be physiologically relevant only under non-equilibrium conditions (*i.e.* during turn-over of the enzyme) or when the redox-center is protected from the surrounding water by the peptide.

The large difference between ferredoxins and HiPIPs, both containing the same cluster but using a different transition, is a clear example of the influence of the peptide on the properties of the redox-center. The redox potentials of the cluster in ferredoxins are shifted to higher values by a large number of hydrogen bonds and a polar binding-pocket, while the

redox potentials of the HiPIP cluster are shifted to relatively lower potentials due to a lower number of hydrogen bonds and a hydrophobic binding-pocket. Moreover, within each of the two classes the redox potentials of the cluster varies over a wide range. For ferredoxins potentials between −250 and −650 mV are found, and for HiPIPs potentials between +50 and +500 mV are found (see Chapters 6 and 7, and [Armstrong, 1992] and references cited therein). The different properties of free and protein-bound flavin also shows that the redox properties of a cofactor can be modified considerably by the protein.

When a protonation site is present on or near the redox-active group in the protein the reduction potentials become dependent on the pH because the relative energy difference between the oxidized and the reduced state is influenced by the positive charge of the proton or the negative charge of the deprotonated acid. In turn, the protonation constant of the group is modified by the charge of the electron(s), resulting in a lower p$K$ for the oxidized form and a higher p$K$ for the reduced form (when the group is present in both oxidation states). For one protonation site the pH-dependence of the reduction potential is given by

$$E^\circ = E^a + \frac{RT}{nF}\ln\left[\frac{[H^+] + K_{red}}{[H^+] + K_{ox}}\right] \tag{1.5}$$

where $E^a$ is the constant potential at low pH. In general the potential is given by

$$E^\circ = E^a + \frac{RT}{nF}\ln\left[\frac{[H^+]^k + \sum_{i=1}^{k}\left([H^+]^{k-i}\prod_{j=1}^{i}K_{red,j}\right)}{[H^+]^l + \sum_{i=1}^{l}\left([H^+]^{l-i}\prod_{j=1}^{i}K_{ox,j}\right)}\right] \tag{1.6}$$

when $k$ protonation sites are present in the reduced form and $l$ in the oxidized form [Clark, 1960]. The slope of the reduction potential *versus* pH becomes 59/$n$ mV (25°C) more negative (or less positive) at pH=p$K_{ox,i}$ and more positive (or less negative) at pH=p$K_{red,i}$. When the difference between two successive p$K$'s is large enough the slope becomes ($m_2$-$m_1$) 59/$n$ mV for the overall half reaction

$$Ox + m_1 H^+ + ne^- \rightleftharpoons Red + m_2 H^+ \tag{1.7}$$

at $pK_i < pH < pK_j$ and 25°C. The formulas for the pH-dependence of the redox potentials given in this thesis follow from general equation (1.6) when the $pK$'s outside the measured range are assumed to be infinitely high or low.


## 1.3 Electrochemistry

Electrochemical methods are useful tools to study the properties of redox species, traditionally metal ions, complexes and organic compounds. A wide range of techniques has been developed to obtain information about redox potentials, the kinetics of the electron transfer process and about chemical reactions, coupled to the electron transfer reaction (see the textbooks [Bard & Faulkner, 1980] and [Southampton Electrochemistry Group, 1985]). Often the current is measured resulting from a time-dependent perturbation of the applied potential (so called voltammetric techniques). With a three-electrode setup the potential of a working electrode is controlled by a potentiostat relative to a reference electrode such as a calomel ($Hg/Hg_2Cl_2$) electrode or an Ag/AgCl electrode. The current passes between the working electrode and an auxiliary (or counter) electrode. This way essentially no current passes through the reference electrode and with proper cell design the resistance of the solution has little or no effect on the potential of the working electrode.

A widely used and theoretically well understood voltammetric technique [Nicholson & Shain, 1964; Nicholson 1965] is cyclic voltammetry. The potential of the working electrode is swept linearly between two limiting potentials. When the electron transfer between the electrode and the redox couple is fast compared to the rate at which the potential is changing, the system is in equilibrium and the concentrations of the oxidized and reduced species near the electrode follow from the Nernst-equation (1.2). This implies that a change of the potential will cause a change in the ratio of the concentrations. When the potential is swept to a more negative potential (*i.e.* in cathodic direction) the oxidized species will be reduced and a negative current will be observed. When the potential is swept in positive (anodic) direction the reduced species is (re)oxidized and a positive current will be observed. When a limiting amount of the redox couple is present, either as an adsorbed layer on the electrode surface or when only a very thin layer of solution is present, a peak-shaped curve of current as function of the potential is obtained (Figure 1.4). The peak is centered around the redox potential of the couple and has a width at half-height of $91/n$ mV at 25°C. The height of the peak is proportional to the scan rate because the absolute amount of charge passed is limited by the amount of material present. When the layer of solution is thick (*i.e.* more than a few tenths of a millimeter), the current will be limited by the mass transfer rate. This diffusion will appear in the voltammogram as a convolution of the peak-shape with the $1/\sqrt{t}$ dependence of the mass transfer and results in the characteristic shape plotted in Figure 1.4. The maximum current is proportional to the square root of the scan rate and the peak-to-peak
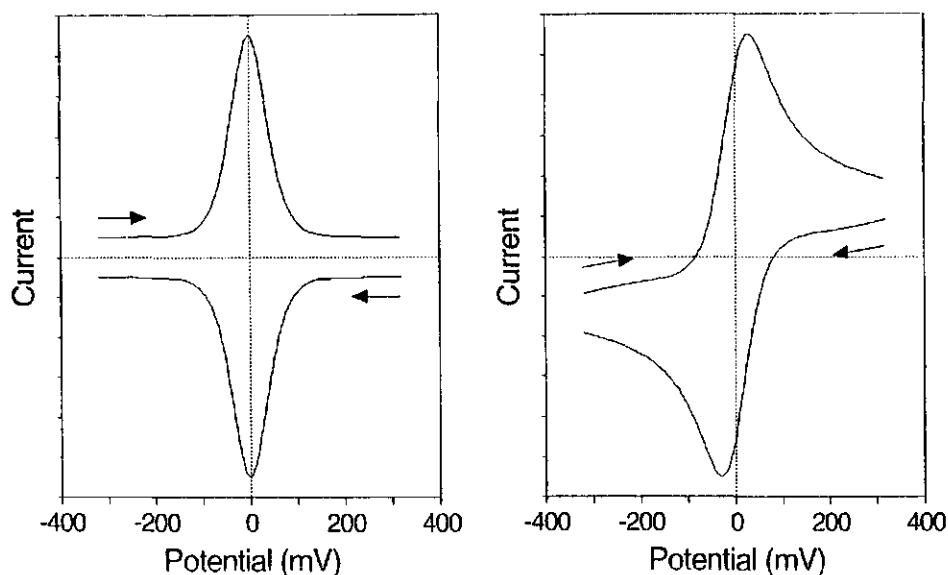
**Figure 1.4.** Theoretical shapes (with arbitrary background) of cyclic voltammograms for a one-electron transferring redox couple. Left: adsorbed onto the electrode or confined in a thin layer. Right: diffusing to a planar electrode.

separation is $59/n$ mV at 25°C. The midpoint potential of the couple can be calculated from the average of the two peak potentials. When the rate of electron transfer becomes rate limiting, the system is no longer in equilibrium. This will appear as a scan rate dependent broadening of the waves and increase of the peak-separation.

Using a digitally controlled potentiostat, the linear time-dependence of the potential in cyclic voltammetry is replaced by a series of small steps. The resulting staircase cyclic voltammetry (SCV) yields in essence the same wave-shape but is also somewhat influenced by the step-size and the moment within the step at which the current is sampled (see [Seralathan *et al.*, 1987] and references cited therein). The digital control of the potential can also be used to modify the staircase sweep with potential pulses. In differential pulse voltammetry (DPV) for example, a pulse is applied at the end of each potential step and the difference between the current at the end of the pulse and just before the pulse is recorded. This enhances the sensitivity and results in a symmetrical peak-shaped voltammogram even when the current is diffusion-controlled. DPV is therefore a useful tool in standard analytical applications but the theory for kinetic convolution and coupled reactions is not as thoroughly understood as for cyclic voltammetry.

## 1.4    Bio-electrochemistry

Electrochemistry is nowadays becoming an important technique to study the properties of redox proteins. However, the first reports of reversible direct electron transfer between redox proteins and electrodes date back only to the late seventies. In many electrochemical studies on metals, metal complexes and organic compounds a mercury electrode was - and still is - used, mainly because of the ability to have a clean and reproducible electrode surface. Most of the early attempts of electrochemistry on redox proteins were therefore done with mercury electrodes. However, it soon became clear that bare metal surfaces and especially mercury cause rapid denaturation of the proteins under study. This severely hampered the development of protein electrochemistry (see [Hill, 1987] and the review of Armstrong [1990] and references cited therein). The break-through came with the discovery of Eddowes and Hill [1977] that at solid electrodes this denaturation could be prevented and the electron transfer enhanced by special additives. They obtained stable and reversible electron transfer between a gold electrode and horse heart cytochrome *c* when the protein was protected from the metal surface by adding 4,4'-dipyridyl. At the same time, Yeh and Kuwana reported on the reversible electrochemistry of cytochrome *c* on a tin oxide electrode.

In the following years a systematic search was done for suitable electrode materials and additives. A number of bifunctional organic compounds were found to stabilize the electrochemical response of cytochrome *c* at a gold electrode [Allen *et al.*, 1984; Frew & Hill, 1988]. Because these compounds enhance the electron transfer but do not take part in the redox reaction itself, the term "promoter" was introduced. Hill and coworkers explained the action of these "XY" promoters by a combination of a group X having a high affinity for the gold surface (*e.g.* thiols or phosphines) and an anionic or weakly basic group Y interacting with the protein. Unpromoted electrochemistry of cytochrome *c* was found to be possible at carbon surfaces. Hill and coworkers [Armstrong *et al.*, 1987] found that a high oxide density on the electrode enhanced the response. Especially the polished edge-plane graphite electrode surface has a large number of negatively charged C-O functionalities, giving favourable electrostatic interactions with the positively charged protein. Hagen [1989] showed that direct, unpromoted electrochemistry of several proteins is possible at a bare glassy carbon electrode. Pretreatment of this electrode by immersion in concentrated nitric acid creates a surface with a large number of quinones, alcohols, ketones and carboxylates. Positively charged cytochromes gave an immediate and reversible diffusion-controlled response at this functionalized electrode. However, the negatively charged proteins (rubredoxin and ferredoxin from *M. elsdenii*) slowly adsorbed onto the electrode and required several hours of scanning to optimize the response. Armstrong, Hill and coworkers found that the electrochemical response of negatively charged redox proteins like flavodoxins or [4Fe-4S] ferredoxins at the edge-plane pyrolytic graphite electrode is enhanced by multivalent cations. Metal ions, complexes like chromium hexamine, positively charged molecules like the aminoglycoside

neomycin, poly-L-lysin or spermine were found to be effective promoters. It is believed that these compounds suppress the Coulombic repulsion. However, further experiments showed that not all combinations of promoter and protein are successful. This indicates that other interactions also play an important role [Armstrong *et al.*, 1987, 1988a; Datta *et al.*, 1992].

In the classical three electrode setup and with semi-infinite diffusion a bulk solution of about 1 ml and a protein concentration of 100 µM is required. However, the supply of proteins is often limiting. Thus, for protein electrochemistry to become practical, the amount of material required needed to be minimized. Hagen [1989] designed an electrochemical cell for microscale electrochemistry of redox proteins with a dismountable inverted disk electrode (Figure 1.5). In this setup the volume of the droplet can be reduced to less than 20 µl with full retention of semi-infinite diffusion down to a scan rate of 1 mV/s. A different approach is to accumulate the protein on the surface of the electrode. This strategy is followed by Armstrong, taking advantage of the observation that a number of proteins often adsorb spontaneously at edge-plane pyrolytic graphite in the presence of suitable coadsorbates like neomycin or polymyxin [Armstrong *et al.*, 1993].
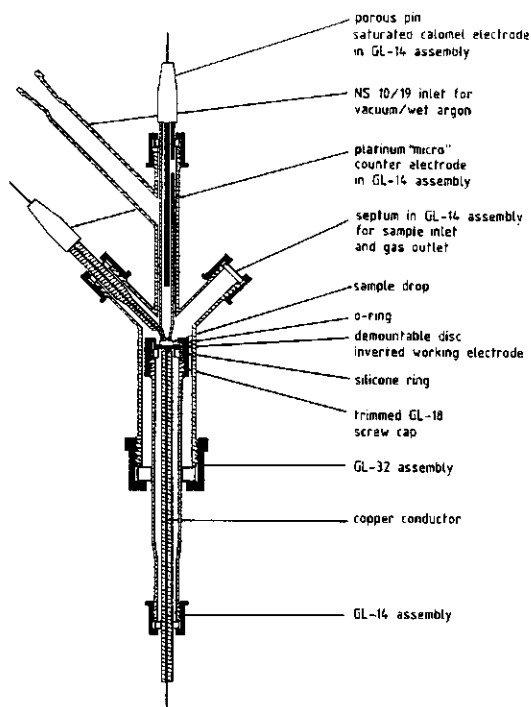


**Figure 1.5.** Electrochemical cell designed by Hagen [1989] for electrochemistry with small sample volumes.

## 1.5 Spectroscopy

Electrochemical measurements can give both equilibrium redox potentials and detailed information about the kinetics of the redox reactions because of the ability to adjust the time scale of the experiment over a wide range. However, electrochemical methods differ fundamentally from spectroscopic methods because, by nature, electrochemistry always involves heterogeneous electron transfer reactions. The interaction of the protein with the electrode surface and with the promoter might alter its properties. The electrode surface can induce changes in the conformation of the protein, and charged groups at the electrode surface and the charged promoter might influence the redox potential of the cofactor. Voltammetric measurements yield a net current as a function of the potential. When one reversible response is observed the interpretation is usually uncomplicated and the midpoint potential is usually equal to the redox potential of the couple in solution. However, the interpretation of the electrochemical response can become difficult when adsorption of protein or the cofactors onto the electrode occurs or when the electron transfer is coupled to homogeneous reactions (*i.e.* preceding or following reactions in solution). It is therefore important to confirm the observed redox potentials and the mechanisms of the coupled reactions deduced from the measured current by spectroscopy.

Redox potentials can be measured by equilibrium redox titrations. A solution of oxidized or reduced sample is titrated by adding small volumes of a reductant or oxidant solution. The potential of the solution is usually measured by a platinum wire with respect to a reference electrode. Alternatively, the electrodes can be used to control the potential of the solution by connecting them to a potentiostat (potentiometric titration). Usually the protein solution also contains a series of "mediators". These small organic molecules (often called redox dyes) are necessary to stabilize the potential of the solution (analogous to buffers in proton-titrations), to establish equilibrium between the solution and the electrode, and to mediate the electron transfer between the reductant or oxidant and the protein (or between the protein and the electrode in the potentiometric titration) [Dutton, 1978]. A characteristic spectral difference between the oxidized and the reduced species can be used to measure their concentrations. A plot of the relative concentration of either the oxidized or the reduced form against the equilibrium potential of the solution results in a Nernst-curve (see *e.g.* Figure 1.6). The redox potential and number of transferred electrons can be determined by a fit of the measured data to equation (1.3).

A useful spectroscopic technique to monitor the oxidation state of the cofactor in redox proteins is Electron Paramagnetic Resonance (EPR) spectroscopy. This technique measures the interaction between paramagnets and an applied magnetic field. In the classical description an electron in vacuo spins around its axis and this moving electric field causes a magnetic moment. In an external magnetic field this paramagnet can align parallel or anti-parallel to the applied field. The energy difference between these states is proportional to the

field strength and electromagnetic radiation can excite the electron from the low to the high energy level. For electrons in molecules the energy difference is influenced by the chemical environment and by the symmetry of the system. This makes EPR spectroscopy a powerful technique to study redox centers such as paramagnetic iron-sulfur clusters, heme-iron and organic radicals like flavin semiquinones. The spectra of these cofactors are often very characteristic and depend strongly on the oxidation state (for a detailed review of EPR on metalloproteins, see [Hagen, 1992]). For example, the 3+ and the 1+ states of the [4Fe-4S] cluster are paramagnetic while the 2+ state is diamagnetic. Thus, EPR-spectra can be observed for reduced ferredoxins and for oxidized HiPIPs. In flavodoxins only the semiquinone state is observed with EPR spectroscopy. An EPR-monitored redox titration can be performed by transferring samples of the solution to EPR-tubes and freezing these in liquid nitrogen [Dutton, 1978; Pierik & Hagen, 1991].

Many redox proteins absorb light in the visible range and have UV/VIS spectra that depend on the oxidation state of the cofactor(s). For example, the flavoquinone in flavodoxin has a yellow colour, the semiquinone has a blue colour and the fully reduced form is colourless. This makes it possible to perform an optically monitored redox titration. However, the use of mediators is restricted because these compounds are usually strongly coloured. An alternative method is the spectrophotometric xanthine/xanthine oxidase titration described by Massey [1990]. The low potential of the xanthine/ureate couple (−350 mV at pH 7) is used together with the ability of xanthine oxidase to transfer the electrons to viologens. A solution of the sample, xanthine, methyl- or benzylviologen and a second redox dye with a potential within 30 mV of the unknown is prepared in a closed anaerobic cuvette. The reduction is started by the addition of xanthine oxidase and spectra are recorded over a period of 1 to 2 hours. The amount of xanthine oxidase must be low to ensure quasi-equilibrium conditions. The potential of the solution is calculated from the spectrum of the redox dye. The main disadvantage of this method is the need for a redox dye with a spectrum that does not interfere with the spectrum of the sample and with a potential close to unknown. This also implies that this "unknown" potential must be estimated.

Redox titrations usually require the presence of mediators to ensure equilibrium between the redox species or between the electrode and the solution. However, a general problem is that many of these redox dyes bind to proteins [Surerus et al., 1994]. This interaction might alter the redox properties of the protein. Disadvantage of EPR-monitored titrations are the need to measure frozen samples and the relatively large amount of protein required. The requirement of equilibrium conditions implies that the potential range is limited by the redox potentials of oxygen and hydrogen. In principle this also applies to voltammetric experiments, but often the reduction and oxidation of water at the electrode surface is very slow and require large overpotentials. For example, carbon electrodes have a high overpotential for the evolution of hydrogen and can be used down to at least −1 Volt [Armstrong et al., 1988b].

Spectroscopic and electrochemical methods both have their eminent advantages and specific problems when applied to study the redox properties of proteins. In many aspects the two fields are complementary to one another and the examples of techniques given above state the usefulness of independent electrochemical and spectroscopic investigations. It is however also possible to integrate voltammetry and spectroscopy in a single spectroelectrochemical experiment. Simultaneous measurement of spectroscopic properties and current as a function of the applied potential promises to offer both the kinetic resolution and control of the redox states by electrochemistry and the molecular specificity and ability to probe the properties of the redox centers by spectroscopy. There are examples in the literature of direct, unmediated spectroelectrochemistry on redox proteins using optically tranparant electrodes like tin oxide, gold mesh or platinum mesh (*e.g.* [Durliat & Comtat, 1982, 1984; Bowden *et al.*, 1982]). However, carbon electrodes have not been applied in unmediated protein spectroelectrochemistry (see Chapter 5).

## 1.6    Aim and outline of this thesis

Direct electron transfer between redox enzymes and solid electrodes can be used to determine redox potentials and to obtain information about the electron transfer kinetics. Moreover, it promises to be a valuable tool to elucidate the interaction between the redox centers within the protein and to measure the catalytic properties of the enzyme (see *e.g.* [Sucheta *et al.*, 1992,1993]). Practical applications are the construction of biosensors and the bio-electrosynthesis of valuable chemicals. For these applications direct communication between the protein and the electrode is not a prerequisite. However, although small organic mediators or conducting polymers can be used to "wire" the enzyme to the electrode [Elmgren, 1993; Bartlett & Cooper, 1993; Heller, 1992, Wring & Hart, 1992], the use of these mediators can cause toxicity and bio-compatibility problems for *in vivo* measurements with biosensors or for the recovery of the products of bio-electrosynthesis. Since many small electron transferring proteins are capable of direct electron transfer at solid electrodes, these proteins might be used as biological mediators. For example, cytochromes can be used to shuttle electrons between the electrode and hydrogenase [Verhagen *et al.*, 1994]. From the electrochemical studies on small electron transferring proteins some understanding has been obtained about the relation between the properties of the protein, the electrode surfaces, and promoters. However, there is still a great deal of "trial-and-error" involved for each new system under study to give a stable and reversible electrochemical response. In particular the direct unmediated electrochemistry of enzymes is not straightforward. This was shown by electrochemical studies in our laboratory on lipoamide dehydrogenase, cytochrome P-450 and superoxide dismutase [Verhagen, 1995].
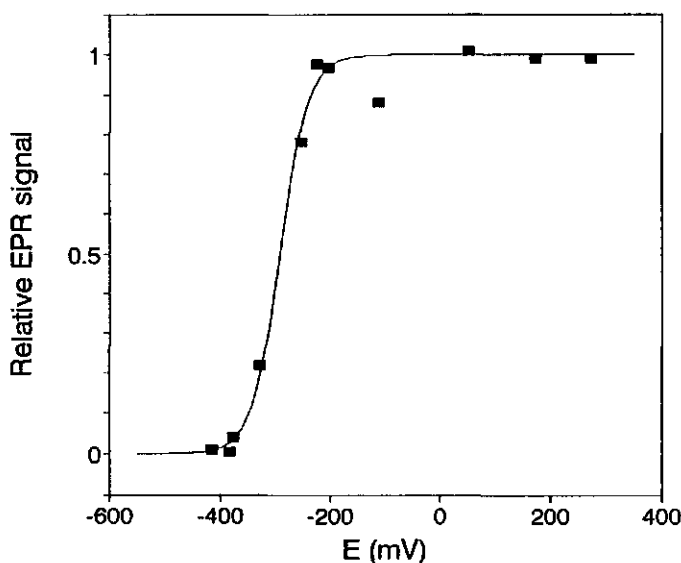
**Figure 1.6.** EPR-monitored redox titration with sodium dithionite of a solution of 46 µM Assimilatory Sulfite Reductase from *D. vulgaris* (H) and a series of 13 mediators (32 µM each) in 50 mM Hepes buffer, pH 7.5 and 50 mM NaCl. The EPR-spectra were recorded on a Bruker 200D EPR spectrometer at a microwave frequency of 9.32 GHz, microwave power of 100 µW, modulation frequency of 100 kHz, modualtion amplitude of 3.2 mT, and at a temperature of 22 K. The relative intensity of the combined $g=2.43/g=2.36$ signal is corrected for dilution. The potentials were measured using a platinum electrode with respect to a saturated calomel electrode and recalculated to the standard hydrogen electrode ($E_{SCE}$=246 mV at 22°C).

One of the problems might be that redox enzymes are larger than most electron transferring proteins. Direct electron transfer between the electrode and the active site can be inhibited by an insulating peptide matrix. Therefore, in view of its low molecular mass (23.5 kDa) the small assimilatory sulfite reductase (ASR) from the sulfite reducing bacterium *Desulfovibrio vulgaris* (Hildenborough) promised to be more readily accessible by electrochemistry. This enzyme catalyses the six-electron reduction of $SO_3^{2-}$ to $S^{2-}$ and contains an iron-sulfur cluster and a low-spin siroheme with EPR lines at $g=2.43$, $g=2.36$, and $g=1.77$. Iron/sulfur analysis, EPR and Mössbauer spectroscopy, and $^{35}S^{2-}$ exchange suggest that the siroheme iron is coupled to a [4Fe-4S] cluster by a bridging $S^{2-}$ [Tan & Cowan, 1991; Huyn *et al.*, 1984; Janick *et al.*, 1983]. An EPR-monitored redox titration with dithionite in the presence of mediators showed that over the whole potential range from +300 to –410 mV no EPR-spectrum was visible for the iron-sulfur cluster, suggesting that the [4Fe-4S] cluster is in the 2+ state with potentials above +350 mV and below –450 mV. Contrarily, the siroheme iron could be reduced reversibly (slow reoxidation with air was possible). The

data points follow a one-electron curve with a midpoint potential of −292 mV at pH 7.5 (Figure 1.6). This potential is similar to the siroheme potential in dissimilatory sulfite reductase from the same bacterium determined by EPR-titration [Pierik & Hagen, 1991].

Direct, unpromoted electrochemistry of ASR did not give any response. This was expected because the negative charge of the protein (p$I$=5.1) and of the glassy carbon electrode predict that a positively charged promoter is required to obtain an electrochemical response. A wide range of "hard" to "soft" positively charged promoters were tried (from magnesium, calcium and rare earth metal ions, to spermine, aminoglycosides like neomycin, and poly-L-lysine) as well as different electrode pretreatments or the addition of the positively charged surfactant dodecyltrimetylammonium bromide. The effect of sulfide and/or sulfiet ions as substrate was also tested. However, non of these combinations resulted in any response. This indicates that the predictive value of the "XY"-hypothesis and of the supposed shielding of Coulombic repulsion is not universal. Recently however, Lui and Cowan [1994] published the square wave voltammetry of the sulfite reductases from *D. vulgaris* (H) at an edge-plane pyrolytic graphite electrode, promoted by $Cr(NH_3)_6^{3+}$. The reported ASR potentials at pH 7.5 of −21 mV, assigned to the siroheme and −303 mV, assigned to the Fe/S cluster differ significantly from our EPR-titration. Square wave voltammetry is a fast-perturbation technique, and the authors used a perturbation of 50 mV at a frequency of 140 Hz. Therefore, it remains to be seen if the square wave potentials reflect the equilibrium values in solution.

It was concluded from the ASR experiments that our understanding of the interactions between proteins and electrodes was not detailed enough to be applied to enzymes. The goal of the project was therefore to obtain more detailed insight in interactions between redox proteins and solid electrodes and the mechanisms of electron transfer. In addition to this, the influence of the protein environment on the redox properties of the active site and the possible influence of the electrode/promoter system on these properties are considered. Electron transferring proteins are used as model systems for redox enzymes. The FMN containing flavodoxins are used as model systems for flavin enzymes such as glucose oxidase. A series of high potential iron-sulfur proteins (HiPIPs) can be regarded as models for proteins containing [4Fe-4S] clusters. The HiPIPs are also of interest because of the high oxidation state of the cluster; the sequences are known and also the three-dimensional structures of some HiPIPs are known.

The electrochemistry of flavodoxins is reported in Chapters 2 and 3. In Chapter 2 the electron transfer between *Desulfovibrio vulgaris* (Hildenborough) flavodoxin and the glassy carbon electrode is studied. A mechanism for the processes at the electrode and in bulk solution is presented. In Chapter 3 the redox properties of wild-type and mutant flavodoxin II from *Azotobacter vinelandii* are compared both by electrochemistry and by EPR spectroscopy. These studies suggest that electron transfer to the FMN cofactor is severely

hampered when these flavins are buried inside wild-type dimers. The electrochemically measured midpoint potentials are the same as the reduction potentials measured by titration in bulk solution. The theory and application of spectroelectrochemistry on redox proteins is reported in Chapters 4 and 5. In Chapter 4 the theory of a long optical path length thin layer electrochemical cell (LOPTLC) is described. In Chapter 5 the usefulness of a glassy carbon LOPTLC is tested for the study of redox proteins. The proposed mechanism for flavodoxin electron transfer is verified by spectroelectrochemistry. In Chapter 6 and 7 the redox properties and electrochemical response of seven HiPIPs with different overall charges are studied. The electrochemical response of the HiPIPs depends on the charge and the addition of promoters and stabilizers. A correlation between protein charge, the optical spectra and the redox potentials is demonstrated. In Chapter 7 the chemical and electrochemical super-reduction of HiPIPs (*i.e.* the further reduction to the $[4Fe-4S]^{1+}$ state) is reported.

## 1.7　References

Allen, P.M., Hill, H.A.O & Walton, N.J. (1984) *J. Electroanal. Chem. 178*, 69.

Armstrong, F.A., Cox, P.A., Hill, H.A.O., Lowe, V.J. & Oliver, B.N. (1987) *J. Electroanal. Chem. 217*, 331.

Armstrong, F.A., Hill, H.A.O. & Walton, N.J. (1988a) *Acc. Chem. Res. 21*, 407.

Armstrong, F.A., George, S.J., Thomson, A.J. & Yates, M.G. (1988b) *FEBS Letters 234*, 107.

Armstrong, F.A. (1990) *Structure and Bonding 72*, 137.

Armstrong, F.A. (1992) *Advances in Inorganic Chemistry 38*, 117.

Armstrong, F.A. (1993) *Methods in Enzymology 227*, 479.

Bard, A.J. & Faulkner, L.R. (1980) *Eelectrochemical methods, Fundamentals and Applications*, Wiley, New York.

Bartlett, P.N. & Cooper, J.M. (1993) *J. Electroanal. Chem. 362*, 1.

Bowden, E.F., Hawkridge, F.M., Chlebowski, J.F., Bancroft, E.E., Thorpe, C. & Blount, H.N. (1982) *J. Am. Chem. Soc. 104*, 7641.

Carter, C.W., Kraut, J., Freer, S.T., Alden, R.A., Sieker, L.C., Adam, E.T. & Jensen, L.H. (1972) *Proc. Nat. Acad. Sci. USA 69*, 3526.

Cammack, R.C. (1992) in *Advances in Inorganic Chemistry, Vol. 38: Iron-Sulfur Proteins*, (Cammack, R.C. & Sykes, A.G., Eds.), Academic Press, San Diego, California, p. 281.

Clark, W.M. (1960) *Oxidation-reduction potentials of organic systems*, Waverley Press, Baltimore.

Datta, D., Hill, H.A.O. & Nakayama, H. (1992) *J. Electroanal. Chem. 324*, 307.

Durliat, H. & Comtat, M. (1982) *Anal. Chem. 54*, 856.

Durliat, H. & Comtat, M. (1984) *Anal. Chem. 56*, 148.

Dutton, P.L. (1978) *Methods in Enzymology 54*, 411.

Eddowes, M.J. & Hill, H.A.O. (1977), *J. Chem. Soc. Chem. Comm. 1977*, 771.

Elmgren, M. (1993) *Amperometric biosensors based on enzymes wired by redox polymers, Comprehensive summaries of Uppsala Dissertations from the Faculty of Sciece 471*, Lindbergs Grafiska HB, Uppsala, Sweden.

Frew, J.E. & Hill, H.A.O. (1988) *Eur. J. Biochem. 172*, 261.

Fraústo da Silva, J.J.R. & Williams, R.J.P. (1993) *The biological chemistry of the elements: The Inorganic Chemistry of life*, Oxford University Press, Oxford.

Hagen, W.R. (1989) *Eur. J. Biochem. 182*, 523.

Hagen, W.R. (1992) in *Advances in Inorganic Chemistry, Vol. 38: Iron-Sulfur Proteins*, (Cammack, R.C. & Sykes, A.G., Eds.), Academic Press, San Diego, California, p. 165.

Heller, A. (1992) *J. Phys. Chem. 96*, 3579.

Hill, H.A.O. (1987) *Pure & Appl. Chem. 59*, 743.

Huyn, B.H., Kang, L., DerVartanian, D.V., Peck, H.D. & LeGall, J. (1984) *J. Biol. Chem. 259*, 15376.

Janick, P.A., Rueger, D.C., Krueger, R.J., Barber, M.J. & Siegel, L.M. (1983) *Biochemistry* *22*, 396.

Link, T.A., Hagen, W.R., Pierik, A.J., Assmann, C. & von Jagow, G. (1992) *Eur. J. Biochem.* *208*, 685.

Lippard, S.J. & Berg, J.M. (1994) *Principles of Bioinorganic Chemistry*, University Science Books, Mill Valley, California.

Lui, S.M. & Cowan, J.A. (1994) *J. Am. Chem. Soc. 116*, 11538.

Massey, V. (1990) in *Flavins and Flavoproteins: Proceedings of the Tenth International Symposium on Flavins and Flavoproteins*, (Curti, B., Ronchi, S. & Zanetti, G., Eds.), Walter de Gruyter & Co., Berlin, p. 59.

Müller, F. (1981) in *Topics in Current Chemistry Vol. 108* (Boschke, F.L., Ed.), Springer, Berlin, p. 71.

Müller, F. (1987) *Free Radical Biology & Medicine 3*, 215.

Nicholson, R.S. & Shain, I. (1964) *Anal. Chem. 36*, 706.

Nicholson, R.S. (1965) *Anal. Chem. 37*, 1351.

Pierik, A.J. & Hagen, W.R. (1991) *Eur. J. Biochem. 195*, 505.

Seralathan, M., Osteryoung, R.A. & Osteryoung, J.G. (1987) *J. Electroanal. Chem. 222*, 69

Southampton Electrochemistry Group (1985) *Instrumental Methods in Electrochemistry*, Ellis Horwood series in Physical Chemistry, Ellis Horwood, Chichester.

Sucheta, A., Ackrell, B.A.C., Cochran, B. & Armstrong, F.A. (1992) *Nature 356*, 361.

Sucheta, A., Cammack, R., Weiner, J. & Armstrong, F.A. (1993) *Biochemistry 32*, 5455.

Surerus, K.K., Chen, M., Van der Zwaan, J.W., Rusnak, F.M., Kolk, M., Duin, E.C., Albracht, S.P.J. & Münck, E. (1994) *Biochemistry 33*, 4980.

Tan, J. & Cowan, J.A. (1991) *Biochemistry 30*, 8910.

Verhagen, M.F.J.M., Wolbert, R.B.G. & Hagen, W.R. (1994) *Eur. J. Biochem. 221*, 821.

Verhagen, M.F.J.M. (1995) *Characterization of redox proteins using electrochemical methods, Ph.D. Thesis*, Agricultural University Wageningen, The Netherlands.

Wring, S.A. & Hart, J.P. (1992) *Analyst 117*, 1215.

Yeh, P. & Kuwana, T. (1977), *Chem. Letters 1977*, 1145.

# Chapter 2

## Complex electrochemistry of flavodoxin at carbon-based electrodes results from a combination of direct electron transfer, flavin-mediated electron transfer, and comproportionation

## 2.1 Introduction

Flavodoxins are small electron transfer proteins that contain one molecule of flavin mononucleotide (FMN) as prosthetic group. Bound to the protein, the cofactor can be reduced by two separate one-electron steps, of which the second low-potential reduction is the physiological important one [Simondsen & Tollin, 1980]. The redox potential of the first reduction (called $E_2$ according the convention of Clark [1960]) of the oxidized quinone to the one electron reduced semiquinone is generally found around −150 mV at pH 7, and exhibits a pH dependence of −59 mV/pH with no p$K$ [Sykes & Rogers, 1982; Sykes & Rogers, 1984; Entsch & Smillie, 1972; Paulsen et al., 1990; Pueyo et al., 1991; Mayhew, 1971; Deistung & Thorneley, 1986; Mayhew et al., 1969]. This is indicative for a protonation upon reduction [Clark, 1960]. The one electron reduced protein has a blue colour. This is characteristic for the neutral form of the semiquinone FMN [Müller, 1981]. The second reduction to the fully reduced hydroquinone has a pH-independent potential ($E_1$) of around −400 mV at high pH and a slope of −59 mV/pH at low pH. The observed redox-linked p$K$ for the protonation of the reduced protein generally is below 7 [Sykes & Rogers, 1982; Sykes & Rogers, 1984; Entsch & Smillie, 1972; Paulsen et al., 1990; Pueyo et al., 1991; Mayhew, 1971; Deistung & Thorneley, 1986; Mayhew et al., 1969].

Flavodoxins are found in many bacteria and in red and green algae, but not in plants or animals. All flavodoxins are strongly anionic and can be divided into two groups according to their molecular masses which are either between 14 and 17 kDa or between 20 and 23 kDa. Some flavodoxins are constitutive while others are induced by low iron concentrations to replace ferredoxin as electron carrier . The amino acid compositions and primary structures of many flavodoxins are known and of some also the three-dimensional structures are known for the different oxidation states [Simondsen & Tollin, 1980; Mayhew & Tollin, 1992; Mayhew & Ludwig, 1975].

The flavodoxin from *Desulfovibrio vulgaris* (Hildenborough) contains 148 amino acids and has a molecular mass of 15.7 kDa. It is localized in the cytoplasm [Curley & Voordouw, 1988] and is the proposed electron donor for the sulphite reduction [Hatchikian et al., 1972; Drake & Agaki, 1977; Moura et al., 1980]. The gene has been cloned and sequenced [Curley & Voordouw, 1988; Krey et al., 1988] and the structure of the three redox states have been

determined with X-ray diffraction [Watenpaugh et al., 1972; Watenpaugh et al., 1973; Watt et al., 1991]. The redox properties and chemical characteristics of the native protein have been determined by Dubourdieu et al. [1975]. By direct potentiometric titration (no mediators) with dithionite of the oxidized/semiquinone couple they found an $E_2$ of $-102$ mV at pH 7 and 25°C with a slope of $-59$ mV/pH. By measuring the equilibrium concentrations of semiquinone and fully reduced flavodoxin spectrophotometrically in the presence of hydrogenase and $H_2$ an $E_1$ of $-431$ mV was found at pH 7.0. An ionization constant of 6.6 for the fully reduced flavodoxin was determined spectrophotometrically in the presence of excess dithionite. The redox properties of the recombinant flavodoxin have been determined by Curley et al. [1991]. By measuring the concentrations of flavodoxin semiquinone and of the oxidized form of a reference dye spectrophotometrically after photoreduction and by potentiometric titration using electrolytic reduction in the presence of redox mediators the $E_2$ was determined to be $-143$ mV at pH 7 with a slope of $-59$ mV/pH. The $E_1$ was determined by measuring the concentration semiquinone during reduction with $H_2$/hydrogenase and also by potentiometric titration using electrolytic reduction in the presence of redox mediators. An $E_1$ of $-440$ mV at pH 7 was found with a p$K$ of 6.8.

Direct electrochemistry of redox proteins at solid electrodes has become feasible over the last two decennia [Eddowes & Hill, 1977; Osteryoung, 1988; Hagen, 1989; Guo et al., 1989; Armstrong, 1990; Armstrong et al., 1993; Hill & Hunt, 1993]. Many low molecular mass proteins such as azurines, cytochromes, ferredoxins and flavodoxins give well-defined and reversible electron transfer without mediators. Most of these proteins in vivo act as electron donor or acceptor for redox enzymes. Direct electrochemistry on larger redox enzymes often gives voltammograms that are not easily explained. Most of these proteins exhibit very slow electron transfer or do not react at all. The smaller electron carrier proteins may serve as models for these larger proteins or may be used as biochemical mediators. This coupled electron transfer can be used to study electron transfer chains or can be applied to construct biosensors without synthetic mediators or as an alternative for the polymer or immobilized mediators used in bioelectrosynthesis. Because flavodoxin is proposed electron donor for the sulphite reductases in D.vulgaris it may be applied as mediator to construct a sulphite biosensor. It can also be considered a model for the flavin enzyme glucose oxidase (GOD), the most frequently used enzyme in studies on biosensors.

Direct electrochemistry of flavodoxins has been reported by several groups. Van Dijk et al. [1982] reported on differential and normal pulse polarography of Megasphaera elsdenii flavodoxin adsorbed onto the mercury electrode. In the presence of poly-L-lysine at pH 7.4 both the quinone/semiquinone and the semiquinone/hydroquinone couples were found at $-114$ and $-392$ mV, respectively. At the pyrolytic graphite electrode, Armstrong and coworkers [1984] only found the semiquinone/hydroquinone couple of M. elsdenii flavodoxin. With square wave voltammetry and in the presence of $MgCl_2$ or $Cr(NH_3)_6^{3+}$ a potential of $-318$

mV was found at pH 5.0. Bianco *et al.* [1988] studied the flavodoxin from *Desulfovibrio vulgaris* (strain Hildenborough) at the pyrolytic graphite electrode with differential pulse voltammetry and cyclic voltammetry. After addition of 15 μM poly-L-lysine the semiquinone/hydroquinone couple was observed. The midpoint potential (−430 mV at pH 7.6) was essentially independent of pH in the range 6-7.6. Hill and coworkers [Barker *et al.*, 1988; Bagby *et al.*, 1991] investigated the flavodoxins isolated from *Azotobacter choococcum* using cyclic voltammetry at a polished edge-plane graphite electrode in the presence of the cationic aminoglycoside neomycin. The semiquinone/hydroquinone potentials of two distinct flavodoxins were found (−305 mV and −520 mV at pH 7.4).

The absence of the quinone/semiquinone response has never been explained and the semiquinone/hydroquinone response has never been characterized in detail. In this chapter the electrochemical response of *D. vulgaris* (Hildenborough) flavodoxin at the glassy carbon electrode is characterized. Numerical analysis shows that the time-dependent response of the semiquinone/hydroquinone couple and the absence of the first redox couple can be explained by a combination of FMN-mediated electron transfer, comproportionation and direct electron transfer.

## 2.2   Experimental procedures

### 2.2.1   Flavodoxin

Flavodoxin from *Desulfovibrio vulgaris*, strain Hildenborough, was purified as described by Le Gall and coworkers [Le Gall & Hatchikian, 1967; Dubourdieu & Le Gall, 1970]. The final ratio $A^{277}/A^{380}$ was 5.4 and the ratio $A^{277}/A^{461}$ was 4.3 (in 10 mM potassium phosphate buffer, pH 7.0). The isoelectric point was 3.6 (determined with a Servalyt Precote 3-11 gel from Serva on a flat-bed Untrophor Unit from Pharmacia).

### 2.2.2   EPR-monitored redox titration

A deaerated, argon-fluxed solution was prepared containing 15 μM of flavodoxin and the redox mediator dyes (15 μM each) phenazine ethosulfate, methylene blue, resorufin, indigo carmine, 2-hydroxy-1,4-naphthoquinone, anthraquinone-2-sulfonate, phenosafranine, safranine O and neutral red in 50 mM Mops/NaOH buffer, pH 7.0. All mediator dyes are two electron acceptors to avoid formation of radicals with EPR spectra interfering with the FMN semiquinone spectrum. The reductant was sodium dithionite, dissolved in a deaerated and argon-flushed 500 mM Mops/NaOH buffer of pH 7.0. The reductive titration was carried out

at $22\pm1°C$ in an anaerobic cell under a constant flow of purified wet argon [Massey & Hemmerich, 1978]. The potential of the solution was measured at a platinum electrode (Radiometer P-1312) with respect to the potential of a saturated calomel electrode (Radiometer K-401) using a Fluka 8022-A multimeter (Fluka, Tilburg, NL). The potentials have been recalculated with respect to the normal hydrogen electrode (NHE) using the potential of −246 mV (NHE) of the saturated calomel electrode (SCE). After each addition of dithionite the solution was stirred until a stable potential (over a period of 1 minute) was obtained. A sample was transferred to an anaerobic EPR-tube connected to a scrubbed argon/vacuum manifold, and was frozen in liquid nitrogen. The relative concentration of the flavodoxin semiquinone in each sample was determined from the intensity of the radical signal and corrected for dilution. The EPR spectra were taken on a Bruker ESR 200 D spectrometer with a microwave frequency of 9.31 GHz and power of 50 µW, a modulation frequency of 100 kHz and a modulation amplitude of 1.25 mT. A temperature of 103 K was maintained by a flow of nitrogen trough a home-built cryostat.

### 2.2.3  Electrochemistry

In the classical three electrode setup and with semi-infinite diffusion a bulk solution of about 1 ml and a protein concentration of 100 µM is required. Instead, an electrochemical cell for microscale electrochemistry of redox proteins with a dismountable inverted disk electrode was used here. A droplet of solution is held between the horizontal working electrode and the flat tip of the reference electrode (a Radiometer K-401 saturated calomel electrode with a porous pin). In this setup the volume of the droplet can be reduced to less than 20 µl with full retention of semi-infinite diffusion down to a scan rate of 1 mV/s [Hagen, 1989].

The working electrode was a glassy carbon disc of 15 mm diameter and 2 mm height (type V25, obtained from Le Carbon Loraine, Rotterdam, NL). Prior to each electrochemical measurement the disc was polished firmly on Microcloth polishing cloth with 6-µm Metadi Diamond Compound spray (both from Buehler, USA), rinsed thoroughly with water and dried. To activate the electrode the lower part was exposed for 30 seconds to a methane flame from a Bunsen-burner. The polished working surface was never in direct contact with the flame and if any inhomogeneity was detected on the surface, the polishing and glowing was repeated. A reproducibly oxidized and clean carbon surface was obtained with this procedure. The counter electrode was a Radiometer P-1312 micro platinum electrode. The electrodes were connected to an Autolab 10 potentiostat (Eco Chemie, Utrecht, NL) controlled by the Eco Chemie GPES software (version 2.0) on a personal computer. After mounting the electrodes the cell was flushed with purified wet argon [Massey & Hemmerich, 1978]. A deaerated, argon-flushed sample was then transferred with a gas-tight Hamilton syringe to the tip of the

reference electrode and the working electrode holder was pushed up until the shape of the droplet was approximately cylindrical. The working area of the glassy carbon electrode was between 15 and 25 mm$^2$ with a diameter of the calomel electrode tip of 4 mm, or 5 to 15 mm$^2$ when a calomel electrode with a trimmed tip was used.

Staircase cyclic voltammetry (SCV) was done with steps of 1.22, 2.44 or 3.66 mV. The cycling was started after equilibration for 1 to 3 minutes at the starting potential. Differential pulse voltammetry (DPV) was done in both directions after 60 s. equilibration at the starting potential with steps of 2.44 mV and 250 ms, modulated by pulses of 20 mV and 100 ms. The experiments were performed at a temperature of $22 \pm 1$ °C and the potentials have been recalculated with respect to the normal hydrogen electrode (NHE) using the potential of $-246$ mV (NHE) of the saturated calomel electrode (SCE).

The dependence of the potential on pH was measured with SCV and with DPV. Each point in the curve was measured on a fresh 5 µl droplet (working surface area 5 to 10 mm$^2$ with a trimmed calomel electrode) containing 0.11 mM flavodoxin and 3.3 mM neomycin B (Sigma) in a buffer of 20 mM citrate, 20 mM bistrispropane and 20 mM Caps, titrated with HCl or NaOH and adjusted with NaCl to a constant ionic strength $I=0.2$ (as calculated from the theoretical ionic composition of the buffers at given pH).

Temperature dependent cyclic staircase voltammograms were obtained by submerging the electrochemical cell in a thermostated waterbath. The dependence of the calomel electrode on temperature ($t$ in °C) was calculated from [Bard & Faulkner, 1980]:

$$E_{SCE} = 244.4 - 0.661\ (t\text{-}25) - 1.75 \cdot 10^{-3}\ (t\text{-}25)^2 - 9.00 \cdot 10^{-7}\ (t\text{-}25)^3\ \ \text{mV} \qquad (2.1)$$

## 2.3  Results and discussion

### 2.3.1  Redox titration

In Figure 2.1 the formation of the semiquinone radical upon reduction of oxidized flavodoxin with dithionite is shown as measured with EPR spectroscopy. The data is fitted to a Nernst curve with $n=1$ and free 100% level. The resulting midpoint potential is $-113$ mV (NHE). This value is comparable to the potentials (at pH 7.0) of $-102$ mV reported by Dubourdieu et al. and $-143$ mV reported by Curley et al. The second reduction could not be determined because the potential is outside the range of the available two-electron mediators. The semiquinone spectrum could be titrated to zero with excess dithionite but no stable reading of the potential could be obtained at low potential because the lowest potential is that of neutral red at $-340$ mV.
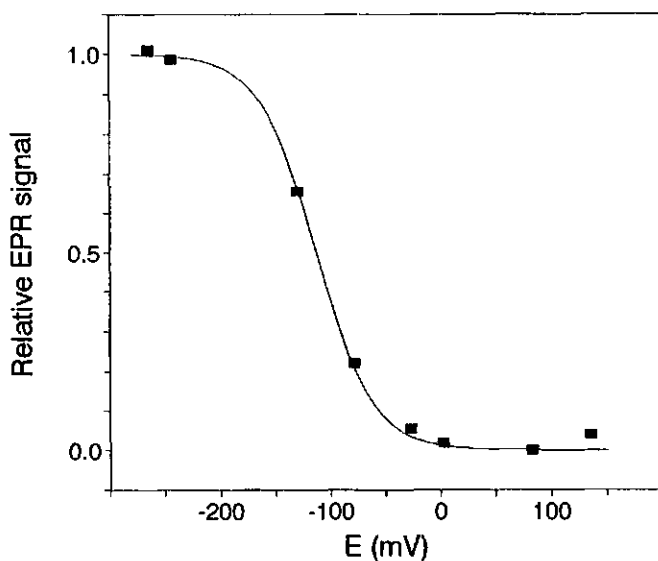
**Figure 2.1.** EPR-monitored titration of the first reduction potential of *D. vulgaris* flavodoxin. The semiquinone radical signal was corrected for dilution and fitted to a one-electron Nernst curve with free 100% level.

### 2.3.2 Electrochemistry

Staircase cyclic voltammetry (Figure 2.2) on a 6 µl droplet containing 0.14 mM fully oxidized flavodoxin in 17 mM potassium phosphate buffer at pH 7.0 results in a voltammogram with only one redox couple around −215 mV (NHE). This is close to the reported potential of FMN [Müller, 1981; Anderson, 1983]. When 0.5 µl of a 50 mM solution of neomycin is added, one additional response is observed around −410 mV, but no reduction or oxidation current was observed around the midpoint potential of −113 mV for the quinone/semiquinone couple. Dithionite reduction experiments of Dubourdieu *et al.* [1975] showed that the rate of reduction of *D. vulgaris* flavodoxin quinone is much lower than the reduction rate of the semiquinone. The re-oxidation with oxygen of the hydroquinone also is much faster than the re-oxidation of the semiquinone. Apparently, this is also true for the electron transfer at the glassy carbon electrode. Recently, Peelen and Vervoort [1994] concluded from two-dimensional NMR studies that the conformation of the isoalloxazine binding region in *D. vulgaris* flavodoxin changes when going from the oxidized to the semiquinone state. No changes were observed when going from the semiquinone to fully reduced state. This might offer an explanation for the observed difference in reduction rates and the resulting absence of the quinone/semiquinone couple in the voltammogram.
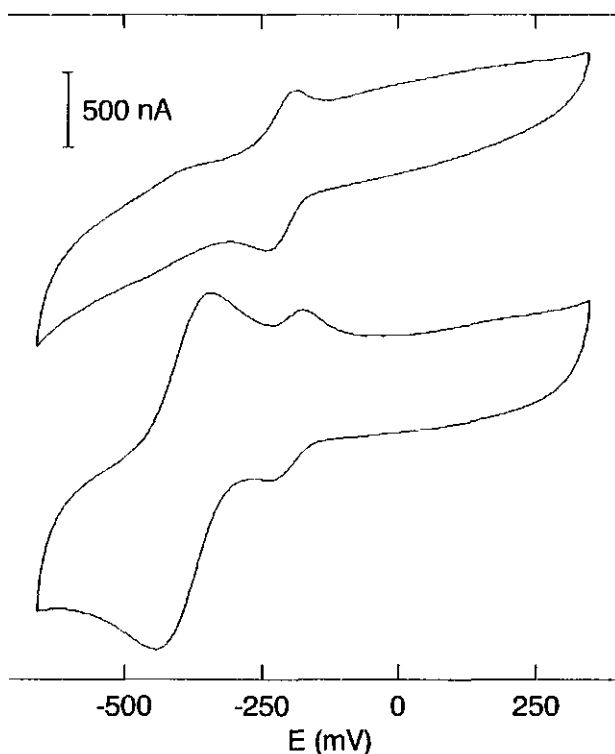
**Figure 2.2.** The effect of neomycin on the cyclic voltammogram of flavodoxin. Staircase cyclic voltammogram with a potential step of 2.44 mV and a scan rate of 20 mV/s on a 6 µl droplet (working surface area 0.2 cm$^2$) containing 2.25 mg/ml (0.14 mM) fully oxidized flavodoxin in 17 mM potassium phosphate buffer at pH 7.0 before and after addition of 0.5 µl 50 mM neomycin.3H$_2$SO$_4$ (titrated with NaOH to pH 7).

The multiple cationic aminoglycoside neomycin is believed to overcome the electrostatic repulsion between the highly negatively charged protein (isoelectric point of 3.6) and the electrode surface that is also negatively charged due to oxidation of the carbon [Armstrong *et al.*, 1988]. Neomycin does not exhibit redox activity in the applied potential range. Other aminoglycosides like kanamycin and gentamycin, positive ions like CaCl$_2$ or organic amines like spermine H$_2$N-(CH$_2$)$_4$-NH-(CH$_2$)$_3$-NH$_2$ are also effective promoters for flavodoxin. Another type of promoter is the cationic surfactant dimethyldidodecyl ammonium chloride. In combination with a glassy carbon electrode, thoroughly polished with aluminiumoxide to obtain an apolar surface (high contact angle with water), this ammonium surfactant is also an effective promoter. The flavodoxin response is however not stable due to denaturation of the protein in the presence of the surfactant. Positively charged proteins like cytochromes show direct, unpromoted electrochemistry at the glassy carbon electrode [Hagen,
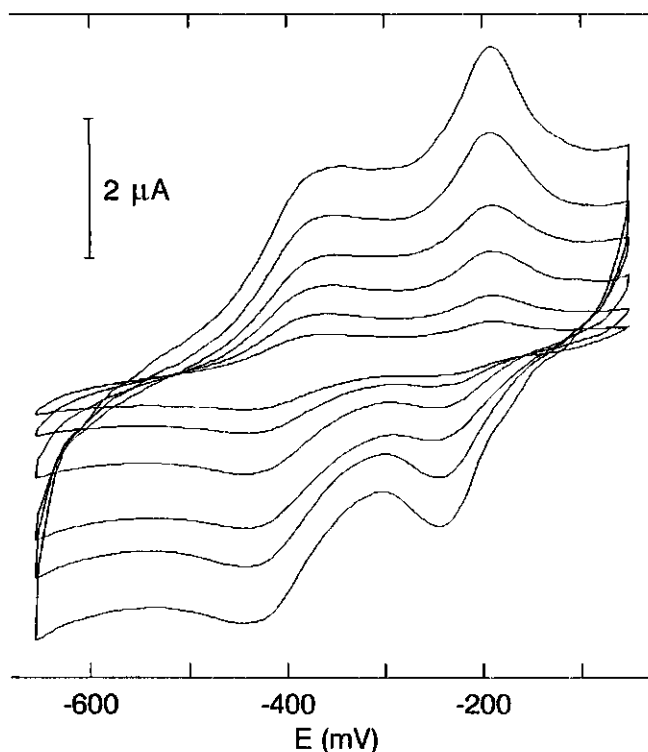
**Figure 2.3.** Flavodoxin voltammograms at scan rates of 5, 10, 20, 30, 50 and 70 mV/s. A 6.5 μl droplet was used (working surface area 15 mm$^2$) containing 0.13 mM flavodoxin and 3.8 mM neomycin in 14 mM potassium phosphate buffer at pH 7.0. The voltammograms were recorded using SCV with a potential step $\Delta E$=2.44 mV.

1989]. Armstrong, Hill and coworkers [Armstrong *et al.*, 1987; 1988] showed that many multiple cations and positively charged complexes are effective promoters for ferredoxin at a graphite electrode. These observations indicate that the general function of a promoter is to form a 'bridge' between the protein surface and the electrode surface. Ionic interactions seem to be dominant, but Van der Waals forces and hydrophobic interactions can become important when the ionic charges are low, compensated by counter ions or screened by a compact double-layer (high salt concentration). The polarity and number of negatively charged sites of the carbon surface can be modified by the degree of polishing and oxdative pretreatment. This allows for a flexible application of promoters.

The scan-rate dependence of the two couples (Figures 2.3 and 2.4) was measured using a 6.5 μl droplet containing 0.13 mM flavodoxin and 3.8 mM neomycin in 14 mM potassium phosphate buffer at pH 7.0. The peak currents of the FMN couple are proportional to the scan
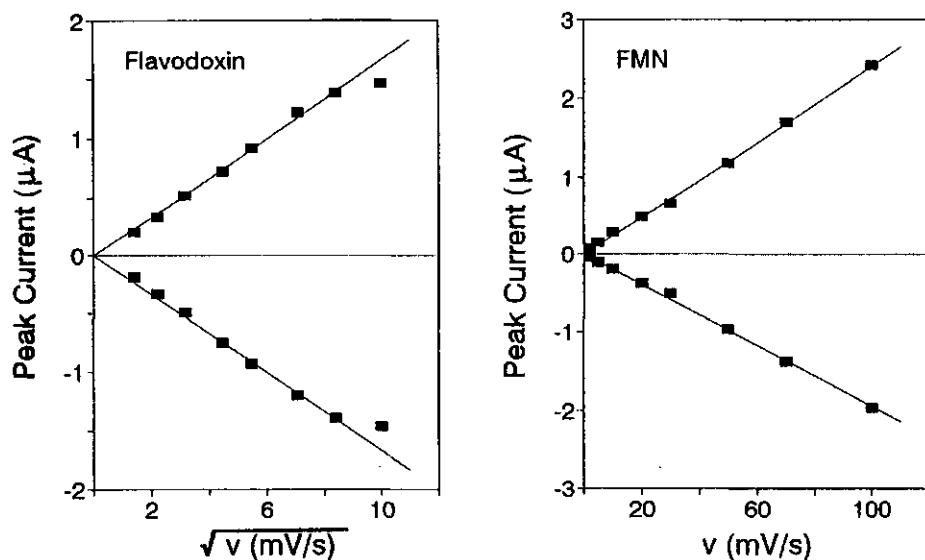
**Figure 2.4.** Scan rate dependence of the peak currents (see Figure 2.3): Flavodoxin peak currents *versus* the square root of the scan rate and FMN peak currents *versus* the scan rate.

rate. This is indicative for the adsorbed nature of the FMN, with a surface concentration of $3.3 \cdot 10^{-7}$ mol/m$^2$ or about 10% occupation assuming an electrode surface area of 15 mm$^2$ and using an area of 51 Å$^2$ per FMN molecule [Müller & Friedrich, 1977]. The peak currents of the low potential flavodoxin couple are proportional to the square root of the scan rate. Assuming a concentration gradient near the electrode that resembles a 100% semiquinone bulk solution (see below) a diffusion constant of $9 \cdot 10^{-11}$ m$^2$/s is calculated. The peak-to-peak separation is 58±2 mV and is independent of the scan rate. This indicates that this response is a reversible one-electron transition. This was also confirmed by the peak widths of the differential pulse voltammograms and of the semi-derivatives of the cyclic voltammograms.

At low scan rates the development of the peak currents of the low potential flavodoxin couple is completed within the first two scans. At faster scan rates the height of the peaks increase with time. This is shown in Figure 2.5 for repetitive cycling with a scan rate of 100 mV/s between –0.2 and –1.0 V SCE and after 5 minutes equilibration at –0.2 V (SCE). For the flavodoxin couple the stationary state is reached after 16 cycles (4 min.). The maximum current is close to the expected current of 2.2 µA (with $A=25$ mm$^2$ and $D=1 \cdot 10^{-10}$ m$^2$/s). The FMN peaks continue to grow with time at a slow rate of about 9 nA per scan or $2.5 \cdot 10^{-14}$ mol adsorption per scan. Because the flavodoxin preparation does not contain excess free FMN initially the protein is slowly loosing its cofactor. However, the observed rate for the decrease of the flavodoxin response after scan number 16 of about 6 nA/scan is equivalent
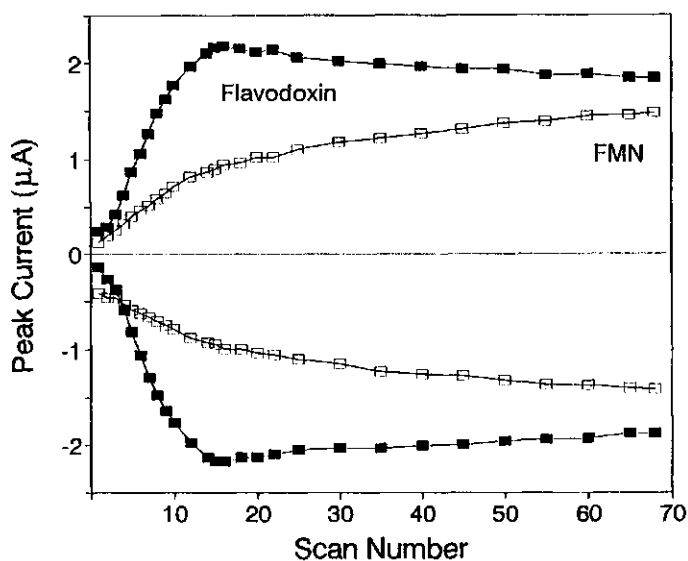
**Figure 2.5.** Development of the flavodoxin and FMN peak currents with time. Repetitive cycling was performed between −0.2 and −1.0 V SCE ($\Delta E$=3.66 mV) with a scan rate of 100 mV/s. A droplet of 15 µl (working surface area 25 mm$^2$) was used containing 0.10 mM flavodoxin in 60 mM potassium phosphate buffer at pH 7.0 and 3.3 mM neomycin. Before starting the cycling the potential was held at −0.2 V SCE for 5 minutes.

to 4 picomoles per scan, much more than the observed rate of FMN adsorption. The total decrease of the flavodoxin response (15% after 70 scans) is also much higher than expected from the amount of adsorbed FMN because only 5% of the protein will be inactivated to supply one full monolayer of adsorbed FMN. This implies that either the concentration of free FMN in solution increases or the available electrode surface for electron transfer to flavodoxin decreases. In the former case the increase of the FMN peaks due to diffusion-controlled current would be about 50 nA per scan. This is much more than observed and also the FMN response is fully proportional to the scan rate, indicating that almost no FMN is present in solution. Therefore, the decreasing flavodoxin response is not caused by denaturation in solution but by partial blocking of the electrode surface by a small amount of denatured flavodoxin at the surface.

### 2.3.3 Dependence of the midpoint potential on pH

The pH dependence of both redox couples is plotted in Figure 2.6. The data was fitted with the equations for redox-linked protonations [Clark, 1960]:
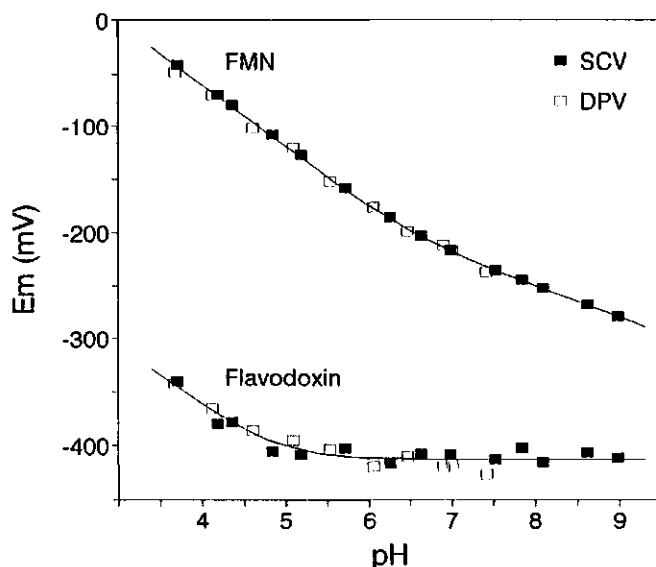
**Figure 2.6.** Dependence of the midpoint potentials of FMN and flavodoxin on pH. The staircase cyclic voltammograms ($\Delta E$=2.44 mV, $v$=10 mV/s) and the differential pulse voltammograms (steps of 2.44 mV and 250 ms, modulated by pulses of 20 mV and 100 ms) were recorded using a fresh 5 μl droplet for each point (working surface area of 5 to 10 mm$^2$) containing 0.11 mM flavodoxin and 3.3 mM neomycin in 20 mM citrate, 20 mM BisTrisPropane and 20 mM Caps, titrated with HCl or NaOH and adjusted to $I$=0.2 with NaCl. The DPV potentials are the average of the potentials measured with a cathodic and an anodic scan.

$$E_m = E^a + \frac{RT}{2F} \ln\left[\frac{[H^+]^3 + K_{red}[H^+]^2}{[H^+] + K_{ox}}\right] \tag{2.2}$$

for FMN and

$$E_1 = E^a + \frac{RT}{F} \ln\left[[H^+] + K_{red}\right] \tag{2.3}$$

for flavodoxin $E_1$. This yielded a p$K$ of 6.5 for the protonation of reduced FMN (with a fixed p$K$ for the oxidized species of 10.4 [Müller, 1981; Anderson, 1983]) and a p$K$ of 4.8 for the reduced flavodoxin.

The fitted midpoint potential of −218 mV at pH 7.0 and the p$K_{red}$ of 6.5 of FMN, adsorbed to glassy carbon are the same as reported for FMN in solution (−219 mV and 6.6)

- 29 -

[Müller, 1981; Anderson, 1983]. This indicates that the oxidized and the reduced forms of FMN are adsorbed equally strongly at glassy carbon, that the N(1) of the isoalloxazine ring is exposed to the solvent and that the electronic structure of the ring is not changed when FMN is adsorbed onto the electrode.

The fitted potential of the flavodoxin couple is $-413$ mV at pH 7.0. This is somewhat higher than the values for the semiquinone/hydroquinone potential $(E_1)$ of $-431$ mV reported by Dubourdieu *et al.* [1975] and $-440$ mV measured by Curley *et al.* [1991]. The pK of 4.8 of the reduced flavodoxin is unusually low. Dubourdieu *et al.* [1975] reported a redox-linked $pK_{red}$ of 6.6 and Curley *et al.* [1991] a $pK_{red}$ of 6.8 for *D. vulgaris* flavodoxin hydroquinone. These values are close to the pK of 6.6 for the protonation of N(1) in reduced free FMN. However, Vervoort *et al.* [1985; 1986a] concluded from NMR measurements using ^{15}N-enriched FMN that the pK of the N(1) is below 6 in the flavodoxins from *Desulfovibrio vulgaris, Megasphaera elsdenii, Clostridium beijerinckii* (MP) and *Azotobacter vinelandii*. Similar work by Franken *et al.* [1984] on *Megasphaera elsdenii* flavodoxin has shown that the N(1) is not protonated at pH 5.5 although the observed redox-linked pK for this flavodoxin is 5.7. Ludwig *et al.* [1990] did not observe any change in the optical spectrum at pH 4.6 and concluded that the pK for the N(1) in *M. elsdenii* flavodoxin must be below 4.0 and that the pK of 5.7 is due to protonation of an acidic group in the vicinity of the FMN. They proposed that the protonation occurs at the carboxylate of Glu 60 in *M. elsdenii* (Glu 59 in *C. beijerinckii*) that is hydrogen bonded to the N3-H. In *D. vulgaris* another negatively charged amino acid might be responsible for the measured pK of 6.6 to 6.8 because the Asp 63 present at this position in the sequence [Curley & Voordouw, 1988; Krey *et al.*, 1988; Dubourdieu *et al.*, 1973; Dubourdieu & Fox, 1977] is not hydrogen bonded to the isoalloxazine ring [Watt *et al.*, 1991]. The very low pK value and higher potential at high pH measured electrochemically might be caused by a conformational change at the electrode. The measured low pK can be caused by a pK shift due to the altered environment of the amino acid residue responsible for the redox linked pK. Alternatively, the residue might be blocked or no longer in the vicinity of the isoalloxazine ring. The measured $pK_{red}$ of 4.8 can be due to protonation of the isoalloxazine at N(1) in this case. The titration data of Curley *et al.* [1991] do not exclude a second $pK_{red}$ around 5 (See also the pH-dependence of *Azotobacter vinelandii* flavodoxin in Chapter 3).

### 2.3.4 Thermodynamics of the redox reactions

The temperature dependence of the flavodoxin midpoint potential as determined by SCV and plotted in Figure 2.7 is linear up to 30°C with a slope of $-1.86$ mV/K. From the relation between potential and the Gibbs energy for the reduction:
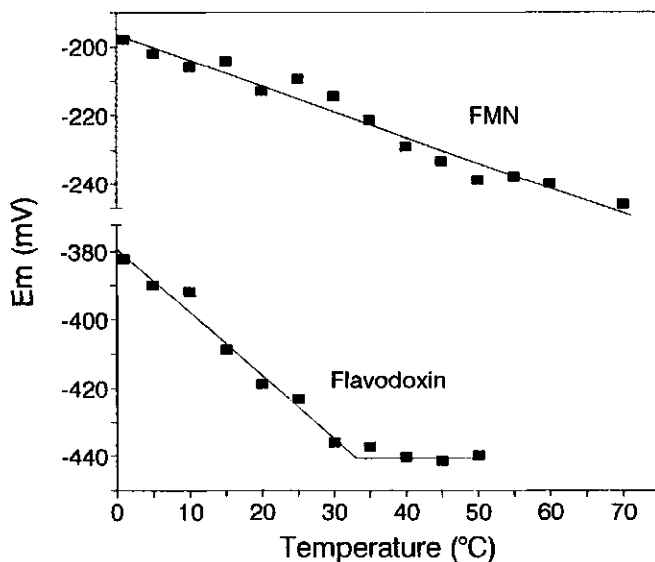
**Figure 2.7.** Dependence of the midpoint potentials of FMN and flavodoxin on temperature. Staircase cyclic voltammograms were recorded with a scan rate of 10 mV/s and $\Delta E$=1.22 mV using a 40 μl droplet containing 93 μM flavodoxin and 2.5 mM neomycin in 31 mM potassium phosphate buffer, pH 7.0.

$$\Delta G^\circ = -\, n\, F\, E_m \tag{2.4}$$

$$\Delta G^\circ = \Delta H^\circ - T\, \Delta S^\circ \tag{2.5}$$

and the entropy change of the reaction center

$$\Delta S^\circ_{rc} = S^\circ_{red} - S^\circ_{ox} = \Delta S^\circ + \Delta S^\circ(H_2) / 2 \tag{2.6}$$

with $\Delta S^\circ(H_2) = 130.4$ J·mol$^{-1}$·K$^{-1}$ [Taniguchi *et al.*, 1980 and references cited therein] follows $\Delta S^\circ = -179$ J·mol$^{-1}$·K$^{-1}$ ($\Delta S^\circ_{rc} = -114$ J·mol$^{-1}$·K$^{-1}$) and $\Delta H^\circ = -12.4$ kJ/mol. The entropic change for the reduction is large compared to that for other redox proteins, indicating a very ordered reduced state [Taniguchi *et al.*, 1980]. This is confirmed by the longer fluorescence lifetimes of the reduced FMN in flavodoxins compared to free FMN and only a single (whole protein) rotational correlation time found for reduced flavodoxins, indicating that the mobility of the reduced FMN is hindered by a rigid protein matrix. This is different for oxidized flavodoxins, where a part of the protein population is characterized by an FMN with some motional freedom [Leenders *et al.*, 1993]. Above 35°C the $E_m/T$ slope becomes

- 31 -

zero. This means that the entropic change upon reduction also becomes zero and thus $\Delta S^\circ_{rc}=$ +65 J·mol$^{-1}$·K$^{-1}$ and $\Delta H^\circ=$ −42.5 kJ/mol. This may be caused by a change in conformation of the protein between 30 and 35°C [Taniguchi et al., 1984]. The reaction entropy becomes positive if the reduced FMN molecule is bound less tightly above 35°C.

The midpoint potential of free FMN shows a linear temperature dependence up to 70°C with a slope of −0.75 mV/K, yielding $\Delta S^\circ=$−145 J·mol$^{-1}$·K$^{-1}$ ($\Delta S^\circ_{rc}=$−80 J·mol$^{-1}$·K$^{-1}$) and $\Delta H^\circ=$−1.5 kJ/mol. This means that the two electron reduction potential is almost fully entropically determined. If the zero reduction entropy of flavodoxin above 35°C is caused by exposing the FMN to the solvent this means that the difference between protein bound FMN and free FMN is small above 35°C. This would indicate that the one electron reduction of the free FMN semiquinone to the hydroquinone is also largely determined by the enthalpic change. The measured entropic change for the two electron reduction of FMN is then dominated by the entropic change of the FMN quinone to the semiquinone reduction and the enthalpic change for this first reduction is about equal but opposite to that of the second reduction step. From $E_2=$−314 mV [Anderson, 1983], $E_m=$−218 mV, $\Delta S_2=$−145 J·mol$^{-1}$·K$^{-1}$ and $\Delta S_1=$0 it follows that $\Delta H_1=$+11.6 kJ/mol and $\Delta H_2=$−13.1 kJ/mol for free FMN. The above interpretation of the data is valid if it is assumed that at pH 7 the single proton involved in the two-electron reduction of free FMN (see Figure 2.6) is transferred to the transient semiquinone FMN (and thus no proton is involved in the semiquinone/hydroquinone transition, similar to protein-bound FMN). This is indicated by the reported p$K$ of 8.3 of the semiquinone species [Müller, 1981].

From the measured potentials together with the potential of −314 mV for the quinone/semiquinone couple of free FMN [Anderson, 1983] the differences between the free energies of binding of FMN in the three oxidation states can be calculated. The FMN semiquinone is bound most tightly to the apo-flavodoxin with a Gibbs energy difference of −19.4 kJ/mol relative to the binding of oxidized FMN (295 K) and the binding of reduced FMN is the weakest with $\Delta G^\circ=$+8.1 kJ/mol relative to the binding of oxidized FMN (295 K). Using the dissociation constant for the FMN quinone of 0.2 nM as determined by Curley et al. [1991] and by Vervoort et al. [1986b] the dissociation constants of the semiquinone and the hydroquinone FMN are $8 \cdot 10^{-5}$ nM and 5.3 nM, respectively. These values are 4 and 12 times lower than those calculated by Curley et al. [1991] due to the higher $E_1$ and $E_2$ measured by us.

From the difference between $E_2$ and $E_1$ the comproportionation constant and the maximum amount of semiquinone at $E=(E_2+E_1)/2$ can be calculated [Clark, 1960]:

$$E_2 - E_1 = \frac{RT}{F}\ln\left(K_{\text{com}}\right) \tag{2.7}$$

$$\frac{[sq]}{[ox]+[sq]+[red]} = \frac{\sqrt{K_{com}}}{2+\sqrt{K_{com}}}$$ (2.8)

At pH 7 and 295 K, this yields $K_{com}=1.3 \cdot 10^5$ and a maximum amount of semiquinone of 99.5%.

## 2.4 Digital simulation

At the electrode, the quinone/semiquinone couple is not observed, but the low potential redox couple in the presence of neomycin has a reversible one electron character. This implies the presence of a high concentration of the one electron reduced flavodoxin semiquinone near the electrode surface, although the starting material was the 100% fully oxidized species (as determined from the absence of absorbance at 580 nm in the optical spectrum). From the increase of the peak current during the first scans at high scan rate (Figure 2.5) and the square root dependence of the peak current on the scan rate (Figures 2.3 and 2.4) it can be concluded that this concentration gradient of semiquinone flavodoxin is generated within a few minutes with a maximum value at some distance from the electrode. This maximum mimics a constant infinite bulk concentration of semiquinone. If no or very little semiquinone is generated directly at the electrode, it is probably formed by a comproportionation mechanism. This can be either the formation of two flavodoxin semiquinone from one fully oxidized and one fully reduced flavodoxin or reduction of oxidized flavodoxin with reduced FMN. Both reactions are known to occur in solution. By consequence, only a few molecules (catalytic amount) of semiquinone are sufficient to generate equilibrium concentrations of semiquinone and hydroquinone near the electrode surface and the development of the voltammogram without a visible first redox couple. A small amount of free or electrode-bound FMN may also act as a mediator to generate the first molecules of semiquinone. A first indication for this mediation is the higher cathodic current compared to the anodic current of the FMN response in the first scans (Figure 2.5).

To prove that this scheme of events yields a stable cyclic voltammogram with only the second reduction visible a digital simulation was performed. Explicit second order Runge-Kutta integration of the diffusion limited electrode reaction was used in combination with a homogeneous comproportionation equilibrium and generation of flavodoxin semiquinone by FMN-mediated electron transfer. The concentration profiles were digitized by the point-method [Britz, 1988].

### 2.4.1 Reaction scheme

The reactions describing the formation of flavodoxin semiquinone by FMN-mediated electron transfer will be treated together with the calculation of the current and boundary conditions. The other reactions are:

$$\text{Fld}^{\text{sq}} + 1\,e^- \underset{}{\overset{E_1^{\text{Fld}}}{\rightleftharpoons}} \text{Fld}^{\text{red}} \tag{2.9}$$

$$\text{Fld}^{\text{ox}} + \text{Fld}^{\text{red}} \underset{k^-}{\overset{k^+}{\rightleftharpoons}} 2\,\text{Fld}^{\text{sq}} \tag{2.10}$$

This scheme can be described by the differential equations:

$$\frac{\partial c_{\text{o}}}{\partial t} = D_{\text{o}} \frac{\partial^2 c_{\text{o}}}{\partial x^2} - k^+ c_{\text{o}} c_{\text{r}} + k^- c_{\text{s}}^2 \tag{2.11}$$

$$\frac{\partial c_{\text{s}}}{\partial t} = D_{\text{s}} \frac{\partial^2 c_{\text{s}}}{\partial x^2} + 2\,k^+ c_{\text{o}} c_{\text{r}} - 2\,k^- c_{\text{s}}^2 \tag{2.12}$$

$$\frac{\partial c_{\text{r}}}{\partial t} = D_{\text{r}} \frac{\partial^2 c_{\text{r}}}{\partial x^2} - k^+ c_{\text{o}} c_{\text{r}} + k^- c_{\text{s}}^2 \tag{2.13}$$

where $c_{\text{o}}$, $c_{\text{s}}$, $c_{\text{r}}$ and $D_{\text{o}}$, $D_{\text{s}}$, $D_{\text{r}}$ are the concentration and diffusion coefficients of oxidized, semiquinone and fully reduced flavodoxin respectively. When the diffusion coefficients are considered to be independent of the oxidation state:

$$D_{\text{o}} = D_{\text{s}} = D_{\text{r}} = D \tag{2.14}$$

and the total concentration flavodoxin is

$$c^* = c_{\text{o}} + c_{\text{s}} + c_{\text{r}} \tag{2.15}$$

only the concentration profiles of oxidized and semiquinone flavodoxin need to be calculated. Changing to dimensionless variables:

$$T = t / \Delta t \qquad \text{with } \Delta t = \Delta E / v \tag{2.16}$$

$$X = x / \Delta x \qquad \text{with } \Delta x = w / N \tag{2.17}$$

$$C_i = c_i / c^* \tag{2.18}$$

$$\lambda = D \Delta t / \Delta x^2 \tag{2.19}$$

$$K_1 = k^+ c^* \Delta t \tag{2.20}$$

and

$$K_2 = k^- c^* \Delta t \tag{2.21}$$

where $\Delta t$ is the time interval, $\Delta x$ is the distance between the grid-points, $\Delta E$ is the potential step used in the simulation, $v$ is the scan rate, $w$ is the width of the electrochemical cell (*i.e.* the distance between the working electrode and the reference electrode in the setup used here) and $N+1$ the number of grid-points gives the new differential equations:

$$\frac{\partial C_o}{\partial T} = \lambda \frac{\partial^2 C_o}{\partial X^2} - COMP \tag{2.22}$$

$$\frac{\partial C_s}{\partial T} = \lambda \frac{\partial^2 C_s}{\partial X^2} + 2\ COMP \tag{2.23}$$

with

$$COMP = K_1 C_o (1 - C_o - C_s) - K_2 C_s^2 \tag{2.24}$$

- 35 -

### 2.4.2 Boundary conditions

At the start of the simulation the potential is well positive of $E_1^{Fld}$ and no hydroquinone is present:

T=0 and at all X: $\qquad C_s = 1 - C_o$ $\hfill (2.25)$

During the simulated cyclic voltammetry the surface concentration of oxidized flavodoxin is calculated from the actual gradient and from the FMN-mediated reaction current $G_o$ as calculated at the end of the previous step (see below) by using a five-point approximation for the surface gradient [Britz, 1988]. The surface concentration of semiquinone flavodoxin is calculated from the Nernst-equilibrium and the total concentration of semi- and fully reduced flavodoxin:

T>0, X=0:

$$C_o(0) = \frac{48C_o(1) - 36C_o(2) + 16C_o(3) - 3C_o(4) - 12G_o}{25} \hfill (2.26)$$

$$C_s(0) = \frac{1 - C_o(0)}{1 + \exp\left(-f(E - E_1^{Fld})\right)} \hfill (2.27)$$

with $f = F / RT$.

At the opposing inert wall (formed by the counter electrode) no real boundary conditions are used but point N is simply treated as a point from which diffusion only occurs in one direction. The diffusional change in concentration at point N

$$\Delta_d C_i(N) = \lambda \{ C_i(N-1) - C_i(N) \} \hfill (2.28)$$

can be derived from the general equation for the diffusion in explicit finite difference simulations

$$\Delta_d C_i(X) = \lambda \{ C_i(X-1) - 2 C_i(X) + C_i(X+1) \} \hfill (2.29)$$

by using half of the diffusional change in concentration occurring when mirror-reflected concentration profiles beyond point N are assumed (*i.e.* $C_i(N+1)=C_i(N-1)$).

### 2.4.3 Current calculation

In general the current $i$ is proportional to the concentration gradient $g$ at the electrode surface:

$$g_{x=0} = -i / nFAD \qquad (2.30)$$

where $A$ is the electrode surface. For a two-step electrode reaction the total current is

$$i_{tot} = FA \{ n_1 D_1 g_1 + n_2 D_2 ( g_1 + g_2 ) \} \qquad (2.31).$$

Using the dimensionless gradient functions for oxidized and semiquinone flavodoxin

$$G_i = g_i \, \Delta x / c^* \qquad (2.32)$$

the dimensionless current function

$$\sqrt{\pi} \, \chi = \frac{i}{nFAc^*} \sqrt{\frac{RT}{nFDv}} \qquad (2.33)$$

becomes

$$\sqrt{\pi} \, \chi = -(2G_o + G_s) \sqrt{\frac{\lambda}{\Delta E} \frac{RT}{F}} \qquad (2.34).$$

The current (gradient) for the reversible semiquinone reduction is calculated using a five-point approximation [Britz, 1988]:

$$G_s = \frac{- 25C_s(0) + 48C_s(1) - 36C_s(2) + 16C_s(3) - 3C_s(4)}{12} \qquad (2.35).$$

The mediated reduction of oxidized flavodoxin by adsorbed FMN can be described by the reactions:

$$\text{FMN}^{\text{red}} + \text{Fld}^{\text{ox}} \xrightarrow{k_f} \text{FMN}^{\text{sq}} + \text{Fld}^{\text{sq}} \tag{2.36}$$

$$\text{FMN}^{\text{ox}} + \text{Fld}^{\text{sq}} \xrightarrow{k_b} \text{FMN}^{\text{sq}} + \text{Fld}^{\text{ox}} \tag{2.37}$$
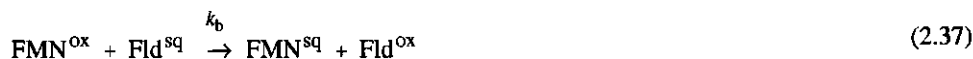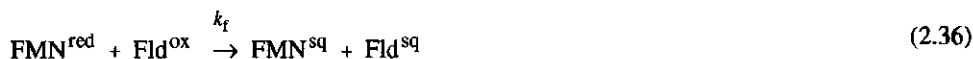
In these reactions an FMN radical is formed that very rapidly reacts to yield a net exchange of one electron between the electrode and flavodoxin:

$$\text{FMN}^{\text{sq}} + 1e^- \rightarrow \text{FMN}^{\text{red}} \tag{2.38}$$

$$\text{FMN}^{\text{sq}} \rightarrow \text{FMN}^{\text{ox}} + 1e^- \tag{2.39}$$

$$2\,\text{FMN}^{\text{sq}} \rightleftharpoons \text{FMN}^{\text{ox}} + \text{FMN}^{\text{red}} \tag{2.40}$$

$$\text{FMN}^{\text{ox}} + 2e^- \rightleftharpoons \text{FMN}^{\text{red}} \tag{2.41}$$

The current due to these reactions can be described by

$$i = n\,F\,A^{\text{FMN}} \{\, k_f\,\Theta^{\text{red}}\,c_o(0) - k_b\,\Theta^{\text{ox}}\,c_s(0) \,\} \tag{2.42}$$

where $n=1$, $A^{\text{FMN}}$ is the area occupied by adsorbed FMN and the relative fractions of reduced and oxidized FMN are determined by the Nernst-equilibrium:

$$\Theta^{\text{red}} = \frac{1}{1 + \exp\left(\dfrac{2F}{RT}(E - E_m)\right)} = 1 - \Theta^{\text{ox}} \tag{2.43}$$

Assuming a driving force for the electron transfer between FMN and flavodoxin according to the Butler-Volmer equation, depending only on the potential difference between the FMN and flavodoxin half-reactions, yields

$$k_f = k°\exp\left(\frac{-\alpha n_\alpha F}{RT}(E_1^{\text{FMN}} - E_2^{\text{Fld}})\right) \tag{2.44}$$

- 38 -

and

$$k_b = k^\circ \exp\left(\frac{(1-\alpha)n_\alpha F}{RT}(E_2^{FMN} - E_2^{Fld})\right) \tag{2.45}$$

where $\alpha$ is the cathodic transfer coefficient, $n_\alpha=1$ the number of transferred electrons in the rate-determining step and $k^\circ$ the standard rate constant for electron transfer between flavodoxin and adsorbed FMN. Changing to the dimensionless constants

$$\phi = A^{FMN} / A \tag{2.46},$$

$$K_f = \phi\, k_f\, \Delta x / D \tag{2.47}$$

and

$$K_b = \phi\, k_b\, \Delta x / D \tag{2.48}$$

yields

$$G_o = K_f\, C_o(0)\, \Theta^{red} - K_b\, C_s(0)\, (1 - \Theta^{red}) \tag{2.49}.$$


### 2.4.4 Implementation

The programme implementing the above scheme was written in Pascal. In Figure 2.8 the core of this programme is shown. The dimensionless parameters $\lambda$, K1, K2, $K_b$ and $K_f$ were kept below 0.5 by choosing a small enough potential step $\Delta E$, N=100 and w=0.5 mm. The transfer coefficient $\alpha$ was set to 0.5, the diffusion constant for flavodoxin (estimated from the scan rate dependence) was $1\cdot10^{-10}$ m$^2$/s, the concentration flavodoxin 0.10 mM, the comproportionation constant was set to the reported value of 2300 M$^{-1}$s$^{-1}$ [Dubourdieu et al., 1975] and the disproportionation rate $k^-$ was calculated from $K_{com} = k^+/k^- = 1.3\cdot10^5$ as determined from equation (2.4). The midpoint potentials $E_1^{FMN} = -122$ mV, $E_2^{FMN} = -314$ mV, $E_1^{Fld} = -413$ mV, $E_2^{Fld} = -113$ mV and $E_m^{FMN} = -218$ mV were used and the upper and lower potential limits were set to +50 and −750 mV respectively.

```
{calculate delta1:}
OX[0]:=(48.0*OX[1]-36.0*OX[2]+16.0*OX[3]-3.0*OX[4]-12.0*GOX)/25.0;
SQ[0]:=(1-OX[0])/(1+exp(-F*(E-E1FLD)));
for x:=1 to N-1 do begin
  COMP:=K1*(1-OX[x]-SQ[x])*OX[x]-K2*SQ[x]*SQ[x];
  D1OX[x]:=Lambda*(OX[x-1]-OX[x]-OX[x]+OX[x+1])-COMP;
  D1SQ[x]:=Lambda*(SQ[x-1]-SQ[x]-SQ[x]+SQ[x+1])+COMP+COMP;
end;
COMP:=K1*(1-OX[N]-SQ[N])*OX[N]-K2*SQ[N]*SQ[N];
D1OX[N]:=Lambda*(OX[N-1]-OX[N])-COMP;
D1SQ[N]:=Lambda*(SQ[N-1]-SQ[N])+COMP+COMP;

{calculate delta2 and new concentrations:}
OX[0]:=(48.0*(OX[1]+D1OX[1])-36.0*(OX[2]+D1OX[2])
      +16.0*(OX[3]+D1OX[3])-3.0*(OX[4]+D1OX[4])-12.0*GOX)/25.0;
SQ[0]:=(1-OX[0])/(1+exp(-F*(E-E1FLD)));
OX1:=OX[0];
OX2:=OX[1]+D1OX[1];
SQ1:=SQ[0];
SQ2:=SQ[1]+D1SQ[1];
for x:=1 to N-1 do begin
  OX3:=OX[x+1]+D1OX[x+1];
  SQ3:=SQ[x+1]+D1SQ[x+1];
  COMP:=K1*(1-OX2-SQ2)*OX2-K2*SQ2*SQ2;
  D2OX:=Lambda*(OX1-OX2-OX2+OX3)-COMP;
  D2SQ:=Lambda*(SQ1-SQ2-SQ2+SQ3)+COMP+COMP;
  OX[x]:=OX[x]+(D1OX[x]+D2OX)/2;
  SQ[x]:=SQ[x]+(D1SQ[x]+D2SQ)/2 ;
  OX1:=OX2;
  OX2:=OX3;
  SQ1:=SQ2;
  SQ2:=SQ3;
end;
COMP:=K1*(1-OX2-SQ2)*OX2-K2*SQ2*SQ2;
D2OX:=Lambda*(OX1-OX2)-COMP;
D2SQ:=Lambda*(SQ1-SQ2)+COMP+COMP;
OX[N]:=OX[N]+(D1OX[N]+D2OX)/2;
SQ[N]:=SQ[N]+(D1SQ[N]+D2SQ)/2;

FMNRED0:=1/(1+exp(2*F*(E-(E1FMN+E2FMN)/2)));
GOX:=KF*OX[0]*FMNRED0-KB*SQ[0]*(1-FMNRED0);
GSQ:=(-25*SQ[0]+48.0*SQ[1]-36.0*SQ[2]+16.0*SQ[3]-3.0*SQ[4])/12.0;
Current:=(-GOX-GOX-GSQ)*sqrt((Lambda)/(dE*F))/0.4463;  {=√π*χ/0.4463}
```

**Figure 2.8.** The core of the Pascal program implementing the reaction scheme.
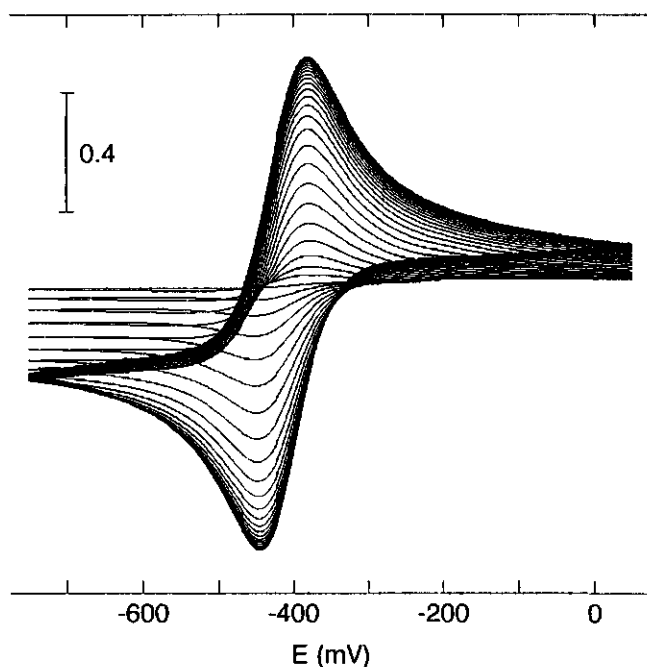
**Figure 2.9.** Simulated development of the flavodoxin response ($\sqrt{\pi}\ \chi\ /\ 0.4463$) with time. Scan numbers 1 to 25 are shown. Simulation parameters: 100 µM flavodoxin, initially fully oxidized; $D$=1·10$^{-10}$ m$^2$/s; $k^+$=2300 M$^{-1}$s$^{-1}$; $K_{com}$=1.3·10$^5$; $E_1^{Fld}$=–0.413 V; $E_2^{Fld}$=–0.113 V; $E_1^{FMN}$=–0.122 V; $E_2^{FMN}$=–0.314 V; $k°$=6.3·10$^{-6}$ m/s; $\alpha$=0.5; $E_{high}$=+0.05 V; $E_{low}$=–0.75 V; $\Delta E$=1 mV; $v$=100 mV/s; $w$=0.5 mm; $N$=100. $A^{FMN}$ increases with time as determined from the area under the FMN peaks in the voltammograms used in Figure 2.5. With 51 Å$^2$ per molecule and a working surface of 25 mm$^2$: $\phi$=0.0134 during scan 1, $\phi$=0.0382 during scan 10, $\phi$=0.0485 during scan 16 and $\phi$=0.0551 during scan 25 (linear in between).

### 2.4.5 Results

In Figure 2.9 the simulated development of the response with time is shown and the resulting current/time curves are compared to the measured data in Figure 2.10. The curves are fitted to the data by varying $k°$ in steps of 1·10$^{-7}$ m/s or the relative concentration semiquinone in steps of 0.001, optimizing the normalization of the measured data by a $\chi^2$-fit and comparing the resulting $\chi^2$-values. A good fit of the data is obtained with a heterogeneous rate constant $k°$=6.3·10$^{-6}$ m/s for the electron transfer between adsorbed FMN and flavodoxin (using the amounts of adsorbed FMN as determined from the area under the FMN peaks in the voltammograms used in Figure 2.5) and setting the maximum current to 2.37 µA (*i.e.* the measured peak height in scan number 16 is equal to 92% of the diffusion-limited maximum
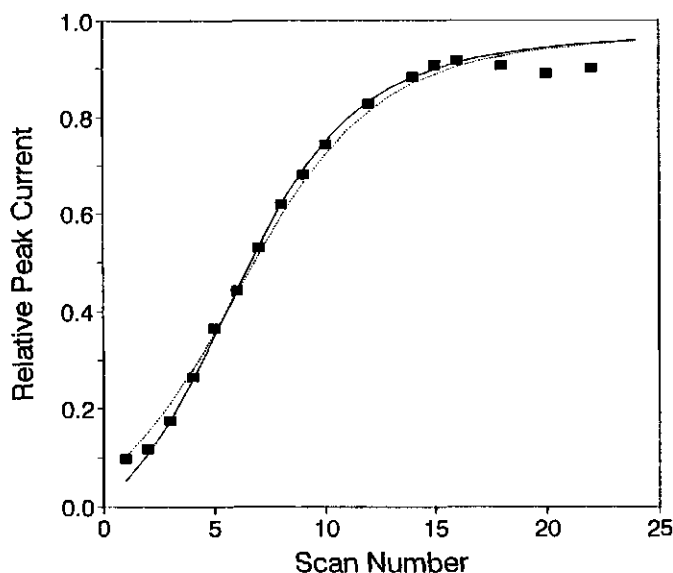
**Figure 2.10.** Comparision of measured anodic peak currents with results of simulations. Simulation parameters for the solid trace are described in Figure 2.9. For the dashed trace: $k°=0$ and initial relative concentration semiquinone 0.058. The measured peaks (see Figure 2.5) are fitted to the solid trace by setting the observed maximum in scan number 16 to 0.9164.

current). When the FMN-mediation rate is set to zero a rather high initial concentration semiquinone (5.8%) is required to fit the data, although the best result is not as close to the measured data as with mediation and no semiquinone was detected at $\lambda=580$ nm in the spectrum of the flavodoxin preparation. When the initial concentration semiquinone is set to 1% or less a higher comproportionation rate (5000 $M^{-1}s^{-1}$ or more) is required to approximate the measured data. This yields too low peak currents during the first scans and results in notable distortion of the first scan at low scan rates (rather like a "catalytic wave", *i.e.* a voltammogram as obtained by a normal $E_rC_i$' mechanism). These distortions were never observed but this might be due to the already heavily distorted first scan due to the presence of traces of oxygen and transient cathodic electrode-signals (also observed without flavodoxin). When FMN-mediated formation of semiquinone is included, no initial semiquinone is required and the comproportionation rate of 2300 $M^{-1}s^{-1}$ causes much less distorted first scans. The third option, mediation by FMN but no comproportionation also yields increasing peak heights with time but an extremely high transfer rate (in the order of $10^{-3}$ m/s) is required to obtain a maximum current around scan 15 to 20. The shape of the curve (very steep initial increase of the peak height and slow subsequent growth) is however very different from the measured data and this scheme is not very realistic.
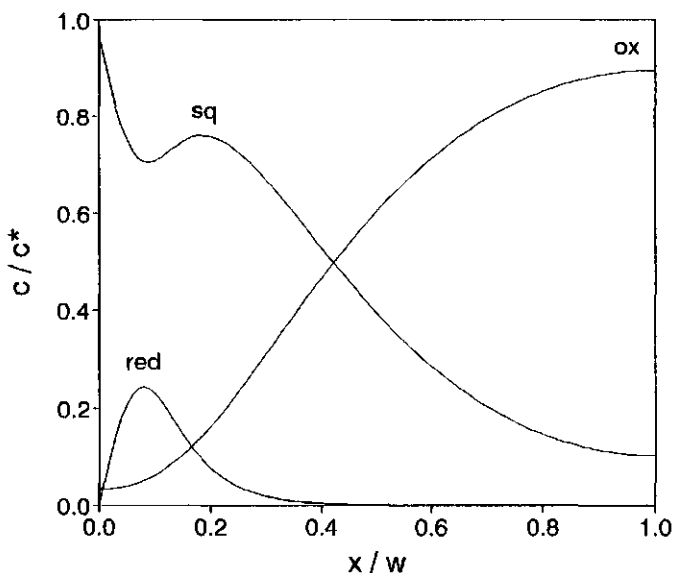
**Figure 2.11.** Concentration profiles of oxidized (ox), semiquinone (sq) and reduced (red) flavodoxin at the end of scan 25. The simulation parameters are described in Figure 2.9.

The concentration gradients indeed are formed as expected (Figure 2.11). The concentration of the fully oxidized flavodoxin becomes zero near the electrode and the concentration gradients of semiquinone and hydroquinone near the electrode are very similar to the gradients obtained when the flavodoxin initially is set to 100% semiquinone, with maximum concentrations semiquinone and fully reduced flavodoxin at time-dependent distances from the electrode surface. These maxima mimic the constant bulk concentrations of semiquinone and hydroquinone as would have been present at large distance from the electrode surface in the absence of fully oxidized flavodoxin. This explains the realistic value for the diffusion coefficient (a value of about $1 \cdot 10^{-10}$ m$^2$/s can be estimated from the molecular mass assuming a globular shape) calculated from the slope of the current *versus* the square root of the scan rate.

## 2.5    Concluding remarks

The results discussed in this chapter indicate that even for the small electron transferring flavin protein flavodoxin the electrochemistry is not straightforward. At the electrode the protonation of the reduced flavodoxin occurs at a much lower pH than in solution. Due to kinetic limitations in combination with a fast comproportionation equilibrium

- 43 -

only the second redox couple is visible at the electrode. Digital simulation shows that the peak currents of the second reduction couple approach a maximum value after a few cycles if comproportionation occurs in solution and a small amount of semiquinone is either present from the start or is generated by mediation of electrode-bound FMN.

The absence of the quinone/semiquinone couple in all previous reported diffusion-limited voltammograms of flavodoxins [Armstrong *et al.*, 1984; Bianco *et al.*, 1988; Barker *et al.*, 1988; Bagby *et al.*, 1991] is consistent with the observations reported in this chapter and indicate that for *Megasphaera elsdenii* and *Azotobacter chroococcum* flavodoxins the quinone/semiquinone redox equilibrium is also slow at the electrode and the comproportionation is fast. Only Van Dijk *et al.* [1982] found both redox couples but in this case the flavodoxin was coadsorbed with poly-L-lysin at the mercury electrode. This disables comproportionation and apparently increases the rate of the first reduction.

These observations have implications for electrochemistry of flavin enzymes. If only one peak is detected in addition to that of free flavin with the characteristics of a one-electron reduction this is not *per se* the expected first reduction step. If the flavin is non-covalently bound (this is the case for most flavoenzymes, *e.g.*, xanthine oxidase [Rodrigues & Wedd, 1991] or glucose oxidase [Bogdanovskaya *et al.*, 1988; Miyawaki & Wingard, 1994; Ianniello *et al.*, 1982; Scheller *et al.*, 1979; Szucs *et al.*, 1989]) the redox couple due to free flavin might easily be mistaken for the expected protein electrochemistry. This was also suggested by Durliat and coworkers [Durliat & Comtat, 1984; Durliat *et al.*, 1988], who monitored the electron transfer between platinum and glucose oxidase from *Aspergillus niger* with thin layer spectro-electrochemistry. They only found peaks centred at the potential of free FAD although the spectroscopy showed that GOD itself is reduced via the intermediate semiquinone state when a constant potential is applied. The molecular activity of the enzyme was unaffected by this electrolysis and a catalytic current was observed in the presence of glucose. Therefore, the development of a catalytic wave when substrate is added does not prove direct interaction between the enzyme and the electrode but can also be accomplished by electron transfer mediated by a small amount of free flavin.

## 2.6    References

Anderson, R.F. (1983) *Biochim. Biophys. Acta 722*, 158.

Armstrong, F.A. (1990) *Structure and Bonding 72*, 137.

Armstrong, F.A., Butt, J.N. & Sucheta, A. (1993) *Methods Enzymol. 227*, 479.

Armstrong, F.A., Cox, P.A., Hill, H.A.O., Lowe, V.J. & Oliver, B.N. (1987) *J. Electroanal. Chem. 217*, 331.

Armstrong, F.A., Hill, H.A.O., Oliver, B.N. & Walton, N.J. (1984) *J. Am. Chem. Soc. 106*, 921.

Armstrong, F.A., Hill, H.A.O. & Walton, N.J. (1988) *Acc. Chem. Res. 21*, 407.

Bagby, S., Barker, P.D., Hill, H.A.O., Sanghera, G.S., Dunbar, B., Ashby, G.A., Eady, R.R. & Thorneley, R.N.F. (1991) *Biochem. J. 277*, 313.

Barker, P.D., Hill, H.A.O., Sanghera, G.S., Eady, R.R. & Thorneley, R.N.F. (1988) *Biochem. Soc. Trans. 16 (626th meeting)*, 959.

Bard, A.J. & Faulkner, L.R. (1980) *Electrochemical Methods, Fundamentals and Applications*, Wiley, New York.

Bianco, P., Haladjian, J., Manjaoui, A. & Bruschi, M. (1988) *Electrochim. Acta 33*, 745.

Bogdanovskaya, V.A., Tarasevich, M.R., Hintsche, R. & Scheller, F. (1988) *Bioelectrochem. Bioenerg. 19 (J. Electroanal. Chem. 253)*, 581.

Britz, D. (1988) *Digital simulation in electrochemistry*, Springer-Verlag, Berlin.

Clark, W.M. (1960) *Oxidation-reduction potentials of organic systems*, Waverly Press, Baltimore.

Curley, G.P., Carr, M.C., Mayhew, S.G. & Voordouw, G. (1991) *Eur. J. Biochem. 202*, 1091.

Curley, G.P. & Voordouw, G. (1988) *FEMS Microbiol. Letters 49*, 295.

Deistung, J. & Thorneley, R.N.F. (1986) *Biochem. J. 239*, 69.

Drake, H.L. & Agaki, J.M. (1977) *J. Bacteriol. 132*, 139.

Dubourdieu, M. & Fox, J.L. (1977) *J. Biol. Chem. 252*, 1453.

Dubourdieu, M. & Le Gall, J. (1970) *Biochem. Biophys. Res. Comm. 38*, 965.

Dubourdieu, M., Le Gall, J. & Favaudon, V. (1975) *Biochim. Biophys. Acta 376*, 519.

Dubourdieu, M., Le Gall, J. & Fox, J.L. (1973) *Biochem. Biophys. Res. Comm. 52*, 1418.

Durliat, H., Barrau, M.B. & Comtat, M. (1988) *Bioelectrochem. Bioenerg. 19 (J. Electroanal. Chem. 253)*, 413.

Durliat, H. & Comtat, M. (1984) *Anal. Chem. 56*, 148.

Eddowes, M.J. & Hill, H.A.O. (1977) *J. Chem. Soc. Chem. Comm. 1977*, 771.

Entsch, B. & Smillie, R.M. (1972) *Arch. Biochem. Biophys. 151*, 378.

Franken, H.-D., Rüterjans, H. & Müller, F. (1984) *Eur. J. Biochem. 138*, 481.

Guo, L.H., Hill, H.A.O., Lawrance, G.A., Sanghera, G.S. & Hopper, D.J. (1989) *J. Electroanal. Chem. 266*, 379.

Hagen, W.R. (1989) *Eur. J. Biochem. 182*, 523.

Hatchikian, E.C., Le Gall, J., Bruschi, M. & Dubourdieu, M. (1972) *Biochim. Biophys. Acta 258*, 701.

Hill, H.A.O. & Hunt, N.I. (1993) *Methods Enzymol. 227*, 501.

Ianniello, R.M., Lindsay, T.J. & Yacynych, A.M. (1982) *Anal. Chem. 54*, 1098.

Krey, G.D., Vanin, E.F. & Swenson, R.P. (1988) *J. Biol. Chem. 265*, 15436.

Leenders, R., Kooijman, M., van Hoek, A., Veeger, C. & Visser, A.J.W.G. (1993) *Eur. J. Biochem. 211*, 37.

Le Gall, J. & Hatchikian, E.C. (1967) *C. R. Acad. Sci. Paris 264*, 2580.

Ludwig, M.L., Schopfer, L.M., Metzger, A.L., Pattridge, K.A. & Massey, V. (1990) *Biochemistry 29*, 10364.

Massey, V. & Hemmerich, P. (1978) *Biochemistry 17*, 9.

Mayhew, S.G. (1971) *Biochim. Biophys. Acta 235*, 276.

Mayhew, S.G., Foust, G. & Massey, V. (1969) *J. Biol. Chem. 244*, 803.

Mayhew, S.G. & Ludwig, M.L. (1975) in *The Enzymes, Vol. 12, Part B*, (Boyer, P.D., Ed.), Academic Press, New York, p. 57.

Mayhew, S.G. & Tollin, G. (1992) in *Chemistry and biochemistry of flavoenzymes Vol. III*, (Müller, F., Ed.), CRC Press, Boca Raton (FL), p. 389.

Miyawaki, O. & Wingard, L. (1994) *Biotechnol. Bioeng. 26*, 1364.

Moura, I., Moura, J.J.G., Bruschi, M. & Le Gall, J. (1980) *Biochim. Biophys. Acta 591*, 1.

Müller, F. (1981) in *Topics in Current Chemistry Vol. 108*, (Boschke, F.L., Ed.), Springer, Berlin, p. 71.

Müller, L. & Friedrich, W. (1977) *Z. Chem. 17*, 70.

Osteryoung, J. (1988) *Methods Enzymol. 158*, 243.

Paulsen, K.E., Stankovich, M.T., Stockman, B.J. & Markley, J.L (1990) *Arch. Biochem. Biophys. 280*, 68.

Peelen, S. & Vervoort, J. (1994) *Arch. Biochem. Biophys. 314*, 291.

Pueyo, J.J., Gomez-Moreno, C. & Mayhew, S.G. (1991) *Eur. J. Biochem. 202*, 1065.

Rodrigues, C.G. & Wedd, A.G. (1991) *J. Electroanal. Chem. 312*, 131.

Scheller, F., Strnad, G., Neumann, B., Kühn, M. & Ostrowski, W. (1979) *Bioelectrochem. Bioenerg. 6 (J. Electroanal. Chem. 104)*, 117.

Simondsen, R.P. & Tollin, G. (1980) *Mol. Cell. Biochem. 33*, 13.

Sykes, G.A. & Rogers, L.J. (1982) *Biochem. Soc. Trans. 10*, 414.

Sykes, G.A. & Rogers, L.J. (1984) *Biochem. J. 217*, 845.

Szucs, A., Hitchens, G.D. & Bockris, J.O'M. (1989) *Bioelectrochem. Bioenerg. 21 (J. Electroanal. Chem. 275)*, 133.

Taniguchi, I., Iseki, M., Eto, T., Toyosawa, K., Yamaguchi, H. & Yasukouchi, K. (1984) *Bioelectrochem. Bioenerg. 13 (J. Electroanal. Chem. 174)*, 373.

Taniguchi, V.T., Sailasuta-Scott, N., Anson, F.C. & Gray, H.B. (1980) *Pure and Appl. Chem. 52*, 2275.

Watenpaugh, K.D., Sieker, L.C. & Jensen, L.H. (1973) *Proc. Nat. Acad. Sci. USA 70*, 3857.

Van Dijk, C., Van Leeuwen, J.W. & Veeger, C. (1982) *Bioelectrochem. Bioenerg. 9 (J.Electroanal. Chem. 141)*, 743.

Vervoort, J., Müller, F., Le Gall, J., Bacher, A. & Sedlmaier, H. (1985) *Eur. J. Biochem. 151*, 49.

Vervoort, J., Müller, F., Mayhew, S.G., van den Berg, W.A.M., Moonen, C.T.W. & Bacher, A. (1986a) *Biochemistry 25*, 6789.

Vervoort, J., van Berkel, W.J.M., Mayhew, S.G., Müller, F., Bacher, A., Nielsen, P. & Le Gall, J. (1986b) *Eur. J. Biochem. 161*, 749.

Watenpaugh, K.D., Sieker, L.C., Jensen, L.H., Le Gall, J. & Dubourdieu, M. (1972) *Proc. Nat. Acad. Sci. USA 69*, 3185.

Watt, W.,Tulinsky, A., Swenson, R.P. & Watenpaugh, F.D. (1991) *J. Mol. Biol. 218*, 195.

# Chapter 3

## Redox properties of wild-type, C69A and C69S *Azotobacter vinelandii* flavodoxin II.

### 3.1 Introduction

Flavodoxin II from *A. vinelandii* strain ATCC 478 consists of 179 amino acids (molecular mass 20 kDa) and belongs to the class of what are called long-chain flavodoxins [Tanaka *et al.*, 1977; Taylor *et al.*, 1990; Van Mierlo *et al.*, 1995]. In nitrogen-fixing cells this flavodoxin is present in ten-fold higher concentrations than in cells grown on ammonium acetate [Klugkist *et al.*, 1986]. $^{31}$P-NMR experiments have shown that flavodoxin II from *A. vinelandii* strain ATCC 478 does not contain a covalently attached phosphate [Van Mierlo *et al.*, 1995; Klugkist *et al.*, 1986], in contrast to flavodoxin from *A. vinelandii* strain OP, Berkeley [Boylan & Edmondson, 1990; Edmondson & James, 1979]. *In vitro* experiments have shown that *Azotobacter* flavodoxins can function as electron donor to nitrogenase [Yates, 1972; Scherings *et al.*, 1977]. This finding has been confirmed for the recombinant *A. vinelandii* flavodoxin II [J.H. Spee, personal communication].

Flavodoxins of various *Azotobacter* strains have been reported to have the lowest semiquinone/hydroquinone midpoint potential $(E_1)$ found within the flavodoxin family: $E_1$ ranges from $-458$ mV to $-524$ mV at pH 8. Most of the reported redox potentials for *Azotobacter* flavodoxins have been determined for flavodoxins from *A. vinelandii* OP strains containing a covalently bound phosphate [Yoch, 1972; Barman & Tollin, 1972; Watt, 1979], and for flavodoxin from *Azotobacter chroococcum* [Deistung & Thorneley, 1986; Barker *et al.*, 1988; Bagby *et al.*, 1991]. Klugkist *et al.* [1986] determined the semiquinone/hydroquinone potential of *A. vinelandii* strain ATCC 478 flavodoxin II with optical spectroscopy in the presence of hydrogen/hydrogenase. However, the hydrogen potential is more positive than the flavodoxin potential found (-520 mV at pH 9). This implies that even at high pH only a small fraction of the flavodoxin was reduced. Therefore, the reported potentials probably are not very accurate. The only other potential determined for an *A. vinelandii* dephospho-flavodoxin was reported by Taylor *et al.* [1990]. By spectrocoulometric titration they measured a potential of $-458$ mV at pH 8 for recombinant *A. vinelandii* flavodoxin (strain OP, Berkeley) expressed in *E. coli*.

It has been observed that dimerization of wild-type *A. vinelandii* flavodoxin occurs both at room temperature and during storage at $-20$ °C and that this results in dimers which lack biological activity [Yoch, 1975; Tollin & Edmondson, 1980]. Using site-directed mutagenesis, van Mierlo *et al.* [1995] obtained proof that this dimerization occurs via

intermolecular disulfide bond formation of the single cysteine residues at position 69, as had previously been suggested by Yoch [1975] and by Tanaka *et al.* [1977]. The X-ray structure of the highly homologous *A. chroococcum* flavodoxin indicates that Cys69 is positioned at the periphery of the protein at 5 Å from the exposed edge of the isoalloxazine ring of the FMN [Thorneley *et al.*, 1993]. It has been found that Cys68 in *Klebsiella pneumoniae* flavodoxin is post-translationally modified by attachment of coenzyme A via a mixed disulfide bond. This post-translational modification was suggested to be part of a regulatory mechanism for electron transfer to nitrogenase [Thorneley *et al.*, 1992]. However, such a phenomenon has not been detected for any other flavodoxin.

Since dimerization of *A. vinelandii* flavodoxin II would seriously hamper studies on the folding and stability of this protein, van Mierlo *et al.* replaced Cys69 by an alanine as well as a serine residue. The goal was to create a flavodoxin mutant of which the folding behaviour, stability and redox potentials are as similar as possible to wild-type flavodoxin. In this chapter the redox properties of the wild-type and the C69A and C69S mutant flavodoxins are reported. Since Cys69 is situated in the immediate vicinity of the FMN cofactor, it is of interest to investigate whether this cysteine plays a role in the modification of the midpoint potentials of the protein. Furthermore, the electrochemical behaviour of the large *A. vinelandii* flavodoxin is compared to that of *D. vulgaris* flavodoxin described in Chapter 2. The potentials obtained by direct electrochemistry were verified by EPR monitored redox-titrations. Direct electrochemistry has been reported for flavodoxins from *Desulfovibrio vulgaris* (Hildenborough) [Bianco *et al.*, 1988; Chapter 2], *Megasphaera elsdenii* [Van Dijk *et al.*, 1982; Armstrong *et al.*, 1984], *K. pneumoniae* [Thorneley *et al.*, 1993] and *A. chroococcum* [Barker *et al.*, 1988; Bagby *et al.*, 1991], but no complete EPR-titration of a flavodoxin has been reported.

## 3.2   Experimental procedures

### 3.2.1   Proteins

Recombinant wild-type, C69A and C69S flavodoxin II from *Azotobacter vinelandii* strain ATCC 478 were expressed in *E. coli* and purified as described previously [Tollin & Edmondson, 1980; van Mierlo *et al.*, 1995].

### 3.2.2   Cyclic Voltammetry

Cyclic voltammograms were measured using either a Wenking POS73 potentiostat (Bank Elektronik, FRG) or a BAS CV-27 potentiostat (Bioanalytical systems, Indiana, USA).

The potential was also measured with a Fluka 8022-A digital multimeter. The data were recorded on a X-Y recorder (Kipp & Zonen, NL). A glassy carbon disc (type V25, Le Carbon Loraine, Rotterdam, NL), a P-1312 micro platinum electrode (Radiometer, Copenhagen, DN) and a K-401 saturated calomel electrode (SCE) (Radiometer, Copenhagen, DN) were used as working, counter and reference electrode, respectively. Prior to each electrochemical measurement the glassy carbon disc was polished on Microcloth with 6 µm Metadi Diamond Compound spray (Buehler, USA) and activated in a methane flame as described in Chapter 2. The three-electrode electrochemical cell used is described in detail by Hagen [1989].

The experiments were performed at $22\pm1°C$ and the potentials have been recalculated with respect to the normal hydrogen electrode (NHE) using 246 mV for the saturated calomel electrode. The sample size was 16 to 20 µl with wild-type, C69A, and C69S flavodoxin final concentrations ranging from 75 to 155 µM. 3 mM neomycin B (Sigma) was always present as a promoter. In case of wild-type flavodoxin the sample also contained 3 mM dithiotreitol (Sigma).

The pH dependence was measured in 60 to 100 mM "Good" buffers (Mes, pH 5.5 and pH 6.0, Bis-Tris pH 6.5, Mops pH 7.0, Hepes pH 7.5, Tricine pH 8.0, and Taps pH 8.5) or sodium acetate buffer (pH 4.0, pH 4.5 and pH 5.0). Cyclic voltammograms were recorded from −0.30 to −1.00 V (pH > 5) or from −0.20 to −0.90 mV (pH < 5.5) versus SCE at a scan rate of 10 mV/s.

The temperature dependence was measured at pH 6 by submerging the cell in a thermostated waterbath. The cell was flushed with argon which was led through 2 meters of 3 mm copper tube submerged in the waterbath. The internal temperature of the cell was measured using a thermocouple inserted into the salt bridge of the calomel electrode. The potentials are corrected for the temperature dependent potential of the calomel electrode as given in Chapter 2, equation (2.1).


### 3.2.3 EPR-monitored redox titrations

Redox titrations were performed at $22\pm1°C$ as described by Pierik and Hagen [1991]. The potential of the solution was measured at a P-1312 micro platinum electrode (Radiometer, Copenhagen, DN) with respect to the potential of a K-401 saturated calomel electrode (Radiometer, Copenhagen, DN) using a Fluka 8022-A digital multimeter. Reported potentials were recalculated with respect to the normal hydrogen electrode ($E_{SCE}$=246 mV). Typically, a solution contained 40 µM wild-type or C69A flavodoxin and equimolar concentrations (40 µM) of the following redox mediator dyes: phenazine ethosulfate, methylene blue, resorufin, indigo carmine, 2-hydroxy-1,4-naphtaquinone, anthraquinone-2-sulfonate, phenosafranine, safranine O, neutral red, benzylviologen, and methylviologen in 100 mM Mes buffer pH 6 (or 100 mM Taps buffer pH 8.5) containing 40 mM sodium chloride. The reductant was

sodium dithionite (Sigma) freshly prepared in an anaerobic 100 mM Mes buffer pH 6 (or 100 mM Taps buffer pH 8.5). When at very low potential it became impossible to reduce the flavodoxin solution with dithionite [Mayhew, 1978], a titanium(III)citrate solution was used as reductant (midpoint potentials of $-440$ mV at pH 6 and $-590$ mV at pH 8.5 [Zehnder, 1976]). After each addition of reductant the solution was stirred until a stable potential was obtained. Subsequently, a 100 µl sample was transferred to an anaerobic EPR-tube connected to an argon/vacuum manifold and frozen in liquid nitrogen. EPR data were collected on a Bruker 200D EPR spectrometer at a microwave frequency of 9.18 GHz with a microwave power of 20 µW. The modulation frequency was 100 kHz, the amplitude of modulation was 1.0 mT. The temperature was kept between 125 and 135 K using a flow of nitrogen through a home-built cryostat. The relative concentration of the flavodoxin semiquinone form was determined from the intensity of the radical signal and corrected for dilution.

## 3.3    Results

### 3.3.1   Cyclic Voltammetry

Without neomycin no response was observed apart from some FMN adsorbed on the electrode (the peak current was proportional to the scan rate). In the presence of the cationic aminoglycoside neomycin one additional response around $-460$ mV *versus* NHE (at pH 7) was observed for the C69A and C69S flavodoxin mutants. No response was observed at $E>E_{FMN}$. The observation that only the semiquinone/hydroquinone couple is present in the cyclic voltammograms although the starting material was always fully oxidized is similar to the observations with *D. vulgaris* flavodoxin reported in Chapter 2.

During the first scans the response was reversible but in subsequent scans the peak-to-peak separation increased. An optimum stability was observed for neomycin end concentrations of 3 mM. Wild-type flavodoxin however, gave a very unstable and broad response in the presence of 3 mM neomycin alone. Addition of dithiotreitol (3 mM end concentration) to the wild-type flavodoxin solution proved essential to obtain a reversible response (Figure 3.1). Under optimum conditions the measured potentials during the first few scans were usually reproducible within 5 mV for all three proteins. The peak currents were a linear function of the square root of the scan rate up to 50 mV/s. The calculated diffusion coefficient for wild-type, C69A and C69S flavodoxin is $(7.4\pm0.9)\cdot10^{-7}$ cm$^2$/s. The heterogeneous electron transfer rate constants were determined by plotting the kinetic parameter obtained from the peak-to-peak separation *versus* the reciprocal square root of the scan rate according to Nicholson [1965]: $k°$ is $(2.1\pm0.7)\cdot10^{-3}$ cm/s for wild-type, C69A and C69S flavodoxin.
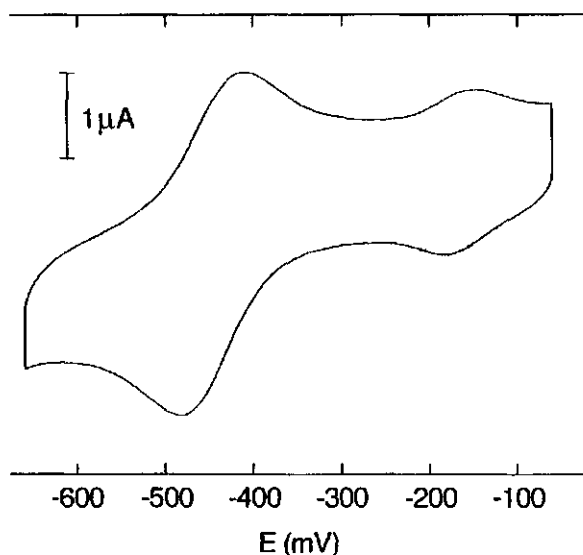
**Figure 3.1.** Cyclic voltammogram of 75 μM wild-type flavodoxin in 100 mM Mes buffer pH 6 in the presence of 3 mM neomycin and 3 mM dithiotreitol. Cyclic voltammograms were recorded from −300 to −900 mV *versus* SCE at a potential scan rate of 10 mV/s. Temperature 22±1°C, working / reference / counter electrodes glassy carbon / SCE / Pt. The potential axis is defined *versus* the normal hydrogen electrode.

The pH dependence of the potentials could accurately be measured between pH 5 and pH 9. Below pH 5 the response became unstable and broad, while the FMN signal increased with time. This indicates that the flavodoxin looses its cofactor at low pH. Above pH 9 the response also deteriorated, probably due to deprotonation of neomycin. As can be seen in Figure 3.2, no significant differences are observed in pH dependence of $E_1$ between wild-type, C69A and C69S flavodoxin. At least two p$K$'s for the reduced species (*i.e.* the hydroquinone form) and one p$K$ for the oxidized species (*i.e.* the semiquinone form) were required to fit the observed pH dependence:

$$E_{\mathrm{m}} = E^{\mathrm{a}} + \frac{RT}{F}\ln\left[\frac{[\mathrm{H}^+]^2 + [\mathrm{H}^+]K_{\mathrm{red},1} + K_{\mathrm{red},1}K_{\mathrm{red},2}}{[\mathrm{H}^+] + K_{\mathrm{ox}}}\right] \tag{3.1}$$

[Clark, 1960] . Points with error bars were not included in the fit because of the unreliability of the observed potential (peak-to-peak separations of 73, 78 and 75 mV for C69A at pH 4.67, and for wild-type at pH 4.5 and 5.0 respectively). Estimated uncertainties for all other
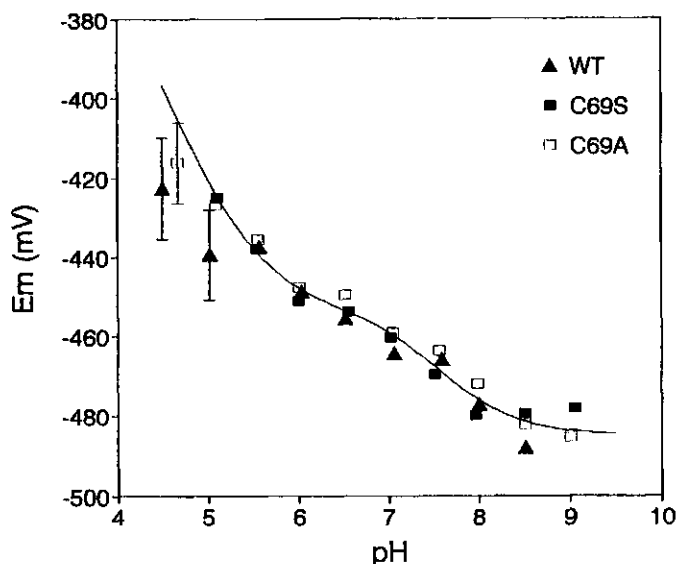
**Figure 3.2.** pH dependence of the semiquinone/hydroquinone redox potentials $E_1$ of wild-type (▲), C69A (□) and C69S (■) flavodoxin. The solid line is a least-squares fit assuming a model with three redox-linked p$K$'s: p$K_{red,1}$ = 5.39 ± 0.08, p$K_{ox}$ = 7.29 ± 0.14, p$K_{red,2}$ = 7.84 ± 0.14. Data points with error bars were not included in the fit. The estimated uncertenties for all other data are between 3 and 9 mV. Experimental conditions were as described in the text.

data were between 3 and 9 mV. An unweighted chi-square fit to the data yields: p$K_{red,1}$ = 5.39 ± 0.08, p$K_{ox}$ = 7.29 ± 0.14, p$K_{red,2}$ = 7.84 ± 0.14, $E_m^7$ = −459 ± 4 mV and a constant potential at high pH of −485 ± 4 mV. A fit of the collected FMN data (not shown) with

$$E_m = E^a + \frac{RT}{2F} \ln \left[ \frac{[H^+]^3 + K_{red}[H^+]^2}{[H^+] + K_{ox}} \right] \tag{3.2}$$

yields a p$K$ of 6.41 ± 0.15 for the protonation of reduced FMN and $E_m^7$ is −215 ± 4 mV when the p$K$ for the oxidized species is fixed at 10.4 [Draper & Ingraham, 1968]. This p$K_{red}$ is in good agreement with the value found in Chapter 2 and the reported values between 6.4 and 6.8 (see [Ksenzhek & Petrova, 1983] and references cited therein).

Measurements of the temperature dependence were performed at pH 6 because of the more stable response under slightly acidic conditions. Within the experimental error no difference was observed in the dependence of $E_1$ on temperature (0 to 30°C) between wild-type and the two mutants (Figure 3.3). No breakpoint was observed as with *D. vulgaris*
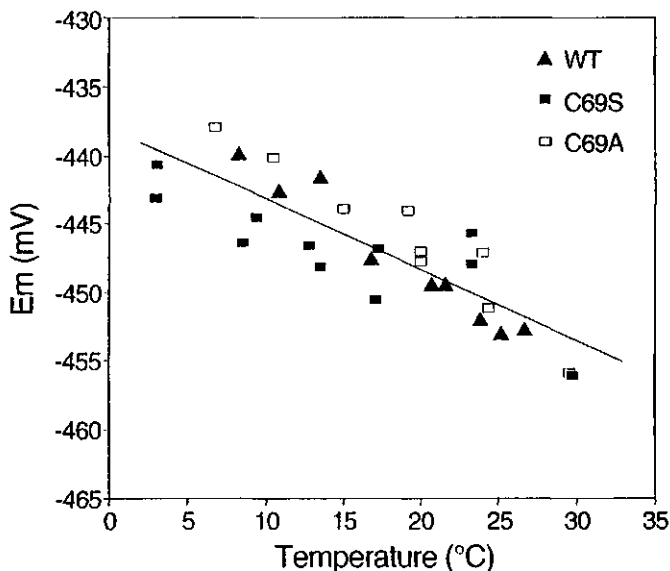
**Figure 3.3.** Temperature dependence of the semiquinone/hydroquinone redox potentials $E_1$ of wild-type (▲), C69A (□) and C69S (■) flavodoxin. The solid line is a least-squares fit using all data. The estimated uncertenties vary between 3 and 9 mV. Experimental conditions were as described in the text.

flavodoxin (Chapter 2), although above 30°C the response became too unstable and the peak-to-peak separation too large to give reliable potential readings. Linear regression using data of the three proteins yields a slope of −0.52 ± 0.06 mV/K ($r^2$ = 0.704728). The calculated potential at 22°C and pH 6 is −449 ± 3 mV, $\Delta H° = 28.6 \pm 1.5$ kJ/mol, $\Delta S° = -50 \pm 6.2$ $J \cdot mol^{-1} \cdot K^{-1}$ and the entropy change of the reaction center $\Delta S°_{rc} = S°_{red} - S°_{ox} = \Delta S° + \Delta S°(H2) / 2 = 15.2 \pm 6.2$ $J \cdot mol^{-1} \cdot K^{-1}$ [Taniguchi *et al.*, 1980 and references cited therein; see also Chapter 2].

### 3.3.2 Redox titrations

The results obtained with cyclic voltammetry were verified by EPR-monitored redox titrations of wild-type and C69A flavodoxin at both high and low pH. Using dithionite it was not possible to obtain potentials below approximately −400 mV at pH 6 and −450 mV at pH 8.5. To obtain data points below these potentials, titanium(III) citrate was used as reducing agent. Although Ti(III) gives pronounced EPR signals around $g$=2, thus overlapping the flavodoxin semiquinone signal, this was not a problem at low concentrations Ti(III). At higher
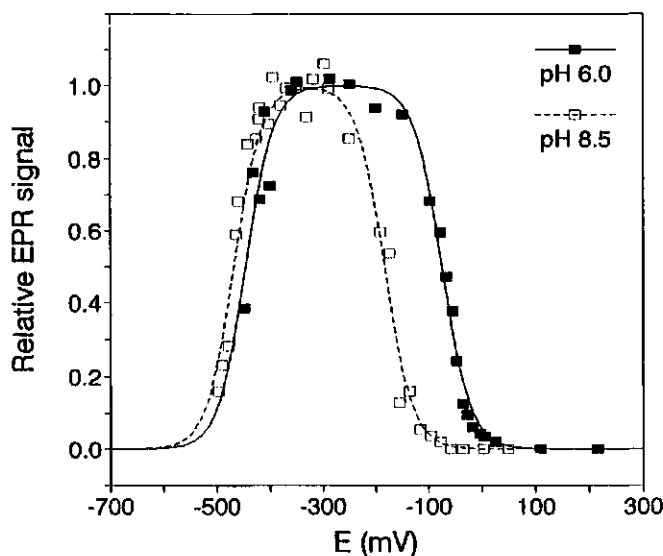
**Figure 3.4.** Mediated redox titration of wild-type flavodoxin at pH 6 (solid squares) and pH 8.5 (open squares) monitored by the EPR spectrum of the semiquinone radical. Data were fitted to the Nernst equation for two consecutive one-electron reductions steps and normalised to the fitted maximum. The semiquinone radical signal was corrected for dilution and relative intensities are shown. Experimental conditions were as described in the text.

concentrations Ti(III) it became difficult to quantitate the semiquinone signal. Moreover, at higher concentrations Ti(III) the potential became unstable due to the lack of stabilizing low-potential mediators until it was no longer possible to lower the potential using Ti(III). Presumably, at these low potentials hydrogen is formed at the platinum electrode. However, a further decrease of the EPR signal of the semiquinone was observed with increasing concentrations of titanium(III) citrate. Subsequent reoxidation by air or by titration with ferricyanide yielded a recovery (> 80%) of the semiquinone signal at intermediate potentials. This observation is indicative for a gradual and reversible reduction of the flavodoxin semiquinone by Ti(III) and dithionite.

Data obtained at stable and reliable potentials from clearly interpretable EPR spectra are collected in Figures 3.4 and 3.5. The data were fitted to the Nernst equation for two consecutive one-electron redox steps:

$$\frac{[sq]}{[Fld_{total}]} = \frac{1}{1 + \exp\left(\frac{F}{RT}(E-E_2)\right) + \exp\left(-\frac{F}{RT}(E-E_1)\right)} \tag{3.3}$$
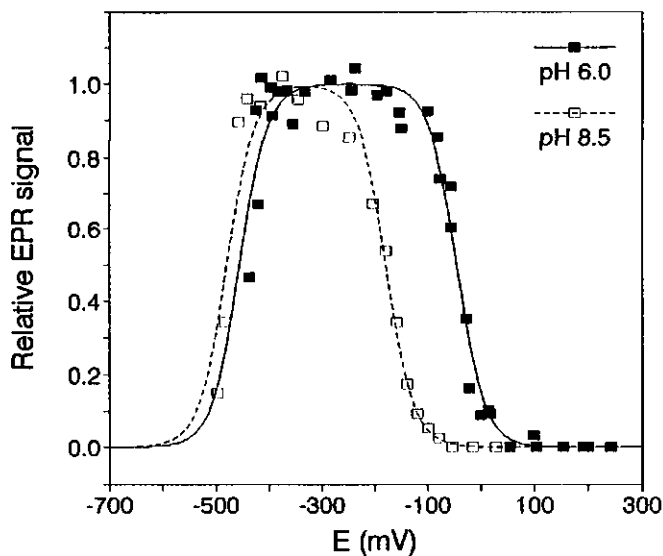
**Figure 3.5.** Mediated redox titration of C69A mutant flavodoxin at pH 6 (solid squares) and pH 8.5 (open squares) monitored by the EPR spectrum of the semiquinone radical. Data were fitted to the Nernst equation for two consecutive one-electron reductions steps and normalised to the fitted maximum. The semiquinone radical signal was corrected for dilution and relative intensities are shown. Experimental conditions were as described in the text.

and normalized to the fitted maximum. The resulting midpoint potentials for the first and second reduction step ($E_2$ and $E_1$, respectively) of wild-type and C69A flavodoxin at both low and high pH are shown in Table 3.1.

## 3.4 Discussion

The electrochemical behaviour of the C69A and C69S flavodoxin mutants is similar to that observed for other flavodoxins: the presence of the promoter neomycin is necessary to obtain a fast en reversible response of the semiquinone/hydroquinone couple at the glassy carbon electrode. Starting with the oxidized form of either C69A or C69S flavodoxin, the response for the semiquinone/hydroquinone couple is fully developed within one scan (10 to 20 mV/s), whereas no response for the quinone/semiquinone transition is observed. Prolonged scanning causes the colour of the flavodoxin solution to change from yellow (indicative for presence of the quinone form) to blue (indicative for presence of the semiquinone form). This confirms the proposed formation of semiquinone by both FMN-mediated electron transfer to

**Table 3.1.** Redox potentials of wild-type, C69A, and C69S flavodoxin obtained by cyclic voltammetry and by EPR-minitored redox titrations.

|  | pH | CV $E_1$ (mV) | EPR $E_1$ (mV) | $E_2$ (mV) |
|---|---|---|---|---|
| Wild-type | 6.0 | −449 ± 4 | −446 ± 10 | −74 ± 10 |
| C69A | 6.0 | −448 ± 3 | −456 ± 10 | −45 ± 10 |
| C69S | 6.0 | −451 ± 4 | | |
| pH-fit | 6.0 | −448 ± 4 | | |
| T-fit | 6.0 | −449 ± 3 | | |
| Wild-type | 8.5 | −488 ± 7 | −468 ± 10 | −183 ± 10 |
| C69A | 8.5 | −483 ± 4 | −480 ± 10 | −179 ± 10 |
| C69S | 8.5 | −480 ± 3 | | |
| pH-fit | 8.5 | −481 ± 4 | | |

the fully oxidized flavodoxin and comproportionation of one quinone and one hydroquinone to two semiquinone flavodoxin molecules (Chapter 2). These findings also show that it is not necessary to start with flavodoxin in the semiquinone form, as was suggested by Bagby *et al.* [1991] for *A. chroococcum* flavodoxin.

In addition to neomycin, dithiotreitol is required to obtain a reversible semiquinone-/hydroquinone response of wild-type *A. vinelandii* flavodoxin II. No significant increase of the free FMN response is observed for wild-type flavodoxin in absence of dithiotreitol. Therefore, it can be concluded that denaturation of the wild-type protein on the carbon surface by sulphur chemistry does not occur. Dithiotreitol is not electrochemically active at the carbon electrode but specifically reacts with cystine bridges (it does not reduce oxidized flavodoxin, as indicated by the observed yellow colour of the protein in the presence of dithiotreitol). It probably prevents electrochemically induced dimerization (*i.e.* oxidation of cysteine residues) of flavodoxin. Presumably, dimerization hampers the electron transfer between the electrode and FMN since FMN molecules in the dimers will be less accessible for electron transfer to the electrode. This finding is consistent with earlier results which demonstrate that flavodoxin dimers have no biological activity [Yoch, 1975].

No significant difference in electrochemical properties between wild-type flavodoxin and the two mutants C69A and C69S flavodoxin were observed (the apparent lower potentials of the C69S mutant in Figure 3.3 are within the estimated uncertainties and are not found in Figure 3.2). This implies that replacement of Cys69 by either an alanine or a serine residue has no measurable influence on the dielectric properties and the structure of the protein although the residue is situated in the immediate vicinity of the FMN. The semiquinone-/hydroquinone potential at pH 8 of $-476 \pm 5$ mV for recombinant *A. vinelandii* flavodoxin II lies in between reported potentials of $-515$ mV at pH 8 for flavodoxin II isolated from *A. vinelandii* (strain ATCC 478) [Klugkist *et al.*, 1986] and $-458$ mV at pH 8 for recombinant dephospho-flavodoxin from *A. vinelandii* (strain OP, Berkeley) expressed in *E. coli* [Taylor *et al.*, 1990].

The observed pH dependence of the semiquinone/hydroquinone redox potential $E_1$ differs significantly from the one-$pK_{red}$ dependencies found for several flavodoxins, including *A. vinelandii* flavodoxin [Chapter 2; Mayhew *et al.*, 1969; Klugkist *et al.*, 1986; Schopfer *et al.*, 1991]. In order to fit the data at least two protonation sites with redox-linked p$K$'s must be assumed to be present in the vicinity of the isoalloxazine ring of FMN. The first p$K_{red}$ of 5.4 is comparable with the low p$K_{red}$ of 4.8 observed for *D. vulgaris* flavodoxin (Chapter 2) and the reported p$K_{red}$ of 5.8 for *M. elsdenii* flavodoxin [Mayhew *et al.*, 1969]. The additional protonation site in *A. vinelandii* flavodoxin (p$K_{ox}$ = 7.3, p$K_{red,2}$ = 7.8) causes a further lowering of the potential by about 30 mV at high pH. It is tentative to ascribe physiological relevance to this observation. Since the internal pH in *A. vinelandii* bacteria is found to be around pH 8 [Laane *et al.*, 1980] the additional protonation site could provide the necessary driving force for electron transfer to nitrogenase.

The temperature dependence of the semiquinone/hydroquinone potential $E_1$ is not very pronounced. The small reaction entropy indicates that there is not much difference in mobility of the FMN between the semiquinone and the hydroquinone form in the protein. The slope of -0.52 mV/K is less steep than the temperature dependence observed for *D. vulgaris* flavodoxin ($-1.86$ mV/K at pH 7, see Chapter 2), but no direct comparison can be made since $\Delta S^\circ$ can be pH-dependent (due to a different number of reactants when reduction is coupled to protonation).

EPR-monitored redox titrations of flavodoxin at pH 6 and 8.5 confirm that the midpoint potentials measured using cyclic voltammetry originate from the semiquinone-/hydroquinone couple of flavodoxin. Table 3.1 shows that neither the promoter neomycin nor dithiotreitol have a measurable influence on the semiquinone/hydroquinone redox potential of flavodoxin as measured in the cyclic voltammetry experiments. The midpoint potentials of the quinone/semiquinone couple $E_2$ at pH 8.5 give essentially identical values for wild-type and C69A flavodoxin. However, at pH 6.0 the potentials differ slightly more than the estimated errors of the redox titration experiments allow for. Since such a difference in $E_2$ at pH 6 would imply that replacement of Cys69 only has an effect on the quinone form below

pH 8.5 but neither on the semiquinone or on the hydroquinone state, it is unlikely that the observed difference at pH 6.0 is significant. It is not clear whether $E_2$ shows a pH-dependent behaviour of $-59$ mV/pH, as was found for other flavodoxins in which reduction of the quinone form to yield the neutral semiquinone is coupled to a protonation [Ludwig & Luschinsky, 1992]. The existence of a p$K$ of 7.3 for the semiquinone state suggests a non-linear dependence of $E_2$, unless a p$K$ of around 7.3 exists for the quinone state. The value for $E_2$ at pH 8.5 ($-180$ mV) is less negative than the reported quinone/semiquinone potential of $-224$ mV at pH 8 for the recombinant dephospho-flavodoxin reported by Taylor *et al.* [1990]. Reported values of the quinone/semiquinone redox potential $E_2$ of *Azotobacter vinelandii* (strain OP and strain OP, Berkeley) flavodoxins containing a covalently attached phosphate group vary from $+50$ mV at pH 8.2 to $-273$ mV at pH 7.7 [Barman & Tollin, 1972; Yoch, 1972; Watt, 1979].

## 3.5    Conclusions

The electrochemical behaviour of the two mutant flavodoxins is similar to that observed with *D. vulgaris* flavodoxin. To obtain a reversible response of wild-type flavodoxin dithiotreitol is required, probably to prevent dimerization by formation of cystine bridges. No difference between the wild-type flavodoxin and the two mutants was observed. This means that Cys69 has no measurable influence on the redox properties of the flavin. The dependence of the semiquinone/hydroquinone midpoint potentials on temperature is not very pronounced. The dependence of the semiquinone/hydroquinone potential on pH does not follow the usual one-p$K$ model reported for flavodoxins. At least two protonation sites with redox-linked p$K$'s are required to fit the data. The semiquinone/hydroquinone midpoint potentials obtained by the EPR-monitored redox titrations and by cyclic voltammetry are equal. This is true for both the wild-type and the C69A mutant and at both high and low pH.

## 3.6 References

Armstrong, F.A., Hill, H.A.O., Oliver, B.N. & Walton, N.J. (1984) *J. Am. Chem. Soc. 106*, 921.

Bagby, S., Barker, P.D., Hill, H.A.O., Sanghera, G.S., Dunbar, B., Ashby, G.A., Eady, R.R. & Thorneley, R.N.F. (1991) *Biochem. J. 277*, 313.

Barker, P.D., Hill, H.A.O., Sanghera, G.S., Eady, R.R. & Thorneley, R.N.F. (1988) *Biochem. Soc. Trans. 16 (626th meeting)*, 959.

Barman, B.G. & Tollin, G. (1972) *Biochemistry 11*, 4755.

Bianco, P., Haladjian, J., Manjaoui, A. & Bruschi, M. (1988) *Electrochim. Acta 33*, 745.

Boylan, M.H. & Edmondson, D.E. (1990) *Biochem. J. 268*, 745.

Clark, W.M. (1960) *Oxidation-reduction potentials of organic systems*, Waverly Press, Baltimore.

Deistung, J. & Thorneley, R.N.F. (1986) *Biochem. J. 239*, 69.

Draper, R.D. & Ingraham, L.L. (1968) *Arch. Biochem. Biophys. 125*, 802.

Edmondson, D.E. & James, T.L. (1979) *Proc. Natl. Acad. Sci. USA 76*, 3786.

Hagen, W.R. (1989) *Eur. J. Biochem. 182*, 523.

Klugkist, J., Voorberg, J., Haaker, H. & Veeger, C. (1986) *Eur. J. Biochem. 155*, 33.

Ksenzhek, O.S. & Petrova, S.A. (1983) *Bioelectrochem. Bioenerg. 11 (J. Electroanal. Chem 156)*, 105.

Laane, C., Krone, W., Konings, W., Haaker, H. & Veeger, C. (1980) *Eur. J. Biochem. 103*, 39.

Ludwig, M.L. & Luschinsky, C.L. (1992) in *Chemistry and biochemistry of flavoenzymes Vol. 3*, (Müller, F., Ed.), CRC press, Boca Raton, p427.

Mayhew, S.G. (1978) *Eur. J. Biochem. 85*, 535.

Mayhew, S.G., Foust, G.P. & Massey, V. (1969), *J. Biol. Chem. 244*, 803.

Nicholson, R.S. (1965) *Anal. Chem. 37*, 1351.

Pierik, A.J. & Hagen, W.R. (1991) *Eur. J. Biochem. 195*, 505.

Scherings, G., Haaker, H. & Veeger, C. (1977) *Eur. J. Biochem. 77*, 621.

Schopfer, L.M., Ludwig, M.L. & Massey, V. (1991) in *Flavins and Flavoproteins Vol. 1990*, Walter de Gruyter & Co, Berlin, p399.

Tanaka, M., Haniu, M., Yasunobu, K.T. & Yoch, D.C. (1977) *Biochemistry 16*, 3525.

Taniguchi, V.T., Sailasuta-Scott, N., Anson, F.C. & Gray, H.B. (1980) *Pure & Appl. Chem. 52*, 2275.

Taylor, M.F., Boylan, M.H. & Edmondson, D.E. (1990) *Biochemistry 29*, 6911.

Thorneley, R.N.F., Abell, C., Ashby, G.A., Drummond, M.H., Eady, R.R., Huff, S., Macdonald, C.J. & Shneier, A. (1992) *Biochemistry 31*, 1216.

Thorneley, R.N.F., Ashby, G.A., Eady, R.R., Kazlauskaite, J. & Hill, H.A.O. (1993), in *9th International congress on nitrogen fixation, Cancun, Mexico*, (Palacios, R., Mora, J. & Newton, W.E., Eds.), Kluwer Academic Publishers, Dordrecht, The Netherlands, p152.

Tollin, G. & Edmondson, D.E. (1980) *Methods in Enzymology 69*, 392.

Van Dijk, C., Van Leeuwen, J.W. & Veeger, C. (1982) *Bioelectrochem. Bioenerg. 9 (J. Electroanal. Chem. 141)*, 743.

Van Mierlo, C.P.M., Van den Berg, W.A.M., Van Berkel, W.J.H., Van Dongen, W.M.A.M. & Steensma, E. (1995), *Folding and stability of wild-type, C69A and C69S Azotobacter vinelandii flavodoxin*, in preparation.

Watt, G.D. (1979) *Anal. Biochem. 99*, 399.

Yates, M.G. (1972) *FEBS letters 27*, 63.

Yoch, D.C. (1972) *Biochem. Biophys. Res. Comm. 49*, 335.

Yoch, D.C. (1975) *Arch. Biochem. Biophys. 170*, 326.

Zehnder, A.J.B. (1976) *Ph.D. Thesis*, Federal Institute of Technology (ETH), Zürich, Switzerland.

# Chapter 4

**Calculation of the absorbance by integration of the concentration distribution in long optical path length thin-layer electrochemical cells.**

## 4.1 Introduction

In common semi-infinite bulk electrochemical techniques only the current, charge and potential are monitored. The observed reactions are located in a thin layer at the electrode and bulk reactions are limited by mass transport. Therefore, it is not always possible to obtain detailed information about processes occurring in the bulk solution. One approach to avoid diffusion limitation involves decreasing the volume of the cell without decreasing the surface area of the electrode. This can be achieved by confining a small volume to a thin layer at the electrode. An additional advantage of such a thin layer electrochemical cell is the small amount of material required. This is important for electrochemistry on redox enzymes. To obtain additional information not accessible by normal electrochemical experiments, one can pass a light beam through the solution (directly or using reflection) and measure the absorbance or the fluorescence. There are two classes of spectroelectrochemical cells. In one type the light beam passes perpendicular to an optically transparent electrode. This electrode may consist of a small film of semiconductor or metal, deposited on a transparent substrate, or be made of a fine wire mesh minigrid or a porous conductor [Tyson & West, 1979; Sagara *et al.*, 1992]. Because the concentration gradient is oriented parallel to the light beam, the overall absorbance can be obtained by integrating (adding) local absorbances and is independent of the distribution of the chromophores [Brewster & Anderson, 1989]. A disadvantage of such cells is the relative insensitivity because of the short path length. In the second type of cell the light beam passes at grazing incidence over the electrode surface [Jan & McCreery, 1986; Xie & Dong, 1990; Nagy & Anderson, 1991]. In this setup there are no restrictions to the electrode material or the volume of the bulk solution. The absorbance can be calculated from the transmittance, integrated perpendicular to the light beam and depends on the distribution of the chromophores [Brewster & Anderson, 1991]. The sensitivity can be increased by increasing the path length of the light beam through the solution.

In two recent publications Wei *et al.* give the theoretical and numerical solution for calculating the concentration distribution and the absorbance during chronoamperometry in long optical path thin-layer electrochemical cells [Wei *et al.*, 1992a; Wei *et al.*, 1992b]. In this chapter some critical remarks are made regarding this work, and a new numerical approximation of the error function will be presented.

- 65 -

## 4.2 Theory

Summarizing the calculations of Wei *et al.* [1992a,b] the absorbance of a long optical path length cell is:

$$A(t) = \log w - \log \int_0^w 10^{-\varepsilon lc(x,t)} dx \tag{4.1}$$

where $w$ is the width of the plane of incidence, $\varepsilon$ is the molar absorption coefficient, $l$ is the path length, $c$ is the concentration of the absorbing species, $x$ is the distance from the electrode and $t$ is the time. This integral equation can be evaluated numerically by a two-point average stepwise integration known as the extended trapezoidal rule [Press *et al.*, 1989]:

$$A(t) = \log n - \log \frac{1}{2}\sum_{j=1}^{n} \left( 10^{-\varepsilon lc(x_{j-1},t)} + 10^{-\varepsilon lc(x_j,t)} \right) \tag{4.2}$$

where n is the number of discrete steps between $x=0$ and $x=w$ and the position $x_k = k \cdot w/n$ ($0 \leq k \leq n$).

For the reaction

$$Ox + ne^- \underset{k_b}{\overset{k_f}{\rightleftharpoons}} Red \tag{4.3}$$

starting with 100% Ox in solution and with a planar electrode at constant potential and a semi-infinite bulk solution, the concentration of Ox is given by

$$c_O(x,t) = c_O^* - \frac{k_f c_O^*}{H\sqrt{D_O}} \left[ \text{erfc}\left( \frac{x}{\sqrt{4D_O t}} \right) - \exp\left( \frac{Hx}{\sqrt{D_O}} + H^2 t \right) \text{erfc}\left( H\sqrt{t} + \frac{x}{\sqrt{4D_O t}} \right) \right] \tag{4.4}$$

with

$$H = k_f/\sqrt{D_O} + k_b/\sqrt{D_R} \tag{4.5}$$

$$k_f = k_s \exp\left[-\alpha n F (E - E^{O'})/RT\right] \tag{4.6}$$

and

$$k_b = k_s \exp\left[(1 - \alpha) n F (E - E^{O'})/RT\right] \tag{4.7}$$

where $c_O^*$ is the bulk concentration of Ox (*i.e.* the initial concentration), $D_O$ and $D_R$ are the diffusion coefficients of Ox and Red and $\alpha$ is the cathodic transfer coefficient. Note, that the equivalent of equation (4.4) given in the work of Wei *et al.* (*cf.* equation (13) in [Wei *et al.*, 1992b]) is incorrect due to errors made in the Laplace back-transformation, *i.e.* the last step in its derivation. When a sufficiently negative potential is applied and $k_f$ is large enough (*i.e.* no kinetic limitation), equation (4.4) is reduced to the equation, descibing the concentration profile under "Cottrell conditions" [Bard & Faulkner, 1980]:

$$c_O(x,t) = c_O^* \operatorname{erf}\left(x / \sqrt{4 D_O t}\right) \tag{4.8}$$

Under the same conditions (Red initially absent, planar electrode, sufficiently negative potential, large $k_f$) but with a cell boundary parallel to the electrode at a distance $w$, the concentration in time of Ox at a distance $x$ from the electrode is given by [Wei *et al.*, 1992b]:

$$c_O(x,t) = c_O^* \frac{4}{\pi} \sum_{m=1}^{\infty} \frac{1}{2m-1} \exp\left[\frac{-(2m-1)^2 D_O \pi^2 t}{(2w)^2}\right] \sin\left[\frac{(2m-1)\pi x}{2w}\right] \tag{4.9}$$

To simplify the equations (4.8) and (4.9), dimensionless time and distance parameters can be defined for the thin layer cell: $t_N = t D_O/w^2$ and $x_N = x/w$. With these parameters, the equations can be written as:

$$c_O(x_N, t_N)/c_O^* = \operatorname{erf}\left[x_N/2\sqrt{t_N}\right] \tag{4.8b}$$

and

$$c_O(x_N,t_N)/c_O^* = \sum_{m=1}^{\infty} \frac{2}{P_m} \exp\left[-P_m^2 t_N\right] \sin\left[P_m x_N\right] \tag{4.9b}$$

with $P_m=(m-\tfrac{1}{2})\pi$. Note that equation (4.8) is only valid in thin layer cells as long as bulk solution with $c_O(x,t)=c_O^*$ is present. This implies that the diffusion layer boundary $\delta$ has not reached the cell wall opposite to the electrode ($\delta<w$). The definition of diffusion layer boundary depends largely on the desired accuracy and on the model used to describe the concentration profile [Bard & Faulkner, 1980; Lyklema, 1991]. Describing diffusion by a random walk model, the one-dimensional root-mean-square displacement $\Delta=\sqrt{(2Dt)}$. Using a linear approximation for the concentration profile, $\delta(t)=2\sqrt{(Dt)}$ is found. The largest value found in literature ([Bard & Faulkner, 1980; Lyklema, 1991] and references cited therein) is $\delta(t)=6\sqrt{(Dt)}$. This means that $\delta<w$ when $t_N<1/36$. This latter value will be used in the present work.

In treating diffusion problems like the above mentioned, one frequently encounters the error function, that is, the integrated normal error curve:

$$\mathrm{erf}(x) = \frac{2}{\sqrt{\pi}} \int_0^x e^{-y^2} dy \tag{4.10}$$

Because this function approaches unity as $x$ becomes large, the complement of the error function can be defined as

$$\mathrm{erfc}(x) = 1-\mathrm{erf}(x) = \frac{2}{\sqrt{\pi}} \int_x^{\infty} e^{-y^2} dy \tag{4.11}$$

The integral has no analytical solution. Therefore, computing equations containing this function is often done numerically, or series approximations are used. The series representations of the error function usually require a large number of terms to obtain an acceptable accuracy and the validity is restricted to a finite range [Press $et\ al.$,1989; Bard & Faulkner, 1980; De Vries, 1965]. Here, an alternative approximation is presented using only three terms and valid for all positive values of $x$:

$$\mathrm{erf}(x) \approx 1-e^{ax+bx^2+cx^3} \qquad (x\geq0) \tag{4.12}$$

when $a$, $b$ and $c$ are negative, or the equivalent form

$$\text{erf}(x) \approx 1-(A\,(B\,(C)^x)^x)^x \qquad\qquad (x\geq 0) \qquad\qquad\qquad (4.12b)$$

with $A=\exp(a)$, $B=\exp(b)$ and $C=\exp(c)$. Note, that both $\text{erf}(x)$ and the right hand side of equation (4.12), $f(x)$, approach unity when $x$ becomes large and $\text{erf}(0)=f(0)=0$. The approximation does not hold for negative values of $x$, but the relation $\text{erf}(-x)= -\text{erf}(x)$ can be used if necessary.

## 4.3  Results and Discussion

### 4.3.1  Approximation of the error function.

The procedure to calculate the values of the parameters a,b and c consists of three steps. Firstly, the integral equation (4.10) has to be evaluated numerically. This is done by two-point average stepwise integration (the extended trapezoidal rule) of the normal error curve:

$$\text{erf}(x_j) = \frac{\Delta y}{\sqrt{\pi}} \sum_{k=1}^{j} (e^{-y_{k-1}^2} + e^{-y_k^2}) \qquad\qquad\qquad (4.13)$$

with $y_k=k\Delta y$, $x_j=j\Delta x$ and $\Delta x=\Delta y$. Here, $\Delta x=0.01$ and the interval $x=0$ to $x=3$ ($j=0$ to $j=300$) are used. The error associated with the step size $\Delta x=0.01$ was estimated to be smaller than $1\cdot 10^{-5}$.

Secondly, starting values for the three parameters have to be found. According to the Leibnitz rule [Bard & Faulkner, 1980] the first derivative of the error function is the normal error curve:

$$\frac{d}{dx} \text{erf}(x) = \frac{2}{\sqrt{\pi}} e^{-x^2} \qquad\qquad\qquad (4.14)$$

Because this is a simple function of $x$, the parameters can now be estimated by evaluating the first, second, and third derivatives ($\phi=1$, 2 and 3) of $\text{erf}(x)$ and the exponential function at $x=0$:

$$\left[\frac{d^\phi}{dx^\phi}\text{erf}(x)\right]_{x=0} = \left[\frac{d^\phi}{dx^\phi}(1-e^{ax+bx^2+cx^3})\right]_{x=0} \qquad\qquad (4.15)$$

Calculation of the first derivatives results in $a=-2/\sqrt{\pi}$. Using this value and the second derivatives yields $b=-2/\pi$. Using these values of $a$ and $b$ and the third derivatives, the parameter $c=(2\pi-8)/(3\pi\sqrt{\pi})$. Without further optimization this already result in a chi-square of $8.80\cdot10^{-4}$ ($n=300$) and a maximum error of 0.36%. The parameter chi-square is the unweighted least-squares parameter and is defined as [Press *et al.*, 1989]:

$$\chi^2(a,b,c,n) = \sum_{j=0}^{n} \left[ 1 - \exp(ax_j + bx_j^2 + cx_j^3) - \mathrm{erf}(x_j) \right]^2 \tag{4.16}$$

The error at any point is the difference between the two functions, relative to the error function:

$$e(x_j,a,b,c) = \frac{1 - \exp(ax_j + bx_j^2 + cx_j^3) - \mathrm{erf}(x_j)}{\mathrm{erf}(x_j)} \tag{4.17}$$

No higher order terms $d\cdot x^4$ or $e\cdot x^5$ are added to the exponential function because the values for the parameters d and e, obtained by evaluating the fourth and fifth derivatives of $f(x)$ and $\mathrm{erf}(x)$ at $x=0$, are small and positive: $d=(4\pi-12)/(3\pi^2)$ and $e=(-3\pi^2+28\pi-48)/(15\pi^2\sqrt{\pi})$. With these terms the function strongly deviates from unity as $x$ becomes large and at small values of $x$ the contribution of these terms is insubstantial.

Finally, a non-linear optimization is performed [Press *et al.*, 1989], using the Optimizer routine in the spreadsheet program Quattro Pro, version 4.0 (Borland International, Inc.). The initial estimates of the variables in each iteration were calculated by linear extrapolation from a tangent vector, forward differencing was used for estimates of partial derivatives and the search direction was computed quasi-Newtonian [Press *et al.*, 1989]. The curve fittings were done by minimizing chi-square starting from the calculated values of the parameters. In Table 4.1, the results are summarized. A very good least-squares fit can be obtained, allowing all three parameters to vary. With this fit, however, the absolute value of the error is large for small values of $x$ (Figure 4.1). The reason for this large error is the large deviation of the first-order parameter, $a$, from its starting point: The limiting value of the error for $x$ approaching zero is given by $-1-\frac{1}{2}a\sqrt{\pi}$ (using l'Hôpital's rule). To obtain a better relative fit, the absolute value of the error at any point $x_j$ was minimized. Because the results from this fit are slightly better when the initial estimates of the variables are used as starting values, as compared to the minima obtained by starting from the chi-square fit results, the former are listed in Table 4.1. As can be seen, the maximum absolute value of the difference between $f(x)$ and $\mathrm{erf}(x)$ is only slightly increased, while the absolute value of the error drops below 0.05% when all three parameters are adjusted. This accuracy will be more than

**Table 4.1.** Comparision of the error function erf(x) and the approximating function $f(x)=1-\exp(ax+bx^2+cx^3)$ for different values of the parameters.

| parameters | | | $\chi^2\times10^5$ | $f(x_j)-\text{erf}(x_j)$ | | $e(x_j)$ | |
|---|---|---|---|---|---|---|---|
| $a$ | $b\times10$ | $c\times10^2$ | | min. $\times10^3$ | max. $\times10^3$ | min. $\times10^3$ | max. $\times10^3$ |
| $a_0$ | $b_0$ | $c_0$ | 88.03 | 0.000 | 3.27 | 0.000 | 3.58 |
| $a_0$ | $b_0$ | −8.260572 | 5.71 | −0.784 | 0.683 | −1.26 | 0.699 |
| $a_0$ | −6.505188 | −6.910211 | 0.960 | −0.254 | 0.345 | −0.313 | 0.113 |
| −1.123326 | −6.639788 | −6.139661 | 0.335 | −0.241 | 0.161 | −4.48 | 0.317 |
| $a_0$ | $b_0$ | −8.499586 | 6.91 | −0.551 | 0.920 | −0.950 | 0.950 |
| $a_0$ | −6.445195 | −7.541600 | 1.90 | −0.349 | 0.474 | −0.487 | 0.487 |
| −1.127942 | −6.470818 | −7.302408 | 1.38 | −0.332 | 0.389 | −0.448 | 0.448 |

The error function is evaluated using equation (4.13), with $\Delta y=0.01$; the minimizations are started from $a_0=-2/\sqrt{\pi}$, $b_0=-2/\pi$ and $c_0=(2\pi-8)/(3\pi\sqrt{\pi})$; chi-square is evaluated using equation (4.16), with $x_j=j\Delta x$, $\Delta x=0.01$, and $n=300$ ($0 \leq x \leq 3$). In the first row the initial values are used. In the second, third and fourth rows the results of the chi-square minimizations (allowing one, two or all three parameters to vary) are tabulated. In the lower three rows the absolute value of the error (equation (4.17)) is minimized.
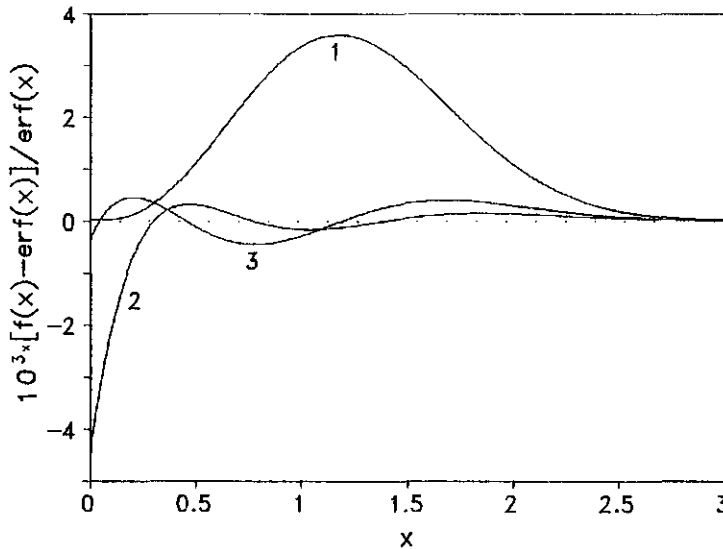


**Figure 4.1.** The difference between the error function erf(x) and the exponential function $f(x)=1-\exp(ax+bx^2+cx^3)$ relative to the error function (The conditions are as in Table 4.1). For trace 1 the initial values of the parameters are used: $a=a_0$, $b=b_0$ and $c=c_0$; for trace 2 the result of the three-parameter chi-square minimization is used: $a=-1.123326$, $b=-0.6639788$ and $c=-0.06139661$; for trace 3 the result of the relative difference optimization is used: $a=-1.127942$, $b=-0.6470818$ and $c=-0.07302408$.
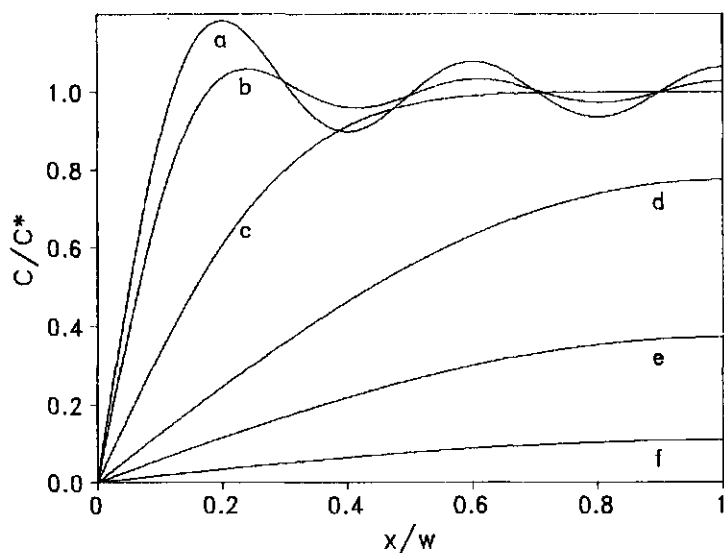
**Figure 4.2.** Concentration profiles at different moments simulated with the first 5 terms of equation (4.9b). Curve a: $t_N=1.757812 \cdot 10^{-5}$; curve b: $t_N-3.375 \cdot 10^{-3}$; curve c: $t_N=1/36$; curve d: $t_N=0.2$; curve e: $t_N=0.5$; curve f: $t_N=1.0$.
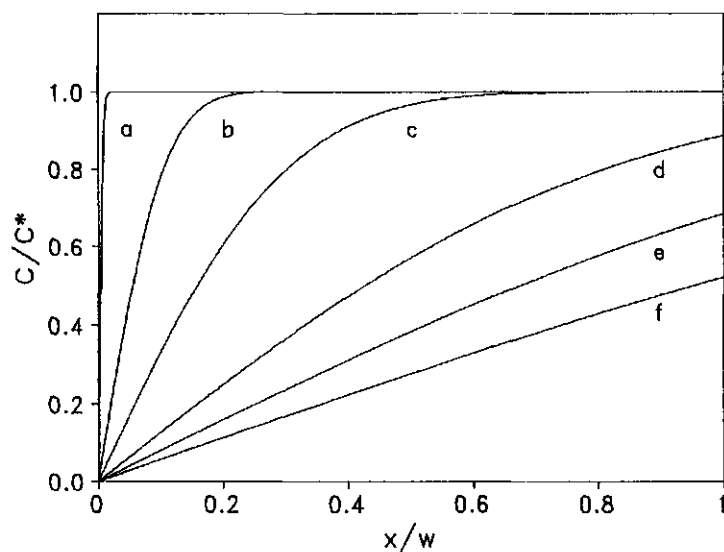


**Figure 4.3.** Concentration profiles at different moments according to the semi-infinite diffusion model (equation (4.8b)). Description of the curves is as in Figure 4.2.
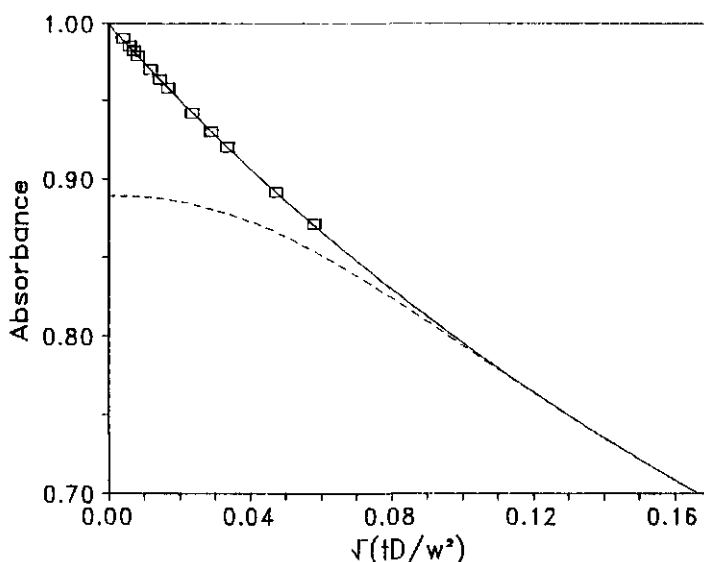
**Figure 4.4.** Simulation of the absorbance *vs.* the square root of time by numerical integration of the concentration profiles. For the integration equation (4.2) is used, n=500 and the initial absorbance is 1. Solid trace: concentrations calculated using equation (4.8b); dashed trace: concentrations calculated using the first 5 terms of equation (4.9b); □ : the "true" absorbance (from Table I in ref. [Wei *et al.*, 1992a]).

sufficient for analyzing measured extinctions. In this chapter, the results of this minimal error fit are used in equation (4.12).

### 4.3.2 Calculation of the concentration profiles and the absorbance.

In Figure 4.2, the concentration profiles at different times are calculated from equation (4.9b) using 5 terms. Trace a and b are the lower and upper limiting times, used by Wei *et al.* (Table I in [Wei *et al.*, 1992a]). In Figure 4.3 the concentration profiles are calculated at the same values of $t_N$ using the semi-infinite diffusion model without kinetic limitation (equation (4.8b)). The error function was calculated using equation (4.12). In Figure 4.4 the concentration profiles are integrated to obtain the absorbance and compared with the "true" values (Table I in [Wei *et al.*, 1992a]). For the integration of the concentration profiles the trapezoidal rule was used (equation (4.2)), the cell width was divided into $n$=500 steps and the initial absorbance $\varepsilon c^* l$=1.

As can be seen clearly, at times $t_N < 1/36$ the approximation of equation (4.9b) with 5 terms is very poor (trace a and b) because of the very steep slope of the concentration

profile. This implies that the "true" absorbance values (Table I in [Wei *et al.*, 1992a]) cannot have been calculated this way. Depending on the actual slope (*i.e.* the timescale) at least 20 to 30 terms are required. At these short times, however, there is still bulk solution present. Therefore, the semi-infinite diffusion model can be applied to calculate the concentration profile. As shown in Figure 4.4, the absorbance values calculated this way are indeed equal (within 0.1%) to the "true" absorbance reported by Wei *et al.* [1992a]. This also implies that the approximation of the error function by equation (4.12) is valid.

At a time $t_N = 1/36$ (trace c in Figures 4.2 and 4.3) the boundary of the diffusion layer reaches the wall of the thin layer cell. Therefore, the semi-infinite diffusion model cannot be used beyond this time. Fortunately, the slope of the concentration profile is now small enough to be approximated by the first 5 terms of equation (4.9b), and the profiles and absorbance values calculated using equations (4.8b) and (4.9b) with 5 terms are equal at $t_N=1/36$. At $t_N > 1/36$ the semi-infinite diffusion model is no longer valid and equation (4.9b) should be used.

## 4.4    Conclusions

In contradiction to the proposal of Wei *et al.* [1992a] the concentration profile in a thin layer electrochemical cell cannot be calculated using only 5 terms of equation (4.9) on a timescale $t_N < 1/36$. Because at these times there is still bulk solution present, the concentrations can instead be calculated using the semi-infinite diffusion model (equations (4.4) or (4.8), depending on the reaction rate). At longer timescales, the diffusion-layer boundary reaches the limit of the thin layer cell. Therefore, equations (4.4) and (4.8) are no longer valid, but now the slope of the concentration profile is small enough to be approximated by the first 5 terms of equation (4.9).

The error function erf($x$) can be approximated to high accuracy (better than 0.05% deviation) for all positive values of $x$ by equation (4.12). This function offers a fast calculation and a good compatibility with the exponential functions that are often combined with the error function. The presented approximation is of importance when the error function has to be recalculated many times or when the separate indices of the exponential terms are too high for computation on a personal computer, as in equation (4.4) at small values of $x$ and $t$.

## 4.5 References

Bard, A.J. & Faulkner, L.R. (1980) *Electrochemical Methods. Fundamentals and Applications*, Wiley, New York, p142; p666; p32; p128; p407; p683.

Brewster, J.D. & Anderson, J.L. (1989) *Appl. Spectr. 43*, 710.

DeVries, W.T. (1965) *J. Electroanal. Chem. 9*, 448.

Jan, C.C. & McCreery, R.L. (1986) *Anal. Chem. 58*, 2771.

Lyklema, J. (1991) *Fundamentals of Interface and Colloid Science. Volume 1: Fundamentals*, Academic Press, London, chapter 6.

Nagy, T.R. & Anderson, J.L. (1991) *Anal. Chem. 63*, 2668.

Press, W.H., Flannery, B.P., Teukolsky, S.A. & Vetterling, W.T. (1989) *Numerical Recipes in Pascal*, Cambridge University Press, pp116-148; pp175-211; pp547-598; pp309-374.

Sagara, T., Koide, T., Saito, H., Akutsu, H. & Niki, K. (1992) *Bull. Chem. Soc. Jpn. 65*, 424.

Tyson, J.F. & West, T.S. (1979) *Talanta 26*, 117.

Wei, W.Z., Xie, Q.J. & Yao, S.Z. (1992a) *J. Electroanal. Chem. 328*, 9.

Wei, W.Z., Xie, Q.J. & Yao, S.Z. (1992b) *J. Electroanal. Chem. 334*, 1.

Xie, Y. & Dong, S. (1990) *J. Electroanal. Chem. 284*, 279.

# Chapter 5

## Monitoring flavodoxin semiquinone by cyclic voltabsorptometry.

## 5.1    Introduction

In Chapter 2 an explanation was presented for the complex electrochemistry of flavodoxins. It was shown for *Desulfovibrio vulgaris* flavodoxin that the peak currents of the semiquinone/hydroquinone couple approach a maximum value after a few cycles if comproportionation of fully reduced and fully oxidized flavodoxin occurs in solution, provided that some semiquinone is generated by mediation of electrode-bound FMN. It was also shown (Chapter 3) that the electrochemical response of *Azotobacter vinelandii* flavodoxin is similar to *D. vulgaris* flavodoxin. In this chapter the validity of the proposed mechanism is verified by measuring the absorbance of the semiquinone form of *D. vulgaris* (Hildenborough) flavodoxin during cyclic voltammetry. The term "cyclic voltabsorptomogram" for the resulting plot of absorbance *versus* potential was introduced by Bancroft *et al.*[1981].

A long optical path length thin layer electrochemical cell (LOPTLC) was used, of which the theoretical properties under "Cottrell conditions" (large overpotential, fast electron transfer) are described in the previous chapter. As can be deduced from an extension of Figure 4.4, under these conditions (*i.e.* $E<<E_m$) the bulk of the cell is reduced for more than 99% after dimensionless time $t_N \geq 2$. The cell used in the experiments described in this chapter has a width of 0.2 mm. This means that the timescale for this cell to behave as a thin layer cell is rather large. For example, with a diffusion coefficient $D=1\cdot10^{-10}$ m$^2$/s of *D. vulgaris* flavodoxin more than 99% reduction of the bulk solution is achieved only after 800 seconds, while the time to reduce ferricyanide ($D_o=7.6\cdot10^{-10}$ m$^2$/s [Xie *et al.*, 1993]) for 99% in this cell is about 100 seconds.

Under scanning conditions, the upper limit for the scan rate that can be applied to achieve full reduction of the bulk before the end of the cathodic scan is reached, depends on the difference between the midpoint potential and the lower potential limit of the scan. For a reversible one-electrode transition, more than 99% reduction is achieved if the applied potential is 118 mV lower than the midpoint potential. If the time between this point and the end of the scan is taken to be critical, the flavodoxin semiquinone/hydroquinone midpoint potential $E_1=-413$ mV and the switching potential $E_{low}=-750$ mV, the upper limit of the scan rate is 0.27 mV/s. For ferricyanide with $E_m=437$ mV and $E_{low}=150$ mV, the upper limit of the scan rate is 1.7 mV/s. But although full reduction is achieved at the end of the scan at this scan rate, a large deviation of the ideal thin layer behaviour is to be expected (for a 0.2 mm

layer, even at a ten times slower scan rate still more than 10% deviation from the ideal TLC peak shape will occur [Bard & Faulkner, 1980]). The electrochemical response will in fact be the intermediate of a true thin layer cell and an infinite-bulk cell. This makes it particularly important to account for the concentration profile perpendicular to the light beam when calculating the absorbance, as described in the previous chapter. It is also important to keep in mind that the resulting absorbance is <u>not</u> proportional to the average concentration in the cell as is the case when the light beam passes perpendicular to the electrode surface [Brewster & Anderson, 1989].

## 5.2    Experimental procedures

### 5.2.1    Spectroelectrochemical cell

A demountable two-piece thin layer cell for absorbance measurements at grazing incidence was designed that snugly fits into a normal 1 ml quartz cuvette with inner dimensions of 10 x 4 mm (Figure 5.1). It consists of a glassy carbon electrode (10 x 7 x 1 mm), machined from a standard disc of 15 mm diameter and 2 mm height (type V25, obtained from Le Carbone Loraine, Rotterdam, NL). The other part is a perspex piece of dimensions 10 x 7 x 3 mm. A thin layer of 0.2 mm was machined out of this blocklet, leaving only four triangular spacers (1.5 x 1.5 mm) in the corners. The two sides perpendicular to the light beam were painted black. To be able to demount the cell, a hole was drilled in the bottom of the cuvette and a rubber stopper was fitted. The glassy carbon electrode was connected to the potentiostat by a platinum wire with a tip flattened to 0.2 mm, snugly fitted between the perspex and the carbon but outside the light beam (behind the spacer). The counter electrode was a piece of platinum foil (0.3 mm thick) in contact with the excess solution on top of the cell. The reference electrode (a Radiometer K-401 saturated calomel electrode) was placed into a small volume of saturated KCl and connected to the cell by a plastic tube (0.3 mm internal diameter and 15 cm long) filled with 5% Agar-agar and saturated KCl, positioned directly above the thin layer. The electrode surface area is 66 mm$^2$ and the cell has a thin layer volume of 13 μl. The minimum volume required to obtain good contact of the counter and reference electrodes is about 40 μl. The area of the light beam is 0.8 mm$^2$.

The glassy carbon electrode was cleaned with water and with ethanol, polished (6 μm Metadi Diamond Compound spray on Microcloth polishing cloth, Buehler, USA), activated by soaking it for a few minutes in concentrated nitric acid, rinsed with 0.5 M K$_3$PO$_4$ and with water and dried prior to use. The backside of the electrode was inactivated by applying a very thin film of silicon vacuum grease. The cuvette was filled with about 100 μl of a degassed solution and the two pieces of the cell were placed in the cuvette, making sure that no gas
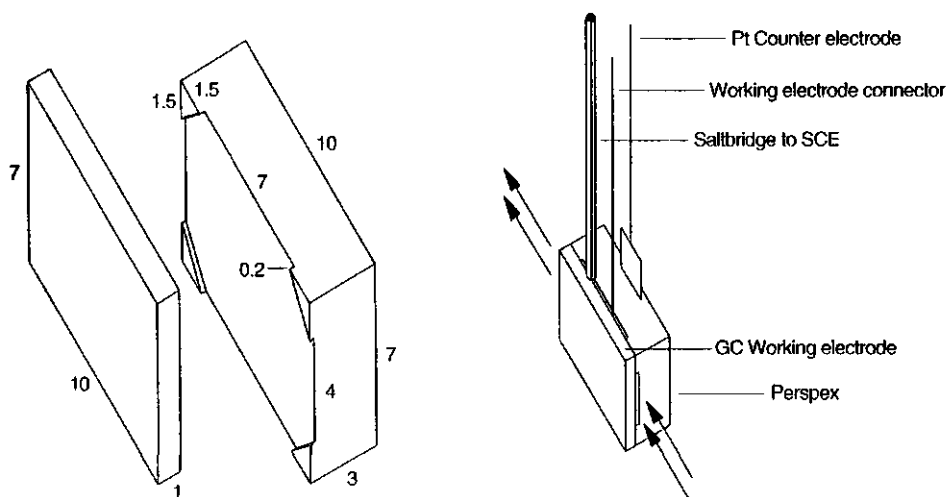
**Figure 5.1.** Schematic representation of the demountable long optical path length spectroelectrochemical cell. The dimensions are given in mm. The two sides of the perspex perpendicular to the light beam were painted black. The whole setup was mounted in a quartz cuvette (10 mm path length and 4 mm wide).

bubbles were trapped in the thin layer. The other components were installed and held in place by a square rubber stopper. The cuvette was kept anaerobic by a steady flow of purified wet argon [Massey & Hemmerich, 1978]. The cuvette was placed in the spectrophotometer (Spectroplus-D, MSE Scientific Instruments, UK) fitted with a black box to accommodate the setup and aligned in the light beam by maximizing the transmittance.

### 5.2.2 Measurement Procedures

The electrodes were connected to an Autolab 10 potentiostat (Eco Chemie, Utrecht, NL) controlled by the Eco Chemie GPES software on a personal computer. Staircase cyclic voltammetry was done with steps of 1.22 mV and sampling parameter $\alpha = 0.5$. The output of the spectrophotometer was fed into a spare AD channel of the potentiostat and recorded simultaneously with the current. The temperature was $22\pm1°C$ and a potential of +246 mV was used for the saturated calomel electrode (SCE) to recalculate the potentials with respect to the normal hydrogen electrode (NHE).

Ferricyanide ($K_3Fe(CN)_6$; Merck) was measured at 423 nm. The starting solution was 0.49 mM (using an extinction coefficient of 1020 $M^{-1}cm^{-1}$ [Winograd et al., 1969]) in 1 mM KCN and 100 mM Mops/NaOH buffer at pH 7.0. The KCN was added to prevent (surface)

decomposition of the complex [Kawiak *et al.*, 1987]. The initial absorbance was set to the calculated value and corrected afterwards for the absorbance of the fully reduced layer. Scans were recorded between 0.5 and −0.1 V *versus* SCE at 1, 0.5, and 0.2 mV/s with 5 minutes equilibration at +0.5 V *versus* SCE between the scans. The same solution was also used to test the reversibility of the ferricyanide response using the setup as described previously [Hagen, 1989], with a glassy carbon electrode pretreated as described above. The response time of the calomel electrode connected to the solution *via* the salt bridge was also tested in this setup by replacing the reference electrode with a holder for the plastic tube.

The flavodoxin semiquinone was measured at 580 nm [Dubourdieu *et al.*, 1975]. The starting solution was 0.1 mM fully oxidized flavodoxin (calculated from the absorbance at 460 nm, using an extinction coefficient of 10700 $M^{-1}cm^{-1}$ [Dubourdieu *et al.*, 1975]) in 3 mM neomycin and 60 mM potassium phosphate, pH 7.0. The starting value for the absorbance at 580 nm was set to zero (no absorbance of the oxidized form at 580 nm). Two scans were recorded between 0 and −1.0 Volt *versus* SCE at a scan rate of 1 mV/s, the cell was equilibrated at 0 V *versus* SCE for 10 minutes, two scans at 5 mV/s were recorded, followed by another 10 minutes equilibration, one scan at 0.2 mV/s, 10 minutes equilibration and two scans at 0.5 mV/s.

### 5.2.3 Simulations

For the simulation of the flavodoxin experiments the programme described in Chapter 2 was used with 0.1 mM flavodoxin, initially fully oxidized and $E_{high}$=+0.25 V, $E_{low}$=−0.75 V; $w$=0.2 mm, N=20, $\phi$(FMN)=0.05, $\lambda$=0.4 ($\Delta E$=2 mV with $v$=5 mV/s, $\Delta E$=0.4 mV with $v$=1 mV/s, $\Delta E$=0.2 mV with $v$=0.5 mV/s, and $\Delta E$=0.08 mV with $v$=0.2 mV/s). The other parameters are the same as used for the simulation in Chaper 2 ($D$=1·10$^{-10}$ m$^2$/s, $k^+$=2300 $M^{-1}s^{-1}$, $K_{com}$=1.3·10$^5$, $E_1^{Fld}$=−0.413 V, $E_2^{Fld}$=−0.113 V, $E_1^{FMN}$=−0.122 V, $E_2^{FMN}$=−0.314 V; $k^\circ$=6.3·10$^{-6}$ m/s, $\alpha$=0.5). The relative absorbance was calculated at 2 mV intervals by integration of the semiquinone concentration distribution as described in the previous chapter. The ferricyanide response was simulated using the same method and general boundary conditions as described for flavodoxin, with initially fully oxidized species, $D$=7.6·10$^{-10}$ m$^2$/s, $E_m$=437 mV, E$_{high}$=0.75 V, $E_{low}$=150 mV, $w$=0.2 mm, N=20, and $\lambda$=0.38 ($\Delta E$=0.05 mV with $v$=1 mV/s, $\Delta E$=0.025 mV with $v$=0.5 mV/s, and $\Delta E$=0.01 mV with $v$=0.2 mV/s).

## 5.3    Results and discussion

### 5.3.1    Ferricyanide

Ferricyanide was used as a model compound to test the properties of the thin layer cell. In Figure 5.2a the measured absorbance at 423 nm is plotted against the applied potential. In Figure 5.2b the normalized derivatives ("Derivative cyclic voltabsorptomograms" [Bancroft *et al.*, 1981; Xie *et al.*, 1993]) are shown. Because the data are too noisy for normal stepwise differentiation the differentiation and noise filtering was done using a Fast Fourier Transform routine. Prior to the transformation of the complete scan a linear baseline was subtracted and the 984 data points were padded to 4096 points with zero's to prevent "wrap-around" upon differentiation. The differentiation was done in Fourier space by complex multiplication of the data set with $i\omega$ ($\omega$ being the potential-based angular frequency) [Engblom, 1992]. Prior to back transformation the noise was filtered by applying the maximum box cutoff without broadening of the peaks: after 45 points for 1 mV/s, after 50 points for 0.5 mV/s, and after 60 points for 0.2 mV/s. The peaks were normalized by multiplication with $(4\ R\ T)\ /\ (F\ A_{max})$ [Xie *et al.*, 1993]. From Figure 5.2 it is clear that although the layer is fully reduced under these conditions, there is considerable hysteresis in the response to the applied potential of the ferricyanide in the layer. The area under the peaks in the voltammograms (Figure 5.3) is not correlated to the scan rate. The average of 649 ± 36 µC corresponds to 6.73 ± 0.37 nmol ferri/ferrocyanide, equal to the calculated amount of material in the thin layer of 6.42 nmol. This indicates that only the thin layer is measured and therefore diffusion from the bulk solution on top of the cell is negligible.

However, from the voltammograms in Figure 5.3 it is clear that the peak-to-peak separation is even larger than the maximum value of 59 mV for a infinite bulk setup (Table 5.1). This means that a large part of the observed hysteresis must be caused either by slow electron transfer, resistance in the solution or a slow reaction time of the salt bridge. This is also clear when the simulated data (Figure 5.4) are compared to the measured data: Some broadening due to diffusion because of the non-ideality of the cell at these timescales is indeed predicted, but much less than measured. In the standard setup (Chapter 2) with a 20 µl droplet almost no broadening was observed. (63 mV with a scan rate of 10 mV/s). When the salt bridge, used in the thin layer cell, was placed between the SCE and the droplet, no additional broadening was observed at 10 mV/s. In both setups the midpoint potential was 445±5 mV (scan rate 10 mV/s). These observations indicate that the salt bridge does not slow down the response of the SCE and shows that some of the broadening observed when using the thin layer cell must be due to uncompensated resistance in the solution layer.

a
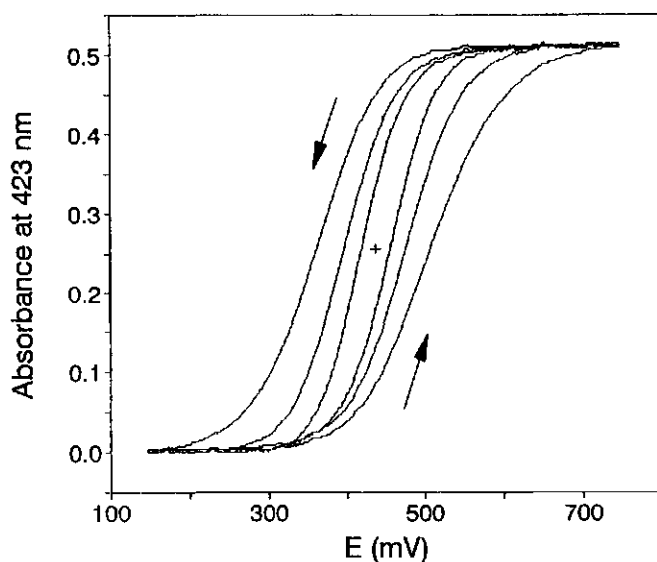


b
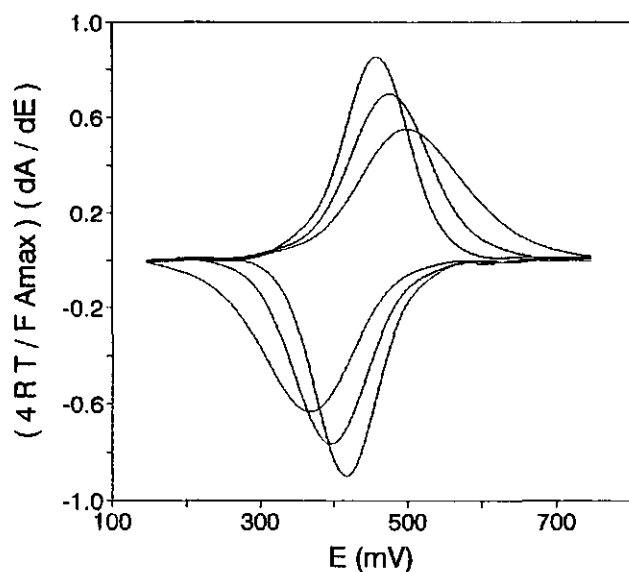


**Figure 5.2. a:** Cyclic voltabsorptomograms of 0.49 mM potassium ferricyanide in 1 mM KCN and 100 mM Mops/NaOH buffer at pH 7.0, measured at 423 nm and corrected for the absorbance of the fully reduced layer. Scans were recorded at $v=1$, 0.5, and 0.2 mV/s after 5 minutes equilibration at +0.75 V. **b:** Calculated derivative cyclic voltabsorptomograms.
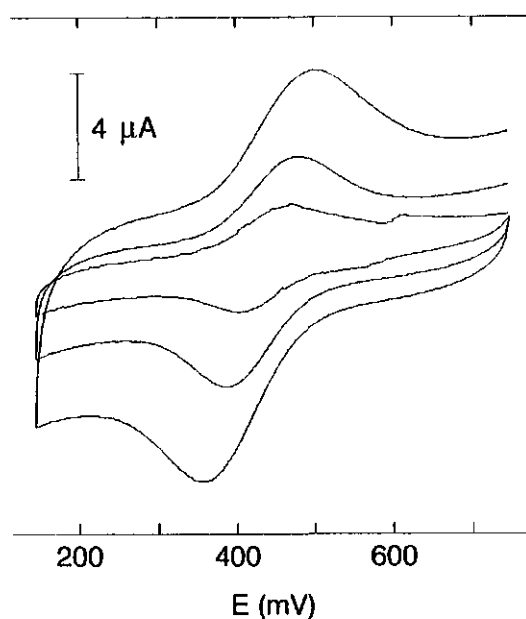
**Figure 5.3.** Staircase cyclic voltammograms of ferricyanide recorded simultaneously with the absorbance in Figure 5.2 ($\alpha$=0.5, $\Delta E$=1.22 mV).
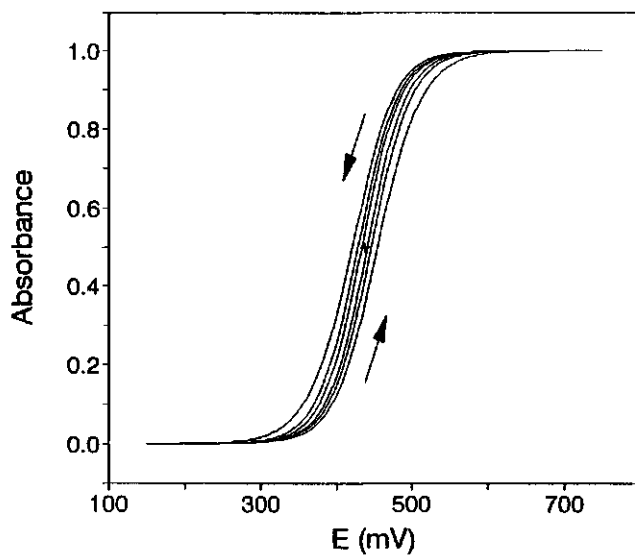


**Figure 5.4.** Simulated cyclic voltabsorptomograms of ferricyanide. $D$=7.6·$10^{-10}$ $m^2$/s, $E_m$=437 mV, $E_{high}$=0.75 V, $E_{low}$=0.15 V, $w$=0.2 mm, N=20, and $\lambda$=0.38 ($\Delta E$=0.05 mV with $v$=1 mV/s, $\Delta E$=0.025 mV with $v$=0.5 mV/s, and $\Delta E$=0.01 mV with $v$=0.2 mV/s).

**Table 5.1.** Measured and simulated peaks in the voltammograms and the derivative voltabsorptomograms of ferricyanide.

| | $v$ | Measured | | Simulated | |
| | | $E_m$ | $\Delta E_p$ | $E_m$ | $\Delta E_p$ |
|---|---|---|---|---|---|
| | mV/s | mV | mV | mV | mV |
| Current | 1 | 432 | 126 | 437 | 30 |
| | 0.5 | 435 | 81 | 437 | 18 |
| | 0.2 | 438 | 55 | 437 | 6 |
| $dA/dE$ | 1 | 433 | 132 | 438 | 28 |
| | 0.5 | 435 | 81 | 438 | 16 |
| | 0.2 | 437 | 40 | 437 | 6 |

### 5.3.2 Flavodoxin

The diffusional hysteresis with flavodoxin is expected to be much more important than with ferricyanide due to the lower diffusion coefficient of flavodoxin. This is demonstrated by a simulation with 100% semiquinone as starting material and neither comproportionation nor mediation by FMN. Figure 5.5 shows that only at a scan rate of 0.2 mV/s or lower full reduction of the semiquinone is achieved at the lower potential limit of −0.75 V. The peak-to-peak separation in the voltammograms (not shown) are 38, 50, 57 and 58 mV at 0.2, 0.5, 1 and 5 mV/s respectively. This indicates that with flavodoxin the cell starts to behave as a normal semi-infinite bulk cell at scan rates of 1 mV/s or higher.

The experimental results are plotted in Figures 5.6 to 5.8. In Figure 5.6 the two cyclic voltabsorptomograms at 1 mV/s show that during the scan the semiquinone concentration increases and decreases periodically and that the whole process is reversible and stable. In Figure 5.7 the single scan results at different scan rates are plotted.

During the cathodic scans (Figure 5.7a) no semiquinone is formed until the potential is below the FMN redox potential. This confirms that no electrons are directly transferred to the oxidized flavodoxin at the quinone/semiquinone midpoint potential of −113 mV, also not at 0.2 mV/s (even with the hysteresis due to diffusion, or resistance in solution some semiquinone should have been visible from −113 mV onwards at this slow scan rate if some electron transfer had occurred). The rapid increase of the absorbance below the FMN potential confirms the proposed FMN mediated electron transfer to the oxidized flavodoxin. With increasing scan rate the offset shifts to lower potential and the slope flattens. This is not only due to the diffusional hysteresis but probably also to the resistance in solution and the
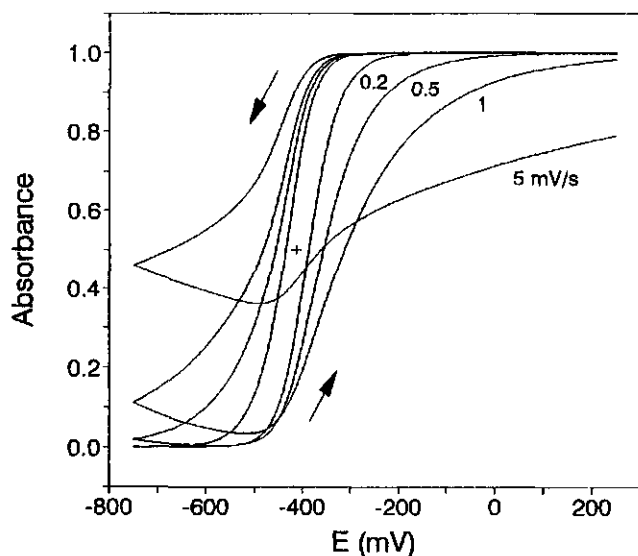
**Figure 5.5.** Simulated cyclic voltabsorptomograms of flavodoxin semiquinone. $D=1\cdot10^{-10}$ m$^2$/s, $E_1^{Fld}=-0.413$ V, $E_{high}=+0.25$ V, $E_{low}=-0.75$ V, $w=0.2$ mm, N=20, $\lambda=0.4$ ($\Delta E=2$ mV with $v=5$ mV/s, $\Delta E=0.4$ mV with $v=1$ mV/s, $\Delta E=0.2$ mV with $v=0.5$ mV/s, and $\Delta E=0.08$ mV with $v=0.2$ mV/s). No oxidation of the semiquinone or comproportionation are included.
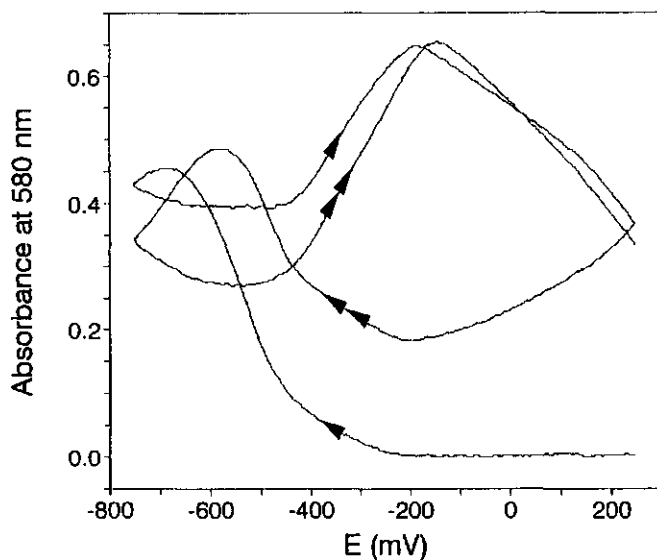


**Figure 5.6.** Cyclic voltabsorptomograms of 0.1 mM *D. vulgaris* (Hildenborough) flavodoxin, initially fully oxidized, in 3 mM neomycin and 60 mM KPi buffer at pH 7.0, measured at 580 nm at a scan rate of 1 mV/s.

a
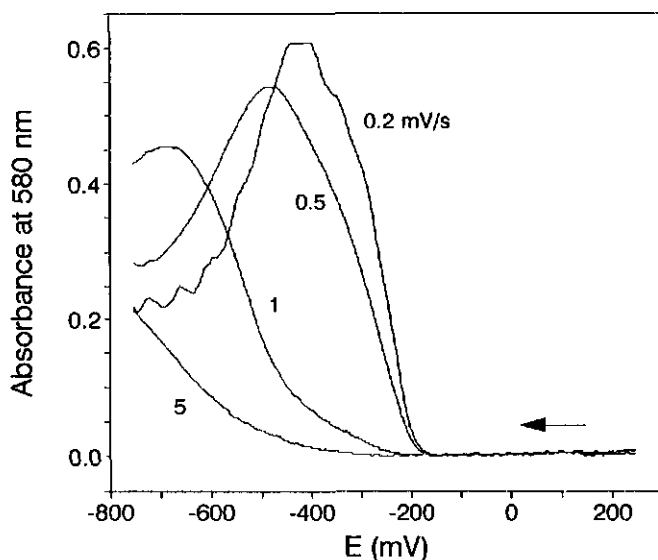


**Figure 5.7.** Cyclic voltabsorptomograms of 0.1 mM *D. vulgaris* (Hildenborough) flavodoxin, initially fully oxidized, in 3 mM neomycin and 60 mM KPi buffer at pH 7.0, measured at 580 nm at scan rates of 0.2, 0.5, 1 and 5 mV/s. **a:** Cathodic scans.

relatively slow electron transfer between FMN and flavodoxin ($k°$=6.3·$10^{-6}$ m/s was found in Chapter 2).

At 1 mV/s a marked increase in the rate of semiquinone formation is observed around −450 mV and also at 5 mV/s the slope is steeper at lower potential. This is most likely due to the proposed autocatalytic comproportionation cycle: reduction of the semiquinone, followed by comproportionation with a quinone to form two semiquinone molecules. At lower potentials and at low scan rates the absorbance drops again due to the depletion of the quinone and the continued reduction of the semiquinone. At lower scan rate the resulting absorption peak is higher and appears at a less negative potential because more time has passed to reduce all quinone in the bulk. This results in a steeper slope due to FMN-mediated semiquinone formation and faster depletion of the quinone in the bulk

The anodic scans (Figure 5.7b) show that as the potential passes the redox potential of the semiquinone/hydroquinone couple, the amount of semiquinone increases again due to oxidation of hydroquinone. When the potential of FMN is passed, the absorbance lowers again at low scan rate. The absorption peak is positioned around −250 mV at $v$=0.2 mV/s and shows the same hysteresis as observed in the cathodic scans. This indicates that at higher potential the semiquinone is oxidized again. This might be due to some direct electron transfer

**b**
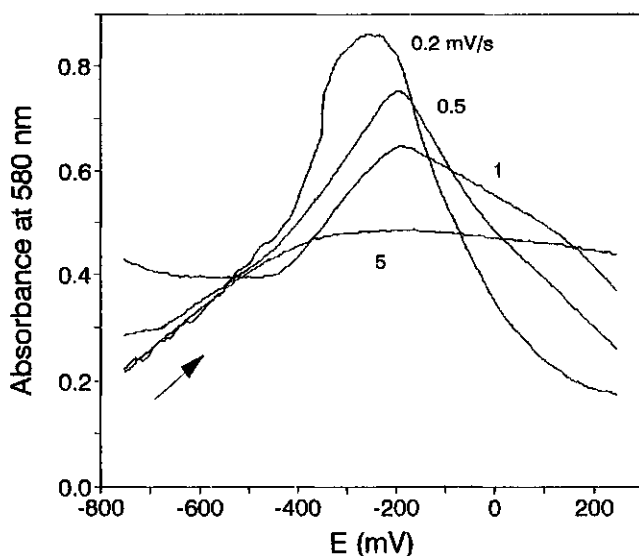


**Figure 5.7.** (Continued) **b:** Following anodic scans.

to the flavodoxin, not included in the model of Chapter 2. Alternatively, the electron transfer is mediated by FMN but this process must then be much faster then predicted by the Butler-Volmer type of driving force assumed in the model.

The voltammograms recorded simultaneously with the voltabsorptomograms are similar to those observed with *D. vulgaris* and *A. vinelandii* flavodoxins under semi-infinite bulk conditions (Chapters 2 and 3), although more low potential background current was observed due to less rigorous anaerobicity and the flavodoxin response is less pronounced due to the very low scan rates and the thin-layer conditions. In none of the voltammograms the direct oxidation of the semiquinone was observed. In Figure 5.8, the voltammograms recorded at 0.5 mV/s are shown. The cathodic and the anodic FMN currents are about 10 times higher then the maximum calculated for a full monolayer of FMN adsorped to the electrode. This is a clear indication for the FMN mediated electron transfer both to the fully oxidized flavodoxin and from the semiquinone.

To show that the given explanation for the observations is plausible, the semiquinone absorbance as a function of the potential was simulated. All parameters were set equal to those used in Figure 2.9. The partial occupation of the surface with FMN was set to 5% because the rate of adsorption measured at 100 mV/s (Figure 2.5) predicts this amount of adsorption halfway the first cathodic scan at 1 mV/s. The results are plotted in Figure 5.9.
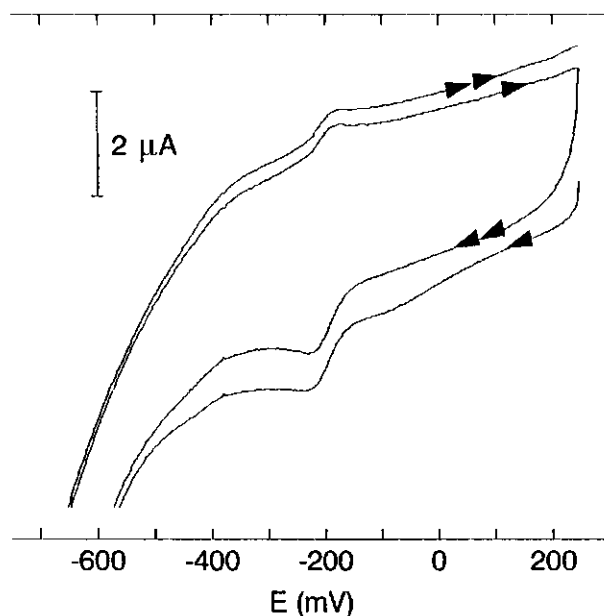
**Figure 5.8.** Staircase cyclic voltammograms of *D. vulgaris* flavodoxin recorded simultaneously with the absorbance in Figure 5.7 ($v$=0.5 mV/s, $\alpha$=0.5, $\Delta E$=1.22 mV).

This shows that for the cathodic scans the observed changes are indeed qualitatively predicted by the model. Quantitatively however, there are some marked differences:
* The observed increase during the scan at 0.5 mV/s is much steeper than simulated. This is probably due to a larger amount of FMN at the electrode because the 0.5 mV/s scans were recorded after the slow 0.2 mV/s scan. Simulations with increasing FMN surface concentrations indeed show an increasing slope.
* The peaks at higher scan rates are more shifted than the simulation predicts and the absorbance does not decay to zero at 0.5 and 0.2 mV/s like the simulation predicts. This is probably caused by the uncompensated resistance in the thin layer as was demonstrated by the ferricyanide experiments.

The anodic scans in the simulation (the 1 mV/s scan is plotted in Figure 5.9) all show an increase of the absorbance to the maximum value. Only at 0.2 mV/s some decrease at high potential is observed due to FMN-mediated oxidation of the semiquinone. Hence, the observed fast oxidation of semiquinone in the anodic scan (Figure 5.7b) is not predicted by the model. As mentioned above, this might be due to some direct electron transfer to the flavodoxin, not included in the model of Chapter 2. However, no current for this direct electron transfer was observed in the voltammograms. Alternatively, the electron transfer is mediated by FMN. The

- 88 -
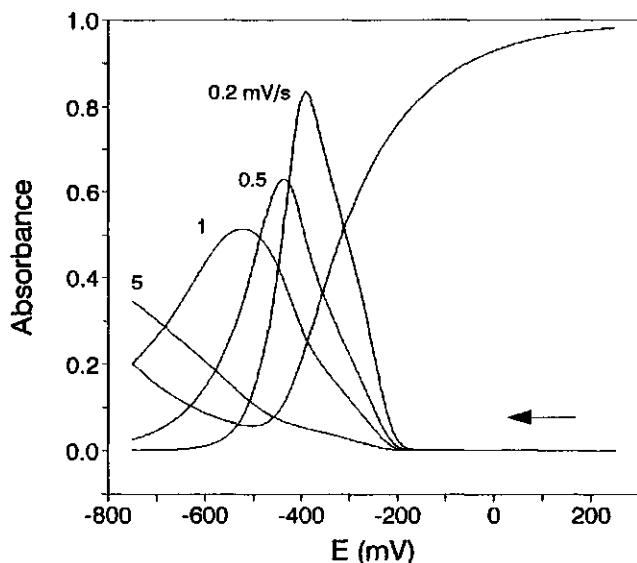
**Figure 5.9.** Simulated voltabsorptomograms of flavodoxin. Simulation parameters: 0.1 mM flavodoxin, initially fully oxidized, $D=1\cdot10^{-10}$ m$^2$/s, $k^+=2300$ M$^{-1}$s$^{-1}$, $K_{com}=1.3\cdot10^5$, $E_1^{Fld}=-0.413$ V, $E_2^{Fld}=-0.113$ V, $E_1^{FMN}=-0.122$ V, $E_2^{FMN}=-0.314$ V, $k°=6.3\cdot10^{-6}$ m/s, $\alpha$(FMN/fld)=0.5, $E_{high}=+0.25$ V, $E_{low}=-0.75$ V, $w=0.2$ mm; N=20, $\phi$(FMN)=0.05, $\lambda=0.4$ ($\Delta E$=2 mV with $v$=5 mV/s, $\Delta E$=0.4 mV with $v$=1 mV/s, $\Delta E$=0.2 mV with $v$=0.5 mV/s, $\Delta E$=0.08 mV with $v$=0.2 mV/s).

observation that the FMN currents (both cathodic and anodic, see Figure 5.8) are much higher than calculated for one monolayer of FMN are a clear indication for this. Also, the decline of the absorbance starts at potentials below the FMN potential (even though the uncompensated resistance and electron transfer kinetics are expected to cause a shift of the response in positive direction).

The rate of electron transfer from the semiquinone to FMN are predicted by the Butler-Volmer type of driving force assumed in the model (Chapter 2, equations (2.44) and (2.45)) to be only about 2% of the rate in the reverse direction due to the unfavourable potential difference. However, simulations with larger $k_b$ (while keeping $k_f=7.5\cdot10^{-6}$ m/s according to equation (2.44) with the previously determined $k°$) yield a much better similarity with the observations. This indicates that not only the potential differences but probably also chemical factors determine the rate of electron transfer between FMN and flavodoxin. One of these factors probabily is the conformational change of the flavodoxin upon oxidation of the semiquinone [Peelen & Vervoort, 1994]. At 5 mV/s not much oxidation of the semiquinone is observed (Figure 5.7b). This means that at 100 mV/s this reaction will be even more insignificant and the general model of Chapter 2 (equations (2.36) to (2.43)) can still be applied, with an apparent $k_f=7.5\cdot10^{-6}$ m/s and $k_b<<k_f$.

An additional indication for the oxidation of the semiquinone by FMN is found when the concentration profiles and the anodic peak during the simulation ($v=1$ mV/s, with $k_b=k_f=7.5\cdot10^{-6}$ m/s) are analyzed. It appears that the anodic absorption peak shifts to more positive potential when more FMN is present at the electrode. This is caused by the increased rate of semiquinone oxidation with more FMN. The formed quinone diffuses to bulk where it reacts with the hydroquinone that has not yet been oxidized due to the diffusional delay. The overall reaction is therefore the formation of one semiquinone. The shift of the peak was indeed observed between the first and second scan at 1 mV/s (Figure 5.6). These were the first two scans recorded and the adsorption of FMN probably increases during these scans.

## 5.4   Conclusions

The measured and simulated cyclic voltabsorptomograms show that the proposed model of FMN-mediated formation of semiquinone flavodoxin and an autocatalytic comproportionation cycle at low potential is valid. However, the physical origin of the rates of electron transfer between FMN and flavodoxin ($k_f$ and $k_b$) probably is more complex than assumed in the Butler-Volmer model (Chapter 2, equations (2.44) and (2.45)). The results in this chapter show that voltabsorptometry is a potentially useful technique to study the electron transfer mechanism and properties of redox proteins. It can be applied to verify the voltammetric response and to elucidate coupled homogeneous chemical reactions.

## 5.5 References

Bancroft, E.E., Sidwell, J.S. & Blount, H.N. (1981) *Anal. Chem 53*, 1390.

Bard, A.J. & Faulkner, L.R. (1980) *Electrochemical Methods, Fundamentals and Applications*, Wiley, New York.

Brewster, J.D. & Anderson, J.L. (1989) *Appl. Spectrosc. 43*, 710.

Dubourdieu, M., Le Gall, J. & Favaudon, V. (1975) *Biochim. Biophys. Acta 376*, 519.

Engblom, S.O. (1992) *J. Electroanal. Chem. 332*, 73.

Hagen, W.R. (1989) *Eur. J. Biochem. 182*, 523.

Kawiak, J., Kulesza, P.J. & Galus, Z. (1987) *J. Electroanal. Chem. 226*, 305.

Massey, V. & Hemmerich, P. (1978) *Biochemistry 17*, 9.

Peelen, S. & Vervoort, J. (1994) *Arch. Biochem. Biophys. 314*, 291.

Winograd, N., Blount, H.N. & Kuwana, T. (1969) *J. Phys. Chem. 73*, 3456.

Xie, Q.,Wei, W., Nie, L. & Yao, S. (1993) *J. Electroanal. Chem. 348*, 29.

# Chapter 6

## The influence of charge and polarity on the redox potentials of High Potential Iron-Sulfur Proteins: Evidence for the existence of two groups.

## 6.1    Introduction

The high-potential iron-sulfur proteins form a group of related and well-studied, small redox proteins (6 to 10 kDa) [Bartsch, 1978; Meyer, 1994]. They form a special class of ferredoxins, containing a [4Fe-4S] cluster bound to the protein by four cysteinyl sulfur ligands and buried in a hydrophobic environment. However, the sequences show no similarity at all to the "bacterial ferredoxins". In oxidized HiPIPs the [4Fe-4S] cluster is in the 3 ferric, 1 ferrous state (overall charge 3+) while oxidized ferredoxins contain a $[4Fe-4S]^{2+}$ (2 ferric, 2 ferrous) cluster. Most HiPIPs are found in purple photosynthetic bacteria but a HiPIP is also present in a halophilic, denitrifying *Paracoccus* species [Bartsch, 1991; Tedro *et al.*, 1977]. The primary structures of many HiPIPs have been determined (see references in Table 6.1) and the crystal structures of the HiPIPs from *Chromatium vinosum*, *Rhodocyclus tenuis* strain 2761, *Ectothiorhodospira halophila* (iso-1) and *Ectothiorhodospira vacuolata* (iso-2) are known [Carter *et al.*, 1974a; Freer *et al.*, 1975; Breiter *et al.*, 1991; Rayment *et al.*, 1992; Benning *et al.*, 1994]. For *Ectothiorhodospira halophila* iso-2 a molecular dynamics model structure has been calculated [Banci *et al.*, 1993a] and NMR structures is reported for *E. halophila* iso-2 and for *C. vinosum* [Banci *et al.*, 1994; Banci *et al.*, 1995]. Recently, a synthetic gene encoding the *E. halophila* iso-1 HiPIP has been constructed and highly expressed in *E. coli* [Eltis *et al.*, 1994]. Apart from the coordinating cysteines, some aromatic residues and some moderately conserved features, the overall homology of the sequences is not very high. However, structural homology is high, especially around the cluster, and cluster geometry and coordination to the protein are highly conserved. There are however differences in the electronic structures of the $[4Fe-4S]^{3+}$ clusters. This has been demonstrated by Nettesheim and by Bertini and coworkers, who studied the distribution of the charges over the iron ions using $^1$H-NMR spectroscopy [Nettesheim *et al.*, 1992; Banci *et al.*, 1993a,b; Bertini *et al.*, 1992; Bertini *et al.*, 1993].

Interestingly, the redox potential of the 3+/2+ transition ranges from +50 to +500 mV [Meyer *et al.*, 1983; Luchinat *et al.*, 1994; Table 6.1]. These large differences in reduction potentials are probably caused by differences in polarity of the cluster environment [Backes *et al.*, 1991; Krishnamoorthi *et al.*, 1989]. The peptide charge, ranging from very negative to quite positive (−13 to +5), might also modulate the redox potentials.

Crystallography and resonance Raman studies of bacterial ferredoxins and HiPIPs show that the structures of the clusters are nearly identical. There are however major differences in the local environment of the clusters in bacterial ferredoxins and HiPIPs. The sequences and folding patterns, the location of the cysteines, the cysteine ligand dihedral angles (close to 180° in HiPIPs) and the position of the hydrogen bonds are completely different. In ferredoxins, eight hydrogen bonds between amide N-H and sulfur ligands are present while in HiPIPs only five are found. The redox potentials of the cluster are probably regulated in part by the number of these NH-S bonds because they stabilize the more negatively charged reduced states [Adman et al., 1975; Jensen et al., 1994; Langen et al., 1992; Backes et al., 1991 and references cited therein]. By comparing bacterial ferredoxins, HiPIPs and synthetic clusters, Carter [1977] found that each hydrogen bond increases the potential by about 80 mV. In HiPIPs the cluster is completely inaccessible to water and surrounded by hydrophobic residues, while the ferredoxin cluster is in a more hydrophilic environment and much more accessible to water [Backes et al., 1991; Orme-Johnson et al., 1983]. The hydrophobic pocket in HiPIPs causes a further lowering of the reduction potentials [Kassner & Yang, 1977]. Carter [1977] observed opposite stereochemistry of the $[4Fe-4S]^{2+}$ cluster in *Chromatium* HiPIP and ferredoxins in the visible CD spectra (although Przysiecki et al. [1985] found that not all HiPIPs show these features). He proposed a destabilization of the transition state for the $[4Fe-4S]^{2+,1+}$ reduction by charge-dipole interactions between the highly conserved tyrosine side chain and the cluster (Tyr19 and $S^*3$ in *C. vinosum*).

These differences result in a shift of the redox potentials of both the 3+/2+ and the 2+/1+ transitions to such an extent that in HiPIPs the second transition, normally observed in bacterial ferredoxins, is shifted out of the biologically useful potential range while the first transition becomes feasible. Calculation of the $[4Fe-4S]^{2+,1+}$ transition potential for the *C. vinosum* HiPIP based on the "Protein Dipoles Lanevin Dipoles" method by Jensen and coworkers yields a value of −1747 mV [Jensen et al., 1994]. Cammack [1973] found that only in solutions containing more than 70% DMSO, the reduced *C. vinosum* HiPIP ($[4Fe-4S]^{2+}$) can be further reduced by dithionite at pH 9. However, a kinetic rather than thermodynamic barrier for the super-reduction of HiPIPs was suggested by the findings of Butler et al. [1980]. They were able to super-reduce *C. vinosum* HiPIP with hydrated electrons (reduction potential −2.9 V) generated by pulse-radiolysis of water, but they observed no reaction with $CO_2^-$ radicals (−2.0 V). They proposed that the ability of the electrons to tunnel through an energy barrier explains the higher reactivity of hydrated electrons compared to $CO_2^-$ radicals.

In this chapter the result of the electrochemical characterization of a number of HiPIPs by direct, unmediated electrochemistry are reported. The charge of the peptide is shown to have a large influence on the electron transfer to the electrode. A correlation between the peptide charge and the redox potentials is proposed. To probe the influence of the local

**Table 6.1.** Redox potentials and general features of the HiPIPs.

| | $E_m{}^7$ | Size | Charge | Number of the amino acids: | | | | Surplus apolar residues |
|---|---|---|---|---|---|---|---|---|
| | | | | H | W,Y,F | S,T, H,N,Q | A,V,L, I,M,P, F,Y,W | |
| | mV | a.a. | (K+R−D−E) | | | | | |
| RGEL[a] | 332[b] 329[c] | 74 | +5 (+10−5) | 1 | 7 | 12 | 35 | 23 |
| RTEN 2761[d] | 302[e] 310[c] | 62 | +5 (+8−3) | 0 | 5 | 12 | 26 | 14 |
| RTEN 3761[f] | 304[e] | 64 | +5 (+8−3) | 0 | 5 | 16 | 27 | 11 |
| CVIN[g] | 356[b] 346[c] | 85 | −3 (+7−10) | 1 | 6 | 17 | 41 | 24 |
| TROS[h] | 342[e] | 85 | −4 (+6−10) | 3 | 6 | 17 | 42 | 25 |
| CGRA[h] | 347[f] | 83 | −5 (+7−12) | 2 | 6 | 16 | 38 | 22 |
| TPFE[i] | 352[b] | 81 | −7 (+4−11) | 4 | 8 | 24 | 34 | 10 |
| PS[j] | 282[b] 360[k] | 71 | −10 (+1−11) | 2 | 6 | 23 | 28 | 5 |
| RSAL[l] | 500[c] | 54 | +1 (+5−4) | 2 | 6 | 15 | 25 | 10 |
| RGLO[m] | 453[e] 432[c] | 57 | +1 (+8−7) | 0 | 4 | 12 | 22 | 10 |
| EV1[n] | 260[e] 259[c] | 72 | −3 (+5−8) | 3 | 6 | 17 | 32 | 15 |
| EV2[n] | 150[e] 172[c] | 71 | −6 (+4−10) | 2 | 7 | 17 | 32 | 15 |
| EH1[o] | 110[e] 120[p] | 71 | −10 (+4−14) | 4 | 8 | 13 | 29 | 16 |
| EH2[q] | 50[e] | 76 | −13 (+3−16) | 4 | 10 | 14 | 32 | 18 |

[a]Tedro *et al.*, 1976. [b]Mizrahi *et al.*, 1980. [c]this chapter. [d]sequence from Tedro *et al.*, 1985a and corrected by Rayment *et al.*, 1992. [e]Przyssieki *et al.*, 1985. [f]sequence from Tedro *et al.*, 1979 and corrected by Rayment *et al.*, 1992. [g]sequence from Dus *et al.*, 1973 and corrected by Tedro *et al.*, 1981. [h]Tedro *et al.*, 1981. [i]Tedro*et al.*, 1974. [j]Tedro *et al.*, 1977. [k]Hori, 1961. [l]Ambler *et al.*, unpublished. [m]Ambler *et al.*, 1993. [n]Ambler *et al.*, 1994. [o]sequence from Tedro *et al.*, 1985b and corrected by Breiter *et al.*, 1991. [p]Eltis *et al.*, 1994. [q]Tedro *et al.*, 1985b.

cluster environment on the potential the positions of the cluster charge-transfer bands are measured and correlated with the thermodynamics of the redox reaction.

## 6.2    Experimental procedures

### 6.2.1    HiPIPs.

The investigated HiPIPs are isolated from *Ectothiorhodospira vacuolata* strain β1 (iso-1 and iso-2), *Chromatium vinosum* strain D, *Rhodocyclus gelatinosus* strain 2.2.1, *Rhodocyclus tenuis* strain 2761, *Rhodopila globiformis* strain 7950 and from *Rhodospirillum salinarum* strain ATCC 35394 (the multimeric HiPIP iso-2). The purifications have been published elsewhere [Bartsch, 1978; Ambler *et al.*, 1994; Bartsch, 1971; Tedro *et al.*, 1976; Tedro *et al.*, 1979; Tedro *et al.*, 1985a; Ambler *et al.*, 1987; Meyer *et al.*, 1990; Meyer, 1994].

The iso-electric points of the reduced HiPIPs were measured by analytical thin-layer gel isoelectric focusing, performed at 4°C in polyacrylamide gel (Serva, servalyt precotes 3-10) using an LKB 2217 Ultrophor electrofocusing unit. A Serva protein mix containing trypsinogen (p$I$=9.30), lentil lectin (p$I$=8.65, 8.45, and 8.15), myoglobin (p$I$=7.35 and 6.85), human carbonic anhydrase B (p$I$=6.55), bovine carbonic anhydrase B (p$I$=5.85), β-lactoglobulin A (p$I$=5.20), soybean trypsin inhibitor (p$I$=4.55), and amyloglucosidase (p$I$=3.50) was used to calibrate the system.

### 6.2.2    UV/VIS spectroscopy.

The UV/VIS spectra of the reduced HiPIPs were obtained on an Aminco DW-2000 spectrophotometer (SLM instruments) interfaced with an IBM PC. The spectra were recorded at 22±1°C with split beam mode, a slit of 3 nm and a scan rate of 2 nm/s with medium filtering. A holmium glass filter was used to calibrate the monochromator using the same slit, scan rate and filtering. The HiPIPs were diluted to approximately 20 μM in 20 mM Hepes buffer pH 7.0. To obtain fully reduced (*i.e.* [4Fe-4S]$^{2+}$) HiPIPs 100 μM of ascorbic acid ($E_m$=58 mV [Clark, 1960]) and 1 μM of the mediator phenazine ethosulphate ($E_m$=55 mV) were added (ferricyanide oxidized HiPIPs could be fully reduced by ascorbate within 5 minutes, even without mediator). Ascorbate does not absorb light above 320 nm, but has a rather high UV absorbance. This was not a problem when the sample was measured against a reference cuvette with the same concentrations of buffer, ascorbate and mediator. The positions of absorption maxima were determined after smoothing the measured curves until one noise-free maximum could be detected and the values of three spectra were averaged.

This way the position of the maximum could be determined with an accuracy of less then 1 nm. Such an accurate measurement is not possible for the oxidized state of all HiPIPs because the maxima are much less distinct; also, the high potential of *R. globiformis* HiPIP and the higher potential and instability of oxidized *R. salinarum* HiPIP [Meyer *et al.*, 1990] make it difficult to obtain fully oxidized protein.

The protein concentrations were estimated from the maximum absorbance around 385 nm using an extinction coefficient of 16 $mM^{-1}cm^{-1}$ [Bartsch, 1978; Przysiecki *et al.*, 1985].

### 6.2.3 Electrochemistry.

The HiPIPs were studied by analogue cyclic voltammetry and by digital staircase cyclic voltammetry. An electrochemical cell for microscale electrochemistry is used with a demountable inverted disk working electrode [Hagen, 1989]. A 10 to 20 µl droplet of buffered protein solution was held between the horizontal working electrode and the tip of the reference electrode which was at approximately 1 mm above the surface of the working electrode. The reference electrode was a Radiometer K-401 saturated calomel electrode with a porous pin. The working electrode was a glassy carbon disc of 15 mm diameter and 2 mm height (type V25 from Le Carbone Loraine). Prior to each electrochemical measurement the disc was polished firmly (Microcloth polishing cloth and 6 µm Metadi Diamond Compound spray, both from Buehler, USA), rinsed with water and with ethanol and activated by exposing the lower part to a methane flame from a Bunsen-burner for 30 seconds. The counter electrode was a Radiometer P-1312 micro platinum electrode. For Staircase CV the electrodes were connected to an Eco Chemie Autolab 10 potentiostat, controlled by the Eco Chemie GPES software version 3.0 on a personal computer. A step of 1.22 mV was applied and a sampling parameter $\alpha=0.5$ (resulting in an averaging of the current during 20 ms around the center of the step) was used to obtain quasi-reversible voltammograms equal to analogue CV measurements [Seralathan *et al.*, 1987]. A 220 µF condenser across the current-output of the potentiostat (Z=100 Ω) was applied as low-pass filter with a resulting cell constant $2\pi RC=0.14$ seconds. The analogue CV measurements were performed using a BioAnalytical Systems Voltammograph CV27 with the internal *RC*-filter set to 0.1 s.

The scan rate used to determine the midpoint potentials was always 10 mV/s and the upper and lower potential limits were at least 150 mV higher and lower than the observed positions of the anodic and cathodic peaks. The cell was flushed with wet purified argon [Massey & Hemmerich, 1978]. The experiments were performed with 25 to 135 µM HiPIP in 10 to 20 mM Hepes buffer pH 7.5 at a temperature of 22±1°C. Promoters: $MgCl_2$ (Merck); $ScCl_3$ (Aldrich); $EuCl_3$ (Fluka); poly-L-lysine, Mw=3300 (Sigma); Morpholin (Janssen Chimica); L-amino acids (Merck); phenol (Merck); 4,4'-dipyridyl (Janssen Chimica).

The buffers used for the determination of the pH-dependency of the midpoint-potentials were 10 to 20 mM of sodiumacetate/acetic acid (Merck) at pH 4 to 5 or the "Good" buffers (Sigma) Mes, BisTris, Mops, Hepes, Epps, Taps, BisTrisPropane, Ches or Caps at pH 5.5 to 11, all titrated with NaOH or HCl.

Temperature dependent cyclic voltammograms were obtained by submerging the cell in a thermostated waterbath. The argon was passed through 2 meters of copper tube (3mm) submerged in the waterbath. The temperature of the cell was measured using a thermocouple inserted into the saltbridge of the calomel electrode. The measurement was started when the internal temperature was within 1°C of the temperature of the waterbath and the average of the temperatures at the start and at the end of the cyclic scan was used. At each temperature a new droplet of solution and a new working electrode were used, unless the stability of the protein was sufficient to measure for a longer period of time (judged by the shape of the voltammogram and by a second measurement after resetting the temperature to a previously measured value). The potentials are corrected for the temperature dependent potential of the calomel electrode as given in Chapter 2, equation (2.1).

The ionic strength dependencies of the potentials were measured in 10 to 20 mM Hepes pH 7.5 and the ionic strength was increased by adding KCl (either by titration of one droplet or by using a new droplet and a new working electrode in case the electron transfer became sluggish). The ionic strength was calculated by adding the concentration of ionized buffer (as calculated from pH and p$K$) to the KCl concentration. The protein itself, promoters or stabilizers are not included in the calculated ionic strength.


## 6.3    Results

### 6.3.1    Optical spectra of the HiPIPs.

The spectra of the reduced HiPIPs are similar to the spectra of oxidized bacterial ferredoxins with a shoulder around 300 nm and one absorption band in the visible region around 385 nm [de Klerk & Kamen, 1966; Dus et al., 1967; Meyer et al., 1973; Bartsch, 1978; Meyer, 1985; Meyer et al., 1990]. The purity indices (ratio $A^{280}/A^{385}$) are comparable to reported values and are listed in Table 6.2.

The absorption maximum in the UV region is located at the same position for all HiPIPs: $\lambda_{max}$=282.6±0.8 nm but there are measurable differences between the positions of the maxima in the visible region (listed in Table 6.2). The meaning of these differences and correlations with observed potentials and thermodynamics of the redox reaction will be discussed.

**Table 6.2.** Characteristics of the HiPIPs.

| | Charge[a] | p$I$ | $\lambda_{max}^{UV}$ | $\lambda_{max}^{VIS}$ | $A^{UV} / A^{VIS}$ |
|---|---|---|---|---|---|
| | | | nm | nm | |
| R. gelatinosus | +5 | 9.35 | 283.0 | 384.9 | 2.28 (2.31[b]) |
| R. tenuis strain 2761 | +5 | 9.08 9.44 | 283.7 | 382.9 | 1.34 (1.58[c]) |
| C. vinosum | −2 | 3.90 4.13 | 283.2 | 386.5 | 2.51 (2.57[b]) |
| R. salinarum iso-2 | +1 | 5.62 | 281.8 | 393.2 | 2.11 (1.9[d]) |
| R. globiformis | +1 | 4.59 | 282.6 | 386.0 | 1.74 (1.8[e]) |
| E. vacuolata iso-1 | −3 | 3.96 4.22 | 281.2 | 390.0 | 2.40 |
| E. vacuolata iso-2 | −6 | 3.48 3.66 | 282.5 | 376.9 | 2.36 |

[a]The charge of the peptide without cysteines or the cluster is given. The ratio of UV and VIS absorbance between parenthesis is the best purity index found in literature. [b]Dus *et al.*, 1967. [c]Bartsch, 1978. [d]Meyer *et al.*, 1990. [e]Przysiecki *et al.*, 1985.

## 6.3.2 Iso-electric points.

The measured iso-electric points are collected in Table 6.2. *E. vacuolata* iso-1 and iso-2, *C. vinosum* and *R. tenuis* HiPIPs focus in two bands, separated by 0.26, 0.18, 0.26 and 0.36 pH units respectively. This is comparable to the lowering of the iso-electric point by 0.2 units upon reduction as reported by Dus *et al.* [1967] for *C. vinosum* HiPIP. Therefore, the band at higher pH probably is the oxidized species. The other three HiPIPs focus in one band. Because the HiPIPs were initially fully reduced, the single bands of the high-potential *R. globiformis* and *R. salinarum* HiPIPs probably are the reduced species.

The measured iso-electric points are as expected from the overall charge of the proteins except for *R. globiformis* and *R. salinarum. R. globiformis* HiPIP has 8 lysines and 7 aspartate and glutamate residues [Ambler *et al.*, 1993] but the protein focused in a single

band at pH 4.6. The *R. salinarum* iso-2 pepetide also has a charge of +1 (Ambler *et al.*, unpublished results) and the HiPIP focused at low pH (p$I$=5.6). This indicates that the net −2 charge of the reduced cluster including cysteine ligands has a large influence on the iso-electric point. The p$I$ values of the other two positively charged HiPIPs (*R. gelatinosus* and *R. tenuis*) are not shifted as dramatically as *R. globiformis* and *R. salinarum* because of the higher peptide charge.


### 6.3.3  Electrochemistry.

The charge of the protein has a large influence on the electrochemical response. Direct, unpromoted electrochemistry is possible with the positively charged *R. gelatinosus*, *R. tenuis* and *R. globiformis* HiPIPs (*R. salinarum* gives only a small anodic response during the first scan), but the negatively charged *C. vinosum* HiPIP and both *E. vacuolata* iso-HiPIPs require a positively charged promoter. This indicates that the electrostatic interactions between the protein surface and the negatively charged glassy carbon electrode are important for the electron transfer reaction. The positively charged promoter is believed to form a bridge between the negative charges [Armstrong *et al.*, 1987, 1988]. However, not all of the "traditional" cationic bridging promoters are suitable in this case. Multivalent cations like $Mg^{2+}$, $Sc^{3+}$ or $Eu^{3+}$ do not promote the response. With the aminoglycoside neomycin a small and rather unstable response is observed. The best promoter proved to be poly-L-lysine. This indicates that the flexibility of the promoter is important. Apparently, the promoter must not only suppress Coulombic repulsion but also be able to adjust its shape to provide a good docking-site for the protein on the electrode.

Other important factors for a reliable measurement of the potential are the stability (persistence) and reversibility (peak-to-peak separation) of the response. The ideal promoter not only provides a bridge between the protein and the electrode surface but also effects a reversible and stable electron transfer. However, poly-L-lysine is not a good promoter in this sense. For the three negatively charged HiPIPs promoted by poly-L-lysine the response is not very stable. The peak-to-peak separation rapidly increases to above 100 mV after a few cycles. This was also observed for the unpromoted positively charged *R. gelatinosus* and *R. tenuis* HiPIPs. This might be caused by a change in conformation of the protein upon adsorption on the electrode, thereby blocking the electron transfer. Probably the protein denatures to a flattened shape with hydrophobic interactions between the apolar residues and apolar patches on the electrode surface [Norde, 1986]. This is confirmed by the observation that the stability of the response is less when the electrode is not activated but only polished, yielding a more hydrophobic surface (large contact angle with water). With this in mind, a number of bifunctional (hydrophobic / hydrophilic, zwitterionic) substances were screened for their ability to prevent or delay the irreversible denaturing of the HiPIPs by adsorption.

In combination with poly-L-lysine, morpholin proved to have a positive effect on the stability of the response. For *C. vinosum*, the optimum is 43 to 72 μM HiPIP with 7.7 to 9.2 mM morpholin and 0.67 to 0.8 mM poly-L-lysine, for *E. vacuolata* iso-1, 27 to 44 μM HiPIP with 7.7 to 9.2 mM morpholin and 0.67 to 0.8 mM poly-L-lysine was used, and for *E. vacuolata* iso-2, a protein concentration of 132 μM with 7.2 mM morpholin and 1.6 mM poly-L-lysine gave the best stability.

The reversibility of the (unpromoted) response of *R. gelatinosus* HiPIP can be improved by adding amino acids. A remarkable observation is that at lower concentrations the response is diffusion-controlled (peak current proportional to the square root of the scan rate), but the addition of more of the amino acid (typically 5 mM or more) causes a gradual shift of the peaks to lower potential, a decreasing peak-to-peak separation and after some time (typically one hour) a peak current proportional to the scan rate, indicating adsorption of the protein in the native conformation at a slow rate. Probably the amino acids prevent denaturation at the electrode surface by intervening between the protein and the electrode but at higher concentration the interactions become too strong for the protein to leave the surface after electron transfer. Another possibility is that at a low concentration of stabilizer only a small amount of protein is adsorped and facilitates electron transfer by "self-mediation" [Verhagen & Hagen, 1992]. For *R. gelatinosus* HiPIP the optimal response without adsorption was obtained by adding 3 mM aspartic acid to 51 μM protein. The reversibility of the response of *R. tenuis* HiPIP also improves when amino acids are added, but the absorption phenomena are less pronounced. The optimal response was obtained with 3 mM tryptophan added to 84 μM protein.

The response of *R. globiformis* HiPIP is much more stable compared to the other HiPIPs and no promoter nor stabilizer is required. This might be due to the almost equal amounts of positive (8) and negative (7) residues. The negative charges apparently prevent (or rather, delay) the denaturing of the protein. For the potential measurements, concentrations of 58 to 68 μM were used but higher concentrations are also possible. In Figure 6.1 a typical voltammogram of *R. globiformis* HiPIP is shown.

The electrochemical response of the large *R. salinarum* HiPIP is extremely unstable. Probably this is due to the degradation of the oxidized form [Meyer *et al.*, 1990]. It was found that none of the promoters nor the stabilizers morpholin or amino acids could improve the response. Only in the presence of phenol (3 mM or more) or 4,4'-dipyridyl (7 mM or more) a reversible but not very stable response was obtained (midpoint potentials equal in both cases). The peak-to-peak separations were around 70 mV in the first scan but rapidly increased. Maybe these aromatic stabilizers bind to hydrophobic patches of the electrode, thereby delaying the adsorption of the protein. They probably also prevent degradation of the oxidized HiPIP. Because phenol is electrochemically active (the high applied potentials are
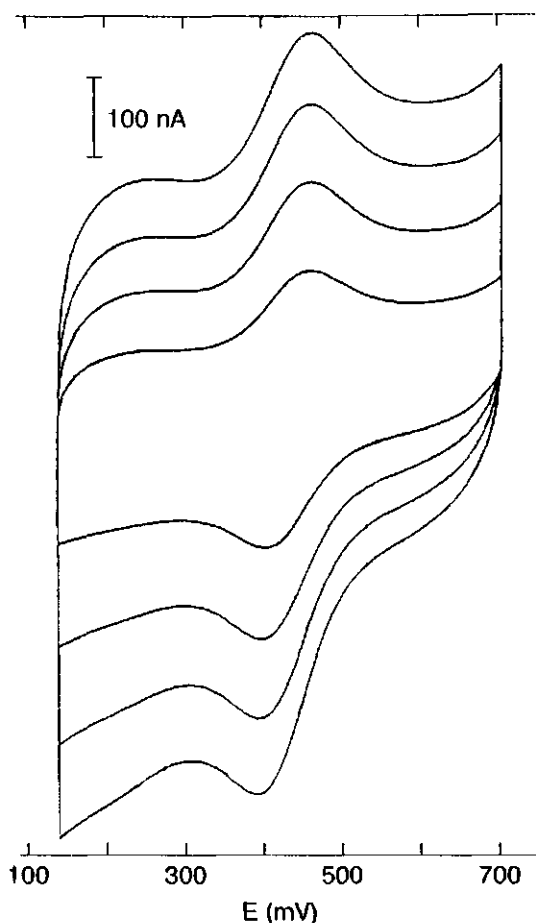
**Figure 6.1.** Cyclic Voltammograms of 41 μM *R. globiformis* HiPIP in 16 mM Hepes pH 7.5. **a:** A 12.5 μl droplet was used on a glassy carbon electrode, activated by glowing in a methane-flame. Conditions: reference/counter electrodes, SCE/Pt; scan rates 5, 10, 15 and 20 mV/s; temperature 22°C. The potential axis is defined *versus* the normal hydrogen electrode.

close to the redox-potential for the oxidation of phenol) it was decided to use 4,4'-dipyridyl as stabilizer. For the potential measurements 11 mM dipyridyl and 67 μM *R. salinarum* HiPIP were applied and only the first and second scans were used.

The measured midpoint potentials are comparable to the values reported before (see Table 6.1). The potential of *R. salinarum* is the highest HiPIP potential ever reported and is close to the upper estimate of 480 mV, based on the absorbance change upon a single addition of ferricyanide before decay of the oxidized HiPIP [Meyer *et al.*, 1990]. The addition of morpholin to the negatively charged HiPIPs promoted by poly-L-lysine or the addition of
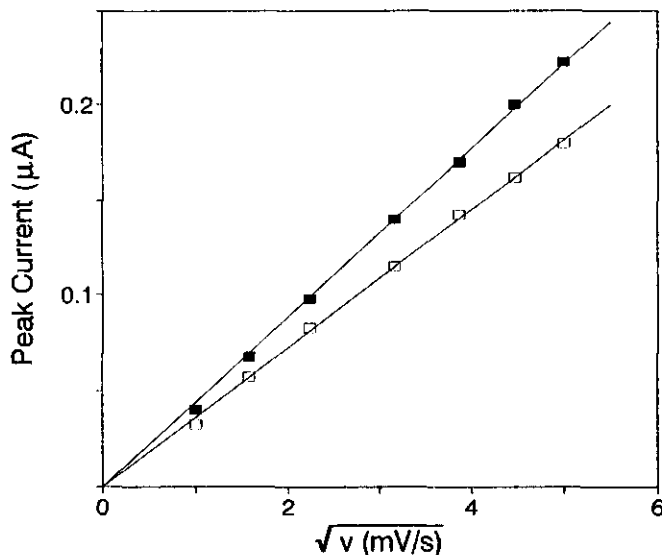
**Figure 6.1.** (Continued) **b:** Scan rate dependence of the anodic $(+i_{pa}; \square)$ and cathodic $(-i_{pc}; \blacksquare)$ peak current. An average diffusion coefficient of $(8\pm2)\cdot10^{-7}$ cm$^2$/s is obtained (working surface 13 mm$^2$).

amino acids to the positively charged HiPIPs does not change the midpoint potentials significantly. This indicates that the broadening of the voltammograms is rather symmetrical and thus the oxidation and reduction are equally hampered by denatured protein. Poly-L-lysine does not have any effect on the midpoint potentials. Addition of 0.8 mM poly-L-lysine to *R. globiformis* HiPIP has no effect on the midpoint potential nor on the peak-current. Without a promoter *C. vinosum* HiPIP gives a very low and poorly reversible response but the midpoint potential is equal to the measured value in the presence of poly-L-lysine.

### 6.3.4   pH dependence of the potentials.

The results of the measurements of the redox potentials at different pH are collected in Figure 6.2 and in Table 6.3. Generally, the response of the HiPIPs (reversibility, current) is independent of pH when the optimum concentrations of protein, promoters and stabilizers are used. Only at high pH ($\geq9.5$) the response of the four positively charged HiPIP becomes less stable and broader. The very weak response of *C. vinosum* HiPIP without promoter or stabilizer becomes stronger and more stable at low pH (4 to 5.5). At pH 4 *E. vacuolata* iso-1 gives a broad response (130 mV peak-to-peak separation) without poly-L-lysine. These observations suggests that some deprotonation occurs at high pH and some protonation of negatively charged groups occurs on the surface of either the protein or the electrode at low
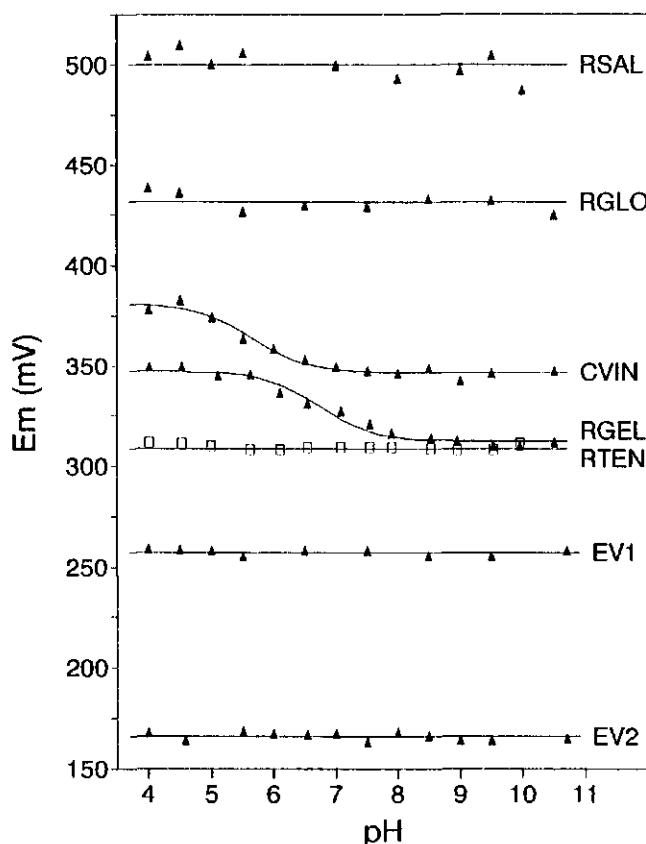
**Figure 6.2.** Dependence of HiPIP redox potentials on pH. Cyclic voltammograms of the HiPIPs (and promoters and/or stabilizers, Table 6.3) in 10-20 mM buffer were recorded at 22°C with a scan rate of 10 mV/s; working / reference / counter electrodes, glassy carbon / SCE / Pt. The potential axis is defined *versus* the normal hydrogen electrode. (*R. tenuis* is given a different symbol for clearness).

pH. Although 4,4'-dipyridyl is protonated around pH 6, no deterioration of the *R. salinarum* response was observed at low pH. Such a deterioration was reported for cytochrome c on a dipyridyl-modified gold electrode [Hagen, 1989]. This indicates that in the case of *R. salinarum* HiPIP on glassy carbon, 4,4'-dipyridyl does not act as a hydrogen-bond accepting promoter but rather as a stabilizer (Like cytochome c, *R. salinarum* HiPIP has a positive surface charge).

At a pH between 4 and 10 protonation of histidines is most likely to cause pH-dependent midpoint potentials. As expected [Luchinat *et al.*, 1994], the potentials of the two HiPIPs without histidines (*R. globiformis* and *R. tenuis*) are independent of pH. This was also found by Krishnamoorthi *et al.* [1989] who observed pH independent ^{1}H-NMR spectra of *R.*

**Table 6.3.** Dependence of HiPIP reduction potentials on pH.[a]

| | $E_m$ (high pH)[b] | $pK_{(ox)}$ | $pK_{red}$ | Slope[c] | $\Delta E_m$ |
|---|---|---|---|---|---|
| | mV | | | mV/pH | mV |
| *R. salinarum* iso-2 | 500.1 ± 7.0 | | | | |
| *R. globiformis* | 431.3 ± 4.5 | | | | |
| *C. vinosum* | 346.5 ± 2.1 | 5.35 | 5.95 | −19.3 | 35.0 |
| | 346.6 ± 2.1 | 5.65 | | −19.9 | 34.7 |
| *R. gelatinosus* | 312.4 ± 3.1 | 6.30 | 6.90 | −19.2 | 34.7 |
| *R. gelatinosus* + asp | 312.5 ± 2.7 | 6.51 | 7.11 | −19.3 | 34.9 |
| *R. gelatinosus*, both | 312.4 ± 3.0 | 6.42 | 7.01 | −19.0 | 34.9 |
| | 312.6 ± 3.1 | 6.71 | | −19.9 | 34.6 |
| *R. tenuis* | 309.6 ± 2.3 | | | | |
| *R. tenuis* + trp | 309.0 ± 1.2 | | | | |
| *R. tenuis*, both | 308.8 ± 1.8 | | | | |
| *E. vacuolata* iso-1 | 257.4 ± 1.4 | | | | |
| *E. vacuolata* iso-2 | 166.1 ± 1.8 | | | | |

[a]Results of chi-square fitting of the data with a $pK_{ox}$ and $pK_{red}$ and with one $pK$. *R. salinarum* HiPIP (67 μM) was measured in the presence of 11 mM 4,4'-dipyridyl, *R. globiformis* (58 μM) without additions, *C. vinosum* (43 μM) with 0.8 mM poly-L-lysine and 9.2 mM morpholin, *R. gelatinosus* (51 μM) both without and with 3 mM aspartate; *R. tenuis* (84 μM) both without and with 3 mM tryptophan, *E. vacuolata* iso-1 (44 μM) with 0.67 mM poly-L-lysine and 7.7 mM morpholin and *E. vacuolata* iso-2 (134 μM) with 1.6 mM poly-L-lysine and 7.2 mM morpholin, all in 10-20 mM buffer. [b]For the pH-independent potentials the average is given. [c]The slope was calculated from the steepest part of the curve over 0.2 pH units.

*tenuis* HiPIP and by Przysiecki *et al.* [1985] who found that the visible CD spectrum of reduced *R. tenuis* is independent of pH.

The potentials of *C. vinosum* and *R. gelatinosus* HiPIPs both show characteristic pH-titration curves with clear plateaus at high and low pH. The potentials at low pH are about 35 mV higher than the potentials at high pH and the maximum slopes are approximately −20 mV/pH. This indicates that the single histidine residue present in both *R. gelatinosus* and *C. vinosum* HiPIP can be titrated. The small difference between the acidic and basic potentials

and the small slopes can be explained in two ways. Either the p$K$ of the histidine residue in the oxidized protein is lower than in the reduced HiPIP, or the p$K$ does not change at all.

In the case of a redox-state dependent p$K$ the Nernst equation for a direct redox-linked protonation can be applied to fit the data:

$$E_m = E_m^a + \frac{RT}{F} \ln\left[\frac{[H^+] + K_{red}}{[H^+] + K_{ox}}\right] \tag{6.1}$$

in which $E_m{}^a$ is the potential at low pH. The charge of the proton influences the redox potential of the cluster and the charge of the extra electron alters the p$K$ of the protonation site. A difference of 35 mV between the potentials at low and high pH and a maximum slope of $-19$ mV/pH are obtained if the difference between p$K_{red}$ and p$K_{ox}$ is about 0.6 units.

When the p$K$ is assumed to be independent of the redox-state of the cluster the effect of pH on the potentials are of an allosteric nature. Protonation of the histidine causes a change in conformation of the protein and the slightly altered environment of the cluster increases its potential by about 35 mV. A Coulombic interaction between the cluster and the protonation site is less likely in this case because a change of p$K$ would then also be expected. A common pH-titration curve can be used to fit the data:

$$E_m = E_m^b + \frac{\Delta E_m}{1 + 10^{pH - pK}} \tag{6.2}$$

with $\Delta E_m = E_m{}^a - E_m{}^b$ and $E_m{}^b$ is the potential at high pH. If the p$K$ is the average of p$K_{ox}$ and p$K_{red}$ and the proper plateau-potentials are used, the maximum slope is slightly steeper compared to the two-p$K$ Nernst curve. However, the curves are virtually indistinguishable if the two-p$K$ curve has p$K_{red}$-p$K_{ox}$<1.

The results of the fits are collected in Table 6.3. For both *R. gelatinosus* HiPIP (using the data both with and without the stabilizing aspartate added) and *C. vinosum* HiPIP the Nernst-fit yields p$K_{red}$-p$K_{ox}$=0.6 and a p$K$ value found with the one-p$K$ titration formula exactly equal to the average of p$K_{ox}$ and p$K_{red}$. For *R. gelatinosus* a p$K$ of 6.71 is found and for *C. vinosum* a p$K$ of 5.65 is obtained. No significant differences of the standard deviations (= $\sqrt{(X^2/N)}$) are found between the one-p$K$ fit and the Nernst-fit.

These p$K$ values are slightly lower compared to reported pH profiles. Nettesheim *et al.* [1983] found from ^{1}H-NMR for both *C. vinosum* and *R. gelatinosus* HiPIP that the p$K$ of the oxidized protein is 6.7 and p$K_{red}$=7.3. Earlier, from pH-perturbation difference spectroscopic studies of *C. vinosum* HiPIP a p$K_{ox}$ of 6.7 and p$K_{red}$ of 6.9, and a p$K$ of about 7 was obtained from electrostatically corrected pH profile for the second order rate constant

of oxidation by ferricyanide [Nettesheim *et al.*, 1980]. The pH dependence of HiPIP redox potentials measured by Mizrahi *et al.* [1976, 1980] suggest a p$K$ below 7 for *C. vinosum* and a p$K$ around 7.5 for *R. gelatinosus*. Przysiecki *et al.* [1985] found that the visible CD spectra of reduced *C. vinosum* and *R. gelatinosus* are different at pH 8.7 and pH 5.1.

The potentials of *E. vacuolata* iso-1 and iso-2 are not pH-dependent in spite of the three and two histidine residues present in these proteins [Ambler *et al.*, 1994]. In *C. vinosum* and *R. gelatinosus* the histidine next to the first cysteine (His42 and Cys43 in *Chromatium*) is responsible for the observed pH-dependence but in both *E. vacuolata* iso-1 and iso-2 this particular histidine is not present. All histidines are located further away in the hydrophilic loop that connects Tyr19 and Cys43 (*Chromatium* numbering). Apparently, protonation of the histidines in this loop does not alter the cluster environment sufficiently to cause a measurable shift of the potential because these residues are more exposed to the solvent [Benning *et al.*, 1994]. The potential of *R. salinarum* HiPIP is also independent of pH. Two histidines are present in this HiPIP (Ambler *et al.*, unpublished) but the sequence is too divergent from the other HiPIPs to model the structure.

The results reported here differ from the pH profiles reported by Luchinat *et al.* [1994]. They used an edge-plane pyrolytic graphite electrode without promoters or stabilizers. The potentials were measured with single-scan differential pulse voltammetry (DPV) and the midpoint potentials were determined by correction of the peak-position by half the pulse amplitude. The observed peaks were reported to be broadened (n=0.8 to 0.9). Unbuffered solutions of 100 to 300 µM HiPIP with 0.5 M NaCl were titrated with concentrated NaOH or HCl. The results for *R. globiformis* (pH-independent), *C. vinosum* (p$K_{ox}$=6.2, p$K_{red}$=6.6) and *R. gelatinosus* (p$K_{ox}$=7.2, p$K_{red}$=7.5) are comparable to the observations reported in this chapter (although they did not find clear plateaus at low pH) but pH-dependent potentials were also found for both *E. vacuolata* iso-HiPIPs.

However, from the observations described here it is clear that the response at a carbon surface without promoters is very unstable and the electron tranfer kinetics are very much dependent on the pH without promoters. Moreover, at higher ionic strength and with the reported high protein concentrations the response also becomes worse. When such quasi-reversible systems are measured by DPV the peak will not only be lower and broader but will also be significantly shifted by an activation overpotential. In an anodic (oxidative) scan the observed potential will be higher and in a cathodic (reductive) scan a lower apparent midpoint potential will be found. It is therefore possible that at least part of the dependence of the potential on pH observed by Luchinat *et al.* originates from a pH-dependent electron-transfer rate. The midpoint potentials obtained with cyclic voltammetry are less sensitive to the electron-transfer rate. For quasi-reversible systems the peak-to-peak separation increases with increasing scan rate, but if the shift is symmetrical this does not influence the measured midpoint potential. The symmetry of the broadening can be examined by altering the scan rate.
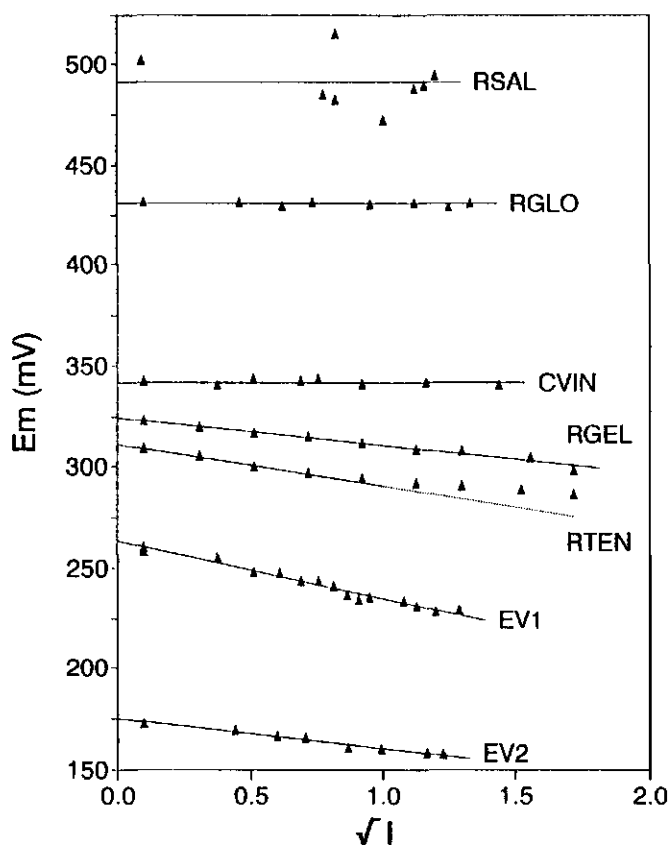
**Figure 6.3.** Dependence of HiPIP redox potentials on the square root of the total ionic strength. Cyclic voltammograms of the HiPIPs (and promoters and/or stabilizers, see Table 6.4) in 10-20 mM Hepes pH 7.5 and increasing concentration KCl were recorded at 22°C with a scan rate of 10 mV/s; working/reference/counter electrodes, glassy carbon/SCE/Pt. The potential axis is defined *versus* the normal hydrogen electrode.

### 6.3.5   Ionic strength dependence of the potentials.

The results of the measurements of the redox potentials at different ionic strength are collected in Figure 6.3 and in Table 6.4. The *R. salinarum, R. globiformis* and *C. vinosum* HiPIPs do not show any dependence of the midpoint potential on the ionic strength (although the data for *R. salinarum* are rather noisy due to the low stability of the electrochemical response at higher ionic strength). The potentials of *R. gelatinosus, R. tenuis* and both *E. vacuolata* HiPIPs decrease with increasing ionic strength but the sensitivity is rather low. The

**Table 6.4.** Dependence of HiPIP reduction potentials on ionic strength[a].

| | $E_m$ (at $I$=0)[b] | Slope | $r^2$ |
|---|---|---|---|
| | mV | mV/$\sqrt{M}$ | |
| *R. salinarum* iso-2 | 490.9 ± 13.1 | 0 | |
| *R. globiformis* | 430.9 ± 1.1 | 0 | |
| *C. vinosum* | 342.2 ± 1.3 | 0 | |
| *R. gelatinosus* | 323.7 ± 1.0 | −14.1 ± 0.6 | 0.9869 |
| *R. gelatinosus* + asp | 324.4 ± 0.3 | −13.0 ± 0.3 | 0.9974 |
| *R. tenuis* | 311.3 ± 0.9 | −21.7 ± 1.3 | 0.9886 |
| *R. tenuis* + trp | 310.9 ± 0.2 | −19.4 ± 0.7 | 0.9988 |
| *E. vacuolata* iso-1 | 263.3 ± 1.8 | −28.0 ± 1.3 | 0.9724 |
| *E. vacuolata* iso-2 | 174.9 ± 1.0 | −14.8 ± 1.0 | 0.9743 |

[a]Results of linear regression analysis of potential *versus* the square root of the ionic strength. *R. salinarum* HiPIP (67 µM) was measured in the presence of 11 mM 4,4'-dipyridyl, *R. globiformis* (58 µM) without additions, *C. vinosum* (43 µM) with 0.8 mM poly-L-lysine and 9.2 mM morpholin, *R. gelatinosus* (51 µM) both without and with 3 mM aspartate; *R. tenuis* (84 µM) both without and with 3 mM tryptophan, *E. vacuolata* iso-1 (27 µM) with 0.8 mM poly-L-lysine and 9.2 mM morpholin and *E. vacuolata* iso-2 (134 µM) with 1.6 mM poly-L-lysine and 7.2 mM morpholin, all in Hepes pH 7.5 and KCl. [b]In case of zero slope the average potential is given.

slopes of the $E_m$ *versus* $\sqrt{I}$ are −13.6, −20.6, -28.0 and −14.8 mV/$\sqrt{M}$ respectively. The slopes are zero when the potential itself is high ($E_m$>=346 mV for *C. vinosum*, *R. globiformis*, *R. salinarum*) but this might be coincidental.

Generally, the stability of the electrochemical response is lower and the electron transfer kinetics slower at high ionic strength (usually above 0.5 M KCl). This is most likely due to shielding of charges and thus weakening of ionic interactions between the protein, the promoter and/or stabilizer and electrode surface. Hydrophobic interactions become dominant at higher salt concentrations and might cause blocking of electrode by denatured protein. It is however not likely that the measured sensitivity of the midpoint potential on the ionic strength is caused by asymmetrical broadening of the voltammograms due to this salt-dependence of the electron transfer kinetics because the potentials are already lowered when the reversibility of the reaction is still good (peak-to-peak separation close to 60 mV up to 0.5 M KCl).
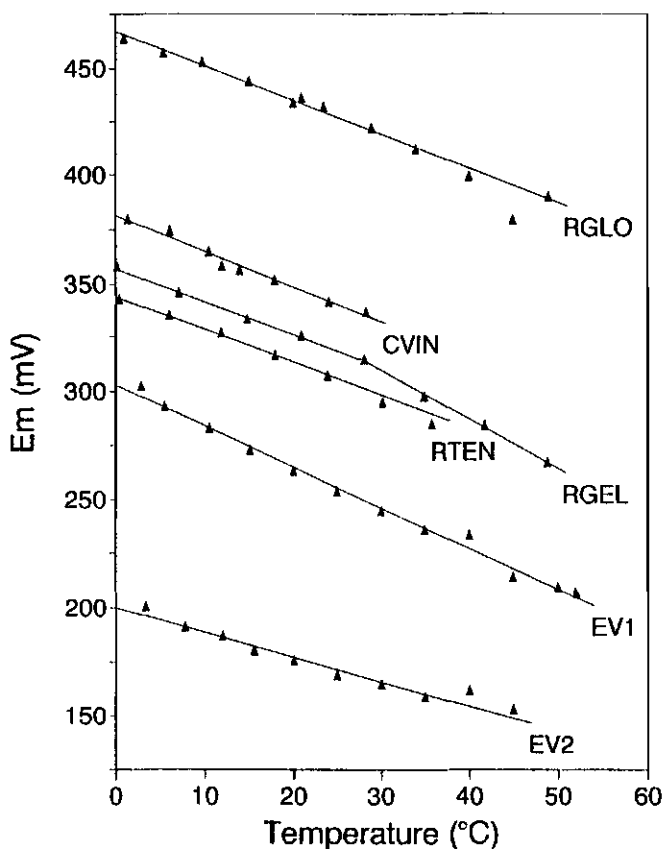
**Figure 6.4.** Dependence of HiPIP redox potentials on the temperature. Cyclic voltammograms of the HiPIPs (and promoters and/or stabilizers, see Table 6.5) in 10-20 mM Hepes pH 7.5 were recorded in an isothermal cell with a scan rate of 10 mV/s; working/reference/counter electrodes, glassy carbon/SCE/Pt. The potential axis is defined *versus* the normal hydrogen electrode.

### 6.3.6 Temperature dependence of the redox reactions.

The results of the measurements of the redox potentials at different temperatures are collected in Figure 6.4 and in Table 6.5. Of the investigated HiPIPs, *R. gelatinosus* HiPIP is the only one with a clear break point in the temperature dependence. The potentials of *E. vacuolata* iso-1 and iso-2 and *R. globiformis* HiPIPs do not have break points up to 45-50°C (Measurements at higher temperatures was not possible because the small droplet evaporated too quickly under the warm argon flow). The response of *C. vinosum* HiPIP disappears at a temperature of 36°C although no significant broadening was observed at 29°C. *R. tenuis*

**Table 6.5.** Dependence of the HiPIP reduction potentials on temperature[a].

| | intercept | Slope | $r^2$ | Range | $\Delta S°$ | $\Delta H°$ |
|---|---|---|---|---|---|---|
| | mV | mV/K | | °C | J/mol·K | kJ/mol |
| R. globiformis | 466.9 ± 2.2 | −1.59 ± 0.05 | 0.9921 | 1-49 | −153.0 | −86.9 |
| C. vinosum | 381.5 ± 2.2 | −1.64 ± 0.09 | 0.9816 | 1-29 | −158.2 | −80.0 |
| R. gelatinosus | 357.0 ± 1.3 | −1.59 ± 0.06 | 0.9959 | 0-29 | −153.4 | −76.4 |
| | 380.0 ± 1.0 | −2.39 ± 0.07 | 0.9985 | 29-49 | −230.2 | −99.5 |
| R. gel. + asp | 357.6 ± 1.4 | −1.49 ± 0.06 | 0.9949 | 0-26 | −144.0 | −73.8 |
| | 374.2 ± 2.6 | −2.12 ± 0.17 | 0.9878 | 26-49 | −204.9 | −92.1 |
| R. tenuis | 344.2 ± 1.4 | −1.52 ± 0.07 | 0.9933 | 0-24 | −146.8 | −73.3 |
| R. tenuis + trp | 344.3 ± 1.5 | −1.56 ± 0.05 | 0.9955 | 0-36 | −150.3 | −74.3 |
| E. vacuolata iso-1 | 302.9 ± 3.1 | −1.89 ± 0.05 | 0.9916 | 3-52 | −182.1 | −79.0 |
| E. vacuolata iso-2 | 199.9 ± 2.7 | −1.13 ± 0.07 | 0.9736 | 2-45 | −109.4 | −49.2 |

[a]Results of linear regression analysis of the potential *versus* the temperature, measured in 10-20 mM Hepes pH 7.5. *R. globiformis* HiPIP (68 µM) was measured without additions, *C. vinosum* (72 µM) with 0.67 mM poly-L-lysine and 7.7 mM morpholin, *R. gelatinosus* (51 µM) both without and with 3 mM aspartate; *R. tenuis* (84 µM) both without and with 3 mM tryptophan, *E. vacuolata* iso-1 (27 µM) with 0.8 mM poly-L-lysine and 9.2 mM morpholin and *E. vacuolata* iso-2 (134 µM) with 1.6 mM poly-L-lysine and 7.2 mM morpholin.

HiPIP could not be measured at 30°C or higher without tryptophan but with this stabilizer a stable response was obtained up to 36°C. *R. salinarum* HiPIP is too unstable to determine a reliable temperature dependence at all (During the adjustment of the temperature the response disappears).

The entropy and enthalpy changes upon reduction are calculated from the $E_m$ *versus* $T$ plots as described in Chapter 2. The slopes of these plots of −1.2 to −1.8 mV/K at low temperature are steep compared to many other redox proteins [Taniguchi *et al.*, 1980]. The resulting large negative $\Delta S°$ values indicate that the reduced protein has a very rigid structure. The observed redox thermodynamics of *C. vinosum* HiPIP differ from the $\Delta H°$=−66.0 kJ/mol and $\Delta S°$=−107 J/mol·K (*i.e.* a slope of −1.1 mV/K) reported by Taniguchi *et al.* [1980]. The break point in the temperature dependence of *R. gelatinosus* HiPIP occurs around 28°C. Averaged over the measurements with and without the stabilizing aspartate added, the slope of the $E_m$ *versus* $T$ plot of *R. gelatinosus* HiPIP changes around 28°C from −1.5 mV/K to

−2.2 mV/K. Below 28°, $\Delta H° = -75.1$ kJ/mol and $\Delta S° = -149$ J/mol·K ($\Delta S°_{rc} = -84$ J/mol·K) and above 28°C $\Delta H° = -95.8$ kJ/mol and $\Delta S° = -218$ J/mol·K ($\Delta S°_{rc} = -153$ J/mol·K). This change to a more negative slope may be caused by a change of conformation around 28°C [Taniguchi *et al.*, 1984].

## 6.4    Discussion

### 6.4.1    Optical spectra, charges and potentials of the HiPIPs.

The position of the absorption band of the reduced cluster might be correlated with the relative polarity of the amino acids surrounding the cluster. In a more polar (less hydrophobic) environment the electronic state of the cluster with highest dipole moment, probably the excited state, will be lowered relative to the ground state. This results in a red-shift of the absorption band [Cantor & Schimmel, 1980; Warshel & Russel, 1984]. Because the electron-rich reduced cluster will be more stable if the cluster is more solvated [Churg & Warshel, 1986], *i.e.* surrounded by more polar residues, a correlation is expected between the position of the absorption band and the redox potential.

The influence of the solvation of the cluster on the visible spectrum and redox-properties of iron-sulfur clusters was already observed by Hill *et al.* [1977]. They examined the effect of DMSO/water mixtures on both the absorption maxima and the reduction potentials of two $[Fe_4S_4(SR)_4]^{2-}$ analogues and of *Clostridium pasteurianum* ferredoxin. Going from pure water to pure DMSO the potentials of the analogues were lowered and the visible maximum was red-shifted proportional to the percentage DMSO. The maximum around 295 nm was solvent-insensitive. The ferredoxin potential and absorption maximum did not change up to 40% DMSO but between 40 and 80% DMSO the maximum around 390 nm shifts to longer wavelength and the potential decreases proportional to the percentage DMSO. A decrease of about 10 mV per nm red-shift can be estimated from the reported data for ferredoxin and 5 to 10 mV/nm for the analogues. The observed increase of the potentials with decreasing percentage DMSO (*i.e.* to a more polar and protic solvent) is consistent with the expected stabilization of the reduced state by solvation and hydrogen bonding in water but the correlated red-shift is opposite to the expected greater difference between the ground state and the exited state in a less polar environment.

The solvent-sensitive band was ascribed to charge transfer from filled orbitals with dominant $S^*$ lone pair character to the highest occupied level with predominant tetrametal antibonding character [Yang *et al.*, 1975]. Apparently the lone pair ground state is stabilized by the hydrogen bonding network of water. If the cluster pockets of the HiPIPs have different (local) polarity but the hydrogen bonding network to the reduced clusters are similar this

different stabilization of the ground state does not occur and a blue-shift with lowering of the polarity will be observed.

A close look at the data indeed suggests a linear correlation between the position of the absorption band around 385 nm and the measured midpoint potentials. Using *E. vacuolata* iso-2, *R. tenuis*, *R. gelatinosus*, *C. vinosum* and *R. salinarum* HiPIP, a regression line with a slope of +19.8 mV per nm red-shift ($r^2$=0.98865) is obtained (not shown). However, the potential of *E. vacuolata* iso-1 is much lower (173 mV) and the potential of *R. globiformis* HiPIP is higher (78 mV) than predicted by this regression line. This correlation between absorption maxima of the reduced HiPIPs and the reduction potential suggests a relation between the polarity of the cluster environment, the stability of the reduced state and the stability of the exited reduced state. The position of the absorption band is not correlated with the total number of (uncharged) polar, apolar or aromatic residues, but this is to be expected because only the polarity of the residues in the vicinity of the cluster are responsible for the solvation.

Before discussing these observations in detail, the overall charges of the HiPIPs must be considered. The potential of the positively charged *R. globiformis* HiPIP is too high and that of the negatively charged *E. vacuolata* iso-1 is too low in a plot of the redox potential against absorption maximum. Also, the data suggest a correlation between the overall charge (or iso-electric point) and the redox potential within the acidic HiPIPs (see Table 6.2). Such a correlation will probably modify the correlation between the potential and the absorption spectrum. However, when other HiPIPs are included in the plot (Figure 6.5a; combining the published potentials and charges listed in Table 6.1) the correlation is lost but the distribution of the charges is not completely random. It appears that the potentials of some HiPIPs are centred closely around an average value of 333 mV, in spite of the variation of the overall charges, ranging from very negative to quite positive. This indicates that the overall charge of these HiPIPs does not influence the potential of the cluster. The potentials of the four highly negatively charged *Ectothiorhodospira* HiPIPs (both *E. vacuolata* and both *E. halophila* iso-HiPIPs) are significantly lower than 333 mV and the potentials of the positively charged *R. globiformis* and *R. salinarum* HiPIPs are higher than the average. This suggests the existence of a group of HiPIPs with potentials that are influenced by the overall charge.

A lowering of the potential with increasing negative charge is expected because of destabilization of the additional negative charge in the reduced state. The simplest model for this is the linear Coulomb model. In this model, one negatively charged electron is introduced in the center of a sphere with radius $r$ with a net charge $z$ on the outside and a uniform dielectric constant inside this sphere. The electrostatic force on the electron is then given by

$$F = \frac{e^2 z}{4\pi\,\varepsilon\,\varepsilon_0 r^2} \tag{6.3}$$

The charge-dependent part of the reduction enthalpy is then given by the work to bring the electron from infinity into the center of the sphere:

$$\Delta h^\circ(z) = \frac{-e^2 z}{4\pi\,\varepsilon\,\varepsilon_0 r} \tag{6.4}$$

per molecule, or

$$\Delta H^\circ(z) = -nFE_m = \frac{-Fez}{4\pi\,\varepsilon\,\varepsilon_0 r} \tag{6.5}$$

per mol. The slope of potential *versus* charge is then

$$\frac{\partial E_m}{\partial z} = \frac{e}{4\pi\,\varepsilon\,\varepsilon_0 rn} \tag{6.6}$$

or

$$\frac{\partial E_m}{\partial z} = \frac{14.4}{\varepsilon\,r} \quad \text{V/unit} \tag{6.7}$$

with $n=1$, $\varepsilon_0=8.8542\cdot10^{-12}$ $C^2N^{-1}m^{-2}$, $e=1.6022\cdot10^{-19}$ C and $r$ in Å.

When both *E. halophila* HiPIPs are included, a regression line with a slope of 29.7 ± 4.2 mV per unit charge ($r^2$=0.92671) and a potential of 404.2 ± 53.9 mV at zero charge is obtained. The *Paracoccus* HiPIP is very acidic and the potential of 282 mV [Przysiecki *et al.*, 1985; Mizrahi *et al.*, 1980] is lower than the mean value (although Hori [1961] reported a potential of +360 mV) but not as low as would be expected from the regression line. Therefore, it may be considered to be a charge-independent HiPIP rather than belonging to the charge-dependent group. The potential and charge of *C. vinosum* HiPIP do not clearly indicate to which group this HiPIP belongs, but sequence homology with *T. roseopersicina* and *C. gracile* and similarities with *R. gelatinosus* HiPIP strongly suggest that it is a charge-independent HiPIP.

With this classification of the HiPIPs it is possible to separate the influence of the overall charge from the measured potentials. The remaining part of the potential then probably is a reflection of differences in the local environment of the cluster (polarity, solvation). Indeed, a strong linear correlation is found when the deviations from the mean potentials of *C. vinosum*, *R. tenuis* and *R. gelatinosus* HiPIPs and the deviations from the regression line of the other HiPIPs are collected and plotted against the positions of the absorption maxima (Figure 6.5b). When *E. vacuolata* iso-1 is excluded, regression yields a line with a slope of 7.01 ± 0.91 mV/nm, crossing the x-axis at 386.2 nm ($r^2$=0.93740). The sign of the slope is in accordance with the expected lowering of the potential and blue-shifting of the absorption band upon lowering of the polarity. The uniform behaviour of both types of HiPIPs indicates that the relative solvation of the cluster has the same effect on the potentials in all HiPIPs and apparently is independent of the influences of charges on the potential. Therefore, the modulation of the potential by charges and by the polarity of the pocket can be assumed to be additive. The line through the charge-dependent HiPIPs and the line through the residual potentials *versus* the absorption maxima can then be optimized by minimizing the chi-square for six HiPIPs. Starting with the values obtained from the regression lines results in general formulas for both groups of HiPIPs:

$$E_m^7 = 332.9 + ( \lambda_{max} - 385.2 ) \cdot 9.661 \text{ mV} \tag{6.8}$$

for the *Chromatium*-like HiPIPs with charge-independent potentials and

$$E_m^7 = 399.3 + z \cdot 24.52 + ( \lambda_{max} - 385.2 ) \cdot 9.661 \text{ mV} \tag{6.9}$$

for the *Ectothiorhodospira*-like charge-dependent HiPIPs. These results are plotted in Figure 6.5 and a comparision between the measured and predicted potentials is made in Table 6.6. The standard deviation $\sqrt{(\chi^2/N)}$ of the predicted potentials from the measured potentials improved from 6.1 to 0.6 mV (*E. vacuolata* iso-1 excluded). The average potential of the charge-independent HiPIPs of 332.9 mV was not included in the minimization because it only serves as a reference point for the potential scale. From the obtained slope of 24.5 mV per unit charge an apparent relative dielectric constant $\varepsilon_{app}$ of 84 can be calculated when an average radius of 7 Å is assumed [Dunham *et al.*, 1991; Carter *et al.*, 1974a; Freer *et al.*, 1975; Rayment *et al.*, 1992; Breiter *et al.*, 1991; Benning *et al.*, 1994]. This is close to the dielectric constant of water, indicating that the influence of the charges is effectively quenched by the peptide matrix and probably also by the water dipoles surrounding the charged groups at the surface [Churg & Warshel, 1986; Warshel & Russel 1984].

Although the two *E. halophila* HiPIPs were not included in the fit, the prediction of the potentials is remarkably accurate. An additional argument to include *E. halophila* and *R. globiformis* in one group are the findings of Nettesheim and of Bertini and coworkers that the
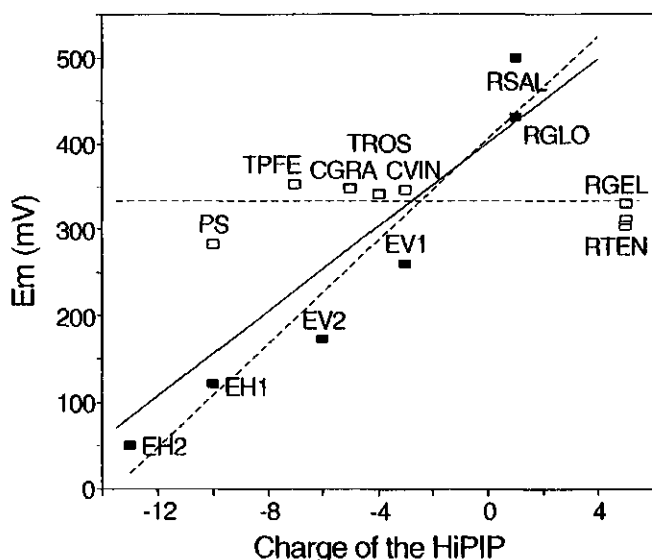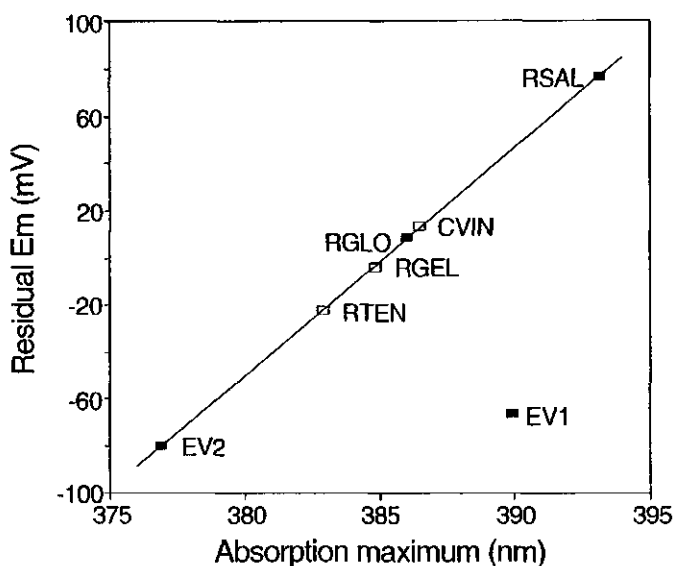
**Figure 6.5.** Influence of peptide charge and cluster solvation on the potentials of HiPIPs.

**a:** Resulting linearized dependence of the potentials on the net charge of the peptide.

**b:** Resulting linear dependence of the residual potential on the position of the absorption band. The dashed lines in Figure (a) are the average potential of the open squares (exept *Paracoccus* sp.) and the regression line for the filled squares. The solid line is the result of a chi-square optimization of the potentials of *R. salinarum* (large iso-2 HiPIP), *R. globiformis* and *E. vacuolata* iso-2 with respect to the *R. gelatinosus*, *R. tenuis* and *C. vinosum* potentials. The residual potential in figure (b) is the redox potential of the HiPIP *minus* the fitted charge-dependent part of the potential.

**Table 6.6.** Midpoint potentials at $I$=0.01 and 22°C, in mV NHE, as obtained from the different measurement series.

| | $E_m^{7.5}$, from dependence on | | | $E_m^7$ | |
| --- | --- | --- | --- | --- | --- |
| | pH | Ionic strength | temp. | average[a] | predicted[b] |
| | mV | | | | |
| *R. salinarum* iso-2 | 500 | (491) | | 500 | 500 |
| *R. globiformis* | 431 | 432 | 432 | 432 | 432 |
| *C. vinosum* | 347 | 343 | 345 | 346 | 345 |
| *R. gelatinosus* | 318 | 323 | 324 | 329 | 329 |
| *R. tenuis* | 309 | 309 | 311 | 310 | 311 |
| *E. vacuolata* iso-1 | 257 | 260 | 261 | 259 | (371) |
| *E. vacuolata* iso-2 | 166 | 173 | 175 | 172 | 172 |

[a]The average potentials at pH 7.0 (also mentioned in Table 6.1) are calculated from the average at pH 7.5 and the pH-dependence. [b]from the chi-square optimization plotted in Figure 6.5.

electronic distribution within the oxidized clusters is in equilibrium between two forms. In one form, Cys-46 is bound to an iron(III) ion and Cys-77 to a mixed-valence iron (with the iron coordinated by Cys-63), in the other form this is reversed. The HiPIPs from *C. vinosum* and *R. gelatinosus* have the cluster mainly in the first form (ratio 70/30 and 80/20) while *E. halophila* iso-2 and *R. globiformis* are found more in the second form (ratio 10/90 and 30/70). The cluster in *E. vacuolata* iso-2 is found in an intermediate 60/40 ratio. [Nettesheim *et al.*, 1992; Banci *et al.*, 1993a,b; Bertini *et al.*, 1992, 1993].

The dependence of the potential of electron transferring proteins on the net charge of the protein was already mentioned by Rees [Rees, 1985]. A slope of 23 mV per charge (intercept +205 mV) was found for the soluble one-electron carrier proteins, including HiPIPs, ferredoxins, flavodoxins, azurins and cytochromes. However, Moore *et al.* [1986] commented that this linear correlation is fortuitous because the different types of proteins are likely to have different contributions of the bonding interactions at the redox center and conformational changes to the redox potentials, and some proteins far from the observed trend were not included. They concluded that the interactions between the redox center charge and the

charges on the protein surface are relatively small compared to interactions with more buried charges. For example, it was found that ionization of a buried propionic acid residue attached to the haem lowers the potential of *Pseudomonas aeruginosa* cytochrome $c_{551}$ by 65 mV. This was explained in terms of a local dielectric constant of 27, quenching the electrostatic repulsion of the electron [Moore, 1983, Rogers *et al.*, 1984].

With this in mind it might be possible to explain why the potentials of a large group of HiPIPs do not depend on the charge of the peptide. The four known structures do not reveal systematic differences between the two groups in exposure of the charges to water, nor in the distances to the cluster. It is unlikely (if not impossible) that the insensitivity of the potentials to charges is caused by a "passive" complete shielding of the charges.

A large effect on the dielectrics of the protein matrix might be expected from the aromatic residues. The number of aromatic residues varies but some are conserved, both in position and in orientation. From the sequences and the four known crystal structures it is clear that Tyr19, and the aromatic residues 76 and 80 (*Chromatium* numbering) are highly conserved and are positioned exactly between the cluster and the hydrophilic loop between Tyr19 and Cys43. The aromatic residues in the twisted antiparallel β-sheet (formed by parts of the peptide between the second and the last cysteine) are positioned at the opposite side of the cluster, separating it from the second hydrophilic loop (residues 51-59) [Carter *et al.*, 1974a; Freer *et al.*, 1975; Rayment *et al.*, 1992; Breiter *et al.*, 1991; Benning *et al.*, 1994]. They are less conserved but it seems that at least one must be present to complete the four-membered ring of aromatic residues located around one side of the cluster. Most likely these aromatic side chains provide an apolar cluster environment in all HiPIPs and thus are (at least in part) responsible for the lowering of the potential relative to ferredoxin clusters. Different positions or even slightly different orientations of the aromatic residues might have a large effect on local dielectric constants in the protein matrix, but no clear differences in the structures can be found between the two groups. However, a numerical correlation might be present between the aromatic residues and the potential (Table 6.1). Within the *Ectothiorhodospira*-like HiPIPs an increasing number of aromatic residues coincides with a decreasing potential, while a more constant number of aromatic residues is present in the charge-independent *Chromatium*-like HiPIPs. This suggests that the potential is also modulated by these residues.

There also is a correlation between the influence of the charge on the potential and the total number of apolar (A, V, L, I, P, M, W, Y, F) and the number of uncharged polar (S, T, H, N, Q) residues (the charged residues are not included because these are all on the outside of the proteins - except Asp46 in *R. tenuis* - and are the ones that are supposed to be shielded). This is most clearly visible when looking at the difference between the two numbers, *i.e.* the surplus hydrophobic residues (listed in Table 6.1). In the group of *Chromatium*-like HiPIPs this number decreases almost linearly with increasing overall charge. A slight increase of the surplus hydrophobic residues with increasing charge is found in the

charge-dependent *Ectothiorhodospira* HiPIPs but this probably reflects the increasing number of aromatic residues. The surplus hydrophobic residues in *R. gelatinosus* HiPIP is comparable to *C. gracile* with an equal but opposite charge. The *R. globiformis* and both *R. tenuis* HiPIPs have a relatively small surplus of hydrophobic residues but this is probably due to their smaller size, causing a higher surface-to-volume ratio. This is also the case for *R. salinarum* iso-2, although this HiPIP forms a large multimer [Meyer *et al.*, 1990; Ambler *et al.*, unpublished].

A striking difference between the *R. tenuis* HiPIPs (strain 2761 and 3761) and the others is the presence of a buried aspartate at position 46 and one inserted amino acid at position 47 (Asn in stain 2761 and Ser in 3761), where most other HiPIPs have a lysine that is exposed to the solvent (both *E. halophila* HiPIPs have a valine, *Paracoccus* HiPIP has an asparagine and *T. pfennigii* HiPIP a tyrosine at the position of the *R. tenuis* Asp46). Also, the nearby phenylalanine that is present in most of the other HiPIPs is replaced by Ile43 (a valine in *R. globiformis*, a tyrosine in *T. pfennigii* and in *E. halophila* iso-1 Phe53 has a different orientation compared to *C. vinosum* and *E. vacuolata* iso-2) [Benning *et al.*, 1994]. It might be that the high positive peptide charge and the relatively low number of hydrophodic residues in the small *R. tenuis* HiPIPs (predicting a high potential) are compensated by substitution of the largely conserved "F(P)(G)K" hairpin turn between the second and third strand of the β-sheet [Carter *et al.*, 1974a] into "IPGDx", with a buried negative charge to lower the potential. In the *Paracoccus* HiPIP the presence of a glutamate (residue 59) in the third strand of the β-sheet near the cluster coincides with a 50 mV lower than expected potential. In the other HiPIPs an uncharged polar or an apolar residue is present at this position. In the *C. vinosum* structure [Carter *et al.*, 1974a] this is Asn72, located next to Trp60 in the second β-strand. The amide is involved in the hydrogen-bonding network of the conserved tyrosine [Rayment *et al.*, 1992]. Only in the two *E. halophila* HiPIPs a positively charged residue (lysine in iso-1 and arginine in iso-2) is present at the equivalent position, but in these HiPIPs the lysine in the largely conserved F(P)(G)K hairpin turn between the second and third strand of the β-sheet [Carter *et al.*, 1974] is substituted by a valine. Maybe charged and aromatic residues in the β-sheet are of special importance for the regulation of the potential. The possible cause of the too low potential of *E. vacuolata* iso-1 will be discussed in relation with the redox thermodynamics.

It seems that the potential around 333 mV of the *Chromatium*-like HiPIPs is maintained by compensating an increasing positive or negative charge by increasing the number of polar residues (but not the aromatic residues forming the local environment of the cluster) and decreasing the number of hydrophobic residues, thereby probably increasing the dielectric constant of the protein matrix and thus shielding the charges more effectively. In *R. tenuis* the buried negative charge compensates the positive charge. This "active" compensation of charges strongly suggests that the potential of 333 mV is of major

importance to the function of these HiPIPs and that the surface charge has to be adjusted, possibly to fit the charge on the redox partners *in vivo*. Apparently the potentials of the *Ectothiorhodospira*-like HiPIPs are not constrained but are tuned by varying the charges of these HiPIPs and maybe also by the number of aromatic residues around the cluster. Recently a synthetic gene encoding *E. halophila* iso-1 has been expressed in *E. coli* [Eltis *et al.*, 1994]. It should be interesting to see what effect mutations of the charged and aromatic residues might have on the redox potential.

An alternative subdivision of the HiPIPs into two groups that are both charge-dependent (either with equal slopes but different intercepts or with uncorrelated lines) might also be possible. However, the correlations are much worse in this case, even with the uncorrelated slopes and hence one additional parameter to fit. Also, the thermodynamics ($\Delta H^o$, see below) are not as well-behaved as in the grouping chosen by us. In fact, reasonably good results can only be obtained by excluding *C. vinosum* HiPIP from the fit because of an exceptionally low potential. Also, no indication for this alternative subdivision can be found in the structures and sequences.

### 6.4.2 pH dependence of the potentials.

If there is a difference in sensitivity of the cluster to charges on the surface of the HiPIPs, a difference in sensitivity to protonation of the histidines might also be expected. For the charge-dependent *E. vacuolata* HiPIPs, protonation of the histidines would cause higher redox potentials and protonation of the histidine in *C. vinosum* and *R. gelatinosus* HiPIPs should have a much smaller effect on the potential. A difference in pH-sensitivity between the two types of HiPIPs is indeed present but opposite to the expected effect: The potentials of *C. vinosum* and *R. gelatinosus* HiPIPs are 35 mV higher at low pH but the *E. vacuolata* HiPIPs do not have pH-dependent potentials. This might be related to the different positions of the histidines.

In the *C. vinosum* and *R. gelatinosus* HiPIPs the histidine is located directly next to the first cysteine and, although facing towards the surface, not fully exposed to water [Nettesheim *et al.*, 1980]. Introduction of a positive charge on this histidine has a larger effect on the potential (35 mV) than have the surface charges in the other, charge-dependent group (25 mV per charge). The distance between the histidine and the cluster is about 8.5 Å in *C. vinosum*, giving an apparent dielectric constant of 48. The shielding of this charge is probably lower than the shielding of the surface charges in the *Ectothiorhodospira*-like HiPIPs ($\epsilon$=84) because the histidine is not fully exposed to water and positioned between the surface of the cluster and above the plane of the aromatic residues surrounding the cluster on the pseudo-symmetry axis.

The histidines in both *E. vacuolata* HiPIPs are located in the hydrophilic loop between the conserved tyrosine and the first cysteine and are fully exposed to water. This might cause the protonation of these histidines to have no effect on the energy of the electron in the cluster because of shielding by the surrounding water and maybe also by the highly aromatic protein matrix between the loop and the cluster. Alternatively, the histidines might not be protonated at all because of the large number of positive charges near the histidines during the formation of a transient co-adsorption "complex" between the HiPIP, poly-L-lysine and the electrode surface. (*i.e.* the p$K$'s of the fully exposed histidines are shifted below 4). At pH 4, *E. vacuolata* iso-1 gives a very unstable and broad response (130 mV peak-to-peak separation) with an apparent midpoint potential of 280 mV. This is 20 mV higher than the potential in the presence of poly-L-lysine (peak-to-peak separation 70 mV) but might be fully caused by asymmetrical broadening.

The lower p$K$ values measured for *C. vinosum* compared to literature probably are not artefacts of the promoter. Within errors, the potentials of the low and unstable response without promoter at pH 4, 5.5, 7, 8 and 10.5 are equal to the values measured with poly-L-lysine and morpholin. Moreover, the midpoint potentials of *R. globiformis* HiPIP with and without 0.8 mM poly-L-lysine are equal. This indicates that the charge of the promoter has no effect on the redox-potential of the cluster.

### 6.4.3 Thermodynamics of the redox reactions.

The increased loss of both enthalpy ($\Delta\Delta H^\circ$=−20.7 kJ/mol) and entropy ($\Delta\Delta S^\circ$=$\Delta\Delta S^\circ_{rc}$=−69 J/mol·K) is tentatively ascribed to the loss of a hydrogen bond in the oxidized state of *R. gelatinosus* HiPIP above 28°C and repair of that bond upon reduction. Krishnamoorthi *et al.* [1986] concluded from the differences in the patterns of exchangeable hyperfine-shifted peaks (^{1}H-NMR) that the two *E. vacuolata* and two *E. halophila* HiPIPs have more H-bonds in the reduced state than in the oxidized state. Carter and coworkers [Carter, 1973; Carter *et al.*, 1974a,b] found from the crystal structures of oxidized and reduced *C. vinosum* HiPIP that the hydrogen bond lengths are longer in the oxidized protein than in the reduced state. Therefore it is likely that at higher temperatures the hydrogen bonds are broken more easily in the oxidized state. The extra loss of enthalpy of 21 kJ/mol above 28°C is an acceptable value for the (re)formation of one extra NH-S hydrogen bond upon reduction [Pogorelyi, 1977; Sheridan & Allen, 1980]. This means that the lowered redox potential above 28°C is *not* caused by additional destabilization of the reduced state but is caused by a loss of entropy that outweighs the more favourable reduction enthalpy at these temperatures.

The unstable response of *C. vinosum* and *R. tenuis* HiPIPs at higher temperature might also be caused by the loss of a hydrogen bond and might be a general feature of all

- 121 -

*Chromatium*-like HiPIPs. This is supported by the suggestion of Backes *et al.* [1991] that the five hydrogen bonds to the cluster in *C. vinosum* HiPIP compared to the eight hydrogen bonds in ferredoxins "represent a compromise between maximal hydrogen bonding for structural stability and minimal hydrogen bonding to achieve a higher cluster oxidation level". Thus, if a hydrogen bond is lost the protein may unfold more readily on the electrode surface, thereby hampering the electron transfer.

As shown in Figure 6.6a, a clear correlation can be found between the temperature dependence and the position of the absorption maximum. A plot of $\Delta S°$ *versus* the visible absorption maximum shows a linear dependence ($r^2$=0.96428) with a slope of $-5.27 \pm 0.51$ $J \cdot mol^{-1} \cdot K^{-1}$ per nm red-shift or $-16.1 \pm 1.5$ mV/nm at 295 K and $\Delta S°(\lambda$=385.2 nm$) = -154.7$ $\pm 5.0$ $J \cdot mol^{-1} \cdot K^{-1}$. All HiPIPs, including *E. vacuolata* iso-1, are reasonably close to the regression line. This indicates that the entropy loss upon reduction is influenced only by the local interaction of the cluster with the peptide in both groups of HiPIPs and not by the overall charge. Apparently, the contribution to the reduction entropy of the polarization of the water-shell around the protein is small or similar for all HiPIPs. It also confirms that the charge-dependence of the potential of the *Ectothiorhodospira*-like HiPIPs is fully determined by a charge-dependent reduction enthalpy, as predicted by the Coulomb model. The negative slope (more negative $\Delta S°$ with more red-shifted band) confirms that a red-shifted absorption band is an indication for a more solvated reduced cluster and thus a more ordered peptide around the cluster.

The $\Delta H°$ of most HiPIPs are between $-75$ and $-85$ kJ/mol. Only *E. vacuolata* iso-2 has a much less negative $\Delta H°$ of $-51$ kJ/mol. As mentioned above, the enthalpy change upon reduction is both influenced by the local polarity of the cluster environment and by the forces of the surface-charges on the electron. The influence of cluster solvation on $\Delta H°$ can be calculated by subtracting the charge-dependent part of the potential from it (A slope of $-2.37$ $kJ \cdot mol^{-1}$ per unit charge can be predicted from the 24.5 mV/unit). A plot of $\Delta\Delta H° = \Delta H° +$ $F \cdot 0.3329$ against the absorption maximum for *R. tenuis*, *R. gelatinosus* and *C. vinosum* and $\Delta\Delta H° = \Delta H° + F \cdot (0.3993 + z \cdot 0.0245)$ for *R. globiformis* and *E. vacuolata* HiPIPs (Figure 6.6b) yields a straight line (when *E. vacuolata* iso-1 is not included in the regression) with a slope of $-2.34 \pm 0.19$ kJ/mol (or $+24.2 \pm 2.0$ mV) per nm red-shift and $\Delta\Delta H°(\lambda$=385.2 nm$)$ $= -44.8 \pm 1.5$ kJ/mol ($r^2$=0.97973). The sign of the slope (more negative $\Delta H°$ with more red-shifted absorption maximum) is consistent with the stabilization of the reduced state by polar residues. Together with the $-16.1$ mV/nm at 295 K for $\Delta S°$ a slope of $+8.1$ mV/nm is obtained, within errors equal to the fitted slope of the residual potentials against $\lambda_{max}$. In other words, there is a net positive shift of the potential when the polarity of the cluster environment increases. Lowering of the potential by increased ordering of the peptide is smaller (at 295 K) than the stabilization of the reduced state by increasing solvation of the cluster. The reduction enthalpy of *E. vacuolata* iso-1 is 8.3 kJ/mol higher than expected. The
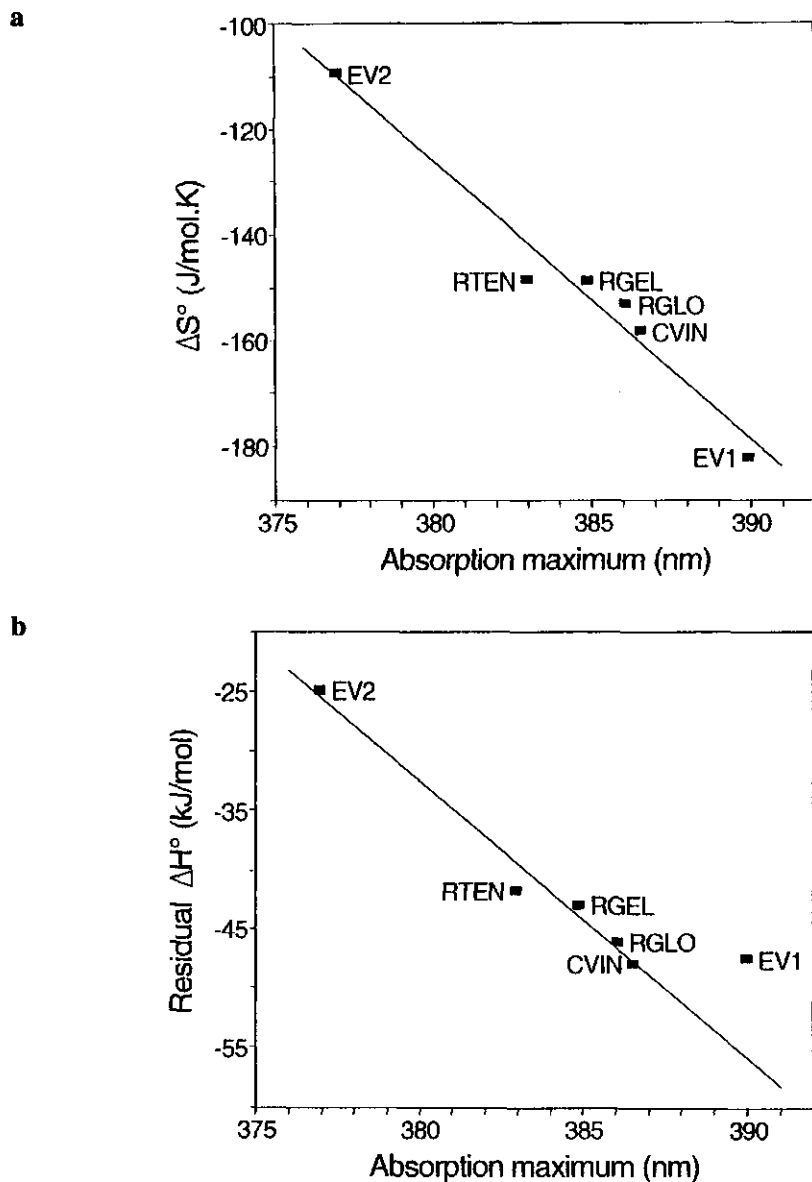
**Figure 6.6.** Linear dependence of the reduction entropy (a) and enthalpy (b) on the position of the absorption band. The entropy change upon reduction is obtained from the temperature coefficients. The residual enthalpy is the measured enthalpy change upon reduction *minus* the charge-dependent part as calculated from the charge-dependency of the potentials. ($\Delta\Delta H^\circ = \Delta H^\circ + F \cdot 0.3329$ for *R. tenuis*, *R. gelatinosus* and *C. vinosum* and $\Delta\Delta H^\circ = \Delta H^\circ + F \cdot (0.3993 + z \cdot 0.02452)$ for *R. globiformis* and *E. vacuolata* HiPIPs).

resulting 86 mV lowering of the potential is, within errors, close to the deviation of −112 mV found from the fitted dependence of the potential on the peptide charge and the position of the absorption band.

The question arises whether *E. vacuolata* iso-1 has an unusually low potential or the position of the absorption maximum is unusually red-shifted. Dipolar interactions might interfere with the suggested relation between the cluster solvation and redox thermodynamics because they can either stabilize or destabilize the excited state and thus cause a shift of the absorption maximum in either direction. However, the linear relations between the position of the absorption band and the reduction entropy and enthalpy implies that the dipolar interactions with the cluster are very similar in all HiPIPs studied in this chapter. The potential of *E. vacuolata* iso-1 is about 100 mV too low, suggesting that the cluster is bound by one H-bond less compared to the other HiPIPs [Carter, 1977]. However, Krishnamoorti *et al.* [1986] concluded from the patterns of moderately slowly exchangeable hyperfine-shifted peaks (^{1}H-NMR) that the *E. vacuolata* HiPIPs have equal numbers of H-bonds in the reduced form. Moreover, the similar dipolar interactions also opposes differences in hydrogen bonding of the reduced cluster. A larger number of hydrogen bonds in oxidized *E. vacuolata* iso-1 might also explain the lowering of the redox potential. However, Krishnamoorti *et al.* [1986] found that oxidized *E. vacuolata* iso-2 HiPIP has three hydrogen bonds that are not present in oxidized iso-1. This would cause more instead of the measured less negative $\Delta H°$ for *E. vacuolata* iso-1. It might well be possible that some of the exchangeable protons are obscured by the high intensity of the major part of the NMR spectra.

A different explanation for the relatively low potential of *E. vacuolata* iso-1 might be a special interaction of one or more negative charges with the cluster, destabilizing the more negatively charged reduced state. This hypothesis is consistent with the observation that the potential difference is almost fully determined by the less negative reduction enthalpy. However, it is not possible to assign a specific residue responsible for this effect, like in the *R. tenuis* and the *Paracoccus* HiPIP.

### 6.4.4 Ionic strength dependence of the potentials.

The midpoint potential of redox proteins is usually proportional to the square root of the ionic strength [Link *et al.*, 1992; Verhagen *et al.*, 1994]. This proportionality can be derived from the Debye-Hückel limiting law for the dependence of the activity coefficient on ionic strength:

$$-\ln(y_i) = A z_i^2 \sqrt{I} \tag{6.10}$$

with $A = 0.5138 \ln(10) = 1.183$ in water at 295 K and ionic strength $I$ in Molarity [Lyklema, 1991]. Only at low salt concentrations ($<=10$ mM) is this dependence valid. At higher ionic strength the dependence is no longer linear:

$$-\ln(y_i) = \frac{A z_i^2 \sqrt{I}}{1 + \beta a_i \sqrt{I}} \tag{6.11}$$

with $\beta=3.290$ and the ionic radius $a_i$ in nm. Substitution of the limiting law into the Nernst equation leads to:

$$E = E_m + \frac{RT}{nF} \ln\left[ \frac{c_{ox}\, y_{ox}}{c_{red}\, y_{red}} \right] \tag{6.12}$$

or

$$E = E_m(I=0) + \frac{RT}{nF}\left[ \ln(y_{ox}) - \ln(y_{red}) \right] \tag{6.13}$$

and gives

$$E = E_m(I=0) - A\frac{RT}{nF}\left( z_{ox}^2 - z_{red}^2 \right)\sqrt{I} \tag{6.14}$$

When $c_{ox} = c_{red}$ (at $E = E_m$):

$$E_m(I) = E_m(0) - A\frac{RT}{nF}\left( z_{ox}^2 - z_{red}^2 \right)\sqrt{I} \tag{6.15}$$

and with $n = 1$ and $z_{red} = z_{ox} - 1$ at 295 K this reduces to

$$E_m(I) = E_m(0) - 60(z_{ox} - \tfrac{1}{2})\sqrt{I} \quad \text{mV} \tag{6.16}$$

and thus a positive slope if $z_{ox}$ is zero or negative.

However, for the HiPIPs and also other redox-proteins the linearity is extended to an ionic strength of 0.5 M or even higher [Link *et al.*, 1992; Verhagen *et al.*, 1994], although

only the limiting law predicts a linear dependence (at higher ionic strength the term $\sqrt{I}$ should be replaced by $\sqrt{I}/(1+\beta a\sqrt{I})$. Moreover, the observed slopes are all zero or negative, independent of the overall charge of the protein and much smaller than the Debye-Hückel theory predicts (even with $z_{ox}=+1$ and $z_{red}=0$ the slope would be higher than the observed slopes). This indicates that not the overall charge of the protein but rather the local charge of the cluster environment is dominant and apparently is positive (the calculated $z_{ox}$ are between $+\frac{1}{2}$ and $+1$).

A partial explanation for the small slopes could be that if the radii $a_{ox}$ and $a_{red}$ decrease with increasing ionic strength the factor $1+\beta a\sqrt{I}$ (with $a=a_{ox}=a_{red}$) becomes less dependent on I and thus the deviation from linearity at higher salt concentration is lower. Reducing this factor to a constant would result in a linearity up to much higher ionic strength but with a much smaller slope. Specific binding of ions can also influence the effects of ionic strength. The binding of chloride ions has been shown to influence the dependence of the potential on ionic strength for horse-heart cytochrome c [Margalit & Schejter, 1973].

The Debye-Hückel theory also predicts that the potential can only be independent of the ionic strength if $z_{ox}=z_{red}$. This can be acomplished by a protonation of the reduced protein and thus a pH-dependent potential. However, the potential of *C. vinosum* HiPIP is independent of ionic strength but the p$K$ of both the oxidized and reduced state are too low for protonation at pH 7. The p$K$ values of the histidine in *R. gelatinosus* HiPIP are closer to 7 but the potential is still lowered by adding salt. Moreover, the potentials of *R. globiformis* and *R. salinarum* HiPIPs are not influenced by salt and are also independent of pH. Protonation upon reduction is therefore not the only explanation for the insensitivity to ionic strength of these HiPIPs.

Probably the ionic strength influences the conformation of the protein, thereby changing the local environment of the cluster and apparently stabilizing the oxidized form or destabilizing the reduced form of the cluster. The relatively high sensitivities to the ionic strength of *R. tenuis* and *E. vacuolata* iso-1 HiPIPs coincide with the proposed special role of a negatively charged residue in the regulation of the potential (Asp46 in *R. tenuis*). The negative slopes indicate an increasing destabilization of the reduced state by the negative charge at higher ionic strength. The opposite effect would be expected for charges exposed to the solvent because of increased shielding, but these charges are probabily not exposed (at least this is true for Asp46 of *R. tenuis*).

There appears to be no correlation between the sensitivity of the potential to ionic strength and the halophillicity of the bacterium, nor to the proposed classification of the HiPIPs.

## 6.5   Conclusions

Direct, unpromoted electrochemistry at the glassy carbon electrode is possible with the positively charged HiPIPs. The negatively charged HiPIPs require the positively charged and flexible bridging promoter poly-L-lysine. The stability of the response can be improved by morpholin in combination with the negatively charged proteins and by monomeric amino acids or 4,4'-dipyridyl with the positively charged HiPIPs. These 'stabilizers' apparently prevent the blocking of the electrode by denatured protein during electrochemistry. Only *C. vinosum* and *R. gelatinosus* HiPIPs show a weak but significant pH dependence of the measured midpoint potentials. This implies that the presence of histidines in the sequence does not *per se* predict a pH-dependent redox potential. The dependence of the midpoint potential on ionic strength cannot be explained by the Debye-Hückel theory alone because the linearity exceeds the limiting concentration, the slopes are much smaller than predicted by this theory and no positive slopes are observed. Combination of the sequences, the optical spectra, the overall charges and the redox thermodynamics suggests a subdivision of the HiPIPs into two distinct groups:

* The first group is formed by the *Chromatium*-like HiPIPs. These are found in *R. tenuis*, *R. gelatinosus*, *C. vinosum*, *Chromatium gracile*, *Thiocapsa roseopersicina* and *Thiocapsa pfennigii*. The *Paracoccus* HiPIP probably also belongs to this group although its potential is about 50 mV lower than expected. These HiPIPs all have potentials around 333 mV that are modulated by the "solvation" of the cluster (hydrophilicity of the environment) as indicated by the position of the absorption maximum in the visible region of the spectrum of the reduced HiPIP. The potentials are independent of the overall charge (histidines excluded) of the HiPIPs in this group, probably because of compensation of the electrostatic forces by modulation of the polarity of the protein matrix. It is tentative to conclude from the temperature dependence of *R. gelatinosus* and the instability of *R. tenuis* and *C. vinosum* at higher temperatures that a hydrogen bond is broken at temperatures above 30°C in all the *Chromatium*-like HiPIPs.

* The second group is formed by the *Ectothiorhodospira*-like HiPIPs. The four HiPIPs from the *Ectothiorhodospira* species, the HiPIP from *R. globiformis* and the large *R. salinarum* iso-2 HiPIP belong to this group. The potentials of these HiPIPs are strongly dependent on the overall charge (histidines excluded) of the peptide because the dielectrics of the protein matrix do not counteract the electrostatic forces. A more negative overall charge destabilizes the reduced state, resulting in a lowering of the redox potential with 25 mV per charge. With an average protein radius of 7 Å, an apparent dielectric constant of 84 can be calculated. The electrostatic interactions are additive to the solvating effect of the local cluster environment. Although the potential of *E. vacuolata* iso-1 is about 100 mV too low, it probably also is a HiPIP with a charge-dependent potential.

## 6.6    References

Adman, E., Watenpaugh, K.D. & Jensen, L.H. (1975) *Proc. Nat. Acad. Sci. USA 72*, 4854.

Ambler, R.P., Meyer, T.E., Cusanovich, M.A. & Kamen, M.D. (1987) *Biochem. J. 246*, 115.

Ambler, R.P., Meyer, T.E. & Kamen, M.D. (1993) *Arch. Biochem. Biophys. 306*, 215.

Ambler, R.P., Meyer, T.E. & Kamen, M.D. (1994) *Arch. Biochem. Biophys. 308*, 78.

Armstrong, F.A., Cox, P.A., Hill, H.A.O., Lowe, V.J. & Oliver, B.N. (1987) *J. Electroanal. Chem. 217*, 331.

Armstrong, F.A., Hill, H.A.O. & Walton, N.J. (1988) *Acc. Chem. Res. 21*, 407.

Backes, G.,Mino, Y., Loehr, T.M., Meyer, T.E., Cusanovich, M.A., Sweeney, W.V., Adman, E.T. & Sanders-Loehr, J. (1991) *J. Am. Chem. Soc. 113*, 2055.

Banci, L., Bertini, I., Capozzi, F., Carloni, P., Ciurli, S., Luchinat, C. & Piccioli, M. (1993a) *J. Am. Chem. Soc. 115*, 3431.

Banci, L., Bertini, I., Ferretti, S., Luchinat, C. & Piccioli, M. (1993b) *J. Mol. Struct. 292*, 207.

Banci, L., Bertini, I., Eltis, L.D., Felli, I.C., Kastrau, D.H.W., Luchinat, C., Piccioli, M., Pierattelli, R. & Smith, M. (1994) *Eur. J. Biochem. 225*, 715.

Banci, L., Bertini, I., Dikiy, A., Kastrau, D.H.W., Luchinat, C. & Sompornpisut, P. (1995) *Biochemistry 34*, 206.

Bartsch, R.G. (1971) *Methods Enzymol. 23*, 644.

Bartsch, R.G. (1978) *Methods Enzymol. 53*, 329.

Bartsch, R.G. (1991) *Biochim. Biophys. Acta 1058*, 28.

Benning, M.M., Meyer, T.E., Rayment, I. & Holden, H.M. (1994), *Biochemistry 33*, 2476.

Bertini, I., Capozzi, F., Ciurli, S., Luchinat, C., Messori, L. & Piccioli, M. (1992) *J. Am. Chem. Soc. 114*, 3332.

Bertini, I., Capozzi, F., Luchinat, C. & Piccioli, M. (1993) *Eur. J. Biochem. 212*, 69.

Breiter, D.R., Meyer, T.E., Rayment, I. & Holden, H.M. (1991) *J. Biol. Chem. 266*,18660.

Butler, J., Sykes, A.G., Buxton, G.V., Harrington, P.C. & Wilkins, R.G. (1980) *Biochem. J. 189*, 641.

Cantor, C.R. & Schimmel, P.R. (1980) *Biophysical Chemistry, part II*, Freeman and Co., San Francisco, pp. 386.

Carter, C.W. (1973) in *Iron-Sulfur Proteins, vol. III* (Lovenberg W., Ed.), Academic Press, New York, pp. 157.

Carter, C.W., Kraut, J., Freer, S.T., Xuong, Ng.H., Alden, R.A. & Bartsch, R.G. (1974a) *J. Biol. Chem. 249*, 4212.

Carter, C.W., Kraut, J., Freer, S.T., & Alden, R.A. (1974b) *J. Biol. Chem. 249*, 6339.

Carter, C.W. (1977) *J. Biol. Chem. 252*, 7802.

Cammack, R. (1973) *Biochem. Biophys. Res. Comm. 54*, 548.

Churg, A.K. & Warshel, A. (1986) *Biochemistry 25*, 1675.

Clark, W.M. (1960) *Oxidation-reduction potentials of organic systems*, Waverly Press, Baltimore.

Dunham, W.R., Hagen, W.R., Free, J.A., Sands, R.H., Dunbar, J.B. & Humblet, C. (1991) *Biochim. Biophys. Acta 1079*, 253.

Dus, K., de Klerk, H., Sletten, K. & Bartsch, R.G. (1967) *Biochim. Biophys. Acta 140*, 291.

Dus, K., Tedro, S. & Bartsch, R.G. (1973) *J. Biol. Chem. 248*, 7318.

Eltis, L.D., Iwagami, S.G. & Smith, M. (1994) *Protein Eng. 7*, 1145.

Freer, S.T., Alden, R.A., Carter, C.W. & Kraut, J. (1975) *J. Biol. Chem. 250*, 46.

Hagen, W.R. (1989) *Eur. J. Biochem. 182*, 523.

Hill, C.L., Renaud, J., Holm, R.H. & Mortenson, L.E. (1977) *J. Am. Chem. Soc. 99*, 2549.

Hori, K. (1961) *J. Biochem. 50* , 481.

Jensen, G.M., Warshel, A. & Stephens, P.J. (1994) *Biochemistry 33*, 10911.

Kassner, R.J. & Yang, W. (1977) *J. Am. Chem. Soc. 99*, 4351.

Klerk, H. de & Kamen, M.D. (1966) *Biochim. Biophys. Acta 112*, 175.

Krishnamoorthi, R., Markley, J.L., Cusanovich, M.A., Przysiecki, C.T. & Meyer, T.E. (1986) *Biochemistry 25*, 60.

Krishnamoorthi, R., Cusanovich, M.A., Meyer, T.E. & Przysiecki, C.T. (1989) *Eur. J. Biochem. 181*, 81.

Langen, R., Jensen, G.M., Jacob, U., Stephens, P.J. & Warshel, A. (1992) *J. Biol. Chem. 267*, 25635.

Link, T.A., Hagen, W.R., Pierik, A.J., Assmann, C. & Jagow, G. von (1992) *Eur. J. Biochem. 208*, 685.

Lyklema, J. (1991) *Fundamentals of Interface and Colloid Science, Vol. 1, Fundamentals*, Academic Press, London, Chapter 5.

Luchinat, C., Capozzi, F., Borsari, M., Battistuzzi, G. & Sola, M. (1994) *Biochem. Biophys. Res. Comm. 203*, 436.

Margalit, R. and Schejter, A. (1973) *Eur. J. Biochem. 32*, 492 and 500.

Massey, V. & Hemmerich, P. (1978) *Biochemistry 17*, 9.

Meyer, T.E., Kennel, S.J., Tedro, S.M. & Kamen, M.D. (1973) *Biochim. Biophys. Acta 292*, 634.

Meyer, T.E., Przysiecki, C.T., Watkins, J.A., Bhattacharyya, A., Simondsen, R.P., Cusanovich, M.A. & Tollin, G. (1983) *Proc. Nat. Acad. Sci USA 80*, 6740.

Meyer, T.E. (1985) *Biochim. Biophys. Acta 806*, 175.

Meyer, T.E., Fitch, J., Bartsch, R.G., Tollin, D. & Cusanovich, M.A. (1990) *Biochim. Biophys. Acta 1017*, 118.

Meyer, T.E. (1994) *Methods Enzymol. 243*, 435.

Mizrahi, I.A., Wood, F.E. & Cusanovich, M.A. (1976) *Biochemistry 15*, 343.

Mizrahi, I.A., Meyer, T.E. & Cusanovich, M.A. (1980) *Biochemistry 19*, 4727.

Moore, G.R. (1983) *FEBS Letters 161*, 171.

Moore, G.R., Pettigrew, G.W. & Rogers, N.K. (1986) *Proc. Natl. Acad. Sci. USA 83*, 4998.

Nettesheim, D.G., Johnson, W.V. & Feinberg, B.A. (1980) *Biochim. Biophys. Acta 593*, 371.

Nettesheim, D.G., Meyer, T.E., Feinberg, B.A. & Otvos, J.D. (1983) *J. Biol. Chem. 258*, 8235.

Nettesheim, D.G., Harder, S.R., Feinberg, B.A. & Otvos, J.D. (1992) *Biochemistry 31*, 1234.

Norde, W. (1986) *Adv. Colloid Interfac. Sci 25*, 267.

Orme-Johnson, N.R., Mims, W.B., Orme-Johnson, W.H., Bartsch, R.G., Cusanovich, M.A. & Peisach, J. (1983) *Biochim. Biophys. Acta 748*, 68.

Pogorelyi, V.K. (1977) *Russ. Chem. Rev. 46*, 316.

Przysiecki, C.T., Meyer, T.E. & Cusanovich, M.A. (1985) *Biochemistry 24*, 2542.

Rayment, I., Wesenberg, G., Meyer, T.E., Cusanovich, M.A. & Holden, H.M. (1992) *J. Mol. Biol. 228*, 672.

Rees, D.C. (1985) *Proc. Natl. Acad. Sci. USA 82*, 3082.

Rogers, N.K., Moore, G.R. & Sternberg, M.J.E. (1984) *J. Mol. Biol. 182*, 613.

Seralathan, M., Osteryoung, R.A. & Osteryoung, J.G. (1987) *J. Electroanal. Chem. 222*, 69.

Sheridan, R.P. & Allen, L.C. (1980) *Chem. Phys. Letters 69*, 600.

Taniguchi, I., Iseki, M., Eto, T., Toyosawa, K., Yamaguchi, H. & Yasukouchi, K. (1984) *J. Electroanal. Chem. 174 (Bioelectrochem. Bioenerg. 13)*, 373.

Taniguchi, V.T., Sailasuta-Scott, N., Anson, F.C. & Gray, H.B. (1980) *Pure and Appl. Chem. 52* , 2275.

Tedro, S.M., Meyer, T.E. & Kamen, M.D. (1974) *J. Biol. Chem. 249*, 1182.

Tedro, S.M., Meyer, T.E. & Kamen, M.D. (1976) *J. Biol. Chem. 251*, 129.

Tedro, S.M., Meyer, T.E. & Kamen, M.D. (1977) *J. Biol. Chem. 252*, 7826.

Tedro, S.M., Meyer, T.E. & Kamen, M.D. (1979) *J. Biol. Chem. 254*, 1495.

Tedro, S.M., Meyer, T.E., Bartsch, R.G. & Kamen, M.D. (1981) *J. Biol. Chem. 256*, 731.

Tedro, S.M., Meyer, T.E. & Kamen, M.D. (1985a) *Arch. Biochem. Biophys. 239*, 94.

Tedro, S.M., Meyer, T.E. & Kamen, M.D. (1985b) *Arch. Biochem. Biophys. 241*, 656.

Verhagen, M.F.J.M. & Hagen, W.R. (1992) *J. Electroanal. Chem. 334*, 339.

Verhagen, M.F.J.M., Wolbert, R.B.G. & Hagen, W.R. (1994) *Eur. J. Biochem. 221*, 821.

Warshel, A. & Russel, S.T. (1984) *Q. Rev. Biophys. 17*, 283.

Yang, C.Y., Johnson, K.H., Holm, R.H. & Norman, J.G. (1975) *J. Am. Chem. Soc. 97*, 6596.

# Chapter 7

# Reversible super-reduction of the cubane $[4Fe-4S]^{(3+;2+;1+)}$ in High Potential Iron-Sulfur Protein under non-denaturing conditions: EPR spectroscopic and electrochemical studies.

## 7.1 Introduction

The high-potential iron-sulfur proteins (HiPIPs) form a group of related and well-studied, small redox proteins (6 to 11 kDa), containing a $[4Fe-4S]^{3+,2+}$ cluster bound to the protein by four cysteinyl sulfur ligands. Most HiPIPs are found in purple photosynthetic bacteria but a HiPIP is also found in halophilic *Paracoccus* species [Bartsch, 1991; Tedro *et al.*, 1977]. Apart from the coordinating cysteines, some aromatic residues and some moderately conserved features, the overall homology of the sequences is low. However, the structural homology is high, especially around the cluster, and the cluster geometry and coordination to the protein are highly conserved [Carter *et al.*, 1974; Freer *et al.*, 1975; Breiter *et al.*, 1991; Rayment *et al.*, 1992; Benning *et al.*, 1994; Banci *et al.*, 1993a; Banci *et al.*, 1994; Banci *et al.*, 1995]. As reported in Chapter 6, the redox potential of the 3+/2+ transition ranges from +50 to +500 mV. The existence of two groups of HiPIPs is proposed. One group consists of *Chromatium*-like HiPIPs with redox potentials between 300 and 350 mV, modulated only by the polarity of the cluster environment (solvation) but not by the overall charge of the protein. The second group is formed by *Ectothiorhodospira*-like HiPIPs with potentials between 50 and 500 mV, largely dependent on the overall charge of the peptide and also modulated by cluster solvation.

In oxidized HiPIPs the [4Fe-4S] cluster is in the 3 ferric, 1 ferrous state (overall charge 3+) while oxidized ferredoxins contain a $[4Fe-4S]^{2+}$ (2 ferric, 2 ferrous) cluster. Crystallography and resonance Raman studies of bacterial ferredoxins and HiPIPs show that the structures of the clusters are nearly identical. There are however major differences in the local environment of the clusters in ferredoxins and HiPIPs. The sequences and folding patterns, the location of the cysteines, the cysteine ligand dihedral angles (close to 180° in HiPIPs) and the position of the hydrogen bonds are completely different. In ferredoxins, eight hydrogen bonds between amide N-H and sulfur ligands are present while in HiPIPs only five are found. The redox potentials of the cluster are probably regulated in part by the number of these NH-S bonds because they stabilize the more negatively charged reduced states [Adman *et al.*, 1975; Jensen *et al.*, 1994; Langen *et al.*, 1992; Backes *et al.*, 1991 and references cited therein]. By comparing ferredoxins, HiPIPs and synthetic clusters, Carter [1977] found that each hydrogen bond increases the potential by about 80 mV. In HiPIPs the

cluster is completely inaccessible to water and surrounded by hydrophobic residues, while the ferredoxin cluster is in a more hydrophilic environment and much more accessible to water [Backes *et al.*, 1991; Orme-Johnson *et al.*, 1983]. The hydrophobic pocket in HiPIPs causes a further lowering of the reduction potentials [Kassner & Yang, 1977]. Carter [1977] observed a pair of bands with opposite signs in the visible CD spectra of *C. vinosum* HiPIP and *P. aerogenes* ferredoxin (although Przysiecki *et al.* [1985] found that not all HiPIPs show these features), and proposed a destabilization of the transition state for the $[4Fe-4S]^{2+,1+}$ reduction by charge-dipole interactions between the highly conserved tyrosine side chain and the cluster (Tyr19 and $S^*3$ in *C. vinosum*).

These differences result in a shift of the redox potentials of both the 3+/2+ and the 2+/1+ transitions to such an extent that in HiPIPs the second transition, normally observed in ferredoxins, is shifted out of the biologically useful potential range while the first transition becomes feasible. Calculation of this potential for *C. vinosum* HiPIP based on the "Protein Dipoles Langevin Dipoles" method by Jensen and coworkers [1994] yields a value of $-1.75$ V. The HiPIP super-reduction potential (*i.e.* the 2+/1+ transition) has not been determined yet under normal conditions. Cammack [1973] found that only in solutions containing more than 70% DMSO, the reduced (*i.e.* $[4Fe-4S]^{2+}$) *C. vinosum* HiPIP can be further reduced by dithionite. The absorbance around 400 nm decreases and an EPR spectrum similar to reduced ferredoxin becomes visible. At pH 9 the midpoint potential is -640 mV or lower, which is about 1000 mV lower than the "normal" potential of +350 mV. However, in DMSO the HiPIP is probably partially denatured. Super-reduction is not possible without DMSO, suggesting a very low second reduction potential of the native HiPIP. Carter [1977] suggested that in 80% DMSO at high pH the conserved Tyr19 might be ionized, thereby disrupting the hydrogen-bonding network (the hydroxyl O accepts a hydrogen bond from amide NH 72 and donates a proton to a water molecule at the protein surface) and hampering the interactions between the tyrosine and the cluster.

However, a kinetic rather than thermodynamic barrier for the super-reduction of HiPIPs was suggested by the findings of Butler *et al.* [1980]. They were able to super-reduce *C. vinosum* HiPIP with hydrated electrons (reduction potential $-2.9$ V) generated by pulse-radiolysis of water, but they observed no reaction with $CO_2^{-\cdot}$ radicals ($-2.0$ V). It was also observed that the electron consumption rate matches the cluster reduction rate, indicating a fast intramolecular transfer or a direct reaction of the electron with the cluster. They proposed that the ability of the electrons to tunnel through an energy barrier explains the higher reactivity of hydrated electrons compared to $CO_2^{-\cdot}$ radicals.

This chapter describes the super-reduction of the high-potential HiPIPs from *R. globiformis* and *R. salinarum* (large iso-2 HiPIP) with titanium(III)citrate at pH 9.5 without DMSO and also by direct reduction at the glassy carbon electrode at pH 7.5. The super-reduced cubane $[4Fe-4S]^{1+}$ in *R. globiformis* HiPIP was studied with EPR spectroscopy.

## 7.2 Experimental procedures

### 7.2.1 HiPIPs.

The investigated HiPIPs are isolated from *Ectothiorhodospira vacuolata* strain β1 (iso-1 and iso-2), *Chromatium vinosum* strain D, *Rhodocyclus gelatinosus* strain 2.2.1, *Rhodocyclus tenuis* strain 2761, *Rhodopila globiformis* strain 7950 and from *Rhodospirillum salinarum* strain ATCC 35394 (the multimeric HiPIP iso-2). The same preparations as described in Chapter 6 were used here.

### 7.2.2 Electrochemistry.

The HiPIPs were studied by analogue cyclic voltammetry and by digital staircase cyclic voltammetry as described in Chapter 6. The experiments were performed in 10 to 20 mM Hepes buffer pH 7.5 at a temperature of 22±1°C. *R. salinarum* HiPIP (67 μM) was measured in the presence of 11 mM 4,4'-dipyridyl (Janssen Chimica) to stabilize the response, *R. globiformis* (58 μM) without additions, *C. vinosum* (43 μM) with 0.8 mM poly-L-lysine (Sigma, Mw=3300) as promoter and 9.2 mM morpholin (Janssen Chimica) to stabilize the response, *R. gelatinosus* (51 μM) with 3 mM L-aspartic acid (Merck) as stabilizer; *R. tenuis* (84 μM) with 3 mM L-tryptophan (Merck) as stabilizer, *E. vacuolata* iso-1 (44 μM) with 0.67 mM poly-L-lysine and 7.7 mM morpholin and *E. vacuolata* iso-2 (134 μM) with 1.6 mM poly-L-lysine and 7.2 mM morpholin. The measured potentials (at a scan rate of 10 mV/s) of the $[4Fe-4S]^{3+/2+}$ couple are +500 mV for *R. salinarum*, +431 mV for *R. globiformis*, +347 mV for *C. vinosum*, +318 mV for *R. gelatinosus*, +309 mV for *R. tenuis*, +257 mV for *E. vacuolata* iso-1 and +166 mV for *E. vacuolata* iso-2 HiPIP.

All potentials are given *versus* the Normal Hydrogen Electrode, using 0.246 V for the Saturated Calomel Electrode at 22°C.

### 7.2.3 EPR spectroscopy.

EPR data were recorded on a Bruker EPR 200 D spectrometer. The samples were cooled with a home-built helium-flow cryostat and the temperature was measured using a calibrated carbon resistor. The spectra were recorded on a personal computer with software written in Asyst for data acquisition, correction of background signals, determination of *g*-values and double integration. The external standard for integration was a 10 mM $CuSO_4$/10 mM HCl/2 mM $NaClO_4$ solution. Reduction of the samples was done anaerobically in the EPR tubes, connected to a vacuum/argon manifold with buffered sodium dithionite (Merck)

and with titanium citrate, prepared in the glovebox from a 15% titanium(III)chloride solution in 1 M HCl (Merck) and an equimolar amount of citrate (trisodium salt), neutralized with NaOH and freshly diluted in anaerobic Ches buffer at pH 9.5. The reductions were carried out at ambient temperature and the samples were frozen in liquid nitrogen. Bulk-oxidation was done in the above described electrochemical cell by replacing the flat glassy carbon disc with a 0.4 ml glassy carbon cup (Le Carbone Loraine). The inner surface was activated by polishing and heating in a methane flame. The counter electrode was a piece of 2 cm 0.3 mm platinum wire, wrapped around the tip of the calomel electrode. A solution of 44 µM *R. globiformis* HiPIP in 200 µl 100 mM Hepes, pH 7.5 was held at +650 mV for 40 minutes while stirring with a small magnetic stirrer. A sample of 100 µl was then transferred to an anaerobic EPR-tube and frozen in liquid nitrogen.

## 7.3   Results

### 7.3.1   EPR spectroscopy.

No super-reduction was observed when sodium-dithionite (0.5 mM) was added to *R. globiformis* HiPIP (final concentration 78 µM) in 200 mM Ches buffer at pH 9.5 and up to 9 hours of equilibration, although the resulting potential was calculated to be about $-0.76$ V at pH 9.5, even if the dithionite is only 60 to 80% pure [Mayhew, 1978]. However, when 250 µM of the strong reducing agent Ti(III)citrate ($E_m = -0.50$ V at pH 7, decreasing with 60 mV per pH unit increase [Zehnder, 1976]) was added to 39 µM of *R. globiformis* HiPIP in 200 mM Ches buffer at pH 9.5 super-reduction was observed but the reaction is extremely slow. The intensity of the spectrum increased from 4% super-reduced HiPIP after 10 minutes equilibration under argon to 23% after 110 minutes and 76% after 10 hours and 40 minutes. A fit of these points with a first-order curve yields a half-life of 229 minutes and an equilibrium at 89% super-reduction. With the total amount of 6.4 equivalents of titaniumcitrate added and a reduction potential for the Ti(IV)/Ti(III) citrate couple of $-0.65$ V at pH 9.5 [Zehnder, 1976], the calculated potential of the solution at equilibrium is $-0.70$ V and the estimated HiPIP super-reduction potential is $-0.64$ V.

After an additional 17 hours incubation the Ti(III) spectrum had completely disappeared, probably due to slow influx of oxygen, but the HiPIP was still partly super-reduced. This gave the opportunity to characterize the complete spectrum of super-reduced *R. globiformis* HiPIP (Figure 7.1). Double integration yields an amount of super-reduced HiPIP of 18 µM or 47% of the total concentration. The above mentioned reduction-percentages in the presence of Ti(III) are calculated by comparing the surface under the $g=2.04$ peak that is not obscured by the Ti(III) spectrum with that of the clean spectrum. The spectrum is very similar to those from reduced [4Fe-4S] ferredoxins (*cf.* [Belinskii, 1993], and
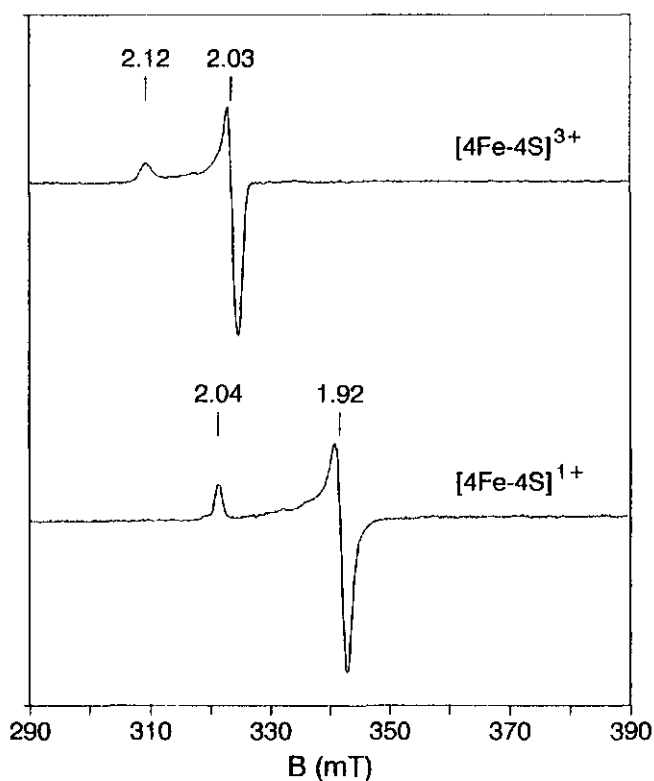
**Figure 7.1.** EPR spectra of *R. globiformis* HiPIP. The super-reduced $[4Fe-4S]^{1+}$ state was obtained by prolongued incubation of 39 μM HiPIP in 200 mM Ches buffer at pH 9.5 with 0.25 mM Ti(III). The oxidized $[4Fe-4S]^{3+}$ state was obtained by reoxidation of the super-reduced HiPIP (37 μM in 95 mM Ches buffer at pH 9.5 with 4.9 mM Ti(III)) with air and 125 μM ferricyanide (final concentration HiPIP 33 μM). EPR conditions for the super-reduced state are: microwave frequency, 9.18 GHz; temperature, 20 K; microwave power, 1.26 mW; modulation frequency, 100 kHz; modulation amplitude, 0.8 mT. For the oxidized state: microwave power, 0.32 mW.

references quoted therein). Particularly, one of the *g*-values is greater than the free electron value $g_e$=2.002, and the other two *g*-values are less than $g_e$. The *g*-values of 2.042 and 1.920 are comparable to the values of 2.04 and 1.93 for *C. vinosum* HiPIP in 80% DMSO as reported by Cammack [1973] but the *R. globiformis* spectrum is sharper. In Figure 7.2 the microwave power saturation at different temperatures is given. Above 40 K the signal broadens considerably.

To check for the reversibility of the reduction, 37 μM *R. globiformis* HiPIP was incubated for 3 hours with 4.9 mM titaniumcitrate (95 mM Ches pH 9.5). The height of the peak at *g*=2.04 indicated complete super-reduction. The excess Ti(III) was oxidized by

- 137 -

**Figure 7.2.** Microwave power saturation of super-reduced *R. globiformis* HiPIP at different temperatures. The $g_\perp$-signals have been normalized to the maximum amplitudes. Other EPR conditions are as in Figure 7.1.



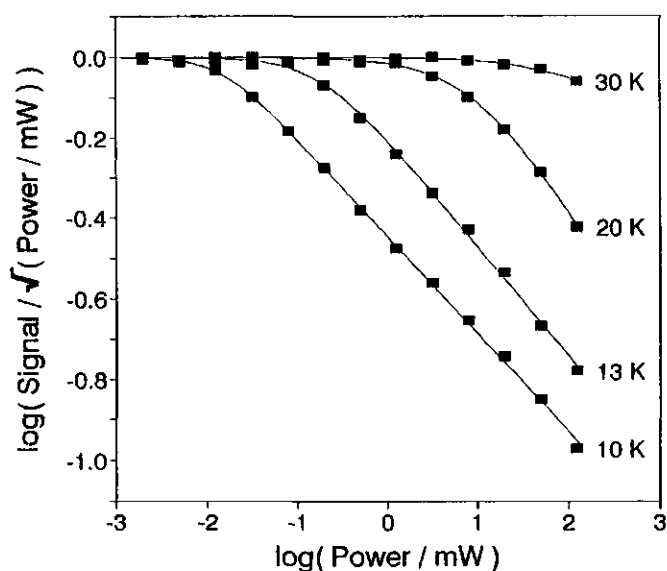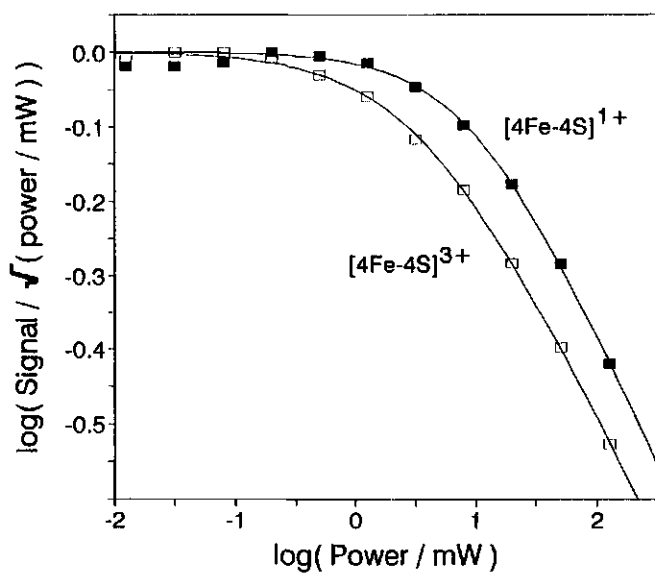**Figure 7.3.** Microwave power saturation of super-reduced and oxidized *R. globiformis* HiPIP at 20 K. The signals are normalized to the maximum values. Other EPR conditions are as in Figure 7.1.
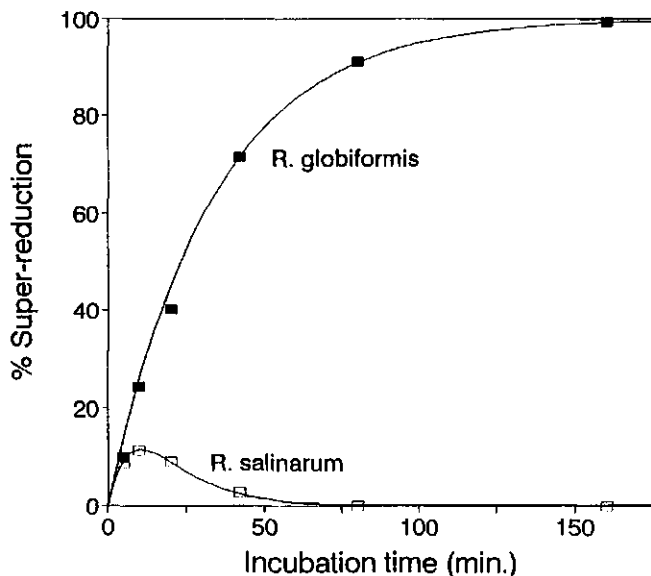
**Figure 7.4.** Time dependence of the super-reduction of *R. globiformis* HiPIP and *R. salinarum* iso-2 with Ti(III), measured by integration of the $g_z$ peak. Conditions: 48 µM HiPIP and 5.24 mM titanium-citrate in 95 mM Ches buffer pH 9.5. EPR conditions are as in Figure 7.1.

bubbling with air and subsequently 4 equivalents of ferricyanide were added to oxidize the HiPIP. The spectrum obtained is identical to that of electrochemically oxidized HiPIP with *g*-values of 2.122 and 2.029 (Figure 7.1) and similar to that of oxidized *C. vinosum* HiPIP [Dunham *et al.*, 1991] and *E. vacuolata* iso-2 [Banci *et al.*, 1993b]. Also, the spectrum of *C. vinosum* HiPIP exhibits additional weak features from a minor species, and the *R. globiformis* spectrum has similar features. From the saturation curve in Figure 7.3 it is apparent that the spin-lattice relaxation for the $[4Fe-4S]^{3+}$ state is slower than for the $[4Fe-4S]^{1+}$ cluster. The power levels required for a 50% reduction of the amplitude are 23 and 55 mW, respectively.

The super-reduction of the other six HiPIPs was attempted and the rate of the reduction was measured under the same conditions: 48 µM HiPIP in 95 mM Ches buffer at pH 9.5 with 5.24 mM titaniumcitrate. EPR-spectra were recorded during the incubation after temporarily freezing the samples in liquid nitrogen. The amount of super-reduced HiPIP was measured by comparing the area under the $g_z$ peak with that of the Ti(III)-free *R. globiformis* spectrum. For the two HiPIPs with the highest 2+/3+ redox potential (*R. globiformis* and *R. salinarum*) super-reduction was observed from the first measurement onwards (Figure 7.4). For the other HiPIPs no signals were observed besides the Ti(III) spectrum under these conditions and incubation up to 36 hours.

- 139 -
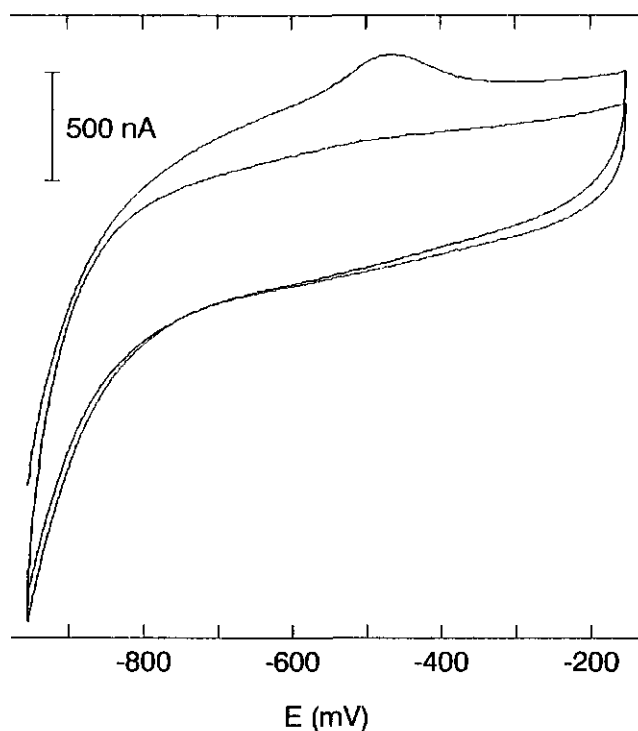
**Figure 7.5.** Staircase cyclic voltammograms of 20 μl 0.10 mM *R. globiformis* HiPIP in 10 mM Hepes at pH 7.5 after 5 min. equilibration at −0.95 V. The first and the second scan are shown (potential scan rate 10 mV/s; current sampling parameter α=0.5; potential step 1.22 mV).

The reduction of *R. globiformis* HiPIP in the presence of 5 mM Ti(III) can be fitted as a pseudo first-order reaction with a half-life of 23.1 minutes. This is much faster than the reduction with 0.25 mM Ti(III) but the rate constant is not linearly dependent on the concentration Ti(III). The addition of 40 μM of both methyl- and benzylviologen as potential mediators did not accelerate the reduction. The reduction rate of *R. salinarum* iso-2 initially is comparable to that of *R. globiformis*. The observed peak is located at $g$=2.050. However, after 10 minutes the signal decreases again. Apparently the super-reduced state is not stable. Using a half-life for the reduction of 23.1 min. a first-order decay half-life of 8.5 minutes is found.
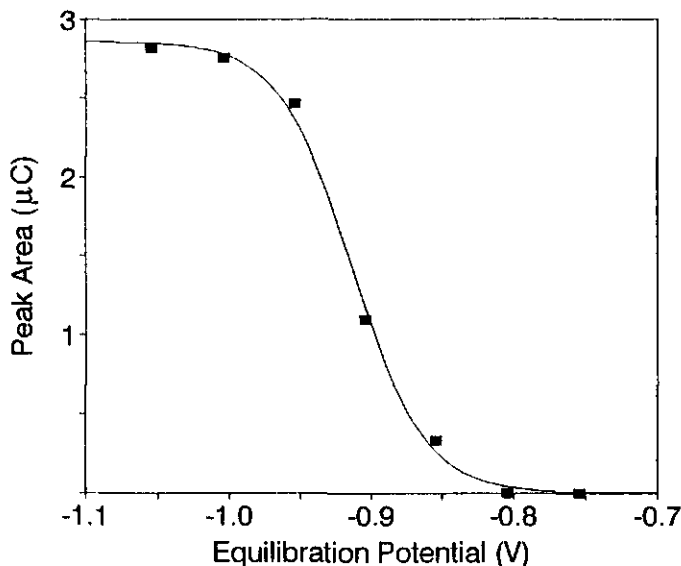
**Figure 7.6.** Dependence of the area under the oxidation peak of the first scan on the equilibration potential (conditions as in Figure 7.5). Between the measurements three scans were recorded and the potentials was held at −0.15 V for one minute. The data have been fitted to a one-electron Nernst curve with a half-wave potential of −0.91 V.

## 7.3.2 Electrochemistry.

No reversible super-reduction was observed using cyclic voltammetry (with potential scan rates down to 2 mV/s) in any of the seven HiPIPs down to potentials of −950 mV. The *R. globiformis* HiPIP was used to study super-reduction in more detail, firstly, because *R. globiformis* HiPIP proved to be more stable in electrochemical experiments than the other HiPIPs (no promoters are required) and, secondly, because the high 3+/2+ reduction potential (431 mV) of *R. globiformis* HiPIP might indicate that the super-reduction potential is also higher than that of the other HiPIPs. Because the reduction with Ti(III) is extremely slow, the super-reduction was attempted by equilibration at low potential with detection of an oxidative peak when scanning toward higher potential. Similar experiments were done by Tong & Feinberg [1994] for the slow reduction of the $[4Fe-4S]^{2+}$ cluster in aconitase, followed by Square Wave Voltammetric detection of the fast reoxidation.

Indeed, a clear oxidation peak was observed around −0.47 V after fixing the potential at −0.85 mV or lower for a few minutes before starting the scan in anodic direction (5 to 25 mV/s). An example is shown in Figure 7.5. This peak was not observed when buffer alone

was treated in the same way. No reduction current was observed and the oxidation current decreased rapidly during the following cycles (even when the lower limit was set at the initial equilibration potential) but after holding the potential at $-0.85$ V again, the oxidation peak fully re-appeared. The height of the peak is proportional to the scan rate and the area in $\mu$C is independent of the scan rate. This means that the reduced species is adsorbed at the electrode. The width at half-height is 100 to 120 mV at 10 mV/s, indicative of slow electron transfer, *i.e.* a quasi-reversible one-electron oxidation.

The peak area increased when the equilibration potential was lowered (Figure 7.6) and could be fitted nicely with a one-electron Nernst curve with a half-wave potential of $-0.91$ V. The fitted plateau-value of 2.86 $\mu$C corresponds to a full monolayer of super-reduced HiPIP. With an electrode surface of 25 mm$^2$ a protein radius of 6.7 Å is obtained. This is comparable to the average radius of 6.5 Å obtained from the X-ray structure of the *R. tenuis* HiPIP [Rayment *et al.*, 1992] with approximately the same mass as the *R. globiformis* HiPIP. When the electrode was held at a low potential for longer times or the electrode was in contact with the solution for a few hours, the peak surface steadily increased and values up to 100 $\mu$C were found (although the peaks were then broadened and some shoulders appeared). This indicates that multilayer adsorbtion occurs at a slow rate. The peak current still depends linearly on the scan rate and the area on the equilibration potential according to a one-electron Nernst curve. For example, after two hours a half-wave potential of $-0.86$ V and a plateau value of 31 $\mu$C were found (not shown).


## 7.4   Discussion


In the electrochemical experiments with *R. globiformis* HiPIP, the area under the reoxidation-peak after equilibration at low potential is directly correlated to the amount of adsorbed super-reduced HiPIP. The Nernst-type dependence of the integrated current on the applied potential indicates that super-reduction of the adsorbed layer is completed within a few minutes. Therefore, the ratio of reduced and super-reduced HiPIP is fully determined by the applied potential, and the fitted midpoint-potential is a reliable value for the reduction-potential. This method to obtain the reduction potential is similar to the well-known potentiometric titration of bulk-species, however, the application to adsorbed species undergoing an electrochemically measurable reoxidation is to our knowledge unprecedented.

The difference between the reduction and oxidation potentials found electrochemically can be explained by a reversible conformational change upon super-reduction. The different spin-lattice relaxation rates for the [4Fe-4S]$^{3+}$ and [4Fe-4S]$^{1+}$ states (Figure 7.3) might also be an indication for a conformational change. In Figure 7.7 a square scheme for the conformational changes and redox reactions is presented. In this scheme the assumptions are made that the super-reduction potentials are independent of pH and that no significant

$E_m = -0.91$ V

$\Delta G = +88$ kJ/mol

I:[4Fe-4S]$^{2+}$ $\rightleftharpoons$ I:[4Fe-4S]$^{1+}$

$\Delta G = -17$ kJ/mol

$K_{II} = 1 \cdot 10^{-3}$

$E_m = -0.64$ V

$\Delta G = +62$ kJ/mol

$\Delta G = -26$ kJ/mol

$K_{II} = 4 \cdot 10^4$

II:[4Fe-4S]$^{2+}$ $\rightleftharpoons$ II:[4Fe-4S]$^{1+}$

$E_m = -0.47$ V

$\Delta G = -45$ kJ/mol
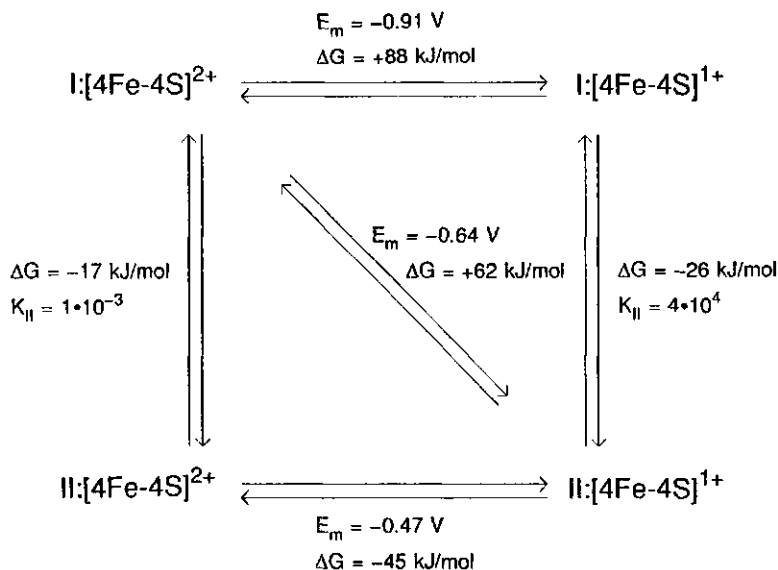
**Figure 7.7.** Square scheme for the super-reduction of *R. globiformis* HiPIP relating the proposed conformational changes and the redox reactions. Conformations are labeled as I and II. The signs of $\Delta G$ are given for the reactions in the direction of the outermost arrows coinciding with the electrochemically observed reactions. The $K_{II}$ values are the estimated formation constants for conformation II.

conformational change has occurred due to adsorption on the electrode. Although the potential of the [4Fe-4S]$^{3+/2+}$ couple in *R. globiformis* HiPIP is independent of pH between pH 4 and 10.5 ([Luchinat *et al.*, 1994] and Chapter 6), the pH-dependency of the 2+/1+ potential remains to be determined.

The conformational changes must be relatively fast because no reduction peak was observed around $-0.47$ V at scan rates up to 25 mV/s and the monolayer is fully converted to the super-reduced conformation within a minute or less. Going from a scan rate of 5 to 25 mV/s, the peak potential shifts about 40 mV in positive direction. This is much more than the theoretical 30 mV per 10-fold increase in the scan rate [Bard & Faulkner, 1980]. This means that some broadening occurs due to slow electron-transfer (A shift in positive direction was also observed when more than one monolayer was adsorbed). This hampers both the determination of the rate of the follow-up reaction and a better estimate of the true redox potential. The lower limits are 5 s$^{-1}$ for the rate constant and $-0.47$ V for the redox potential. Interestingly, this potential is similar to values found for the 2+/1+ transition in ferredoxins.

The reduction potential found from the slow equilibration with Ti(III) is the thermodynamic equilibrium potential for the overall reaction of electron-uptake plus conformational change. The estimated value of $-0.64$ V is aproximately equal to the average

of the two potentials found electrochemically, but this is not required under the model of Figure 7.7. The potential is less negative compared to the reduction potential found electrochemically because some of the reduction energy is provided by the conformational change. The equilibrium constants for the conformational changes (Figure 7.7) show that the reduced HiPIP is almost completely in the "native" conformation I while the super-reduced state is fully in the other conformation (II). A very small amount of reduced (2+) HiPIP in the super-reduced conformation (about 0.1%) would explain the very slow reaction with Ti(III). The redox potential of the Ti(IV)/Ti(III) couple at pH 9.5 is not low enough to directly reduce the HiPIP with the native conformation, but is sufficient for reduction of the very small fraction of the HiPIP in conformation II. The conformational change itself is probably not the rate-determining step: The estimated lower limit for the rate of formation of conformation II is $\approx 5 \cdot 10^{-3}$ s$^{-1}$. This is ten times higer than the measured rate of reduction with 5.2 mM Ti(III). This indicates that the electron transfer from Ti(III) to the HiPIP is slow. For the other HiPIPs no EPR-signals could be detected. This means either that the super-reduction did not occur or that the spectrum is completely obscured by that of Ti(III). In the former case this would indicate that the redox potential of the HiPIP in the super-reduced conformation is well below −0.7 V.

The electrochemical super-reduction behaviour of *R. globiformis* HiPIP shows a noteworthy similarity to the reduction of the [4Fe-4S]$^{2+}$ cluster in aconitase reported recently by Tong & Feinberg [1994]. Using Square Wave Voltammetry, they did not observe direct reduction between −100 and −1100 mV but did observe a reoxidation peak at −450 mV when the potential was held at −1100 mV prior to scanning in positive direction. Analogous to our observations the magnitude of the reoxidation peak increased as a function of the equilibration time. They proposed a very slow reduction and a fast reoxidation. It might well be that a square scheme similar to Figure 7 is also valid for the [4Fe-4S]$^{2+/1+}$ aconitase couple. Furthermore, these authors also transiently observed oxidation of the [4Fe-4S]$^{2+}$ cluster in aconitase to the putative 3+ form at an apparent oxidation potential of +100 mV [Tong & Feinberg, 1994].

The reduction potential of −0.91 V of the HiPIP with the native conformation of the 2+ state is much higher than the potential of −1.75 V, calculated by Jensen and coworkers [1994] from the crystal structure of *C. vinosum* HiPIP. The difference of 1.34 V between the potentials of the 3+/2+ and the 2+/1+ transitions in the native conformation is comparable to the separation between the two steps found for *C. pasteurianum* ferredoxin: Armstrong *et al.* [1982] found an upper limit of +0.86 V for the potential of the irreversible "super-oxidation". This is 1.26 V above the potential of −0.40 V for the 2+/1+ transition [Smith & Feinberg, 1990].

An intriguing question is whether there is a trend in the separation between the reduction steps in the series [2Fe−2S], [4Fe−4S], [6Fe−6S]. For the [2Fe-2S] cluster in the soluble fragment of the Rieske protein from bovine heart $bc_1$ complex, reversible super-

reduction was observed at −0.85 V. This is 1.15 V below the first reduction potential of +0.30 V [Verhagen *et. al.*, 1995]. For model [4Fe-4S] clusters, separations between the 2+/1+ and the 3+/2+ transitions of 0.7 to 1.3 V are reported [Kassner & Yang, 1977; Ciurli *et al.*, 1990]. For the [6Fe−6S] cluster in the Prismane proteins found in *Desulfovibrio vulgaris* and in *Desulfovibrio desulfuricans*, three potentials were found in a relatively small potential range: around −0.2 V, 0 V, and +0.3 V [Pierik *et al.*, 1992; van den Berg *et. al*, 1994]. These observations suggest a decreasing separation between the redox states with increasing cluster size. However, the differences between the potentials of 1.3 V found in both HiPIP and ferredoxin do not support this idea.

## 7.5    Conclusions

The EPR data show that super-reduction of the high-potential HiPIPs from *R. globiformis* and *R. salinarum* with Ti(III) is possible but extremely slow. The electrochemical reduction of *R. globiformis* HiPIP indicates that a reversible conformational change occurs upon super-reduction. The rate of super-reduction with Ti(III) is limited by the small amount (0.1%) of the HiPIP in the 2+ state with the super-reduced conformation. The quantitative super-reduction of *R. globiformis* HiPIP under non-denaturing conditions offers the opportunity for further spectroscopic characterization of this reduction state.

## 7.6    References

Adman, E., Watenpaugh, K.D. & Jensen, L.H. (1975) *Proc. Nat. Acad. Sci. USA 72*, 4854.

Armstrong, F.A., Hill, H.A.O. & Walton, N.J. (1982) *FEBS Letters 150*, 214.

Backes, G.,Mino, Y., Loehr, T.M., Meyer, T.E., Cusanovich, M.A., Sweeney, W.V., Adman, E.T. & Sanders-Loehr, J. (1991) *J. Am. Chem. Soc. 113*, 2055.

Banci, L., Bertini, I., Capozzi, F., Carloni, P., Ciurli, S., Luchinat, C. & Piccioli, M. (1993a) *J. Am. Chem. Soc. 115*, 3431.

Banci, L., Bertini, I., Ciurli, S., Ferretti, S., Luchinat, C. & Piccioli, M. (1993b) *Biochemistry 32*, 9387.

Banci, L., Bertini, I., Eltis, L.D., Felli, I.C., Kastrau, D.H.W., Luchinat, C., Piccioli, M., Pierattelli, R. & Smith, M. (1994) *Eur. J. Biochem. 225*, 715.

Banci, L., Bertini, I., Dikiy, A., Kastrau, D.H.W., Luchinat, C. & Sompornpisut, P. (1995) *Biochemistry 34*, 206.

Bard, A.J. & Faulkner, L.R. (1980) *Electrochemical methods; fundamentals and applications*, J. Wiley & Sons, New York.

Bartsch, R.G. (1991) *Biochim. Biophys. Acta 1058*, 28.

Belinskii, M. (1993) *Chem. Phys. 172*, 189.

Benning, M.M., Meyer, T.E., Rayment, I. & Holden, H.M. (1994) *Biochemistry 33*, 2476.

Breiter, D.R., Meyer, T.E., Rayment, I. & Holden, H.M. (1991) *J. Biol. Chem. 266*, 18660.

Butler, J., Sykes, A.G., Buxton, G.V., Harrington, P.C. & Wilkins, R.G. (1980) *Biochem. J. 189*, 641.

Carter, C.W., Kraut, J., Freer, S.T., Xuong, Ng.H., Alden, R.A. & Bartsch, R.G. (1974) *J. Biol. Chem. 249*, 4212.

Carter, C.W. (1977) *J. Biol. Chem. 252*, 7802.

Cammack, R. (1973) *Biochem. Biophys. Res. Comm. 54*, 548.

Ciurli, S., Carrié, M., Weigel, J.A., Carney, M.J., Stacks, T.D.P., Papaefthymiou, G.C. & Holm, R.H. (1990) *J. Am. Chem. Soc. 112*, 2654.

Dunham, W.R., Hagen, W.R., Fee, J.A., Sands, R.H., Dunbar, J.B. & Humblet, C. (1991) *Biochim. Biophys. Acta 1079*, 253-262.

Freer, S.T., Alden, R.A., Carter, C.W. & Kraut, J. (1975) *J. Biol. Chem. 250*, 46.

Jensen, G.M., Warshel, A. & Stephens, P.J. (1994) *Biochemistry 33*, 10911.

Kassner, R.J. & Yang, W. (1977) *J. Am. Chem. Soc. 99*, 4351.

Langen, R., Jensen, G.M., Jacob, U., Stephens, P.J. & Warshel, A. (1992) *J. Biol. Chem. 267*, 25635.

Luchinat, C., Capozzi, F., Borsari, M., Battistuzzi, G. & Sola, M. (1994) *Biochem. Biophys. Res. Comm. 203*, 436.

Mayhew, G. (1978) *Eur. J. Biochem. 85*, 535.

Orme-Johnson, N.R., Mims, W.B., Orme-Johnson, W.H., Bartsch, R.G., Cusanovich, M.A. & Peisach, J. (1983) *Biochim. Biophys. Acta 748*, 68.

Pierik, A.J., Hagen, W.R., Dunham, W.R. & Sands, R.H. (1992) *Eur. J. Biochem. 206*, 705.

Przysiecki, C.T., Meyer, T.E. & Cusanovich, M.A. (1985) *Biochemistry 24*, 2542.

Rayment, I., Wesenberg, G., Meyer, T.E., Cusanovich, M.A. & Holden, H.M. (1992) *J. Mol. Biol. 228*, 672.

Smith, E.T. & Feinberg, B.A. (1990) *J. Biol. Chem. 265*, 14371.

Tedro, S.M., Meyer, T.E. & Kamen, M.D. (1977) *J. Biol. Chem. 252*, 7826.

Tong, J. & Feinberg, B.A. (1994) *J. Biol. Chem. 269*, 24920.

Van den Berg, W.A.M., Stevens, A.A.M., Verhagen, M.F.J.M, van Dongen, W.M.A.M. & Hagen, W.R. (1994) *Biochim. Biophys. Acta 1206*, 240.

Verhagen, M.F.J.M., Link, T.A. & Hagen, W.R. (1995) *FEBS Letters 361*, 75.

Zehnder, A.J.B. (1976) *Ph.D. Thesis*, Federal Institute of Technology (ETH), Zürich, Switzerland.

# Summary and conclusions

The goal of the project was to obtain more detailed insight in interactions between redox proteins and solid electrodes and the mechanisms of electron transfer. In addition to this, the influence of the protein environment on the redox properties of the active site and the possible influence of the electrode/promoter system on these properties have been considered. Because redox enzymes do not often give an unambiguous and reversible electrochemical response (if at all), electron transferring proteins have been studied. The FMN containing flavodoxins have been used as model systems for flavin enzymes such as glucose oxidase. A series of high potential iron-sulfur proteins (HiPIPs) can be regarded as models for proteins containing [4Fe-4S] clusters. The HiPIPs are also of interest because of the high oxidation state of the cluster; the sequences are known, and the three-dimensional structures of some HiPIPs are known.

In Chapter 2 the electrochemical behaviour of flavodoxin from *Desulfovibrio vulgaris* (Hildenborough) has been characterized by staircase cyclic voltammetry (SCV) and differential pulse voltammetry (DPV). Fully oxidized flavodoxin at the bare glassy carbon electrode gave one redox couple at a potential of −218 mV (NHE) at pH=7.0 with an SCV peak current proportional to the scan rate. This response is caused by FMN, dissociated from the protein and adsorbed onto the electrode. The midpoint potential and the p$K$ of 6.5 are equal to the values measured with free FMN in solution. When the cationic promoter neomycin was added one additional and diffusion controlled response was observed. This positively charged aminoglycoside is believed to form a flexible bridge between the negative charges on the surface of both the protein and the electrode. The midpoint potential of the observed redox couple is −413 mV (NHE) at pH 7.0 with a redox-linked p$K$ for the reduced form of 4.8. The temperature dependence is −1.86 mV/K, yielding $\Delta S°=−179$ J·mol$^{-1}$·K$^{-1}$ and $\Delta H°=−12.4$ kJ/mol. This response is believed to be the semiquinone/hydroquinone transition. Although the starting material was 100% quinone, no response was observed around the midpoint potential of the quinone to semiquinone reduction of −113 mV (NHE) at pH 7.0, determined in an EPR-monitored titration with dithionite. Digital simulation shows that the peak currents of the second reduction couple approach a maximum value after a few cycles if comproportionation of fully reduced and fully oxidized flavodoxin occurs in solution and a small amount of semiquinone is either present initially or is generated by mediation of electrode-bound FMN. In the latter case the observed increase of the peak height can be fitted with a Butler-Volmer type heterogeneous electron transfer rate between adsorbed FMN and flavodoxin of 6.3·10$^{-6}$ m/s. This anomalous behaviour might have implications for the interpretation of electrochemistry on flavin enzymes like glucose oxidase. The observed peak is not *per se* the expected protein response or the expected (first) reduction step. The

development of a catalytic current when substrate is added is no prove for direct interaction between the protein and the electrode, but can also be accomplished by electron transfer mediated by a small amount of free flavin.

In Chapter 3 the detailed electrochemistry and complete EPR-monitored titrations of flavodoxin II of *Azotobacter vinelandii* (ATCC 478) are reported. Since wild-type flavodoxin dimerizes via disulphide bond formation between cysteine 69 residues, Cys69 has been replaced by an alanine as well as a serine residue. Redox properties of the C69A and C69S flavodoxin mutants were compared to those of wild-type flavodoxin. In the presence of the promoter neomycin, C69A and C69S flavodoxin showed a reversible response of the semiquinone/hydroquinone couple at the glassy carbon electrode, similar to the observations with *D. vulgaris* flavodoxin. However, addition of dithiotreitol proved to be necessary for the stabilization of the wild-type flavodoxin response. Dithiotreitol probably prevents dimerization of the protein by formation of cystine bridges. EPR-monitored redox titrations of wild-type and C69A flavodoxin at high and low pH confirm the cyclic voltammetry data. The pH dependence of the semiquinone/hydroquinone redox potentials cannot be described with a simple one-$pK_{red}$ model. Instead, the presence of at least two redox-linked protonation sites is suggested: $pK_{red,1} = 5.39 \pm 0.08$, $pK_{ox} = 7.29 \pm 0.14$ and $pK_{red,2} = 7.84 \pm 0.14$ with $E_m^7$ = $-459 \pm 4$ mV and a constant potential at high pH of $-485 \pm 4$ mV. The dependence of the semiquinone/hydroquinone potential on temperature is $-0.52 \pm 0.06$ mV/K, yielding $\Delta H^\circ =$ $28.6 \pm 1.5$ kJ/mol and $\Delta S^\circ = -50 \pm 6.2$ J·mol$^{-1}$·K$^{-1}$. No significant differences in redox properties of wild-type, C69A and C69S flavodoxin were observed. The electrochemical data suggest that replacement of Cys69 in the vicinity of FMN by either an alanine or a serine residue does not have a measurable influence on the structure of the protein.

In Chapter 4 a theoretical solution of the concentration distribution in long optical path length thin layer spectroelectrochemical cells is given by a convergent infinite summation of terms. At short times a large number of terms is required to obtain a good approximation. Alternatively, on a timescale at which the boundary of the diffusion layer has not reached the cell wall opposite to the electrode the concentration profile of the thin layer cell is equal to the profile of a semi-infinite bulk electrochemical cell. This profile is described by an error function, for which no analytical solution is available. A new three-parameter exponential approximation for this error function is presented with an accuracy better than 0.05% for all positive values of *x*. When the diffusion layer boundary reaches the cell wall the semi-infinite bulk model is no longer valid but then the slope of the profile has become small enough to be approximated by only the first five terms of the summation. When the composition of the bulk solution is measured by a light beam passing at grazing incidence over the electrode surface, the absorbance can be calculated from the concentration distribution by integration of the transmittance perpendicular to the light beam.

In Chapter 5 the validity of the mechanism proposed in Chapter 2 for the flavodoxin response has been verified by measuring the absorbance of the semiquinone form of *D.*

*vulgaris* flavodoxin during cyclic voltammetry. A long optical path length thin layer electrochemical cell (LOPTLC) was used with a layer width of 0.2 mm. Despite the non-ideal behaviour of this cell, the resulting "cyclic voltabsorptomograms" clearly show the proposed formation of semiquinone by FMN-mediated electron transfer, and comproportionation of flavodoxin in solution occurs. Simulated voltabsorptomograms qualitatively confirm this, although the observed reoxidation of flavodoxin semiquinone at low scan rates is not predicted by the Butler-Volmer model of Chapter 2.

In Chapter 6 the High Potential Iron-Sulfur Proteins (HiPIPs) from *Ectothiorhodospira vacuolata* (iso-1 and iso-2), *Chromatium vinosum*, *Rhodocyclus gelatinosus*, *Rhodocyclus tenuis* (strain 2761), *Rhodopila globiformis* and the large (multimer) HiPIP (iso-2) from *Rhodospirillum salinarum* have been investigated by direct electrochemistry. Using a glassy carbon electrode with a negatively charged surface, direct, unpromoted electrochemistry was possible with the positively charged HiPIPs. With the negatively charged HiPIPs the positively charged and flexible bridging promoter poly-L-lysine was required. The stability of the response could be improved by morpholin in combination with the negatively charged proteins and by monomeric amino acids or 4,4'-dipyridyl with the positively charged HiPIPs. These 'stabilizers' apparently prevent the blocking of the electrode by denatured protein during electrochemistry. The redox potential of 500 mV found for the large HiPIP from *R. salinarum* is the highest HiPIP potential reported. The presence of histidines in the sequence does not *per se* predict a pH-dependent redox potential. Only *C. vinosum* and *R. gelatinosus* HiPIPs show a weak but significant pH dependence with a difference of 35 mV between the low and the high pH form and maximum slopes of about $-20$ mV/unit. Either the coupling of electron and proton transfer is indirect ('allosteric') or $pK_{ox}$ is only 0.6 units lower than $pK_{red}$. In the latter case an apparent dielectric constant of 48 can be calculated. The dependence of the midpoint potential on ionic strength cannot be explained by the Debye-Hückel theory alone because the linearity exceeds the limiting concentration, the slopes are much smaller than predicted by this theory (0 to $-28$ mV/$\sqrt{M}$) and no positive slopes are observed. Combination of the sequences, the optical spectra, the overall charges and the redox thermodynamics suggests the existence of two major groups of HiPIPs. One group consists of *Chromatium*-like HiPIPs with redox potentials between 300 and 350 mV, modulated only by the solvation of the cluster but not by the overall charge of the protein. The second group is formed by *Ectothiorhodospira*-like HiPIPs with potentials between 50 and 500 mV, largely dependent on the overall charge of the peptide and also modulated by cluster solvation. From the slope of 25 mV per unit charge an apparent dielectric constant of 84 is calculated.

In Chapter 7 the reversible 2 x 1 $e^-$ reduction of the cubane cluster from oxidized to reduced to super-reduced: $[4Fe-4S]^{3+} \rightleftharpoons [4Fe-4S]^{2+} \rightleftharpoons [4Fe-4S]^{1+}$ has been studied in the HiPIPs of Chapter 6. Super-reduction to the 1+ state was not observed in any of these seven HiPIPs tested during cyclic voltammetry (down to $-0.95$ Volt). However, equilibration at low potential (pH 7.5) of *Rhodopila globiformis* HiPIP yielded a transient peak around $-0.47$ V

due to the oxidation of super-reduced HiPIP adsorbed at the electrode. The peak area depends on the equilibration potential according to a one-electron Nernst curve with a half-wave potential at −0.91 V. Reduction of *R. globiformis* HiPIP with titanium(III)citrate at pH 9.5 is very slow (pseudo first-order half-life of 23 min. with hundred-fold excess Ti(III)) but is reversible, and the EPR spectrum with *g*-values of 2.04 and 1.92 is similar to that of reduced [4Fe–4S]$^{1+}$ ferredoxins. Chemical or electrochemical reoxidation of the super-reduced form resulted in an EPR spectrum with $g_{\parallel} = 2.12$ and $g_{\perp} = 2.03$, *i.e.* identical to that of oxidized HiPIP. From the equilibrium concentration of super-reduced HiPIP at low concentration of Ti(III) a reduction potential of −0.64 V can be estimated. Super-reduction of the large HiPIP (iso-2) from *Rhodospirillum salinarum* is also possible with Ti(III) ($g_z = 2.05$) but the super-reduced state is unstable. No super-reduction with Ti(III) was observed for the other HiPIPs. The difference between the electrochemically observed reduction potential and oxidation potential is explained by a fast and reversible conformational change upon super-reduction. The rate of super-reduction with Ti(III) is limited by the small amount (0.1%) of the HiPIP in the 2+ state with the super-reduced conformation.

It can be concluded that the interaction of redox enzymes with the glassy carbon electrode is determined primarily by the charge of the protein and of the electrode surface. With positively charged proteins no promoter is required to obtain direct electron transfer at the negatively charged electrode surface. A positively charged promoter must be added to obtain a response with negatively charged proteins. A flexible promoter that can adjust its shape to fit both the protein surface and the electrode surface gives the best results. However, the response usually deteriorates in time. This is probably caused by denaturing of the protein on the electrode surface. Van der Waals forces and hydrophobic interactions probably play an important role in this process. The electrode thereby becomes gradually less accessible for electron transfer. A good promoter therefore not only forms a flexible bridge that compensates the electrostatic repulsion, but must also protect the protein from the hydrophobic patches on the electrode. Neomycin apparently has this double-function as promoter for flavodoxins. However, the HiPIP studies show that although poly-L-lysine promotes the response of the negatively charged proteins, the response is not stable. A separate "stabilizer" can be added to improve the voltammetry of both positively and negatively charged HiPIPs. The wild-type *Azotobacter vinelandii* flavodoxin II is a special case where dithiotreitol stabilizes the response by preventing the formation of dimers in which the FMN is no longer accessible to the electrode.

The redox potential of a protein is not always influenced by the charges of the peptide. This is true for both the permanent charges and for the pH-dependent charges. The HiPIP studies show that the distance between the charge and the redox-center, the dielectrics of the peptide in between, and the exposure of the charged groups to water are important factors. The dependence of the redox potentials on pH, measured with electrochemistry, do not always

agree with the results of bulk-titrations. This can just be an indication that the electrochemical measurements have a much better accuracy, but some influence of the electrode surface and/or the promoter on the protein structure cannot be excluded. It is therefore important to compare the electrochemical data with the results of independent spectroscopic redox-titrations. Simultaneous spectroscopic measurements of the solution during the voltammetric experiments can give useful additional information for the deconvolution of coupled homogeneous reactions.

# Samenvatting


Een belangrijke groep eiwitten wordt gevormd door de eiwitten die electronen kunnen opnemen of afstaan. Deze "redoxeiwitten" bevatten tenminste één maar vaak meerdere centra waarin één of meer electronen kunnen worden opgeslagen. Dit kunnen organische verbindingen zijn zoals flavines, clusters van ijzer- en zwavelionen, ionen van overgangsmetalen zoals bijvoorbeeld koper, of metaalionen gebonden door organische verbindingen zoals porfyrines. Een belangrijke eigenschap van een dergelijke electronendrager is de relatieve energie van het electron omdat dit informatie geeft over de plaats die een redoxenzym inneemt in het metabolisme van de cel. Deze energie wordt gegeven door de standaard redoxpotentiaal (evenwichtspotentiaal). Dit is de potentiaal waarbij precies de helft van de verbinding is gereduceerd (d.w.z. een electron heeft opgenomen). Een meer negatieve potentiaal geeft een hogere energie van het electron aan. Deze evenwichtspotentiaal kan bijvoorbeeld worden bepaald door de verbinding in de geoxideerde vorm te titreren met een reductor (d.w.z een verbinding met een lage potentiaal die electronen kan afstaan). Tijdens de titratie wordt de potentiaal gemeten met een voltmeter en twee electroden en worden regelmatig monsters genomen. Met een spectroscopische techniek kan het percentage gereduceerde verbinding voor elk van deze monsters worden bepaald. De hoeveelheid materiaal die voor een dergelijke titratie nodig is hangt af van de gevoeligheid van de meettechniek. Redoxeiwitten kunnen vaak goed worden gemeten met EPR (Electron Paramagnetische Resonantie) maar de beschikbare hoeveelheid eiwit is in veel gevallen nauwelijks genoeg voor een EPR-redoxtitratie. Als het eiwit echter direct electronen kan opnemen van, of afgeven aan het oppervlak van een electrode, kan informatie worden verkregen omtrent de eigenschappen van de redoxcentra door de spanning over de electrode (dat wil zeggen de energie van de electronen in het electrodemateriaal) te variëren en de stroom te meten die daardoor gaat lopen (voltammetrie). Een groot voordeel is dat hiervoor maar weinig eiwit nodig is. En omdat de potentiaal van de electrode met een vaste snelheid kan worden verhoogd of verlaagd, kan ook informatie worden verkregen over de snelheid van de electronenoverdracht.

Redoxenzymen zijn eiwitten die een specifieke reactie katalyseren (versnellen) waarbij electronenoverdracht plaatsvindt. Als een dergelijk enzym electronen kan opnemen van, of afstaan aan een electrode en ook in staat is deze electronen door te geven aan het substraat of op te nemen van het substraat, gaat er een stroom lopen die evenredig is met de concentratie substraat in oplossing. Dit betekent dat deze enzym-electrode dan in principe kan worden gebruikt als zeer selectieve en gevoelige detector, dat wil zeggen als amperometrische biosensor. Als het enzym niet direct met de electrode reageert, kan vaak een "mediator" worden toegevoegd. Dit is een verbinding die voor het transport van electronen tussen eiwit en electrode zorgt. Een dergelijke sensor die in de praktijk wordt toegepast is de glucose

biosensor. Deze bevat het enzym glucose oxidase en wordt gebruikt voor het meten van de concentratie glucose in het bloed van suikerpatienten. Anderzijds kan het systeem worden gebruikt voor de produktie van fijnchemicaliën en natuurlijk voor het bestuderen van de redoxenzymen zelf. Helaas echter geven deze in het algemeen grote eiwitten vaak in het geheel geen of hooguit een slecht gedefinieerde electrochemische respons en wordt ook lang niet altijd een katalytische stroom waargenomen.

Naast de redoxenzymen zijn in een cel ook eiwitten aanwezig die uitsluitend electronen opnemen van, en afstaan aan andere eiwitten, zonder direct een reactie te katalyseren. Deze eiwitten zijn essentieel voor het functioneren van een cel omdat ze de de verschillende onderdelen van het metabolisme met elkaar verbinden. Het zijn i.h.a. kleine eiwitten met relatief eenvoudige structuur. De redox-actieve centra in deze eiwitten komen overeen met die welke in veel redoxenzymen worden gevonden. Onder de juiste condities geven deze eiwitten in het algemeen echter wel eenduidige en reversibele voltammogrammen. Daarom zijn het ideale modelsystemen voor de veelal complexe redoxenzymen. Ook zouden deze eiwitten kunnen worden gebruikt om electronen te transporteren tussen de electrode en een redoxenzym. Op deze manier kan dan een biosensor worden gemaakt met een enzym dat niet direct met de electrode reageert zonder gebruik te maken van de veelal giftige synthetische mediatoren. Een andere interessante mogelijkheid is de reconstructie van (delen van) de electronentransport keten zoals die in de cel aanwezig is. De moeilijkheid zit echter vaak in het vinden van de "juiste condities". In praktische termen betekent dit het zoeken naar het optimale electrode materiaal, de optimale voorbehandeling van het oppervlak van die electrode en het vinden van de optimale combinatie van hulpstoffen. Deze hulpstoffen worden "promotoren" genoemd omdat ze de directe interactie van het eiwit met de electrode vergemakkelijken en stabiliseren, zonder zelf deel te nemen aan de electronenoverdracht. De werking van degelijke promotoren is echter slechts ten dele bekend.

De in dit proefschrift beschreven experimenten hadden dan ook tot doel meer inzicht te krijgen in de wetmatigheden die gelden voor het verkrijgen van een optimale electrochemische respons en in de wijze waarop de electronenoverdracht plaatsvindt. Hiervoor werd gebruik gemaakt van een zogenaamde "glassy carbon" electrode, een electrode gemaakt van glasachtige koolstof. Deze electrode heeft een negatief geladen oppervlak waarvan de eigenschappen enigszins kunnen worden gevarieerd door de manier van voorbehandelen. Daarnaast was ook de relatie tussen eiwitstructuur en redoxeigenschappen een belangrijk onderwerp van studie. Het derde thema in dit proefschrift is de relatie tussen de informatie die verkregen wordt uit de electrochemie en de eigenschappen van diezelfde eiwitten wanneer deze worden bestudeerd met behulp van spectroscopische technieken. Dit is van belang omdat electrochemie kijkt naar de stoom die loopt als gevolg van de som van reacties die zich voordoen zowel aan het oppervlak als in oplossing. Met spectroscopie daarentegen kan specifiek één component in oplossing worden gevolgd.

Als modelsysteem voor flavine bevattende enzymen, zoals het algemeen als modelenzym voor biosensoren gebruikte enzym glucose oxydase, werden flavodoxines bestudeerd. Deze bevatten een niet covalent gebonden flavine mononucleotide (FMN) als cofactor, een derivaat van vitamine B2. De vrije verbinding FMN kan twee electronen in een enkele stap opnemen of afstaan. Gebonden in het flavodoxine echter vindt de reductie plaats in twee stappen, met een potentiaalverschil van 300 à 400 mV. *In vivo* wordt de tweede, lage potentiaal, reductiestap benut. Uit de literatuur is bekend dat de eerste reductiestap traag is en electrochemisch niet wordt waargenomen. De electrochemische respons van flavodoxines wordt in detail bestudeerd.

Als modelsystemen voor enzymen die clusters van ijzer- en zwavelionen bevatten werd een serie HiPIPs uit verschillende organismen bestudeerd. De afkorting HiPIP staat voor "High Potential Iron-Sulfur Protein", hoge potentiaal ijzer-zwavel eiwit. Deze eiwitten bevatten een bij benadering kubusvormige [4Fe-4S] cluster ("cubaan") met een lading van 3+ in de geoxydeerde toestand. Dit is de hoogste oxydatiegraad waargenomen voor dergelijke clusters in eiwitten. Een andere groep electronentransporterende eiwitten met één of twee van deze cluster, de ferredoxines, benutten de 2+/1+ overgang en hebben een veel lagere potentiaal dan de HiPIPs. Het is daarom interessant om zowel de *in vivo* benutte 3+/2+ overgang als de 2+/1+ overgang in de HiPIPs te bestuderen. Daarnaast hebben de HiPIPs zeer uiteenlopende redoxpotentialen en zeer verschillende netto ladingen. Dit geeft de mogelijkheid om de invloed van die lading op zowel de electrochemische respons (interactie met de electrode) als op de redoxpotentiaal te bestuderen.

In Hoofdstuk 2 wordt het electrochemische gedrag van het flavodoxine uit de bacterie *Desulfovibrio vulgaris*, stam Hildenborough, gekarakteriseerd met behulp van cyclische en "differential pulse" voltammetrie. Volledig geoxydeerd flavodoxine zonder toevoegingen gaf alleen een reversibele respons rond −218 mV (pH=7.0) met een piekhoogte die evenredig is met de scansnelheid. Deze respons kan worden toegeschreven aan de cofactor FMN, gedissociëerd van het eiwit en geadsorbeerd aan de glassy carbon electrode. De gemiddelde potentiaal en p$K$=6.5 zijn gelijk aan de waarden van vrij FMN in oplossing. Na toevoegen van de promotor neomycine werd één extra reversibele en diffusie-gecontroleerde respons waargenomen. De werking van neomycine berust waarschijnlijk op het vermogen van deze positief geladen aminoglycoside om een flexibele brug te vormen tussen het negatief geladen eiwitoppervlak en de eveneens negatief geladen electrode. De gemiddelde potentiaal van het waargenomen koppel is −413 mV (pH=7.0), met een p$K$=4.8 in de gereduceerde vorm. De afhankelijkheid van de temperatuur is −1.86 mV/K, wat een entropieverschil $\Delta S°$=−179 J·mol$^{-1}$·K$^{-1}$ en een enthalpieverschil $\Delta H°$=−12.4 kJ/mol oplevert. Deze respons wordt toegeschreven aan de overgang van de 1-electron gereduceerde toestand (semiquinon) naar de 2-electron gereduceerde toestand (hydroquinon). Hoewel het uitgangsmateriaal volledig geoxydeerd was (d.w.z. in de quinon-vorm), werd geen electrochemische respons

waargenomen rond de evenwichtspotentiaal van de quinon / semiquinon overgang. Een EPR-redoxtitratie met natriumdithioniet leverde een waarde van −113 mV bij pH=7.0 op voor deze potentiaal. Numerieke analyse laat zien dat de hoogte van de flavodoxinepiek toeneemt in de tijd en na enkele scans maximaal wordt, als aangenomen wordt dat er comproportionering plaatsvindt in oplossing van één volledig geoxydeerd en één volledig gereduceerd flavodoxine tot twee semiquinon moleculen en als een kleine hoeveelheid semiquinon vanaf het begin aanwezig is of wordt gevormd door mediatie van het aan de electrode gebonden FMN. In dit laatste geval kan de gemeten toename van de piekhoogte in de tijd worden gefit met een heterogene electronoverdracht snelheid (volgens Butler-Volmer) tussen het geadsorbeerde FMN en het flavodoxine van $6.3 \cdot 10^{-6}$ m/s. Dit anomale gedrag kan gevolgen hebben voor de interpretatie van de electrochemische respons van flavine bevattende enzymen zoals glucose oxydase. De waargenomen piek hoeft niet de respons van het eiwit te zijn en als dit wel het geval is, is het wellicht niet de verwachtte (eerste) reductiestap. Een katalytische stroom in aanwezigheid van substraat is geen bewijs voor directe interactie tussen het enzym en de electrode, maar kan ook worden verkregen wanneer de electronen overdracht plaatstvindt via de vrije cofactor.

In Hoofdstuk 3 worden de electrochemie en de complete redoxtitratie, gemeten met EPR, van flavodoxine II uit *Azotobacter vinelandii* (ATCC 478) beschreven. Omdat wild-type flavodoxine dimeriseert door de vorming van een disulfidebrug tussen cysteïne 69 zijketens, is dit aminozuur vervangen door een alanine (C69A mutant) en door een serine (C69S mutant). De redoxeigenschappen van beide mutanten werden vergeleken met het wild-type flavodoxine. In aanwezigheid van neomycine werd met de beide mutanten een reversibele respons waargenomen van het semiquinon / hydroquinon koppel aan de glassy carbon electrode, overeenkomstig met de waarnemingen met *D. vulgaris* flavodoxine. Echter, de toevoeging van dithiotreitol bleek noodzakelijk voor het stabiliseren van de electrochemische respons van wild-type flavodoxine. Dithiotreitol voorkomt dimerisatie door de vorming van disulfidebruggen. De evenwichtspotentialen die werden verkregen uit de EPR- redoxtitraties bij pH=6 en pH=8.5 bevestigen de voltammetrisch bepaalde waarden. De gemeten pH-afhankelijkheid van de semiquinon/hydroquinon potentiaal kan niet worden beschreven met een enkele p$K$ voor de gereduceerde toestand, zoals algemeen wordt aangenomen voor flavodoxines. De metingen suggereren de aanwezigheid van tenminste twee protoneerbare groepen met reductietoestand afhankelijke p$K$'s: p$K_{red,1}$ = 5.39 ± 0.08, p$K_{ox}$ = 7.29 ± 0.14 en p$K_{red,2}$ = 7.84 ± 0.14 met $E_m{}^7$ = −459 ± 4 mV en een constante potentiaal bij hoge pH van −485 ± 4 mV. De temperatuur-afhankelijkheid van de semiquinon/hydroquinon potentiaal is −0.52 ± 0.06 mV/K, wat $\Delta H^{\circ}$ = 28.6 ± 1.5 kJ/mol en $\Delta S^{\circ}$ = −50 ± 6.2 J·mol$^{-1}$·K$^{-1}$ oplevert. Er werden geen significante verschillen waargenomen tussen de redoxpotentialen van het wild-type flavodoxine en de C69A en C69S mutanten. De electrochemische data suggereren derhalve, dat de vervanging van de cysteïne in de nabijheid van de FMN cofactor door alanine of door serine geen meetbare invloed heeft op de structuur van het eiwit.

In hoofdstuk 4 wordt de theorie van de dunne laag electrochemische cel behandel. De concentratiedistributie kan worden beschreven door sommatie van een convergente oneindige reeks termen. Vooral op korte tijdschaal, waar de gradiënt stijl is, zijn veel termen nodig voor een goede benadering. Als alternatief hiervoor kan het concentratieprofiel van de oneindige-bulk cel worden gebruikt, mits de grens van de diffusielaag de wand tegenover de electrode nog niet heeft bereikt. Dit profiel wordt beschreven door een z.g.n. errorfunctie, waarvoor geen analytische oplossing voorhanden is. Een nieuwe exponentiële benadering voor deze functie wordt gepresenteerd, met slechts 3 parameters en een nauwkeurigheid die beter is dan 0.05% voor alle positieve waarden van $x$. Wanneer de grens van de diffusielaag de wand tegenover de electrode bereikt, kan het oneindige-bulk model niet meer worden gebruikt. De helling van het concentratieprofiel is dan echter klein genoeg geworden om benaderd te worden door slechts de eerste vijf termen van de sommatie. Wanneer de samenstelling van de bulk wordt gemeten door een lichtbundel evenwijdig aan de electrode, kan de resulterende absorptie van het licht worden berekend uit het concentratieprofiel door de logaritme uit de integratie (sommatie) van de transmissie als functie van de plaats te bereken.

In hoofdstuk 5 wordt het mechanisme voor de respons van flavodoxines, zoals voorgesteld in hoofdstuk 2, geverifieerd door de absorptie te meten van de semiquinon vorm van *D. vulgaris* flavodoxine tijdens cyclische voltammetrie. Hiervoor werd een dunne laag cel gebruikt (0.2 mm laagdikte) waarin de lichtbundel evenwijdig aan het electrodeoppervlak passeert. Ondanks het niet-ideale gedrag van deze cel laten de resulterende "voltabsorptomogrammen" duidelijk zien dat de voorgestelde vorming van semiquinon door FMN-gemedieerde electronoverdracht en de vorming van twee semiquinon moleculen uit een quinon en een hydroquinon flavodoxine (comproportionering) plaatsvinden. Gesimuleerde voltabsorptomogrammen bevestigen dit kwalitatief, hoewel de waargenomen heroxydatie van flavodoxine semiquinon bij lage scansnelheid niet wordt voorspeld door het Butler-Volmer model zoals in hoofdstuk 2 werd gebruikt.

In hoofdstuk 6 wordt de directe electrochemie van HiPIPs bestudeerd, geïsoleerd uit de bacteriën *Ectothiorhodospira vacuolata* (iso-1 and iso-2), *Chromatium vinosum*, *Rhodocyclus gelatinosus*, *Rhodocyclus tenuis*, *Rhodopila globiformis* en uit *Rhodospirillum salinarum* (de multimere HiPIP iso-2). Het bleek dat directe electrochemie zonder promotor mogelijk is met de HiPIPs die een netto positieve oppervlakteloading hebben. De negatief geladen HiPIPs gaven echter alleen een electrochemische respons wanneer een positief geladen promotor werd toegevoegd. Poly-L-lysine gaf de beste resultaten, waarschijnlijk omdat deze promotor een zeer flexibele brug vormt naar het negatief geladen oppervlak van de glassy carbon electrode. De stabiliteit van de respons kon worden verbeterd door naast poly-L-lysine ook morpholine toe te voegen. Voor de positief geladen HiPIPs kon de respons worden gestabiliseerd door sommige aminozuren of door 4,4'-dipyridyl. Deze "stabilisatoren" verhinderen waarschijnlijk dat de electrode wordt geblokkeerd door het neerslaan van gedenatureerd eiwit. De redoxpotentiaal van 500 mV die werd gemeten voor de HiPIP uit *R.*

*salinarum* is de hoogste HiPIP potentiaal tot dus verre gerapporteerd. De aanwezigheid van histidines in de sequentie blijkt niet *per se* een pH-afhankelijkheid van de redoxpotentiaal te voorspellen. Alleen de *C. vinosum* en *R. gelatinosus* HiPIPs lieten een zwakke maar significante pH-afhankelijkheid zien, met een verschil van 35 mV tussen de potentialen bij hoge en bij lage pH en een maximale helling van $-20$ mV per pH-eenheid. Dit betekent dat òf de koppeling tussen electron- en protonoverdracht indirect is ("allosteer"), òf dat $pK_{ox}$ slechts 0.6 eenheden lager is dan $pK_{red}$. In dit laatste geval is er een ladingsinteractie tussen de plaats van protonering en de ijzer-zwavel cluster met een schijnbare diëlectrische constante van 48 voor het medium ertussenin. De gevoeligheid van de potentialen voor de ionsterkte kan niet volledig worden verklaard door de Debye-Hückel theorie: De lineaire afhankelijkheid van de wortel uit de ionsterkte werd ook bij hoge ionsterkte waargenomen, de gemeten hellingen (0 tot $-28$ mV/$\sqrt{M}$) zijn veel kleiner dan voorspeld door deze theorie en er werden geen positieve hellingen gevonden. De combinatie van de aminozuursamenstellingen, de optische spectra, de netto ladingen en de gegevens uit de temperatuurafhankelijkheden van de HiPIPs suggereert dat de HiPIPs kunnen worden onderverdeeld in twee groepen. De eerste groep bestaat uit *Chromatium*-achtige HiPIPs met potentialen tussen 300 en 350 mV, onafhankelijk van de eiwitlading en uitsluitend beïnvloed door lokale interacties met de peptide. De tweede groep wordt gevormd door de *Ectothiorhodospira*-achtige HiPIPs, met potentialen variërend van 50 tot 500 mV. De potentialen zijn sterk afhankelijk van de netto lading van het eiwit en worden ook beïnvloed door lokale interacties met het peptide. Uit de helling van 25 mV per ladingseenheid volgt een schijnbare diëlectrische constante van 84 voor de interactie tussen de oppervlaktelading en de cluster.

In hoofdstuk 7 wordt de reversibele 2 x 1 $e^-$ reductie bestudeerd van de 'cubaan' cluster van geoxydeerd naar gereduceerd naar supergereduceerd: $[4Fe-4S]^{3+} \rightleftarrows [4Fe-4S]^{2+} \rightleftarrows [4Fe-4S]^{1+}$ in de HiPIPs genoemd in hoofdstuk 6. In geen van deze zeven HiPIPs werd superreductie tot de 1+ vorm waargenomen met cyclische voltammetrie. Wanneer echter de electrode gedurende langere tijd werd vastgehouden op een lage potentiaal, werd met de HiPIP uit *Rhodopila globiformis* in de eerste scan een piek waargenomen rond $-0.47$ V (pH=7.5) afkomstig van de oxydatie van aan de electrode geadsorbeerde en supergereduceerde HiPIP. Het oppervlak onder deze piek is afhankelijk van de potentiaal waarop de electrode wordt vastgehouden: de gemeten waarden volgen een één-electron Nernst-curve met een evenwichtspotentiaal van $-0.91$ V. De reductie van *R. globiformis* HiPIP met titaan(III)citraat bij pH=9.5 is erg traag (een pseudo eerste orde halfwaarde tijd van 23 min. werd waargenomen met honderdvoudige overmaat Ti(III)), maar is reversibel. Het EPR-spectrum van de supergereduceerde vorm met $g$-waarden van 2.04 en 1.92 is gelijk aan dat van gereduceerde $[4Fe-4S]^{1+}$ ferredoxines. Heroxydatie van de supergereduceerde HiPIP, zowel electrochemisch als met ferricyanide, resulteerde in een EPR-spectrum met $g_\parallel = 2.12$ en $g_\perp = 2.03$, identiek aan geoxydeerde $[4Fe-4S]^{3+}$ HiPIP. Uit de evenwichtsconcentratie supergereduceerde HiPIP bij lage concentratie Ti(III) kan een reductiepotentiaal van $-0.64$

V worden geschat. Superreductie van de multimere HiPIP (iso-2) uit *Rhodospirillum salinarum* met Ti(III) is ook mogelijk, maar de supergereduceerde vorm ($g_z$ = 2.05) is niet stabiel. Superreductie werd niet waargenomen voor de andere vijf HiPIPs. Het verschil tussen de electrochemisch waargenomen superreductie en heroxydatie potentialen en de potentiaal geschat uit de reductie met Ti(III) kan worden verklaard met een snelle en reversibele conformatieverandering tijdens de superreductie. De reductiesnelheid met Ti(III) is gelimiteerd door een lage relatieve concentratie (0.1%) van de HiPIP in de 2+ vorm met de conformatie van de supergereduceerde vorm.

Uit de beschreven experimenten kan worden geconcludeerd dat de interactie van redoxeiwitten met de glassy carbon electrode primair wordt bepaald door de lading van het eiwit en het electrodeoppervlak. Met positief geladen eiwitten kan zonder toevoeging van promotoren electronenoverdracht worden gemeten. Een positief geladen promotor is echter nodig om directe electronenoverdracht te krijgen tussen negatief geladen eiwitten en de negatief geladen electrode. Een flexibele promotor die zich zowel naar de structuur van het eiwitoppervlak als naar de electrode kan vormen geeft het beste resultaat. Meestal neemt de respons echter af in de tijd. Waarschijnlijk wordt dit veroorzaakt door het denatureren (ontvouwen) van het eiwit aan de electrode. Hierbij spelen Van der Waals en hydrofobe interacties een belangrijke rol. De electrode wordt hierdoor geleidelijk minder toegankelijk voor electronenoverdracht. Een goede promotor zal daarom naast de functie als flexibele brug voor het compenseren van de gelijke ladingen, ook voor een afscherming van de ongeladen en hydrofobe plaatsen op de electrode moeten zorgen. Neomycine heeft een dergelijke dubbelfunctie als promotor voor flavodoxines. Uit de HiPIP studies bleek dat voor positief geladen eiwitten en voor negatief geladen eiwitten die ondanks de promotor een instabiele respons geven, als alternatief ook een aparte "stabilisator" kan worden toegevoegd. De waargenomen verbetering van de stabiliteit van de respons van zowel de positief als de negatief geladen eiwitten (plus promotor) naarmate een meer oxyderende voorbehandeling van de electrode werd gekozen is ook een aanwijzing dat hydrofobe interacties een ongunstige invloed hebben. Het wild-type *Azotobacter vinelandii* flavodoxine II is een speciaal geval waarin dithiotreitol de respons stabiliseert door de vorming van dimeren tegen te gaan waarin het FMN niet meer toegankelijk is voor de electrode.

De redoxpotentiaal van een eiwit wordt niet altijd door de ladingen in de peptide beïnvloed. Dit geldt zowel voor de permanente ladingen als voor de pH-afhankelijke groepen. De HiPIP studies laten zien dat de afstand tussen de lading en het redoxcentrum, de diëlectrische eigenschappen van de peptide ertussenin en de mate waarin de geladen groep is gesolvateerd door water belangrijke factoren zijn. De pH-afhankelijkheid van de redoxpotentialen gemeten met electrochemie komt niet altijd overeen met de resultaten van bulktitraties. Dit kan enerzijds worden veroorzaakt door de grotere nauwkeurigheid van de electrochemische metingen en anderzijds door de invloed van het electrodeoppervlak en/of

de gebruikte promoter. Het is derhalve van belang om de electrochemische data te verifiëren met onafhankelijke spectroscopische redoxtitraties. Simultane spectroscopische meting van de oplossing tijdens de voltammetrische experimenten kan een belangrijk hulpmiddel zijn bij het ophelderen van gekoppelde homogene reacties.

# Curriculum Vitae

Hendrik Adriaan Heering (Dirk) werd geboren op 27 oktober 1964 te Utrecht. In 1984 behaalde hij het V.W.O. diploma aan de Scholengemeenschap Zandvliet te Den Haag, waarna hij begon aan zijn studie Moleculaire Wetenschappen aan de Landbouwuniversiteit (toen nog Landbouwhogeschool) te Wageningen. Tijdens de doctoraalfase werden afstudeervakken gevolgd bij de vakgroepen Biochemie, Proceskunde en Organische Chemie. In augustus 1990 studeerde hij af als Moleculair Wetenschapper in de chemische, de chemisch-biologische en de fysisch-chemische oriëntaties. In de periode van 1 september 1990 tot 1 januari 1995 was hij als onderzoeker in opleiding (OIO) verbonden aan de vakgroep Biochemie aan de Landbouwuniversiteit Wageningen, alwaar het in dit proefschift beschreven onderzoek werd uitgevoerd onder supervisie van dr. W.R. Hagen en prof. C. Veeger. Vanaf 1 januari 1995 is hij als "postdoc" werkzaam bij dr. F.A. Armstrong aan het Inorganic Chemistry Laboratory van de Universiteit van Oxford, Engeland.

*Happiness lies in being privileged to work hard for long hours in doing whatever you think is worth doing. One man may find happiness in supporting a wife and children. Another may find it in robbing banks. Still another may labour mightily for years in persuing pure research with no discernible result. Each man or women must find for himself that occupation in which hard work and long hours make him happy.*

[R.A. Heinlein, To sail beyond the sunset.]

# List of Publications

1.    Hilhorst, R., Wolbert, R., Fijneman, P., Heering, D., Rietveld, P., Dekker, M., van 't Riet, K. and Bijsterbosch, B.H., "Factors affecting protein transfer from an aqueous phase into a reversed micellar phase", in *Biocatalysis in Non-Conventional Media*, J. Tramper et al. Eds., Elsevier Science Publishers 1992, pp. 299-306.

2.    Hilhorst, R., Fijneman, P., Heering, D., Wolbert, R.B.G., Dekker, M., van 't Riet, K. and Bijsterbosch, B.H., "Protein extraction using reversed micelles.", *Pure & Applied Chemistry 64* (1992) 1765-1770.

3.    Heering, H.A. and Hagen, W.R., "Anomalous direct electron transfer of flavodoxin at the glassy carbon electrode.", *Journal of Inorganic Biochemistry 51* (1993) 25.

4.    Heering, H.A. and Hagen, W.R., "Calculation of the absorbance by integration of the concentration distribution in long optical path length thin layer electrochemical cells.", *Journal of Electroanalytical Chemistry 364* (1994) 235-240.

5.    Vervoort, J., Heering, D., Peelen, S. and van Berkel, W., "Flavodoxins." in *Methods in Enzymology, volume 243, Inorganic Microbial Sulfur Metabolism*, H.D. Peck and J. LeGall Eds., Academic Press 1994, pp. 188-203.

6.    Hilhorst, R., Sergeeva, M., Heering, D., Rietveld, P., Fijneman, P., Wolbert, R.B.G., Dekker, M. and Bijsterbosch, B.H. ,"Protein extraction from an aqueous into a reversed micellar phase: The effect of water content and reversed micellar composition.", *Biotechnology and Bioengineering 46* (1995) 375-387.

7.    Heering, H.A. and Hagen, W.R., "Complex electrochemistry of flavodoxin at carbon-based electrodes results from a combination of direct electron transfer, flavin-mediated electron transfer, and comproportionation. ", *Journal of Electroanalytical Chemistry*, 1995, in press.

8.    Heering, H.A., Bulsink, Y.B.M., Hagen, W.R. and Meyer, T.E., "Reversible super-reduction of the cubane $[4Fe\text{-}4S]^{(3+;2+;1+)}$ in High Potential Iron-Sulfur protein under non-denaturing conditions: EPR spectroscopic and electrochemical studies.", *European Journal of Biochemistry*, 1995, in press.

9       Heering, H.A., Bulsink, Y.B.M., Hagen, W.R. and Meyer, T.E., "Influence of charge and polarity on the redox potentials of High-Potential Iron-Sulfur Proteins: Evidence for the existence of two groups.", *Biochemistry*, submitted March 1995.

10      Steensma, E., Heering, H.A., Hagen, W.R. and van Mierlo, C.P.M., "Redox properties of wild-type, C69A and C69S *Azotobacter vinelandii* flavodoxin II.", *European Journal of Biochemistry*, submitted July 1995.

The results described in Chapter 2 of this thesis are published in numbers 3 and 7 of this list, Chapter 3 is published as number 10, Chapter 4 is published as number 4, Chapter 6 is published as number 9, and Chapter 7 is published as number 8 of this list.